

**Quantitative remote sensing of  
Norway spruce (*Picea abies* (L.) Karst.):  
Spectroscopy from needles to crowns to canopies**

**Promotor:**

Prof. Dr. M. E. Schaepman

Hoogleraar Geo-Informatiekunde mbav Remote Sensing, Wageningen Universiteit  
(Nederland)

**Co-promotoren:**

Dr. Ir. J. G. P. W. Clevers

Universitair hoofddocent bij het Laboratorium voor Geo-Informatiekunde en Remote  
Sensing, Wageningen Universiteit (Nederland)

Dr. P. Cudlín

Hoofd van het Laboratorium voor Boscologie, Instituut voor Systeembioogie en  
Ecologie, Tsjechische Academie van Wetenschappen (Tsjechische Republiek)

**Promotiecommissie:**

Prof. Dr. R. B. Myneni – Boston University (USA)

Prof. Dr. S. Jacquemoud – Université Paris 7 – Denis Diderot (France)

Prof. Dr. Ir. G. M. J. Mohren – Wageningen Universiteit (Nederland)

Dr. F. Gascon – European Space Agency – ESTEC (Nederland)

Dit onderzoek is uitgevoerd binnen de C.T. de Wit onderzoekschool  
'Production Ecology and Resource Conservation (PE&RC)'

**Quantitative remote sensing of  
Norway spruce (*Picea abies* (L.) Karst.):  
Spectroscopy from needles to crowns to canopies**

Zbyněk Malenovský

**Proefschrift**

ter verkrijging van de graad van doctor  
op gezag van de rector magnificus  
van Wageningen Universiteit,  
Prof. Dr. M.J. Kropff,  
in het openbaar te verdedigen  
op vrijdag 13 oktober 2006  
des namiddags te vier uur in de Aula

Zbyněk Malenovský, 2006.

Cover drawings done by Tereza Juráčková (3 years-old), 2006.

Quantitative remote sensing of Norway spruce (*Picea abies* (L.) Karst.):  
Spectroscopy from needles to crowns to canopies.

PhD Thesis, Wageningen University, Wageningen, The Netherlands, 141 pp.  
– with summaries in English, Dutch and Czech –

Keywords: imaging spectroscopy / remote sensing / optical/ quantitative / forest / Norway  
spruce (*Picea abies*) / up-scaling/ leaf optical properties / radiative transfer /  
PROSPECT / DART / AISA Eagle / chlorophyll / LAI

ISBN 90-8504-503-7

**Quantitative remote sensing of  
Norway spruce (*Picea abies* (L.) Karst.):  
Spectroscopy from needles to crowns to canopies**

Zbyněk Malenovský

**Thesis**

to fulfil the requirements to obtain the degree of doctor  
on the authority of the rector magnificus  
of Wageningen University,  
Prof. Dr. M.J. Kropff,  
to be public defended  
in the Auditorium on Friday, October 13<sup>th</sup>, 2006, at 16.00 hours.

---

This work was supported by:

- Sabbatical Fellowship Programme 1K04, the Ministry of Education, Youth and Sports of the Czech Republic
- NATO Science Fellowships Programme
- Fellowship Programme of the Netherlands Ministry of Agriculture, Nature Management and Fisheries
- Centre for Geo-Information and Remote Sensing, Wageningen University
- Institute of Systems Biology and Ecology, Academy of Sciences of the Czech Republic
- Centre d'Etudes Spatiales de la Biosphère, France
- Argus Geo-System, Czech Republic

**Promoter:**

Prof. Dr. sc. nat. M. E. Schaepman

Professor in Geo-Information Sciences with specialisation in Remote Sensing,  
Wageningen University (The Netherlands)

**Co-promoters:**

Dr. Ir. J. G. P. W. Clevers

Associated professor in the Laboratory for Geo-Information Sciences and Remote  
Sensing, Wageningen University (The Netherlands)

Dr. P. Cudlín

Head of the Laboratory of Forest Ecology, Institute of Systems Biology and Ecology,  
Academy of Sciences of the Czech Republic.

**Examining committee:**

Prof. Dr. R. B. Myneni – Boston University (USA)

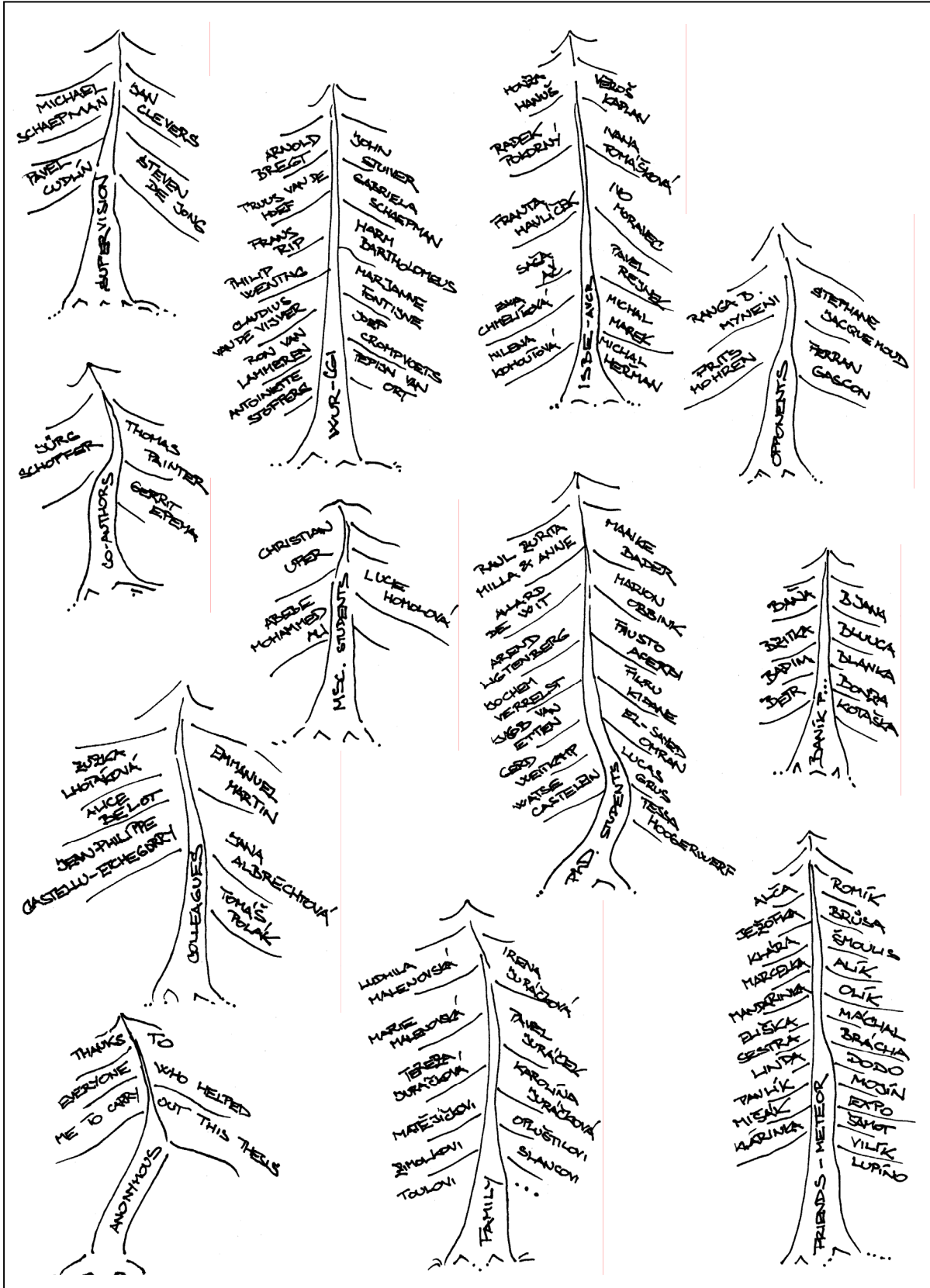
Prof. Dr. S. Jacquemoud – Université Paris 7 – Denis Diderot (France)

Prof. Dr. Ir. G. M. J. Mohren – Wageningen University (The Netherlands)

Dr. F. Gascon – European Space Agency – ESTEC (The Netherlands)

---

# Forest of acknowledgement



---

*In memory of my father and grandfathers  
Jaroslav (1951-1993) and Jaroslav (1921-2002) Malenovský  
and Jan Opluštíl (1911-2003)*



---

## Abstract

---

Mountain ecosystems represent nearly one fourth of the Earth's land surface, and provide (ecosystem) services to a significant part of the world's human population. As was noted in the 1992 United Nations Conference on Environment and Development (UNCED) in Rio de Janeiro (Agenda 21), these ecosystems are experiencing rapid degradation due to environmental and human impact at the local scale having, however, a global spread. This work contributes to the spatial monitoring of mountain forest ecosystems dominated by Norway spruce trees (*Picea abies* (L.) Karst.) through developing new quantitative approaches using optical hyperspectral remote sensing.

A common denominator for all experiments described and performed throughout this work is *spectroscopy*, used in combination with ecological reasoning and physically based *bottom-up* scaling approaches. The spectral information acquired at the level of leaves (needles) is scaled up to the level of tree crowns and then to the level of forest canopies by means of radiative transfer modelling. This *up-scaling* method is based fully on cause-effect relations of vegetation-photon interaction allowing for its subsequent numerical inversion. We have employed radiative transfer models to develop an inversion routine for the retrieval of quantitative forest canopy biochemical (concentration of chlorophyll) and biophysical (leaf area index) parameters based on hyperspectral data acquired by the Airborne Imaging Spectroradiometer (AISA) Eagle.

The starting point of this work was the calibration and validation of the leaf radiative transfer model PROSPECT (leaf optical PROPERTIES SPECTra) for Norway spruce needles at wavelengths ranging from 450-1000 nm. Simultaneously, an investigation on the variability in hemispherical-directional reflectance, transmittance and absorptance of sunlit spruce needle samples was carried out for environmental stress resistant and stress resilient spruce crowns. Recalibration of the PROSPECT chlorophyll and dry matter specific absorption coefficients  $k_{ab}(\lambda)$  and  $k_m(\lambda)$  resulted in close agreement of the PROSPECT simulated needle optical properties with the spectral measurements of three investigated needle age-classes. The root mean square error (RMSE) between simulated and measured needle reflectance, transmittance, and absorptance signatures was 1.74%, 1.53%, and 2.91%, respectively. Testing the adjusted PROSPECT model for total chlorophyll concentration, dry matter content, and leaf water content retrieved simultaneously from laboratory based spectrometer measurements of independent needle samples showed an improved performance.

When comparing sunlit needles of primary shoots of the two environmental stress response classes, significant quantitative differences were discovered at red edge (710-715 nm) and green (540-565 nm) wavelengths with respect to the variability in needle optical properties. These differences are related to the changes in the concentration of the foliar pigments, which proved to be significantly lower for needles of stress resilient trees. High variability in qualitative spectral characteristics was found at wavelengths relating to far-red (740 nm) and green (530 nm) fluorescence emissions. No significant spectral variation was found within the near infrared wavelengths of the tested needles. Consequently, we conclude that sunlit needle samples of a specific age-class collected from a randomly selected branch within two tested crown parts were representative for both of them, but they are optically different if collected from stress resistant or stress resilient crowns.

---

The needle optical properties were up-scaled to the crowns and to the canopies by the 3-dimensional Discrete Anisotropic Radiative Transfer (DART) model. A detailed sensitivity analysis investigating the effect of woody elements introduced into the DART model on the nadir bidirectional reflectance factor (BRF) was performed at a very high spatial resolution (0.4 m) before its direct use for the Norway spruce canopy. The sensitivity analysis was performed separately for both sunlit and shaded parts of the simulated forest canopy and it was validated against BRF measurements at the same spatial resolution acquired over the simulated forest stand by the AISA sensor. Results showed a nadir BRF for the Norway spruce canopy modelled as pure foliage to be similar to the one for foliage including only robust woody constituents (i.e., trunks and branches of first order). The incorporation of small woody parts in DART caused the nadir canopy reflectance to decrease in the near-infrared (NIR) about 4%, in the red edge about 2%, and in the green bands less than 1%. These findings stressed the importance of including fine woody elements in radiative transfer based retrievals of the forest canopy properties at very high spatial resolution, especially if the NIR wavelengths are exploited.

The coupled radiative transfer models PROSPECT and DART were employed to develop and test the sensitivity of a robust chlorophyll estimating optical index for a heterogeneous coniferous forest canopy. A newly proposed index named ‘Area under curve Normalized to Maximal Band depth between 650-725nm’ (ANMB<sub>650-725</sub>) is based on the continuum removal method applied on reflectance spectra. The approach is taking advantage of the fine spectral resolution and sampling interval of hyperspectral images to isolate the chlorophyll absorption feature between 650 and 725 nm. The results, obtained from simulated hyperspectral data with a pixel size of 0.9 m, showed a strong linear relationship of the ANMB<sub>650-725</sub> with spruce crown  $C_{ab}$  concentration ( $r^2 = 0.9798$ ) and an insensitivity for varying canopy structural features such as LAI and canopy closure. Chlorophyll concentration retrieval using the ANMB<sub>650-725</sub> index remained stable also after introduction of the spectral information of epiphytic lichen (*Pseudevernia* sp.) and an increased sensor noise (signal to noise ratio equal to five).

It can be concluded from this work that up-scaling procedures from needles to crowns to canopies can be successfully applied in mountain ecosystems. In particular the quantitative, physical based approaches proved to be robust and further helped to refine radiative transfer based models. In the near future, we will be seeing a number of spaceborne missions being realized (e.g., either of hyper- or super-spectral nature), where the presented up-scaling approaches can significantly contribute to increased variable retrieval accuracy. The integration of such derived products into an assessment programme for monitoring and forecasting the development of forest ecosystem services (e.g., Global Monitoring for Environment and Security (GMES)) is a logical consequence of this work.

## Samenvatting

---

Bergachtige ecosystemen vertegenwoordigen bijna een vierde deel van het landoppervlak op aarde en staan in dienst van een significant deel van de wereldbevolking. Zoals al opgetekend tijdens de UNCED conferentie, de VN conferentie over Milieu en Ontwikkeling, gehouden in Rio de Janeiro in 1992, ondergaan deze ecosystemen een snelle achteruitgang ten gevolge van milieu en menselijke invloeden op lokale schaal, echter met een mondiale verbreiding. Het hier beschreven onderzoek levert een bijdrage aan het ruimtelijk monitoren van bergachtige bos-ecosystemen die gedomineerd worden door fijnspar (*Picea abies* (L.) Karst.) door middel van het ontwikkelen van nieuwe, kwantitatieve benaderingen gebaseerd op optische, hyperspectrale remote sensing.

Een gemeenschappelijke noemer voor de beschreven en uitgevoerde experimenten in dit proefschrift vormt het gebruik van spectroscopie met ondersteuning van een ecologische redenering en een fysische aanpak voor een “bottom-up” schaling. De spectrale informatie die op het bladniveau (de naalden) verkregen wordt, wordt opgeschaald naar het niveau van de boomkronen en vervolgens naar het niveau van bosopstanden door middel van modellering van de interactie van straling met de vegetatie. Deze opschalingmethoden zijn volledig gebaseerd op oorzaak-gevolg relaties van de interactie van fotonen met de vegetatie om zodoende te zorgen dat numerieke inversie vervolgens mogelijk is. Stralingsinteractiemodellen zijn toegepast om een inversiemethode te ontwikkelen voor het afleiden van kwantitatieve biochemische (chlorofylconcentratie) en biofysische (leaf area index) bosparameters gebaseerd op hyperspectrale gegevens verkregen met de Airborne Imaging Spectroradiometer (AISA) Eagle.

Het beginpunt van dit onderzoek was de ijking en validatie van het stralingsinteractiemodel PROSPECT voor naalden van de fijnspar voor golflengten van 450–1000 nm. Tegelijkertijd werd een studie naar de variabiliteit in hemisferisch-directionele reflectie-, transmissie- en absorptiefactoren van naalden van de fijnspar uitgevoerd voor naalden van kronen die ongevoelig zijn voor omgevingsstress (resistent) en voor naalden die zich herstellen na een periode van omgevingsstress (veerkrachtig). Herijking van de specifieke absorptiecoëfficiënten voor chlorofyl  $k_{ab}(\lambda)$  en droge stof  $k_m(\lambda)$  in PROSPECT resulteerde in een goede overeenstemming tussen de met PROSPECT gesimuleerde optische eigenschappen van naalden en de spectrale metingen aan drie leeftijdsklassen die onderzocht zijn. De gemiddelde fout (“root mean square error”, RMSE) tussen gesimuleerde en gemeten reflectie-, transmissie- en absorptiefactoren van naalden bedroeg respectievelijk 1,74%, 1,53% en 2,91%. Het testen van het aangepaste PROSPECT model voor het simultaan afleiden van de totale chlorofylconcentratie, het droge stof gehalte en het watergehalte uit spectrometermetingen verricht in het laboratorium aan een onafhankelijk monster van naalden toonde een verbeterde prestatie.

Bij het vergelijken van de naalden van primaire takken van de twee omgevingsstressklassen werden significante, kwantitatieve verschillen in de optische eigenschappen van naalden gevonden bij golflengten op de overgang van rood naar nabij-infrarood (710-715 nm) en in het groen (540-565 nm). Deze verschillen zijn gerelateerd aan veranderingen in de concentratie aan pigmenten in de naalden, die significant lager was in de naalden van bomen die zich herstelden van stress. Er werd een hoge variabiliteit in kwalitatieve spectrale eigenschappen gevonden bij golflengten die gerelateerd waren aan verrood (740 nm) en groen

(530 nm) fluorescentie-emissies. Er werd geen significante spectrale variatie gevonden voor de nabij-infrarode golflengten van de onderzochte naalden. Daarom kunnen we concluderen dat monsters van naalden van een specifieke leeftijdsklasse representatief zijn voor een willekeurig geselecteerde tak binnen twee onderzochte kroondelen, maar dat ze optisch verschillend zijn voor stressresistente en stressherstellende kronen.

De optische eigenschappen van naalden werden opgeschaald naar kronen en opstanden door middel van het 3-dimensionele DART (Discrete Anisotropic Radiative Transfer) model. Een gedetailleerde gevoeligheidsanalyse werd uitgevoerd om het effect van de introductie van houtachtige elementen in het DART model op de bidirectionele reflectiefactor (BRF) vanuit nadir bij een zeer hoge ruimtelijke resolutie (0,4 m) te onderzoeken voordat het direct bij opstanden van fijnspaar zou worden gebruikt. De gevoeligheidsanalyse werd afzonderlijk uitgevoerd voor delen van de bosopstand die direct door de zon beschenen werden en voor beschaduwde delen en de resultaten werden gevalideerd met BRF-metingen verkregen voor de gesimuleerde bosopstand bij dezelfde ruimtelijke resolutie met behulp van de AISA sensor. Resultaten voor de BRF vanuit nadir waren gelijk voor een fijnspaaropstand gemodelleerd als naalden alleen en een opstand gemodelleerd als naalden en houtachtige delen (dat wil zeggen stammen en eerste orde takken). Het in rekening brengen van kleine houtachtige delen binnen DART leverde een lagere gewasreflectie vanuit nadir in het nabij-infrarood (NIR) op van ongeveer 4%, op de rood-NIR overgang van ongeveer 2% en in het groen van minder dan 1%. Deze bevindingen versterkten het belang van opname van kleine houtachtige delen in het afleiden van boseigenschappen bij een zeer hoge ruimtelijke resolutie met behulp van stralingsinteractiemodellen, in het bijzonder indien NIR golflengten gebruikt worden.

De gekoppelde stralingsinteractiemodellen PROSPECT en DART zijn gebruikt om een robuuste optische index voor de schatting van de chlorofylconcentratie van een heterogeen naaldbos te ontwikkelen en de gevoeligheid ervan te testen. De nieuwe index genaamd “Area under curve Normalized to Maximal Band depth between 650-725 nm” ( $ANMB_{650-725}$ ) is gebaseerd op de zogenaamde “continuum removal” methode toegepast op reflectiespectra. Deze methode maakt gebruik van de fijne spectrale resolutie en bemonsteringsinterval van hyperspectrale beelden om de absorptiekenmerken van chlorofyl tussen 650 en 725 nm te isoleren. De resultaten, verkregen uit gesimuleerde hyperspectrale gegevens met een pixelafmeting van 0,9 m, toonden een sterke, lineaire relatie van de  $ANMB_{650-725}$  met de chlorofylconcentratie van kronen van de spar ( $r^2 = 0.9798$ ), terwijl de index ongevoelig was voor structureigenschappen zoals de LAI en de bedekkingsgraad. Het afleiden van de chlorofylconcentratie met behulp van de  $ANMB_{650-725}$  bleef ook stabiel na introductie van de spectrale informatie van epifytische korstmossen (*Pseudevernia* sp.) en een toegenomen sensorruis (met een signaal-ruis-verhouding van vijf).

Uit dit onderzoek kan geconcludeerd worden dat opschalingprocedures van naalden naar kronen en vervolgens naar opstanden succesvol toegepast kunnen worden in bergachtige ecosystemen. In het bijzonder kwantitatieve, fysische benaderingen bleken robuust te zijn en droegen bij aan het verder verfijnen van modellen gebaseerd op de stralingsinteractie met vegetatie. In de nabije toekomst zullen een aantal satellietmissies gerealiseerd worden (bijvoorbeeld van hyper- of superspectrale aard), waarbij de gepresenteerde opschalingbenaderingen wezenlijk kunnen bijdragen aan een toegenomen nauwkeurigheid van afgeleide variabelen. De integratie van dergelijke afgeleide producten in een programma voor de monitoring en voorspelling van de ontwikkeling van de rol van bosecosystemen (bijvoorbeeld Global Monitoring for Environment and Security (GMES)) is een logisch gevolg van dit werk.

## Abstrakt

---

Horské ekosystémy zaujímají téměř jednu čtvrtinu zemského povrchu a poskytují své funkce významné části lidské populace planety Země. Jak vyplynulo ze závěrů konference Spojených národů „O životním prostředí a rozvoji“, konané v Rio de Janeiru v roce 1992 (Agenda 21), tyto ekosystémy prochází v současnosti rychlým úpadkem způsobeným přírodními a lidskými vlivy působícími především v lokálních měřítcích, nicméně s globálním dosahem. Tato práce přispívá k monitorování stavu horských lesních ekosystémů s převládajícím zastoupením smrku ztepilého (*Picea abies* (L.) Karst.) navržením nových kvantitativních postupů optického hyperspektrálního dálkového průzkumu Země.

Společným jmenovatelem všech experimentů popsanych a uskutečněných v rámci této studie je *spektroskopie*, kombinovaná s ekologickými poznatky a fyzikálně založenou vzestupnou (*bottom-up*) generalizací z úrovně vyššího prostorového měřítka na měřítko nižší (metoda obecně známá jako *up-scaling*). Spektrální informace získaná na úrovni listů (jehlic) je převedena na úroveň korun stromů a následně lesních porostů pomocí modelů přenosu slunečního záření (tzv. radiativního transferu). Tato *up-scaling* metoda je postavena na matematických rovnicích popisujících vzájemné interakce vegetace a fotonů, jež umožňují jejich numerickou inverzi. Modely radiativního transferu byly použity jako základní nástroje vývoje inverzních postupů pro odhad kvantitativních biochemických a biofyzikálních parametrů lesních porostů (koncentrace chlorofylů a indexu listové plochy) z leteckých hyperspektrálních dat nasnímaných spektrometrem AISA Eagle.

V první kroku studie byla provedena kalibrace a vyhodnocení použitelnosti modelu radiativního transferu zvaného PROSPECT (leaf optical PROPERTIES SPECTra) pro simulaci optických vlastností jehlic smrku ztepilého v intervalu vlnových délek 450-1000 nm. Současně s těmito analýzami probíhalo vyhodnocení variability hemisféricky-jednosměrné odrazivosti, propustnosti a absorpce slunečního záření smrkových jehlic, jež byly odebrány z korun stromů rezistentních a resilientních vůči stresu vytvářeného podmínkami životního prostředí. Nová kalibrace modelu PROSPECT, upřesnění jeho specifických absorpčních koeficientů pro chlorofyly a sušinu  $k_{ab}(\lambda)$  a  $k_m(\lambda)$ , vyústila v blízkou shodu mezi modelem simulovaných a v laboratoři naměřených optických vlastností tří zkoumaných ročníků smrkových jehlic. Střední kvadratická chyba od průměru (Root Mean Square Error – RMSE) simulovaných a naměřených hodnot odrazivosti, propustnosti a absorpce jehlic činila 1,74%, 1,53%, a 2,91%. Vhodnost nově kalibrovaného PROSPECT modelu pro smrkové jehlice byla ověřena i dostatečně přesnými výsledky odhadu celkové koncentrace chlorofylů, obsahu listové sušiny a vody, získaných inverzí modelu z laboratorních spektrometrických měření.

Na okraji červené (710-715 nm) a v zelené části (540-565 nm) elektromagnetického spektra byly zjištěny statisticky významné rozdíly optických vlastností jehlic primárních výhonů smrkových korun dvou rozdílných stresových reakcí: stresu rezistentními a stresu resilientními stromy. Tyto rozdíly byly prokazatelně způsobeny změnou koncentrace listových barviv, jež byla nižší v jehlicích stresu resilientních stromů. Vysoká variabilita kvalitativních spektrálních vlastností smrkových jehlic byla objevena pro vlnové délky vzdálené červené (740 nm) a zelené (530 nm) fluorescenční emise. Spektrální charakteristiky blízkých infračervených vlnových délek nevykazovaly žádné statisticky významné rozdíly. Na základě těchto výsledků bylo konstatováno, že vzorky přímým slunečním zářením osvětlených jehlic jedné věkové kategorie, odebrané nahodile z kterékoliv větve dvou

zkoumaných funkčních částí korun smrku ztepilého, jsou reprezentativní pro obě tyto části, ale opticky se liší v závislosti na tom, zda pochází z koruny stromu stresu rezistentního či stresu resilientního.

Optické vlastnosti jehlic byly *up-scaling* metodou převedeny na úroveň smrkových korun celého porostu pomocí trojrozměrného diskretního anisotropického modelu radiativního transferu DART (Discrete Anisotropic Radiative Transfer). Před vlastní aplikací byl DART model podroben analýze vlivu nově navržených dřevních částí lesního porostu na intenzitu dvousměrného faktoru odrazivosti BRF (Bidirectional Reflectance Factor), simulovaného pro *nadir* pozici ve velmi vysokém prostorovém rozlišení 0,4 m. Analýza senzitivity byla provedena odděleně pro osluněné a zastíněné části modelovaného lesního porostu. Její výsledky byly porovnány se skutečným BRF hodnotami naměřenými ve stejném prostorovém rozlišení nad simulovaným porostem leteckým obrazovým senzorem AISA. Z výsledků vyplynulo, že *nadir* BRF je shodný jak pro koruny smrků ztepilého modelované čistě jako shluky listů, tak pro koruny modelované jako kombinace listů a robustních dřevních částí (tj. kmenů a větví prvního řádu rostoucích přímo z kmenů stromů). Po rozšíření simulací o scénář zahrnující také jemné dřevní části korun stromů (drobné větvičky) se snížila jejich simulovaná *nadir* odrazivost v blízké infračervené části spektra přibližně o 4%, na okraji červené části o 2% a v zelených vlnových délkách o méně než 1%. Tyto výsledky upozornily na důležitost modelace jemných dřevních částí lesních porostů při odhadech jejich kvantitativních parametrů inverzí modelů radiativního transferu z obrazových dat velmi vysokého prostorového rozlišení, obzvláště pak v případech kdy jsou využívány vlnové délky blízké infračervené části spektra.

Kombinace dvou modelů radiativního transferu PROSPECT a DART byla použita k vývoji a ověření stability optického indexu pro odhad koncentrace chlorofylů korun stromů vysoce heterogenních jehličnatých porostů. Nový index, pojmenovaný „plocha pod křivkou odrazivosti normalizovaná maximální hloubkou spektrálního pásma mezi 650-725 nm“ (Area under curve Normalized to Maximal Band depth between 650-725nm – ANMB<sub>650-725</sub>), byl navržen na základě vyjmutí a transformace kontinua specifické části křivky odrazivosti. Tento postup využívá jemného spektrálního rozlišení a vysoké frekvence spektrálních pásem hyperspektrálních obrazových dat k izolaci odrazivosti vegetace v intervalu vysoké absorpce slunečního záření chlorofyly mezi 650 a 725 nm. Výsledky získané ze simulovaných hyperspektrálních dat o velikosti strany obrazového prvku 0,9 m prokázaly silnou lineární regresi indexu ANMB<sub>650-725</sub> na koncentraci chlorofylů korun smrků ( $r^2 = 0,9798$ ), a jeho nízkou senzitivitu vůči měnícím se strukturálním charakteristikám korun, tj. proměnlivému indexu listové plochy a korunovému zápoji. Odhad koncentrace chlorofylů pomocí ANMB<sub>650-725</sub> indexu zůstal stabilní i po zavedení rušivého spektrálního účinku epifytického lišejníku *Pseudevernia* sp. a zvýšení šumu senzoru (poměr signálu ku šumu senzoru roven pěti).

Výsledky práce demonstrovaly úspěšnou aplikaci *up-scaling* metody převodu spektrální informace listů (jehlic) na úroveň korun stromů a následně lesních porostů horských smrkových ekosystémů. Byla prokázána účinnost fyzikálně založených kvantitativních přístupů a jejich schopnost přispět k dalšímu rozvoji modelů radiativního transferu. V blízké budoucnosti budeme svědky realizace několika nových satelitních optických systémů Země (hyper- či super-spektrální povahy), kde může prezentovaná *up-scaling* metoda významně přispět ke zvýšení přesnosti odhadů parametrů vegetace. Integrace těchto satelitních produktů do programu monitoringu stavu lesních ekosystémů, zabývajícího se též predikcí jejich vývoje (např. program Globálního monitoringu životního prostředí a bezpečnosti – Global Monitoring for Environment and Security (GMES)), je logickým pokračováním této práce.

---

## Table of contents

---

Forest of acknowledgement.....	i
Abstract.....	iii
Samenvatting.....	v
Abstrakt.....	vii
Table of contents .....	ix
List of figures.....	xiii
List of tables.....	xix
List of acronyms.....	xxi
List of symbols.....	xxv
Sub- and superscripts.....	xxvi
CHAPTER 1 General introduction.....	1
1.1 Quantitative remote sensing of ecosystems .....	2
1.1.1 Parameterization and validation of land-biosphere models .....	3
1.1.2 Monitoring environmentally stressed vegetation .....	4
1.2 Background .....	4
1.2.1 Motivation .....	4
1.2.2 Objectives and research questions.....	6
1.2.3 Structure .....	7
1.3 References .....	8
CHAPTER 2 Scaling in spectroscopy using physically based radiative transfer modelling .....	11
2.1 Introduction .....	13
2.1.1 Scale definitions and parameters in imaging spectroscopy.....	13
2.1.2 Scaling up and down in spectroscopy .....	16
2.2 Types of radiative transfer models.....	17
2.3 Scaling by radiative transfer modelling .....	19
2.3.1 Scaling of the optical properties.....	19
2.3.2 Up-scaling and testing vegetation optical indices .....	20
2.4 Discussion on scaling by means of radiative transfer models.....	22
2.5 References .....	23
CHAPTER 3 Applicability of the PROSPECT model for Norway spruce needles.....	29
3.1 Introduction .....	31
3.2 Material and Methods.....	33
3.2.1 Study site and sampling set-up.....	33
3.2.2 Laboratory measurement of the foliar pigments .....	35

3.2.3	Measurement protocol of the optical and biophysical properties of spruce needles .....	36
3.2.4	Set-up of methodology for PROSPECT applicability analyses .....	37
3.2.5	Verification of PROSPECT for Norway spruce needles .....	37
3.2.6	Stratified recalibration of PROSPECT specific absorption coefficients .....	39
3.2.7	Validation of updated PROSPECT .....	40
3.3	Results .....	41
3.3.1	Retrieved values of the N parameter and PROSPECT suitability validation .....	41
3.3.2	Adjusted specific absorption coefficients and new N parameters .....	42
3.3.3	Forward validation of the recalibrated PROSPECT model .....	43
3.3.4	Multiple retrieval of the PROSPECT inputs .....	45
3.4	Discussion .....	47
3.5	Conclusions .....	52
3.6	Acknowledgements .....	53
3.7	References .....	54
CHAPTER 4	Differences in leaf optical properties of environmentally stressed Norway spruce ( <i>Picea abies</i> (L.) Karst.) crowns .....	59
4.1	Introduction .....	61
4.2	Materials and methods .....	63
4.2.1	Study site and sampling set-up .....	63
4.2.2	Laboratory determination of the foliar pigments .....	63
4.2.3	Analysis of the needle anatomy .....	63
4.2.4	Measurement of the spruce needles optical and biophysical properties .....	64
4.2.5	Methods of needle optical properties assessment .....	64
4.2.6	Statistical tests .....	65
4.3	Results .....	65
4.3.1	Differences in biochemical and anatomical parameters of the needle categories .....	65
4.3.2	Differences in optical properties of spruce needles and statistical relations to biochemical and biophysical parameters .....	68
4.3.3	Spectral differences and relationships with anatomical features of C+2 needles .....	72
4.4	Discussion .....	73
4.4.1	Understanding the quantitative differences in optical properties of needle categories .....	73
4.4.2	Interpretation of the qualitative differences in relation to the needle properties and processes .....	75
4.5	Conclusions .....	75
4.6	Acknowledgements .....	76
4.7	References .....	76



CHAPTER 5	Influence of woody elements of a Norway spruce canopy on nadir reflectance simulated by the DART model at very high spatial resolution .....	79
5.1	Introduction .....	81
5.2	Material and Methods.....	82
5.2.1	Test site .....	82
5.2.2	Methodological concept .....	83
5.2.3	The DART model.....	83
5.2.4	Parameterization of the spruce forest stand in the DART model.....	85
5.2.5	DART modelled images.....	90
5.2.6	AISA Eagle airborne image data.....	91
5.2.7	Comparison of DART and AISA Eagle BRF's .....	92
5.2.8	NDVI and AVI vegetation indices .....	93
5.3	Results .....	93
5.3.1	Effect of non-photosynthetic woody elements on nadir spruce canopy BRF.....	93
5.3.2	Validation of the DART scenarios against the AISA BRF measurements.....	97
5.3.3	Relation of vegetation indices with LAI at high spatial resolution.....	99
5.4	Discussion .....	100
5.4.1	Influence of the woody elements on simulated reflectance .....	100
5.4.2	Reliability of the DART simulations .....	103
5.4.3	Consequences on LAI retrieval and vegetation indices .....	103
5.5	Conclusions .....	104
5.6	Acknowledgements .....	105
5.7	References .....	105
CHAPTER 6	A new hyperspectral index for chlorophyll estimation of a forest canopy: Area under curve Normalized to Maximal Band depth between 650-725 nm .....	111
6.1	Introduction .....	113
6.2	Methods.....	114
6.2.1	Design of the ANMB <sub>650-725</sub> index.....	114
6.2.2	Radiative transfer models.....	115
6.2.3	Parameterization of the RT models and generation of the BRF database .....	116
6.2.4	ANMB <sub>650-725</sub> validation and sensitivity analysis .....	118
6.3	Results .....	120
6.4	Conclusions .....	121
6.5	Acknowledgements .....	124
6.6	References .....	124
CHAPTER 7	Synthesis.....	127
7.1	Conclusions on spectroscopy of Norway spruce canopies.....	128
7.2	Recent advances in the retrieval of biochemical and -physical properties in Norway spruce canopies .....	130

---

7.2.1	Mapping the chlorophyll concentration of spruce crowns .....	130
7.2.2	Spatial estimation of forest stand leaf area index.....	132
7.2.3	Scaling up to coarser spatial resolution of satellite data .....	132
7.3	General synopsis and outlook .....	133
7.4	References .....	134
	PE&RC PhD Education Statement Form .....	137
	Curriculum Vitae .....	138
	List of publications .....	139

## List of figures

---

Figure 2.1: Spectral resolution ('full-width-half-maximum' – FWHM), extent ( $\lambda_{\max} - \lambda_{\min}$ ) and sampling interval of imaging spectroscopy data.....	14
Figure 2.2: Graph of a vegetation canopy reflectance in the principal plane with the highest intensity at the hotspot ( $\rho_{HS}$ ) and the lowest intensity at the darkspot ( $\rho_{DS}$ ) viewing direction. ....	21
Figure 3.1. General location of the study area at the Šumava Mts., Czech Republic (close to the Modrava village). ....	33
Figure 3.2. A universal carrier of conifer needles used for measurement of the directional hemispherical optical properties in a LI-COR integrating sphere LI-1800-12: a/ technical layout; b/ sample needles mounted in the universal carrier, placed at the sample port of the integrating sphere LI-1800-12 and illuminated in the reflectance measurement mode. ....	35
Figure 3.3. Flowchart of the basic methodological steps used in the study for verification, recalibration and validation of the original and updated PROSPECT source code (n is the number of the samples within each dataset). ....	38
Figure 3.4. Direct comparison of the PROSPECT simulated and measured average optical properties of the training and testing dataset (solid grey areas represents +/- one standard deviation, RMSE = root mean square error). a), b), and c) show simulations of the original PROSPECT version 3.01 using the sample specific retrieved N values and inputs of the training sample set; d), e), and f) show results of the updated PROSPECT version 3.01.S using the sample specific retrieved N values; g), h), and i) show outputs of the updated PROSPECT version 3.01.S using the universally identified N values (see table 3.3). ....	43
Figure 3.5. Mean root mean square errors (RMSE) for each of the investigated wavelength (450-1000 nm) computed between the reflectance, transmittance, and absorption values of the training dataset samples and values simulated by a) the original PROSPECT version 3.01; b) the recalibrated PROSPECT version 3.01.S. ....	44
Figure 3.6. Comparison of the newly retrieved a) dry matter ( $k_m$ ) and b) chlorophyll ( $k_{ab}$ ) specific absorption coefficients used for the PROSPECT model update per three investigated Norway spruce needle age-classes (n = number of the samples; solid grey represents area of all the standard deviations of newly recalibrated $k_{ab}$ and $k_m$ ). ....	45
Figure 3.7. Comparison of the newly retrieved a) dry matter ( $k_m$ ) and b) chlorophyll ( $k_{ab}$ ) specific absorption coefficients sorted per stress shoot type classes of Norway spruce needles ( $J_{RN}$ = primary stress resistant needle samples of the juvenile crown part, $P_{RN}$ = primary, stress resistant needle samples of the production crown part, $J_{RT}$ = primary, stress resilient needle samples of the juvenile crown part, $P_{RT}$ = primary stress resilient needle samples of the production crown part, $S_{RT}$ = regenerative secondary stress resilient needle samples of the production crown part; n = number of the samples; solid grey represents area of all the standard deviations of newly recalibrated $k_{ab}$ and $k_m$ ). ....	46
Figure 3.8. Relationship of the N structural parameters estimated for the samples of the training dataset (110 samples) by inversion of the original and the recalibrated PROSPECT model (solid line represents a one-to-one relationship, $R^2$ = coefficient of determination, RMSE = root mean square error). ....	47

Figure 3.9. Mean root mean square errors (RMSE) for each of the investigated wavelength computed between the reflectance, transmittance, and absorption measurements of the independent testing dataset (48 samples) and the updated PROSPECT simulations using: a) the N numbers retrieved for each testing sample; and b) the ‘universal’ N values generated for each stress category from the training dataset samples (see table 3.3). .....	48
Figure 3.10. Results of the partially unconstrained inversion of the original (graphs in left column) and recalibrated (graphs in right column) PROSPECT, retrieving concurrently all the model inputs ( $C_{ab}$ , $C_m$ , $C_w$ , and N) using 48 samples of the testing dataset. The merit function was based on the spectral information and expert knowledge on the variability limits of the retrieved parameters (see equation 3.6), (RMSE = root mean square error between measured and simulated values; solid line represents a one-to-one relationship function; N from single retrieval = structural parameters retrieved only for the purpose of direct PROSPECT simulations, N from multiple retrieval = structural parameters retrieved together with all other PROSPECT inputs for a verification purpose).....	50
Figure 3.11. Results of the constrained inversion of the original (graphs in left column) and recalibrated (graphs in right column) PROSPECT retrieving concurrently all the model inputs ( $C_{ab}$ , $C_m$ , $C_w$ , and N) using 48 samples of the testing dataset. The merit function was not based only on the spectral information, but it was constrained by measured ‘a priori’ knowledge on targeting values and variability limits of the retrieved parameters (see equation 3.7), (RMSE = root mean square error between measured and simulated values; solid line represents a one-to-one relationship function; N from single retrieval = structural parameters retrieved only for the purpose of direct PROSPECT simulations, N from multiple retrieval = structural parameters retrieved together with all other PROSPECT inputs for a verification purpose). .....	51
Figure 4.1. Results of the one-way ANOVA analysis for (a) the concentrations of the measured needle biochemical compounds ( $C_{ab}$ – concentration of the chlorophylls a+b, $C_{xc}$ – concentration of the total carotenoids, $C_m$ – dry matter content) and (b) the mean volumes of the whole needles and basic needle internal structures for selected three years old samples (10 samples per category). Bar represents one standard error. Columns with different superscripts represent a statistically significant difference between the categories ( $P = 0.05$ ). Values in parenthesis represent the volume ratio of the mesophyll, dermal and central cylinder tissue against the intercellular air spaces. ....	66
Figure 4.2. The average measured optical properties of the needle categories in (a) green, (b) red, (c) red edge (RE) and (d) near infrared (NIR) part of the electromagnetic spectrum. For description of needle categories: $J_{RN}$ , $J_{RT}$ , $P_{RN}$ , $P_{RT}$ and $S_{RT}$ see legend of figure 4.1.....	67
Figure 4.3. Statistical one-way ANOVA differences of the integrated areas under the (a) reflectance, (b) transmittance and (c) absorption curve of the green (505-600 nm), red (600-685 nm), red edge (RE, 685-760 nm) and near infrared (NIR, 760-800 nm) spectral intervals. Bar represents one standard error. Columns with different superscripts represent a statistically significant difference between the categories ( $P = 0.1$ ). For needle categories see legend of figure 4.1.....	69
Figure 5.1. Location of the experimental research site Bily Kriz at the Moravian-Silesian Beskydy Mountains (East border between Czech Republic and Slovakia). .....	83
Figure 5.2 Flowchart of the methodological approach (scenario F – only foliage elements were simulated; scenario FW – the foliage elements together with trunk and first order branches were simulated; scenario FWT – foliage elements with trunk and first order	

branches plus small twigs were simulated; CC = canopy closure, LAI = leaf area index, NDVI = normalised difference vegetation index, AVI = angular vegetation index, BRF = bidirectional reflectance factor).....	84
Figure 5.3 a) Vertical projection of the DART Norway spruce stand representation with canopy closure of 60% (four representative trees); b) DART output – greyscale image of three spectral band composition (NIR, red, and green band; white = sunlit background, light grey = sunlit crowns, dark grey = shaded crowns, black = deeply shaded crowns and background).....	87
Figure 5.4. Measured optical properties (hemispherical-directional reflectance and transmittance) of the surfaces used to parameterize the DART simulations: a) ranges of the Norway spruce needle optical properties defined from base to top of the crown, b) optical properties of woody elements (bark of stem, branches and twigs) and background (litter and bare soil).....	89
Figure 5.5. Six ortho-rectified flight lines acquired by the airborne AISA Eagle imaging spectroradiometer in a multi-directional pattern with the pixel size of 0.4 m over the permanent experimental research site Bily Kriz (Beskydy Mts., Czech Republic; 18.54°E, 49.50°N, altitude 936 m above sea level; greyscale image of NIR, red, and green band composition).....	90
Figure 5.6. BRF validation matrices, used also for the measurement of the forest stand leaf area index (LAI), plotted over the grey-scale AISA Eagle band (738 nm). M1-M12 stands for centres of 12 validation matrices of 3x3 points (10x10 m; one circle represents one sampling point).....	92
Figure 5.7. Relation of DART nadir bidirectional reflectance factor (BRF) and LAI simulated at 559, 671, 727, and 783 nm within the Norway spruce canopy composed of i) only foliage (scenario F: a-d), ii) leaves and major woody parts (scenario FW: e-h), and iii) leaves, trunks, branches of first order, and twigs smaller than one cm in diameter (scenario FWT: i-l). Light grey dashed lines represent BRF of sunlit crown pixels of 10 canopy closures (CC = 50-95% with step of 5%), black dotted lines represent BRF of shaded crown pixels of 10 canopy closures, and dark grey full lines represents BRF of 10 canopy closures of the whole spruce crowns.....	95
Figure 5.8. Detailed relationship of the canopy leaf area index (LAI) and the bidirectional reflectance factor (BRF) of the sunlit and shaded crown parts at 783 nm simulated by the DART model for five different canopy closures (CC = 55, 65, 75, 85, and 95%) for each of the three scenarios: i) scenario F – only foliage (a, b), ii) scenario FW – leaves and major woody parts (c, d), and iii) scenario FWT – leaves, trunks, main branches, and small twigs (e, f).....	96
Figure 5.9. Validation of the AISA Eagle image radiometric and atmospheric corrections by comparison with ground measured ASD reflectance of three natural surfaces (50 scans per spot, three spots per surface): clay cover (tennis court – a, b), gravel cover (forest road – c, d), and homogeneous vegetation cover (grassland – e, f). The upper graphs show the reflectance signatures of both instruments, the lower graphs represent the relationship between the ground measured reflectances (HDRF) and the image-derived reflectances in the spectral range of 450-800 nm (RMSE = root mean square error).....	98
Figure 5.10. Direct comparison of the AISA Eagle bidirectional reflectance factor (BRF) obtained from 12 sample areas (10x10 m) and corresponding DART simulated BRF for comparable fraction of sunlit and shaded crown parts, as well as whole spruce canopy for three scenarios: i) scenario F – only foliage (a, b, c), ii) scenario FW – leaves and	

major woody parts (d, e, f), and iii) scenario FWT – leaves, trunks, main branches, and small twigs (g, h, i) (RMSE = root mean square error).....	99
Figure 5.11. Relationship between spruce canopy leaf area index (LAI) and normalised difference vegetation index (NDVI) displayed for sunlit, shaded, and total canopy reflectance simulated by the DART model within three scenarios: i) scenario F – only foliage (a, b, c), ii) scenario FW – leaves and major woody parts (d, e, f), and iii) scenario FWT – leaves, trunks, main branches, and small twigs (g, h, i). Each line represents one of ten simulated canopy closure categories (CC = 50, 55, 60, 65, 70, 75, 80, 85, 90, and 95%).....	101
Figure 5.12. Relationship between spruce canopy leaf area index (LAI) and angular vegetation index (AVI) plotted for sunlit, shaded, and total canopy reflectance simulated by the DART model within three scenarios: i) scenario F – only foliage (a, b, c), ii) scenario FW – leaves and major woody parts (d, e, f), and iii) scenario FWT – leaves, trunks, main branches, and small twigs (g, h, i). Each line represents one of ten simulated canopy closure categories (CC = 50, 55, 60, 65, 70, 75, 80, 85, 90, and 95%).....	102
Figure 6.1. Description of continuum removal and band depth calculation to generate the ANMB <sub>650-725</sub> index from sunlit vegetation spectral signatures of a “green” (high C <sub>ab</sub> ), “yellow” (very low C <sub>ab</sub> ), and “brown” (dead tree without C <sub>ab</sub> ) coloured crown of a deciduous tree extracted from an AISA Eagle atmospherically corrected hyperspectral image: a) delineation of the reflectance feature at the chlorophyll absorption between 650 and 725 nm; b) maximal band depth (MBD <sub>650-725</sub> ) and area under reflectance continuum-removed curve (AUC <sub>650-725</sub> ).....	115
Figure 6.2. Flowchart illustrating the creation of the BRF database used to develop the ANMB <sub>650-725</sub> index, and to establish its statistical relationship with chlorophyll content.....	116
Figure 6.3. Map of one research plot at the Sumava Mts. National Park (Czech Republic) used in DART to generate hyperspectral images for accuracy assessment of the ANMB <sub>650-725</sub> index.....	122
Figure 6.4. A false colour RGB composition of DART simulated nadir AISA bands (R = 800, G = 552 and B = 681 nm) for the research plot depicted in figure 6.3. ....	122
Figure 6.5. Relationship of the optical parameters and canopy chlorophyll concentration computed from the BRF database: a) Integrated area under continuum-removed reflectance between 650-725 nm (AUC <sub>650-725</sub> ); b) Maximal band depth of continuum-removed reflectance between 650-725 nm (MBD <sub>650-725</sub> ). ....	123
Figure 6.6. Statistical relationships between chlorophyll concentration and chlorophyll optical indices generated from the BRF database: a) Linear regression of canopy C <sub>ab</sub> concentration on the area under curve normalised to maximal band depth between 650-725 nm (ANMB <sub>650-725</sub> ); b) Logarithmic statistical relationship of C <sub>ab</sub> concentration and the optical indices ratio TCARI/OSAVI.....	123
Figure 6.7. One-to-one relationship and linear regression of chlorophyll concentration measured for 13 sample spruce crowns and estimated by the optical index: a) ANMB <sub>650-725</sub> ; b) TCARI/OSAVI.....	123
Figure 7.1. Chlorophyll concentration map of a sunlit Norway spruce canopy located around the experimental research site Bily Kriz at the Moravian-Silesian Beskydy Mts. (Czech Republic). The map was generated using four AISA spectral bands selected to compute the ANMB <sub>650-725</sub> chlorophyll index (see text for details, C <sub>ab</sub> represents the concentration	

---

of chlorophyll  $a+b$ ; the map projection is set to Universal Transverse Mercator, zone 34N). ..... 128

Figure 7.2. Accuracy assessment of the chlorophyll  $a+b$  concentrations ( $C_{ab}$ ) measured in the laboratory and estimated from the AISA image for ten spruce crowns using the ANMB<sub>650-725</sub> computed from: a) four spectral bands, and b) nine spectral bands. Each circle represents a tree crown, full circles are crowns used for validation, and the empty circle is an outlier which was excluded from the validation process (horizontal bars represent two standard deviations in  $C_{ab}$  measured within the vertical crown levels; vertical bars represent two standard deviations of  $C_{ab}$  estimation within sunlit AISA pixels;  $r^2$  is coefficient of determination for a linear regression  $y = a x$ ; RMSE is root means square error computed between measured and estimated  $C_{ab}$ ). ..... 131





## List of tables

---

Table 2.1: Parameters of the four-dimensional scale concept for spectroscopic data (FWHM = ‘full-width-half-maximum’, IFOV = ‘instantaneous-field-of-view’). .....	13
Table 3.1. Sampling scheme applied on the selected Norway spruce trees and the average properties per homogeneous unit (values in parentheses are standard deviations). .....	34
Table 3.2. Boundary values for the biochemical and structural variables retrieved by means of the original and recalibrated PROSPECT inversions, using the $M_j^{\text{spectral}}$ and $M_j^{\text{prior}}$ retrieval functions. ....	41
Table 3.3. The values of the structural parameter N retrieved from optical properties of the training dataset by inversion of the original and recalibrated PROSPECT model. The universally identified (rounded) N values and statistically different categories (one-way ANOVA test; $\alpha$ -level of significance = 0.005) are presented.....	42
Table 4.1. The coefficients of determination ( $r^2$ ) for linear regressions between needle hemispherical optical properties (reflectance, transmittance, and absorption) per wavelength and biochemical needle characteristics.....	70
Table 4.2. Result of the one-way ANOVA combined with the Tukey-Kramer and Kuskal-Wallis test appointing statistically significant differences among continuum removed (CR) hemispherical optical properties between 505-800 nm: (a) reflectance, (b) transmittance, and (c) absorption. ....	71
Table 4.3. The coefficients of determination ( $r^2$ ) for linear regressions between continuum removed (CR) values of the reflectance, transmittance, and absorption per wavelength and biochemical needle properties. ....	72
Table 4.4. Pearson correlation coefficients (R) and coefficients of determination ( $r^2$ ) for linear regressions between continuum removed (CR) values of the reflectance and transmittance per wavelength and biochemical and anatomical properties of 30 selected three years old needle samples.....	74
Table 5.1 Description of the three DART modelled scenarios. ....	85
Table 5.2. Input parameters for the DART scenes used to generate multispectral images for all three study scenarios. ....	86
Table 5.3. Measured parameters of the trees modelled in DART for simulation of all three study scenarios. Values in parenthesis stand for standard deviation (STDEV). ....	88
Table 5.4. Root mean square errors (RMSE) computed for BRF of four spectral bands of the experimental spruce canopy obtained from 12 matrices (10 x 10 m) placed over the AISA Eagle image and corresponding DART simulated BRF for all three considered scenarios.....	97
Table 6.1. Basic inputs acquired for the radiative transfer simulation of the Norway spruce stands of Sumava Mts. in Czech Republic.....	117
Table 6.2. Universal tree characteristics used for building the BRF database. ....	117
Table 6.3. Spectral description of simulated AISA bands.....	118
Table 6.4. Biophysical and biochemical properties of 13 sample spruce crowns simulated in DART for the sensitivity analyses of ANMB <sub>650-725</sub> .....	119



## List of acronyms

<i>Acronym</i>	<i>Meaning</i>
1D	One-dimensional
3D	Three-dimensional
AISA	Airborne Imaging Spectroradiometer
ALA	Average Leaf Angle
ANMB <sub>650-725</sub>	Area under curve Normalized to Maximal Band depth between 650-725 nm (index)
ANOVA	ANalysis Of VAriance
ASCII	American Standard Code for Information Interchange
ATA	Average Twig Angle
ATCOR-4	Atmospheric / Topographic CORrection for airborne imagery, v.4
AUC	Area Under Curve
AUC <sub>650-725</sub>	Area Under the continuum-removed reflectance Curve between 650-725 nm
AVI	Angular Vegetation Index
BNA	Band depth normalised to an area of an absorption feature
BNC	Band depth normalised to a wavelength at a centre of an absorption feature
BRDF	Bidirectional Reflectance Distribution Function
BRF	Bidirectional Reflectance Factor
BTDF	Bidirectional Transmission Distribution Function
C	Current year needles
C+1	Two growing periods old needles
C+2	Three growing periods old needles
C <sub>ab</sub>	Chlorophyll a+b concentration
CC	Canopy Closure
CCD	Charged Coupled Device
CESBIO	Centre d'Etudes Spatiales de la BIOSphere
CHRIS	Compact High Resolution Imaging Spectrometer
CNES	Centre National d'Etudes Spatiales
CO <sub>2</sub>	Carbon dioxide
CR	Continuum Removal
DART	Discrete Anisotropic Radiative Transfer (model)
DBH	Diameter at Breast Height
DEM	Digital Elevation Model
DGPS	Differential Global Positioning System
DLR	Deutsches Zentrum für Luft- und Raumfahrt
DMF	Dimethylformamide
DMI	DART Modelled Images
EM	ElectroMagnetic spectrum
EnMAP	Hyperspectral sensor for Environmental Mapping and Analysis
ENVISAT	ENVironmental SATellite, ESA
EO-1	Earth Observer-1
EOS	Earth Observing System (NASA programme)
EOS AM	Earth Observing System Terra platform

<i>Acronym</i>	<i>Meaning</i>
EOS PM	Earth Observing System Aqua platform
ESA	European Space Agency
F	"Foliage" scenario
fAPAR	Fraction of Absorbed Photosynthetically Active Radiation
FLIGHT	Forest LIGHT interaction model
FluorMOD	Integrated vegetation fluorescence leaf-canopy model
FLUXNET	Flux (global) network
FOV	Field Of View
FW	"Foliage + robust Woody parts" scenario
FWHM	Full Width at Half the Maximum
FWT	"Foliage + robust Woody parts + tiny Twigs" scenario
GENACS	GMES Europeanwide Network Assistance and Coordination Support
GF	Gap Fraction
GF <sub>R</sub>	Gap Fraction in Reflectance mode
GF <sub>T</sub>	Gap Fraction in Transmittance mode
GHOST	G-function and HOt SpoT reflectance model
GIS	Geographic Information System
GMES	Global Monitoring for Environment and Security
GMT	Greenwich Mean Time
GPS	Global Positioning System
HDRF	Hemispherical-Directional Reflectance Factor
HDS	Hot-Dark Spot (index)
IDL	Interactive Data Language
IFER	Institute of Forest Ecosystem Research
IFOV	Instantaneous Field Of View
IMU	Inertial Measurement Unit
INFORM	INvertible FOrest Reflectance Model
J_RN	Primary needles from the stress resistant juvenile crown part (chapter 4)
J_RT	Primary needles from the stress resilient juvenile crown part (chapter 4)
J <sub>RN</sub>	Primary, stress resistant needle samples of the juvenile crown part (chapter 3)
J <sub>RT</sub>	Primary, stress resilient needle samples of the juvenile crown part (chapter 3)
KM	Kubelka-Munk (theory)
LAD	Leaf Angle Distribution
LAI	Leaf Area Index
LANDSAT 7 ETM+	Land remote sensing satellite Enhanced Thematic Mapper Plus
LIBERTY	Leaf Incorporating Biochemistry Exhibiting Reflectance and Transmittance Yields (model)
MBD <sub>650-725</sub>	Maximal Band Depth of the continuum-removed reflectance curve between 650-725 nm
MC	Monte Carlo (ray tracing method)
MCARI	Modified Chlorophyll Absorption in Reflectance Index

<i>Acronym</i>	<i>Meaning</i>
MERIS	MEDium Resolution Imaging Spectrometer
MISR	Multiangle Imaging SpectroRadiometer
MLH	Maximum LikeliHood (classification)
MODIS	MOderate Resolution Imaging Spectroradiometer
NASA	National Aeronautics and Space Administration
NDHD	Normalized Difference between Hotspot and Darkspot (index)
NDVI	Normalized Difference Vegetation Index
NIR	Near Infra-Red (part of the electromagnetic spectrum)
NPP	Net Primary Productivity
OSAVI	Optimized Soil-Adjusted Vegetation Index
P_RN	Primary needles from the stress resistant production crown part (chapter 4)
P_RT	Primary needles from the stress resilient production crown part (chapter 4)
PARAS	Semi-physical forest reflectance model
PCA	Plant Canopy Analyzer
POLDER	POLarization and Directionality of the Earth Reflectances (instrument)
P <sub>RN</sub>	Primary, stress resistant needle samples of the production crown part (chapter 3)
P <sub>RT</sub>	Primary, stress resilient needle samples of the production crown part (chapter 3)
PROBA	PRoject for On Board Autonomy (space platform)
PROSPECT	Leaf optical PROPERTIES SPECTra model
R mode	Reflective mode
RAMI	RAdiation Model Intercomparison (exercise)
RAYTRAN	Ray tracing model to compute light scattering in 3-D heterogeneous media
RE	Red Edge
REF	(Flux of) radiation reflected from reference standard
REIP	Red-Edge Inflection Point
RGB	Red Green Blue (colour composition)
RMSE	Root Mean Square Error
RN	Stress resistant tree
RS	Remote Sensing
RT	Radiative Transfer (chapters 1, 2, 4 – 7)
RT	Stress resilient tree (chapter 3)
S_RT	Secondary needles from the stress resilient production crown part (chapter 4)
SAIL	(Light) Scattering by Arbitrary Inclined Leaves (model)
SAILH	Scattering by Arbitrarily Inclined Leaves, with implemented Hot spot (model)
Sentinel-2	Superspectral imaging mission for terrestrial applications
SNR	Signal to Noise Ratio
SO <sub>2</sub>	Sulphur dioxide
SPOT 5 HRG	Systeme pour l'Observation de la Terre satellite with High Resolution Geometric instruments
STR	(Flux of) Stray Light Radiation
S <sub>RT</sub>	Secondary (regenerative), stress resilient needle samples of the production crown part (chapter 3)
SURS	Systematic Uniform Random Sampling
T mode	Thermal mode

---

<i>Acronym</i>	<i>Meaning</i>
TAD	Twig Angle Distribution
TAI	Twig Area Index
TCARI	Transformed Chlorophyll Absorption in Reflectance Index
TOA	Top Of Atmosphere
TOC	Top Of Canopy
UTM	Universal Transverse Mercator (geographic projection)
Ven $\mu$ s	Vegetation and Environment monitoring on a New Micro Satellite
VIS	Visible (part of the electromagnetic spectrum)
VIS/NIR	Visible and Near Infra-Red (part of the electromagnetic spectrum)
VNIR	Visible and Near Infra-Red (part of the electromagnetic spectrum)

---

## List of symbols

<i>Symbol</i>	<i>Meaning</i>	<i>Unit</i>
$a$	$a$ parameter of horizontal hole distribution	relative
$b$	$b$ parameter of horizontal hole distribution	relative
$C_{ab}$	Chlorophyll (a+b) concentration	$\mu\text{g cm}^{-2}$
$C_m$	Dry matter concentration	$\text{g cm}^{-2}$
$C_w$	Thickness of water inside of needles (water depth)	cm
$C_{xc}$	Concentration of total carotenoids	$\mu\text{g cm}^{-2}$
$E_s$	Incident solar irradiance	$\text{Wm}^{-2}$
$f(\lambda_i^*)$	Mean height $h$ of the spectral signature at two successive wavelengths ( $\lambda_i$ and $\lambda_{i-1}$ )	relative
$k_0(\lambda)$	Spectral absorption coefficient of a fresh leaf (for a given wavelength)	
$k_{ab}(\lambda)$	Chlorophyll specific absorption coefficient (for a given wavelength)	$\text{cm}^2 \mu\text{g}^{-1}$
$k_e(\lambda)$	Coefficient of non-zero absorption of an albino leaf up to a wavelength of 480 nm	
$k_m(\lambda)$	Dry matter specific absorption coefficient (for a given wavelength)	$\text{cm}^2 \text{g}^{-1}$
$k_w(\lambda),$	Water specific absorption coefficient (for a given wavelength)	$\text{cm}^{-1}$
$l$	Vertical crown level	
$L_v$	Reflected radiance	$\text{Wm}^{-2}\text{sr}^{-1}$
$M_j^{\text{spectral}}$	Merit function based on spectral information of the samples	
$M_j^{\text{prior}}$	Merit function based on spectral and 'a priori' information of the samples	
$n$	Refractive index of material (chapter 3)	
$n$	Number of integrated wavelengths within defined spectral interval (chapter 4)	
$n$	Number of used spectral bands (chapter 6)	
$N$	Structural parameter $N$ of leaf mesophyll layers	
$R$	Earth surface reflectance (chapter 2)	relative
$R$	Pearson correlation coefficient	relative
$r$	Horizontal distance of cell center from a tree trunk	relative
$R(\lambda)$	Corresponding value to a reflectance at the interpolated continuum line (chapter 4)	
$R^2, r^2$	Coefficient of determination	
$R_{\text{TOTAL}}$	(Flux of) radiation reflected from the sample in reflectance mode	$\text{Wm}^{-2}\text{sr}^{-1}$
$t$	Time frequency of the observation	day
$t_{\text{max}} - t_{\text{min}}$	Temporal extent (time interval between the last and the first observation of the same location)	day
$T_{\text{TOTAL}}$	(Flux of) radiation transmitted from the sample in transmittance mode	$\text{Wm}^{-2}\text{sr}^{-1}$
$V_j$	Estimated value of the variable $j$	
$V_j^{\text{prior}}$	Measured prior value of the variable $j$	
$V_j^{\text{max}}, V_j^{\text{min}}$	Maximum and minimum values of the measured variable $j$	
$x,y$	Spatial coordinates	m, km
$\alpha$	Incident angle (chapter 3)	rad, °
$\alpha$	$\alpha$ parameter of horizontal leaf distribution (chapter 5)	relative
$\alpha(\lambda)$	Absorption (for given wavelength)	relative

<i>Symbol</i>	<i>Meaning</i>	<i>Unit</i>
$\beta$	$\beta$ parameter of horizontal leaf distribution	relative
$\gamma$	$\gamma$ parameter of horizontal leaf distribution	relative
$\varepsilon$	Surface emissivity	relative
$\theta$	Transmission coefficient of the plate	
$\kappa$	$\kappa$ parameter of horizontal leaf distribution	relative
$\lambda$	Spectral wavelength	$\mu\text{m}$ , nm
$\lambda_{max} - \lambda_{min}$	Spectral extent (range); difference between the minimum and maximum wavelength in which measurements are made	$\mu\text{m}$ , nm
$\mu_f$	Leaf volume density	$\text{m}^2 \text{m}^{-3}$
$\mu_t$	Twig volume density	$\text{m}^2 \text{m}^{-3}$
$\theta_r, \phi_r$	Surface reflection direction (chapter 5)	rad, $^\circ$
$\theta_s, \phi_s$	Sun zenith and azimuth angle	rad, $^\circ$
$\theta_v, \phi_v$	Viewing zenith and azimuth angle	rad, $^\circ$
$\rho_{DS}$	Reflectance at the darkspot	relative
$\rho_{green}$	Reflectance at green part of the electromagnetic spectrum	relative
$\rho_{HS}$	Reflectance at the hotspot	relative
$\rho_j, \rho_{j+1}$	Value of continuum removed reflectance at the $j$ and $j+1$ bands	relative
$\rho_{NIR}$	Reflectance at near infra-red part of the electromagnetic spectrum	relative
$\rho_{red}$	Reflectance at red part of the electromagnetic spectrum	relative
$\rho(\lambda)$	Reflectance (for given wavelength)	relative
$\sigma_f$	Signal standard deviation of real recorded image	$\text{Wm}^{-2}\text{sr}^{-1}$
$\sigma_n$	Signal standard deviation of zero-mean noise image	$\text{Wm}^{-2}\text{sr}^{-1}$
$\tau(\lambda)$	Transmittance (for given wavelength)	relative
$\phi$	Relative azimuth angle (difference of the viewing and illumination azimuth angle)	rad, $^\circ$
$\Omega_v, \Omega_s$	Angular viewing geometry of the sun-object-sensor system (chapter 2)	rad, $^\circ$
$\Omega_v, \Omega_s$	Viewing and illumination projected solid angle (chapter 2)	sr

### Sub- and superscripts

<i>Symbol</i>	<i>Meaning</i>
ab	Chlorophyll a+b
d	Directional
dh	Directional-hemispherical
hd	Hemispherical-Directional
m	Dry matter
max	Maximum value
min	Minimum value
s	Illumination geometry (sun)
v	Viewing geometry
w	Water
xc	Total carotenoids
$\alpha$	Absorption
$\rho, R, r$	Reflectance
$\tau, T$	Transmittance



---

# CHAPTER 1

## General introduction

## 1.1 Quantitative remote sensing of ecosystems

---

Major key messages coined by the board of the Millennium Ecosystem Assessment (2005) included three noteworthy statements:

- *'Humans have made unprecedented changes to ecosystems in recent decades to meet growing demands for food, fresh water, fiber, and energy.'*
- *'The pressures on ecosystems will increase globally in coming decades unless human attitudes and actions change.'*
- *'Even today's technology and knowledge can reduce considerably the human impact on ecosystems. They are unlikely to be deployed fully, however, until ecosystem services cease to be perceived as free and limitless, and their full value is taken into account.'*

The vegetative part of terrestrial ecosystems is a major component of the biosphere devoted to the primary function of biomass production and it is playing an important role in biochemical cycles as well as surface-atmosphere interactions (e.g., the carbon cycle and carbon sequestration). However, the extent, structure and functioning of the world's ecosystems have changed more rapidly in the twentieth century than at any time in human history. Complementing the above statements, more land was converted to cropland in the 30 years after 1950 than in the 150 years between 1700 and 1850 (Millennium Ecosystem Assessment, 2005a), due to the industrial revolution and technical progress between 1850 and 1950. Human demands and impacts on ecosystem services are unsustainably increasing, especially in countries exploiting their natural resources on the expense of biodiversity and stability of ecosystems. Such a decline of ecosystems is inducing and accelerating changes in the whole biosphere (e.g., global climate change) that consequently results in a negative and potentially irreversible impact on future development of human society. Remote sensing does not represent the solution how to decrease global pressure on ecosystems, but it provides knowledge and operational technologies for spatial and temporal assessment of terrestrial as well as aquatic ecosystems. Optical remote sensing analysis can provide actual information on changes in ecosystem status, as well as produce input parameterization and output validation for modelling approaches forecasting a future development of ecosystems. Global Monitoring for Environment and Security (GMES) (GENACS, 2005), a joint initiative of the European Commission and the European Space Agency, is showing a particular example how remote sensing should make environmental and security-related Earth observing information available to the people and the organisations who need it.

A significant advancement was achieved in remote sensing (i.e., airborne and space-borne) monitoring of the biotic and abiotic quantitative characteristics of Earth's ecosystems during the past few decades. A considerable contribution to this development can be assigned to a relatively young technology for Earth observation named imaging spectroscopy. Spectroscopy is a physical-based approach concerned with the production, transmission, measurement, and interpretation of electromagnetic spectra (Swain & Davis, 1978), and has been existing since the discovery of the dispersion of light in 1704 (Newton, 1704). It is studying light fluxes emitted, reflected or transmitted from solid or liquid materials or from gases as a function of spectral wavelengths. These spectral signals can be measured using non-imaging or imaging

spectroradiometers in the laboratory or field, as well as from airborne or satellite platforms. Imaging spectroscopy (Gamon et al., 2004) is an imaging technique able to record a distinct portion of the electromagnetic spectrum for each pixel (Meer & Jong, 2001). It is an indispensable part of passive optical remote sensing and has also been named imaging spectrometry, hyperspectral remote sensing, or ultraspectral imaging (Kumar et al., 2001). The introduction of imaging spectroscopy in the mid-1980s brought a new and expanded perception of the term *scale* in remote sensing, mainly in the spectral domain. Imaging spectrometer data, in contrast to multispectral data, contain a high number of narrow spectral bands. Moreover, imaging spectrometers have lately also been acquiring multi-angular data, i.e. images from oblique viewing angles (e.g., the Compact High Resolution Imaging Spectrometer (CHRIS) on board of the PROBA (PRoject for On-Board Autonomy) platform (Barnsley et al., 2004; Guanter et al., 2005)).

Newly designed modern optical spectroradiometers offer unprecedented measurement precision and very good calibration accuracy. The broader availability of more accurate spectroscopic data fostered the development of physically based algorithms, being developed in remote sensing of vegetation since the late 1980s and early 1990s on the basis of the radiative transfer (RT) theory (Asrar, 1989; Fukshansky et al., 1993; Combal et al., 2003). Quantitative statistical approaches (Curran et al., 2001; Schlerf & Atzberger, 2006), based mostly on correlation relations between vegetated surface variables and their spectral response recorded by a remote sensing sensor, are simple and fast (swiftly developed), but usually site-specific and unable to explain a causality behind the statistical relationship. Nowadays, more frequently used physically based quantitative approaches (Kimes & Kirchner, 1982; Knyazikhin et al., 1998; Lyapustin & Wang, 2005) are built on mathematical equations describing the cause-effect relationship of vegetation-photon interactions. They are more universal and flexible (clear improvement path, can be extended to include more complex approaches), but because of pertinent abstraction of the reality they remain complex (consequently requiring a large number of input parameters and variables) and their development is time demanding. Finally, hybrid models, combining advantages and overcoming shortcomings of both, statistical and physical models, are being designed and used for estimation of vegetation biochemical and/or biophysical properties from optical remote sensing data (Fang et al., 2003).

### *1.1.1 Parameterization and validation of land-biosphere models*

An ecological forecasting of biotic and abiotic changes in the biosphere (Nemani, 2005) is becoming an efficient way of predicting the future evolution of ecosystems under influence of the global climate change. This prediction is relying on physically based dynamic vegetation models of land surface processes, initialized and/or validated using Earth observing sensors. Optical remote sensing can provide either categorical input variables for ecological models, like thematic maps of land cover/land use or functional plant types, as well as a spatial distribution of quantitative continuous variables such as the fraction of absorbed photosynthetically active radiation (fAPAR), leaf area index (LAI), fractional vegetation cover (fcover or canopy closure), leaf biomass, leaf chlorophyll content, etc. (Schaeppman et al., 2005). In spite of the fact that many state-of-the-art process-based land-biosphere models, (e.g., Lund-Potsdam-Jena Dynamic Global Vegetation Model (LPJ; Sitch et al., 2003)), are designed to use or capable of accepting some of the above variables, they still do not make full use of remote sensing products to their full capabilities. Therefore, we must strive to comprehensively incorporate today's remote sensing products to calibrate, initialise and

validate these models, such that we will be in a position to take full advantage of future advances in both, remote sensing science and dynamic vegetation model development (Waring, 1983).

### 1.1.2 *Monitoring environmentally stressed vegetation*

Airborne and space-borne optical remote sensing represents an ideal tool for operational monitoring of the state of an ecosystem ranging from local to regional and national scales. Terrestrial ecosystems are exposed to pressures of disturbing natural and anthropogenic stress events of various intensity and duration. Stress of a plant is according to Larcher (1995) defined as being a significant deviation from the optimal living conditions, which negatively affects function, growth or development of the plant organism. The reaction of plants to stress impacts involves both short-term physiological responses and long-term physiological, structural and morphological modifications (Dickson & Isebrands, 1991). In the early 1980s Horler et al. (1983) discovered a spectral shift of the red-edge leaf reflectance (680-740 nm) towards shorter wavelengths induced by early stages of plant stress responses. An optical index called the red-edge inflection point (REIP) was developed based on this phenomenon as a spectral indicator of plant *pre-visual* stress reactions (Rock et al., 1988; Malenovský et al., 2006). The current state of the art in plant research using imaging spectroscopy allows not only the identification of vegetation stress response, but also the quantitative assessment and monitoring of plant stress indicators. Combination of these continuous indicators, retrieved from imaging spectrometer acquired data, can assess the actual state of vegetation. In addition, it has become feasible to track the type of stress impact, including acute (short-term) stress influence (e.g., fast decrease of total chlorophyll concentration), or chronic (long-term) stress influence (e.g., defoliation of the plants decreasing the total leaf area), which may help to more accurately identify the individual environmental stressors.

## 1.2 Background

---

### 1.2.1 *Motivation*

Many vegetation processes of global importance are occurring at the leaf level and thus need to be *scaled up* (Hu et al., 2004) across scales to higher levels (local – canopies, regional – regions, and global – continents) (Curran et al., 2001), taking into account their spatial, directional, and temporal variability. This *bottom-up* concept of ecological modelling (Wang et al., 2004), established on cause-effect interactions, represents a mechanistic approach leading to understand the underlying processes and the resulting properties within and between heterogeneous terrestrial ecosystems.

An ecosystem of particular interest is the Boreal forest, which is in certain regions dominated by Norway spruce (*Picea abies* (L.) Karst.) trees. Norway spruce is a typical tree species of high altitude mountain forest ecosystems. It plays a predominant role in the Euro-Asian high latitude boreal biome called Taiga, representing about 20% of the world's landmass according to Walker & Kenkel (2000). This species belongs to the significant group of coniferous trees that are difficult to be modelled and used in quantitative optical remote sensing approaches due to its highly heterogeneous multi-scale modular architecture.

The particular motivation for this work is primarily based on the up-scaling process from Norway spruce needles to crowns to canopies using ecological reasoning. A basic module (element) of a spruce crown is a leaf that has a small size and a specific acicular shape, which is usually referred to as a *needle*. Needles of the same age-class are growing in small twigs named *shoots*, which are forming *branches* of several orders. Branches of first order are growing directly from the trunk while branches of higher order  $n$  are growing from the branches of order  $n-1$ . Clumps of branches of various orders within one tree create a *crown*. An accumulation of all crowns within a forest stand is considered as being a forest *canopy*.

On average up to seven latest needle age-classes (Cudlín, personal communication), grouped in three types of shoot formations (i.e., proleptic, regular and proventitious) (Gruber, 1994), can be allocated within three functional crown parts (i.e., juvenile, production and saturation). These crown parts have specific physiological functions and reactions to environmental stressors, allowing the spruce trees to be discriminated into two stress response classes: the so-called stress resistant and stress resilient trees (Malenovský et al., 2006). The genetically based crown structural heterogeneity of these stress response classes, supported by extreme montane or boreal environmental conditions, can create a significant variability in needle characteristics, including variability in optical properties. A good knowledge of the variability in leaf optical properties within and in-between the individual spruce crowns is essential for the appropriate set-up of field and laboratory spectroscopic experiments, as well as for reliable parameterization and validation of radiative transfer models for spruce canopies.

Direct measurement of needle optical properties is a tedious and time consuming procedure (Harron & Miller, 1995a; Mesarch et al., 1999; Daughtry et al., 2000a). Therefore, modelling of needle optical properties by means of a leaf RT model (e.g., PROSPECT) (Jacquemoud & Baret, 1990) based on measurable input biochemical and biophysical variables is an efficient and time saving approach. Moreover, a leaf RT model coupled with a canopy model can be inverted for the quantitative estimation of biochemical compounds originating from the measured forest canopy reflectance. However, the canopy RT model must be able to offer an appropriate representation of details as well as an adequate parameterization of the structural heterogeneity of the forest ecosystem, by matching the high spatial resolution.

Following the already introduced bottom-up approach, the simulations of the RT model and the air- or space-borne reflectance measurements must be performed at such a spatial resolution that they are able to capture representative details for each tree crown, thus being able to quantify processes behind multiple reactions to environmental stressors. For this reason, the spatial resolution of the imaging spectrometer data and the inverted RT model must allow mapping and understanding the spatial variability in biochemical and structural quantitative characteristics of separate spruce crowns (especially sunlit vs. shaded parts of the crown). A spatial resolution of 0.4 m is considered to be sufficiently high to do so.

A 3-dimensional Discrete Anisotropic Radiative Transfer (DART) model (Gastellu-Etchegorry et al., 1996; Gastellu-Etchegorry et al., 2004) was adjusted to incorporate a more realistic radiative transfer through a coniferous canopy at the required spatial resolution. The improvements to obtain the increased level of detail focused on the forest structural (architectural) parameterization of the model. The particular functions of the vertical and horizontal distribution of the leaf biomass (including specific defoliation zones), the improvement on trunk construction, and the simulation of woody elements (i.e., branches of first order represented as pyramidal geometrical objects and tiny woody twigs of shoots represented as a woody turbid medium) were incorporated (Malenovský et al., 2006).

Consequently, such an improved DART model was tested for its performance and accuracy in the forward mode through a systematic sensitivity analysis, before running it in the inverse mode.

Finally, the RT models can be used in an inverse mode to retrieve biochemical (e.g., concentration of foliar pigments) or structural (e.g., LAI) properties of a forest canopy (Gastellu-Etchegorry & Bruniquel-Pinel, 2001; Gastellu-Etchegorry et al., 2004; Zarco-Tejada et al., 2004a; Schaepman et al., 2005). Any inversion method should be robust, operational and accurate enough to fulfil the requirements of a given application. For example, the use of total chlorophyll concentration as a bio-indicator of stress response in a Norway spruce stand requires an inversion routine that corrects for the forest structural influence. Furthermore, the routine must be easily adjustable or extendable, and still being capable to retrieve the spatially distributed chlorophyll concentration with a given standard error (lower than  $\pm 7.5 \mu\text{g cm}^{-2}$  (Malenovský et al., 2006)). Moreover, the inversion process should also be based on spectroscopic data with sufficiently high spatial resolution (Pinty et al., 2001), because the nature and intensity of the stress reactions can be highly tree specific (Malenovský et al., 2006). Such approach will finally allow a sound estimation of chlorophyll concentration for individual spruce crowns.

### *1.2.2 Objectives and research questions*

Based on the motivation discussed in the previous chapter, four main scientific objectives were defined for this work:

1. Sensitivity analysis, adaptation and validation of the existing leaf RT model PROSPECT for Norway spruce needles.
2. Understanding the variability of leaf optical properties of environmentally stressed Norway spruce crowns for subsequent scaling approaches from needles to canopies.
3. Appropriate parameterization and sensitivity analysis of the canopy RT model DART for Norway spruce canopies.
4. Development of a simple and robust methodology for estimating chlorophyll concentration of Norway spruce crowns using RT models applied at very high spatial resolution.

Based on the above scientific objectives of this work, the following research questions were identified:

- I. How and to what extent can the RT model PROSPECT be used to simulate leaf optical properties of Norway spruce needles?
- II. What are the statistically significant differences in leaf optical properties of Norway spruce needles within and in-between crowns of two different environmental stress responses, with regard to their use in quantitative remote sensing methods?
- III. What is the influence of the presence of woody elements on the reflectance of a Norway spruce canopy simulated using the DART model?
- IV. On what basis can a robust, operational and reliable chlorophyll concentration retrieval approach be designed for a heterogeneous Norway spruce canopy at very high spatial resolution?

Answers on the defined research questions should extend our knowledge on physically based remote sensing used for quantitative assessment of Norway spruce ecosystems. A unique characteristic of this work is testing the integration of the ecological features of the

Norway spruce crown architecture (e.g., spatially specific foliage distribution and defoliation, presence of woody elements, etc.), including reactions on environmental stressors, into the coupled leaf and canopy RT models of vegetation. These newly introduced structural and stress response factors were expected to increase the reliability of the spruce top of canopy reflectance simulated by the RT models, and to prepare these models for designing retrievals of biochemical and biophysical properties of Norway spruce canopies.

### 1.2.3 *Structure*

The content of this thesis work is structured into seven chapters. This first chapter is discussing a general introduction to quantitative remote sensing approaches used for biochemical and biophysical compound retrieval, resulting in the above motivation, the scientific objectives and four research questions. Chapter 2 reviews various categories and scaling capabilities of physically based radiative transfer models. It focuses on scaling leaf optical properties up to the canopy level, with an outlook on having bidirectional leaf reflectance and transmittance information in addition. Chapter 2 is primarily based on '*Scaling dimensions in spectroscopy of soil and vegetation*' (Malenovský et al., 2006) and has been complemented by specific parts not discussed in the paper, but of relevance to this work.

Chapters 3 and 4 present two parallel studies sharing a common input dataset, but answering two different research questions. Chapter 3 entitled '*Applicability of the PROSPECT model for Norway spruce needles*' (Malenovský et al., 2006) investigates applicability and subsequent adjustment of the PROSPECT RT model for Norway spruce needles. The study resulted in a specific update of PROSPECT for three needle age-classes, which was tested in direct as well as inverse mode. Chapter 4 entitled '*Differences in leaf optical properties of environmentally stressed Norway spruce (*Picea abies* (L.) Karst.) crowns*' (Malenovský et al., 2006) discusses the leaf optical properties measured and used in Chapter 3. This experiment investigated the variability in hemispherical-directional reflectance, transmittance and absorbance of spruce needle samples ranging from 505-800 nm collected from three types of shoots growing within two functional crown parts of two stress response classes.

The up-dated DART model was put through a sensitivity analysis testing the influence of woody elements on the modelled Norway spruce canopy reflectance with regard to the retrieval of forest stand LAI. Results of this analysis are discussed in Chapter 5 '*Influence of woody elements of a Norway spruce canopy on nadir reflectance simulated by the DART model at very high spatial resolution*' (Malenovský et al., 2006). The PROSPECT and DART models were subsequently coupled and used to develop a hybrid (combined physical and statistical) method for estimation of the total leaf chlorophyll concentration potentially uninfluenced by the heterogeneous structure of Norway spruce. This approach is described in Chapter 6 '*A new hyperspectral index for chlorophyll estimation of a forest canopy: Area under curve Normalized to Maximal Band depth between 650-725 nm*' (Malenovský et al., 2006).

Finally, the research questions postulated in Chapter 1 are put in a broader context following the outcomes of Chapters 2-6 in a synthesis (Chapter 7). This final chapter also contains the recent advances on mapping the chlorophyll content and LAI of a Norway spruce canopy from airborne data with very high spatial resolution, and discusses the outlooks on scaling of these methods up to the coarser spatial resolution of satellite based imaging spectroradiometers (e.g., CHRIS/PROBA and potential successors).

### 1.3 References

---

- Asrar, G. (1989), Theory and applications of optical remote sensing. In A. K. Jin (Ed.), *Wiley series in remote sensing* (pp. 734). New York: John Wiley & Sons.
- Barnsley, M. J., Settle, J. J., Cutter, M. A., Lobb, D. R., & Teston, F. (2004), The PROBA/CHRIS mission: A low-cost smallsat for hyperspectral multiangle observations of the earth surface and atmosphere. *Ieee Transactions on Geoscience and Remote Sensing*, 42, 1512-1520.
- Chen, D. X., & Coughenour, M. B. (2004), Photosynthesis, transpiration, and primary productivity: Scaling up from leaves to canopies and regions using process models and remotely sensed data. *Global Biogeochemical Cycles*, 18, 1-15.
- Clevers, J. G. P. W., De Jong, S. M., Epema, G. F., Van der Meer, F. D., Bakker, W. H., Skidmore, A. K., & Scholte, K. H. (2002), Derivation of the red edge index using the MERIS standard band setting. *International Journal of Remote Sensing*, 23, 3169-3184.
- Cudlin, P., Novotny, R., Moravec, I., & Chmelikova, E. (2001), Retrospective evaluation of the response of montane forest ecosystems to multiple stress. *Ekologia-Bratislava*, 20, 108-124.
- Curran, P. J., Dungan, J. L., & Peterson, D. L. (2001), Estimating the foliar biochemical concentration of leaves with reflectance spectrometry: Testing the Kokaly and Clark methodologies. *Remote Sensing of Environment*, 76, 349-359.
- Daughtry, C. S. T., Biehl, L. L., & Ranson, K. J. (1989), A new technique to measure the spectral properties of conifer needles. *Remote Sensing of Environment*, 27, 81-91.
- Dickson, R. E., & Isebrands, J. G. (1991), Leaves as regulators of stress response. San Diego, New York, London: Academic Press, 4-34.
- Fukshansky, L., Remisowsky, A. M. v., McClendon, J., Ritterbusch, A., Richter, T., & Mohr, H. (1993), Absorption-spectra of leaves corrected for scattering and distributional error - a radiative-transfer and absorption statistics treatment. *Photochemistry and Photobiology*, 57, 538-555.
- Gascon, F., Gastellu-Etchegorry, J. P., Lefevre-Fonollosa, M. J., & Dufrene, E. (2004), Retrieval of forest biophysical variables by inverting a 3-D radiative transfer model and using high and very high resolution imagery. *International Journal of Remote Sensing*, 25, 5601-5616.
- Gascon, F., Gastellu-Etchegorry, J. P., & Lefevre, M. J. (2001), Radiative transfer model for simulating high-resolution satellite images. *Ieee Transactions on Geoscience and Remote Sensing*, 39, 1922-1926.
- Gastellu-Etchegorry, J. P., & Bruniquel-Pinel, V. (2001), A modeling approach to assess the robustness of spectrometric predictive equations for canopy chemistry. *Remote Sensing of Environment*, 76, 1-15.
- Gastellu-Etchegorry, J. P., Demarez, V., Pinel, V., & Zagolski, F. (1996), Modeling radiative transfer in heterogeneous 3-D vegetation canopies. *Remote Sensing of Environment*, 58, 131-156.
- Gastellu-Etchegorry, J. P., Martin, E., & Gascon, F. (2004), DART: a 3D model for simulating satellite images and studying surface radiation budget. *International Journal of Remote Sensing*, 25, 73-96.
- GENACS Consortium (2005), GMES - Global Monitoring for Environment and Security. <http://www.gmes.info>, June 29th, 2006.
- Goetz, A. F. H., Vane, G., Solomon, J. E., & Rock, B. N. (1985), Imaging Spectrometry for Earth Remote-Sensing. *Science*, 228, 1147-1153.
- Gruber, F. (1994), Morphology of coniferous trees: possible effects of soil acidification on the morphology of Norway spruce and Silver fir. In D. L. Godbold, & A. Hüttermann (Ed.), *Effects of acid rain on forest processes* (pp. 265-324). New York: Wiley-Liss.
- Guanter, L., Alonso, L., & Moreno, J. (2005), First results from the PROBA/CHRIS hyperspectral/multiangular satellite system over land and water targets. *Ieee Geoscience and Remote Sensing Letters*, 2, 250-254.



- Harron, J. W., & Miller, J. R. (1995), An alternative methodology for reflectance and transmittance measurements of conifer needles. *17th Canadian Symposium on Remote Sensing*, 1995, Saskatchewan: Saskatoon, 654-661.
- Horler, D. N. H., Dockray, M., & Barber, J. (1983), The red edge of plant leaf reflectance. *International Journal of Remote Sensing*, 4, 273-288.
- Jacquemoud, S., & Baret, F. (1990), Prospect - a model of leaf optical properties spectra. *Remote Sensing of Environment*, 34, 75-91.
- Kimes, D. S., Knyazikhin, Y., Privette, J. L., Abuelgasim, A. A., & Gao, F. (2000), Inversion methods for physically-based models. *Remote Sensing Reviews*, 18, 381-439.
- Knyazikhin, Y., Martonchik, J. V., Diner, D. J., Myneni, R. B., Verstraete, M., Pinty, B., & Gobron, N. (1998), Estimation of vegetation canopy leaf area index and fraction of absorbed photosynthetically active radiation from atmosphere-corrected MISR data. *Journal of Geophysical Research D: Atmospheres*, 103, 32239-32256.
- Kumar, L., Schmidt, K., Dury, S., & Skidmore, A. (2001), Imaging spectrometry and vegetation science. In F. D. v. d. Meer, & S. M. d. Jong (Ed.), *Imaging spectrometry - basic principles and prospective applications* (pp. 403). Dordrecht, Boston, London: Kluwer Academic Publishers.
- Larcher, W. (1995), *Physiological plant ecology*. Berlin, Heidelberg: Springer Verlag, pp. 321-323.
- Liang, S. L., Fang, H. L., Kaul, M., Van Niel, T. G., McVicar, T. R., Pearlman, J. S., Walthall, C. L., Daughtry, C. S. T., & Huemmrich, K. F. (2003), Estimation and validation of land surface broadband albedos and leaf area index from EO-1 ALI data. *Ieee Transactions on Geoscience and Remote Sensing*, 41, 1260-1267.
- Lyapustin, A., & Wang, Y. J. (2005), Parameterized code SHARM-3D for radiative transfer over inhomogeneous surfaces. *Applied Optics*, 44, 7602-7610.
- Malenovský, Z., Albrechtová, J., Lhotáková, Z., Zurita-Milla, R., Clevers, J. G. P. W., Schaepman, M. E., & Cudlín, P. (2006a), Applicability of the PROSPECT model for Norway spruce needles. *International Journal of Remote Sensing*, in press.
- Malenovský, Z., Bartholomeus, H. M., Acerbi-Junior, F. W., Schopfer, J. T., Painter, T. H., Epema, G. F., & Bregt, A. K. (2006b), Scaling dimensions in spectroscopy of soil and vegetation. *International Journal of Applied Earth Observation and Geoinformation*, accepted.
- Malenovský, Z., Lhotáková, Z., Albrechtová, J., Clevers, J. G. P. W., Schaepman, M. E., & Cudlín, P. (2006c), Differences in leaf optical properties of environmentally stressed Norway spruce (*Picea abies* (L.) Karst.) crowns. *Trees - Structure and Function*, in preparation.
- Malenovský, Z., Martin, E., Gastellu-Etchegorry, J. P., Cudlín, P., & Clevers, J. G. P. W. (2003), Heterogeneity description improvements of spruce crown architecture simulated using the 3D radiative transfer model DART. *Proceedings of the 2nd SPECTRA Workshop*, 28. - 30. October 2003, ESTEC, Noordwijk, The Netherlands: European Space Agency.
- Malenovský, Z., Martin, E., Homolová, L., Gastellu-Etchegorry, J. P., Zurita-Milla, R., Schaepman, M. E., Pokorný, R., Clevers, J. G. P. W., & Cudlín, P. (2006d), Influence of woody elements of a Norway spruce canopy on nadir reflectance simulated by the DART model at very high spatial resolution. *Remote Sensing of Environment*, accepted.
- Malenovský, Z., Ufer, C. M., Lhotáková, Z., Clevers, J. G. P. W., Schaepman, M. E., Albrechtová, J., & Cudlín, P. (2006e), A new hyperspectral index for chlorophyll estimation of a forest canopy: Area under curve Normalized to Maximal Band depth between 650-725 nm. *EARSeL eProceedings*, 5, 161-172.
- Meer, F. D. v. d., & Jong, S. M. d. Remote sensing and digital image processing (2001), *Imaging spectrometry - basic principles and prospective applications*. Dordrecht, Boston, London: Kluwer Academic Publishers, pp. 403.
- Mesarch, M. A., Walter-Shea, E. A., Asner, G. P., Middleton, E. M., & Chan, S. S. (1999), A revised measurement methodology for conifer needles spectral optical properties: Evaluating the influence of gaps between elements. *Remote Sensing of Environment*, 68, 177-192.

- Millennium Ecosystem Assessment (2005a), *Ecosystems and Human Well-being: Synthesis*. Washington DC: Island Press, pp. 137.
- Millennium Ecosystem Assessment (2005b), Living beyond our means - Natural assets and human well-being. <http://www.millenniumassessment.org>, June 9th, 2006.
- Myneni, R. B., & Ross, J. (1991), *Photon - vegetation interactions: Applications in optical remote sensing and plant ecology*. Berlin Springer-Verlag, pp. 565.
- Nemani, R. R. (2005), Ecological forecasting - Monitoring, modeling, and forecasting the impacts of climate variability and change on ecosystems. <http://ecocast.arc.nasa.gov/>, June 11th, 2006.
- Newton, S. I. (1704), *Opticks: or, a treatise of the reflections, refractions, inflections and colours of light*. London: Printed for W. and J. Innys, pp. 378.
- Peterson, G., Allen, C. R., & Holling, C. S. (1998), Ecological resilience, biodiversity, and scale. *Ecosystems*, 1, 6-18.
- Rock, B. N., Hoshizaki, T., & Miller, J. R. (1988), Comparison of in situ and airborne spectral measurements of the blue shift associated with forest decline. *Remote Sensing of Environment*, 24, 109-127.
- Schaepman, M. E. (2005), Imaging spectroscopy in ecology and the carbon cycle: Heading towards new frontiers. In B. Zagajewski, & M. Sobczak (Ed.), *Imaging Spectroscopy – New Quality in Environmental Studies, The 4th Workshop on Imaging Spectroscopy, Warsaw, Poland, 27.3.-29.3.2005* (pp. 26). Warsaw University and European Association of Remote Sensing Laboratories (EARSeL).
- Schaepman, M. E., Koetz, B., Schaepman-Strub, G., & Itten, K. I. (2005), Spectrodirectional remote sensing for the improved estimation of biophysical and -chemical variables: two case studies. *International Journal of Applied Earth Observation and Geoinformation*, 6, 271-282.
- Schlerf, M., Atzberger, C., & Hill, J. (2005), Remote sensing of forest biophysical variables using HyMap imaging spectrometer data. *Remote Sensing of Environment*, 95, 177-194.
- Sitch, S., Smith, B., Prentice, I. C., Arneeth, A., Bondeau, A., Cramer, W., Kaplan, J. O., Levis, S., Lucht, W., Sykes, M. T., Thonicke, K., & Venevsky, S. (2003), Evaluation of ecosystem dynamics, plant geography and terrestrial carbon cycling in the LPJ dynamic global vegetation model. *Global Change Biology*, 9, 161-185.
- Swain, P. H., & Davis, S. M. Remote sensing: the quantitative approach. (1978), *Remote sensing: the quantitative approach*. New York: McGraw-Hill International Book Company, pp. 406.
- Walker, D. J., & Kenkel, N. C. (2000), The adaptive geometry of boreal conifers. *Community Ecology*, 1, 13-23.
- Wang, Q., Tenhunen, J., Falge, E., Bernhofer, C., Granier, A., & Vesala, T. (2004), Simulation and scaling of temporal variation in gross primary production for coniferous and deciduous temperate forests. *Global Change Biology*, 10, 37-51.
- Waring, R. H., & Running, S. W. (1999), Remote sensing requirements to drive ecosystem models at the landscape and regional scale. In J. D. Tenhunen, & P. Kabat (Ed.), *Integrating hydrology, ecosystem dynamics, and biogeochemistry in complex landscapes : report of the Dahlem Workshop on Integrating Hydrology, Ecosystem Dynamics, and Biogeochemistry in Complex Landscapes, Berlin, January 18-23, 1998* (pp. 367). Chichester, New York: Wiley.
- Zarco-Tejada, P. J., Miller, J. R., Harron, J., Hu, B., Noland, T. L., Goel, N., Mohammed, G. H., & Sampson, P. (2004), Needle chlorophyll content estimation through model inversion using hyperspectral data from boreal conifer forest canopies. *Remote Sensing of Environment*, 89, 189-199.

## CHAPTER 2

### **Scaling in spectroscopy using physically based radiative transfer modelling**

Partially based on the review paper: \*

Malenovský, Z., Bartholomeus, H.M., Acerbi-Junior, F.W., Schopfer, J.T., Painter, T.H., Epema, G.F., Bregt, A.K., 2006: Scaling dimensions in spectroscopy of soil and vegetation. *International Journal of Applied Earth Observation and Geoinformation*, accepted.

---

\* Reprinted with permission from Elsevier © 2006.

## **Abstract**

---

The review clarifies definitions of the term *scale* and *scaling* conversions for imaging spectroscopy with a special focus on vegetation. We demonstrate a four-dimensional scale concept for spectroscopy that includes not only spatial but also the spectral, directional and temporal components. Radiative transfer (RT) models are overviewed to demonstrate their capacity for spatial and spectral up-scaling and directional down-scaling within a heterogeneous environment. Detailed laboratory/field spectral measurements (leaf optical properties) and spectral derivatives (vegetation indices), are shown to be scaled or developed and tested by means of radiative transfer. Finally, a future development in measurement and simulation of the bidirectional leaf optical properties and a potential application of the successive radiative transfer modelling for physical up-scaling from the ecosystem level to the biome level is discussed.

*Keywords:* scale, spatial, spectral, directional, temporal scaling, radiative transfer modelling, imaging spectroscopy, leaf optical properties.

## 2.1 Introduction

### 2.1.1 Scale definitions and parameters in imaging spectroscopy

An imaging spectroscopy measurement of the Earth surface reflectance  $R$  is predominantly a function  $f_R$  defined by spatial, spectral, directional, and temporal scale (Baret, personal communication):

$$R = f_R(x, y; \lambda; \Omega_s, \Omega_o; t) \quad (2.1)$$

where  $x, y$  are spatial coordinates,  $\lambda$  is the wavelength of the electromagnetic spectra,  $\Omega_s, \Omega_o$  describes the angular viewing geometry of the sun-object-sensor system, and  $t$  is the time frequency of the observation. A definition of remote sensing spectral image scale must consider all of these four dimensions. Adjusting the scale definition of Quattrochi (1993) we can state that the *spectroscopy scale* of optical imaging data is the combination of four dimensions: i) space, ii) electromagnetic wavelengths, iii) angular geometrical vectors – directions, and iv) time over which a spectrometric measurement is made. Descriptive parameters of each dimension are summarized in table 2.1.

Table 2.1: Parameters of the four-dimensional scale concept for spectroscopic data (FWHM = ‘full-width-half-maximum’, IFOV = ‘instantaneous-field-of-view’).

Scale dimension	Resolution	Extent	Sampling interval
Spatial	Image pixel-size	$x_{\max}, y_{\max} - x_{\min}, y_{\min}$	–
Spectral	FWHM	$\lambda_{\max} - \lambda_{\min}$	Spacing between band centres
Directional	IFOV <sup>1</sup>	$\Omega_{\max} - \Omega_{\min}$	Spacing between angular vectors
Temporal	Integrating time	$t_{\max} - t_{\min}$	Spacing between the sensor visits

<sup>1</sup>IFOV is applicable only for imaging spectrometers. FOV (field-of-view) of the optical set applies in case of numeric spectroradiometers.

A more precise definition may be reached by extension of the term *support* (Olea, 1991). The original specification of *support* includes the geometrical shape, size, and orientation of the volume. The volume of *spectroscopy support* should enclose, in addition to the spatial and geometrical content, a spectro-directional component and the time intervals between successive observations.

Traditional parameters describing the scale of remote sensing image data are *resolution* (*grain*) and *extent* (see table 2.1). Consequently, considering the four-dimensional spectroscopy scale scheme, *spatial resolution* is equal to the elementary pixel size of a remotely sensed image and *spatial extent* corresponds to the total area covered within an image swath. These spatial parameters are functions of the digital matrix of the spectral sensor and the ‘instantaneous field of view’ (IFOV) given by the optical system, flight altitude, and its flight velocity respectively (Forshaw et al., 1983).

Spectral resolution is described by Lillesand and Kiefer (1994) as ‘the ability to discriminate fine spectral differences’. The *spectral resolution* of a sensor is often defined by the ‘full-width-half-maximum’ (FWHM) of the instrument response to a monochromatic

source (Liang, 2004). The *spectral extent*, also named spectral range, is the difference between the minimum and maximum wavelengths in which measurements are made ( $\lambda_{\max} - \lambda_{\min}$ ). A new parameter, *spectral sampling*, has to be introduced to describe the number and position of the spectral channels. *Spectral sampling interval* is the spacing between sample points in the spectrum (Liang, 2004). As shown in figure 2.1, the sampling interval is independent of the spectral resolution, which implies that there can be overlap between consecutive bands. This is usually the case in imaging spectroscopy instruments, since their aim is to derive a contiguous spectrum where over-sampling reduces the amount of incoming noise but at the cost of information redundancy. Spectral and spatial resolutions of the multi- and/or hyperspectral images are in an inverse relationship due to the technical constraints on the sensor side. There is usually a trade off between high spectral and low spatial resolution or vice versa, because of the limited extent and minimal element size of a ‘charged-coupled device’ (CCD) array recording the spectral image. Lower spatial resolution caused by the binning of the spatial array columns allows a narrowing of the FWHM and, subsequently, increasing spectral resolution. Conversely, spectral binning of the wavelengths widens the FWHM and gives opportunity to increase the spatial resolution. More traditional multispectral satellite instruments operate at high spatial resolution and lower spectral resolution with a small temporal sampling interval (e.g., LANDSAT 7 ETM+ or SPOT 5 HRG). New imaging spectroscopy satellite sensors acquire data with coarser spatial resolution and higher spectral sampling interval and resolution (e.g., Medium Resolution Imaging Spectrometer – MERIS on the ENVISAT satellite), as well as at both high spatial and spectral resolutions (e.g., the Hyperion sensor on board of the satellite EO-1).

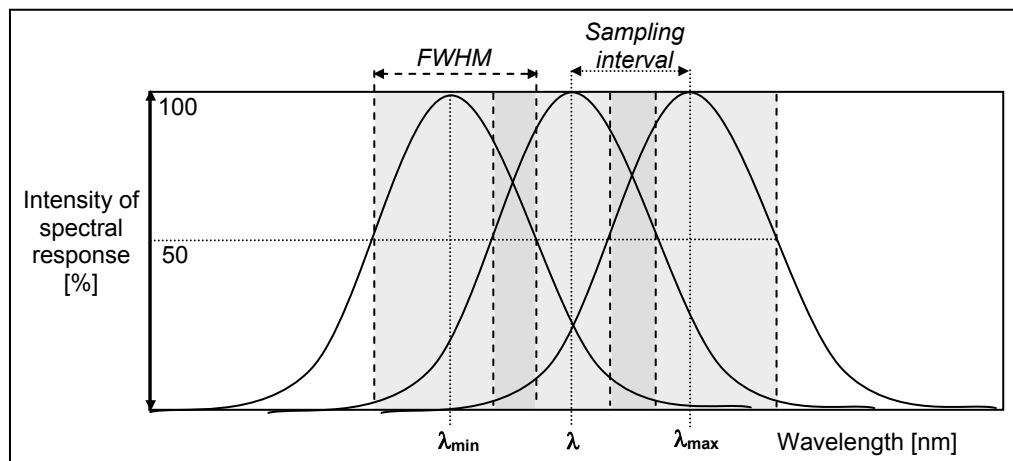


Figure 2.1: Spectral resolution (‘full-width-half-maximum’ – FWHM), extent ( $\lambda_{\max} - \lambda_{\min}$ ) and sampling interval of imaging spectroscopy data.

Reflectance by the Earth’s surface and scattering by atmospheric particles and gases have a strong directional behaviour. This phenomenon is scientifically described by the concept of the bi-directional reflectance distribution function (BRDF). The BRDF is a conceptual quantity that describes the reflectance of a target as a function of the independent variables describing viewing and illumination angles and variables determining the geometrical and optical properties of the observed target (Nicodemus et al., 1977; Deering, 1989; Combal et

al., 2003; Liang, 2004). The BRDF describes the scattering of a parallel beam of incident light from one direction in the hemisphere into another direction in the hemisphere (Schaepman-Strub et al., 2004). The incident and viewing directions are each defined by the zenith and azimuth angles of illumination (in nature sun zenith  $\theta_s$  and azimuth  $\phi_s$  angle) and view of sensor (viewing zenith  $\theta_v$  and azimuth  $\phi_v$  angle). Difference of the viewing and illumination azimuth angle is called the relative azimuth angle ( $\phi = \phi_v - \phi_s$ ) (Schönermark et al., 2004). Then the BRDF [ $\text{sr}^{-1}$ ] can be expressed as a reflectance function  $f_{\text{BRDF}}$  of source illumination projected solid angle  $\Omega_s$ , viewing projected solid angle  $\Omega_v$ , and wavelength  $\lambda$ :

$$\text{BRDF} = f_{\text{BRDF}}(\Omega_s, \Omega_v, \lambda) = \frac{dL_v(\theta_s, \phi_s; \theta_v, \phi_v; \lambda)}{dE_s(\theta_s, \phi_s; \lambda)} \quad (2.2)$$

where  $L_v$  is reflected radiance and  $E_s$  is incident solar irradiance. The unitless bi-directional reflectance factor (BRF) is proportional to the BRDF according to the relation:  $\text{BRF} = \pi \times \text{BRDF}$ . Finally, the reflectance acquired under illumination of the ambient hemispherical sky is called the hemispherical-directional reflectance factor (HDRF). The HDRF is physically defined in the same way as the BRF, except that the HDRF includes illumination coming from the entire hemisphere (Schaepman-Strub et al., 2004). Any outdoor HDRF measurement depends not only on the scattering optical properties of the observed object, but also on atmospheric conditions, the surrounding of the object, the topography, and wavelength. The spectral field measurements of the HDRF are often performed by a goniometer device. In order to obtain a high accuracy, goniometer reflectance measurements are usually performed at a local scale and on a specific vegetation or soil (snow) surface. Still, natural spatial patterns are not uniformly distributed within the space and their expanse covers the whole range from micro to macro scale (e.g., cell structure, leaves, branches, trees, forest). Details of ground directional reflectance measurements are given in Bruegge et al. (2000).

Accordingly to the BRDF concept, the *directional resolution* of the angular spectral image data is represented by the IFOV given by the parameters of the optical set, size of the CCD array basic element, tilt, motion speed and altitude of a sensor. *Directional extent* is specified by the interval between minimal viewing direction ( $\theta_{v \text{ min}}, \phi_{v \text{ min}}$ ) and maximal viewing direction ( $\theta_{v \text{ max}}, \phi_{v \text{ max}}$ ) aside (maximal - minimal oblique viewing angles). Finally, *directional sampling* is expressed by the total number of viewing directions and their angular position within the hemispherical space. Presently, only a few real multi-angular imaging spectroscopy satellite sensors are operational. Examples of successful missions are the Compact High Resolution Imaging Spectrometer (CHRIS) sensor on board the PROBA satellite, providing five angular images in 63 spectral bands (NADIR, +/- 36°, +/- 55°), or the Multiangle Imaging SpectroRadiometer (MISR) on the NASA EOS Terra platform consisting of nine cameras capturing four VIS/NIR spectral bands in nine backwards and forwards along track viewing directions. Developments in remote sensing technology and radiative transfer modelling indicate that angular signatures can be exploited to provide not only improved accuracies relative to single-angle approaches but also unique diagnostic information about the Earth's atmosphere and surface, e.g. identification of atmospheric aerosol, cloud, or surface vegetation type (Diner et al., 1999), capitalizing on both the geometric aspects of the technique as well as the radiometric variations in signal with angle.

Temporal scale must be considered, since geochemical or geophysical constituents of the surface (e.g., concentration of various chemical compounds, or water content) exhibit specific spectral features that vary over time. Monitoring the variation over time becomes more important when ecosystems and their reactions to climate effects are observed. Some authors traditionally refer to temporal resolution as the image frequency which depends on the revisit time of a sensor; in other words, how often is an image acquired over a specific location on Earth (Franklin, 2001). However, strictly following the foregoing concept of the imaging spectroscopy spatial and spectro-directional scale, we propose the sensor revisit time to be called the *temporal sampling interval* rather than temporal resolution. Since image spatial resolution is given by size of the smallest CCD array element then similarly the *temporal resolution* should be defined as the time span needed to integrate the reflected radiative information by the CCD array into the image. Nevertheless, this parameter is commonly called an integration and/or dwell time of a sensor. *Temporal extent* is taken as the time interval between the last and first observation of the same location ( $t_{\max} - t_{\min}$ ), which can be several years for a given satellite platform. Perhaps the most important temporal characteristic, revisit frequency of the satellite driven by the orbit parameters and viewing extent varies from mission to mission. Among low revisiting frequency satellite platforms are LANDSAT 7, and EO-1 (both 16 days) or SPOT (26 days). Examples of the high frequency revisiting sensors are the Moderate Resolution Imaging Spectroradiometer (MODIS) aboard the Terra (EOS AM) and Aqua (EOS PM) satellites viewing the entire Earth's surface every one to two days or the Medium Resolution Imaging Spectrometer (MERIS) with the revisit frequency of three days. Note that the theoretical temporal sampling interval is usually higher than the practical one, due to cloudiness that can cover the location of interest during the time of the sensor overpass.

The increasing availability of remote sensing sensors provides the possibility of choosing the systems that are best adapted for specific research interests. Various factors such as cost, availability at a certain time and place, sensor characteristics (spatial, spectral, temporal, directional resolution) and, of course, specific research interests determine the final decision. Sensor characteristics and research interests are strongly related and this is where scale considerations play a major role. The choice of the appropriate scale for every dimension in a particular application depends on several factors and is a function of the type of environment and the kind of information desired (Woodcock & Strahler, 1987).

### 2.1.2 *Scaling up and down in spectroscopy*

Transfer of data content from one scale to another one is called *scaling*. According to Dungan (2001), *scaling* when applied in remote sensing and GIS is a procedure that changes the size of a measurement unit. Basically, scaling can be performed by means of two approaches: bottom-up and top-down. The bottom-up approach *up-scales* information from smaller to larger observational scales, while the top-down approach *down-scales*, in other words decomposes, information at a certain geographical scale into its constituents at smaller scales (Marceau & Hay, 1999). Considering the four-dimensional scale concept for spectroscopy, the *up-scaling* procedure is decreasing spatial, spectro-directional, and temporal spectroscopic resolution, while the *down-scaling* procedure is increasing these resolutions. Much literature has been published on scaling in environmental research, with the vast majority concerning spatial scaling (Cao & Lam, 1997; Goodchild & Quattrochi, 1997; Tate & Atkinson, 2001). Availability of hyperspectral images and frequently revisiting satellites induced several studies considering the spectral and temporal scaling. Yet, only a few studies



have been conducted on directional scaling thus far. Use of the directional spectral information is currently growing in remote sensing research, so one may expect rapid progress in directional methods supporting development of a new multi-angle optical sensor.

As mentioned by Jarvis (1995), scaling represents a scientific challenge because of the non-linear nature between processes and variables, and heterogeneity of characteristics determining the rates of processes. Therefore, the objective of this review is focused on physically based spatial, spectral and directional up- or downscaling in spectroscopy using the radiative transfer (RT) models. The discussed techniques represent scaling of both: i) measured spectral signatures (hemispherical leaf optical properties), and ii) spectral derivatives (optical vegetation indices).

## 2.2 Types of radiative transfer models

---

The radiative transfer theory was originally developed for turbid media problems in astrophysics, nuclear and atmospheric physics (Chandrasekhar, 1960; Marchuk & Lebedev, 1971; Sobolev, 1975). The original radiative transfer equation was a linear integrodifferential equation which has proved to be remarkably intractable (Hapke, 1993). Therefore, numerical/geometrical computer simulated models had to be used to reach an appropriate and desired solution accuracy (Stamnes et al., 1988).

The radiative transfer theory describes the modelling of the path of solar emitted photons from the moment of their penetration into the atmosphere layers, through interactions with the Earth surface and atmosphere particles, up to the backward reflection and detection by an airborne or satellite sensor. In fact, the equation of radiative transfer can be solved only if at least upper and lower boundaries conditions of a model are defined. For a simple radiative transfer (RT) model that couples an atmosphere with a canopy, the top of the atmosphere with only direct incoming solar radiation represents the upper boundary, while the lower boundary is the Earth surface beneath the vegetation reflecting radiation directionally in terms of the BRDF. Such an RT model, having horizontally homogeneous and infinite but vertically variable and finite layers of atmosphere and canopy, is called one-dimensional (1D) (Liang, 2004). Optical properties of the atmospheric medium are determined by the characteristics of the aerosol particles and atmospheric gasses causing multiple scattering and absorption of photons. Atmospheric radiative transfer equations can be solved by means of numerical (Lenoble, 1985) or approximate solutions (Fang & Liang, 2005). The medium at the Earth surface could be a bare soil, snow or understory canopy layer. Liang and Townshend (2005) improved the original Hapke soil bidirectional reflectance model (Hapke, 1981; Hapke & Wells, 1981; Hapke, 1984; 1986) using a new arbitrary directional distribution of the sky irradiance and multiscattering based on a four-stream approximation. Also numerical soil and snow RT models have been developed, e.g. Mishchenko et al. (1999). Finally, the vegetation canopy of a 1D RT model is assumed to be a turbid medium with randomly distributed leaf clumps and gaps (voids) in between (Pinty et al., 2001). Canopy architecture is described by means of leaf area index (LAI – one-sided leaf area per unit of ground area), leaf angle distribution (LAD – probability density of the distribution of the leaf normals with respect to the upper hemisphere) (Bunnik, 1978; Goel & Strelb, 1984), and dimensions of the leaf shape (length and width) to account properly the hotspot effect (Qin & Xiang, 1994). According to the so called bi-Lambertian scattering model (Shultis & Myneni, 1988), leaf

optical properties are composed by the combined specular-Lambertian reflectance and Lambertian transmittance.

The simple turbid medium concept is not applicable in case of a horizontally heterogeneous or discontinuous vegetation canopies, e.g. forest stands with individual tree crowns. Kimes and Kirchner (1982), therefore, developed a first RT model handling heterogeneous canopy that was extended by Gastellu-Etchegorry et al. (1996; 2004) into the three-dimensional (3D) model named Discrete Anisotropic Radiative Transfer (DART). A DART scene is a 3D matrix of parallel-piped cells containing the landscape components (e.g., leaves, trunks, branches, water, soil, atmosphere) characterized by their optical properties (scattering phase functions, and structural parameters). In spite of several extensive studies of Myneni et al. (Myneni et al., 1989; 1992; Combal et al., 2003) showing that 3D RT models can properly handle any form of the heterogeneous canopy, other types of less computational time-consuming models are developed. Nilson and Peterson (1991) developed an approximate approach to non homogeneous canopies, Kuusk (1994; 2004) designed the so called Markov canopy reflectance model, Goel and Grier (1986) made a hybrid two-dimensional model for row-planted vegetation, Gobron et al. (1997) introduced a semidiscrete RT model, and recently Shabanov et al. (2000) applied a stochastic theory commonly used in hydrodynamics to simulate local inhomogeneities within the canopies.

Similar to atmospheric RT models, there are two basic solutions available for canopy RT modelling: i) approximate and ii) numerical. First approximate solutions were based on the Kubelka-Munk (KM) theory solving the differential equations of upward and downward fluxes. Allen et al. (1970) included into this two-flux theory the third: direct solar flux. Consecutively, Suits (1971-1973) added a flux at the sensor viewing direction, and Verhoef (1984) transformed this four-flux theory into the SAIL (light Scattering by Arbitrary Inclined Leaves) model. Most of the recent canopy RT models are using two-stream (Nilson & Peterson, 1991; Pinty et al., 2004) or four-stream approximations (Liang & Strahler, 1995) for the multiple scattering estimation. The numerical solutions are more accurate in multiple scattering computation, and work well in both 1D and 3D geometries. They can be applied in vegetation by means of several representative algorithms: the discrete ordinates (Shultis & Myneni, 1988; Combal et al., 2003), the Gauss-Seidel algorithm (Liang & Strahler, 1993), the integral equation method (Gutschick & Wiegel, 1984) and successive orders of scattering approximations (Myneni et al., 1987). A new solution is represented by the geometric optical models. These create a canopy from the geometrical shapes like cones, ellipsoids, cylinders, etc., distributed through the ground surface in a predefined pattern. Fractions of sunlit and shaded components within the scene are taken into account during computation of the anisotropic scattering, based on geometric optical principles. Evaluation of most of these canopy models is available in review of Chen et al. (2000). There are also few geometric optical models designed for a soil surface, e.g. the models described by Irons et al. (1992) or by Cierniewski and Verbrugge (1997).

Once a representative structural 3D scene of the plants is created out of the geometrical elements (e.g., triangular facets covered by the parametric surfaces), a Monte Carlo (MC) ray tracing method may be applied to simulate the photon trajectories within the vegetation canopy (Disney et al., 2000). Rays may be traced either 'forward' (from illumination source to a sensor) or 'reverse' (photon trajectories from the sensor are tracing the scattering which could have originated at the illumination source). MC simulation is highly demanding computationally, but its processing time does not increase dramatically as scene variability increases. Secondly, a single photon path can be used to simulate reflectance of several

wavebands without additional cost. This concept called ‘ray bundle’ (Lewis, 1999) was applied by Dawson et al. (1999) to generate high spectral resolution data of a forest. Mentioned advantages makes the ray tracing method the most appropriate spatial and spectral ‘scaling able’ solution for radiative transfer. Alternative to the MC ray tracing is a method of radiosity (Borel et al., 1991; Goel et al., 1991; Qin & Gerstl, 2000; Qin et al., 2002). Radiosity, also called radiant exitance (Nicodemus et al., 1977), is given by the amount of total energy leaving a surface per unit time per unit area (flux density). The main advantage of the radiosity model is that once a radiative transfer solution is found canopy reflectance can be simulated for any view angle. Unfortunately, it requires high initial computational load to simulate a complex canopy with a number of geometrical scattering particles, which limits radiosity to be used only for simple scenes.

A recent overview of the state-of-art in the theory of radiative transfer is available in Liang (2004) and partly also in Schönermark et al. (2004). Mutual performance comparison of several radiative transfer models was carried out in two phases of the Radiation Model Intercomparison (RAMI) exercise by Pinty et al. (2001; 2004) and by Widlowski et al. (2004). Detailed information about mathematical canopy RT modelling can be found in the extensive textbook of Myneni and Ross (2003) or Asrar (1989).

## 2.3 Scaling by radiative transfer modelling

### 2.3.1 *Scaling of the optical properties*

Solving the radiative transfer equations of the modern 3D RT models provides a physical scaling of the spectro-directional and spatial information. A highly heterogeneous natural environment is composed of different spectrally behaving surfaces placed into the 3D space according to a specific geometry. Such a complex environment can be represented by a virtual 3D scene assembled from various geometrical primitives. The surface optical properties of created 3D objects must be specified in order to compute multiple-scattering phase functions. Directional-hemispherical optical properties of the object can be measured in the laboratory or field by a spectroradiometer coupled with an integrating sphere that averages the reflected and/or transmitted radiation signal (Li-Cor, 1983). The surface absorption  $\alpha(\lambda)$  can be easily computed from measured directional-hemispherical reflectance  $\rho(\lambda)$  and transmittance  $\tau(\lambda)$  following the relation:  $\alpha(\lambda) = 1 - \rho(\lambda) - \tau(\lambda)$  (Despan & Jacquemoud, 2004).

Spectral resolution and sampling interval of the optical properties can be very high, e.g. a FWHM of 1 nm per wavelength in a given spectral range (extent) of an instrument (‘visible’ – VIS and ‘near infrared’ – NIR part of the ‘electromagnetic’ – EM spectrum). Any 3D radiative transfer simulation is in principle a bottom-up procedure, scaling spectro-directional information within a heterogeneous scene. The simplified geometrical distribution of 3D objects characterized by the spectral properties is mostly up-scaled and ‘mixed’ on the lower spectral resolution and sampling interval of targeting remote sensing data. The spectral resolution of simulated imaging spectroscopy data is usually coarser (e.g., FWHM about 5-10 nm) but, indeed, the original very small FWHM can be maintained. A similar logic applies to the spectral sampling. Hypothetically, if the spectral sampling interval of the optical properties would be regular, not too broad, and with narrow bands, then an interpolation technique could be used to down-scale the spectral sampling and produce an image with even

more wavelengths than the original one contained. However, use of this top-down technique is not common, because the specific absorption features (caused by gasses, chemical compounds, minerals, etc.) can occur at the wavelengths where the interpolation takes place, and thus the resulting reflectance can be erroneous.

The RT modelling offers a unique opportunity for directional scaling. The 3D radiative transfer and geometric-optical models facilitate generation of spectral data at not only nadir view but also arbitrary oblique (off-nadir) viewing direction is defined. The HDRF and consequently BRDF (respectively BRDF) of a simulated scene can be projected into the sensor plane if the required sensor characteristics are specified ('field-of-view' – FOV, IFOV, flight altitude and speed, etc.). The surface directional reflectance is computed at the top of the atmosphere (TOA), if the atmosphere RT is involved, or at the top of the canopy (TOC) in the case of a vegetation surface simulation without atmosphere. Since the directional resolution is given by the technical properties of the sensor and the extent is limited by the directional hemisphere, radiative transfer can only be used to scale the directional sampling interval. The object optical properties are commonly measured as the directional-hemispherical signatures. Consequently, the RT model can scale these spectral signatures down into the several combinations of the incident and observing directions. On the other hand, these signatures might be measured as the bi-directional optical properties with a high directional sampling rate (Briottet, 2004; Bousquet et al., 2005). In that case one could adjust the RT model for a directional up-scaling and integrate the original number of viewing angles into the few viewing directions specific for a given sensor (this topic is discussed further in section 2.4).

Spatial up-scaling is a primary aim of most radiative transfer techniques. The simulated radiation budget is expected to be expressed on the coarser spatial resolution of simulated airborne or satellite products. The computer-generated spatial extent depends on the size of the representative landscape scene. This must be specified reasonably with the available hardware computational power. Spatial down-scaling can not be accomplished at all, because RT models are not designed for this purpose.

Finally, temporal resolution, temporal sampling interval, and temporal extent are not direct functions of radiative transfer. All of these scale parameters must be defined by the operator controlling the RT simulations. Still, one must be aware of the necessity of synchronizing the entire model input, i.e. all the information must be collected and/or measured at the same date or within a reasonably representative time span.

### *2.3.2 Up-scaling and testing vegetation optical indices*

Physical radiative transfer also offers an opportunity for scaling spectral derivatives, especially tuning and testing of various spectral indices computed at different spatial, spectral and directional resolutions. Spectral indices are specifically designed to detect changes in physical or chemical properties of the observed objects from their reflected radiation. For instance, the Normalized Difference Vegetation Index (NDVI) was designed to distinguish vegetation from other objects (bare soil, snow, water, clouds) (Lillesand & Kiefer, 1994; Williams, 1995) based on reflectance differences at visible and NIR wavelengths caused by different chemical and structural characteristics of surfaces. Early research indicated a close statistical relationship between the NDVI and LAI (Jordan, 1969; Tucker, 1979), but several later studies reported low correlation of these variables in dense canopies (Fassnacht et al., 1997; Turner et al., 1999; Lee et al., 2004), most probably due to the fact that a large foliage density saturates the NDVI values (Birky, 2001). Currently, Gascon et al. (2004) showed by means of RT modelling that the NDVI-LAI relationship weakens for a very high spatial

resolution image. The DART model was used to simulate images of a tropical forest at 1 and 50 m resolution in the VIS and NIR domains. The coefficient of determination for the NDVI-LAI exponential regression was equal to 0.96 in case of a 50 m resolution image, but only 0.47 for an image of 1 m spatial resolution. Authors explained this poor relationship by the fact that the variance in NDVI values of the same tree crown pixels is very high, for any value of forest LAI. This demonstrates that the methods retrieving biophysical variables by means of the RT modelling must be adapted at very high spatial resolution.

Spectral indices, used for estimation of the vegetation biophysical and chemical variables, can first be established on the leaf level from narrow-band optical properties and afterwards spectrally and spatially up-scaled to the canopy level through radiative transfer models (Zarco-Tejada et al., 2001). However, not all leaf spectral indices are directly applicable on the higher spatial scale of the canopy because of heterogeneity and geometry of the surrounding environment. Haboudane et al. (2002) gave a typical example of how radiative transfer models can be used to develop an optical index performing optimally on a higher scale. They used a leaf RT model called PROSPECT coupled with the SAILH canopy RT model to establish and test the ratio of two spectral indices ‘Transformed Chlorophyll Absorption in Reflectance Index’ – TCARI (Daughtry et al., 2000a) and ‘Optimized Soil-Adjusted Vegetation Index’ – OSAVI (Steven, 1998) as an appropriate vegetation index for estimation of chlorophyll content from hyperspectral imagery. The TCARI/OSAVI ratio, simulated for a corn field, was shown to be a robust chlorophyll bio-marker, minimally influenced by the reflectance of the underlying soil and variation in the crop LAI.

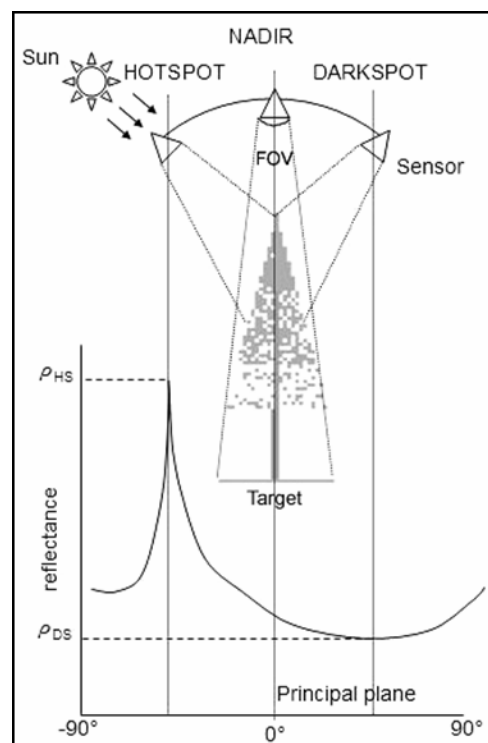


Figure 2.2: Graph of a vegetation canopy reflectance in the principal plane with the highest intensity at the hotspot ( $\rho_{HS}$ ) and the lowest intensity at the darkspot ( $\rho_{DS}$ ) viewing direction.

A similar concept has been applied to develop spectral indices for vegetation canopy structure. Irregular leaf distribution can be described by the clumping index (Nilson, 1971), which measures the foliage aggregation within and between crowns. If the angular positions of sun and sensor are equal ( $\theta_v = \theta_s$  and  $\phi_v = \phi_s$ ), then the canopy reflectance in the principal plane has a maximum ( $\rho_{HS}$ ) in a position called the *hotspot* (mainly first order backward scattered specular reflectance) and minimum ( $\rho_{DS}$ ) in the opposite position called *darkspot* (only diffused forward scattered reflectance), as described in figure 2.2. Reflectance at both positions is explained by optical properties of the foliage and the background, and by canopy architecture determining the number of photon interactions, as well as the canopy shadow fraction in the case of the darkspot. According to the gap distribution probability, a sensor will see less sunlit elements in a clumped canopy than in a random medium. Following this, Lacaze et al. (2002) and Chen et al. (2004) directionally down-scaled the G-function and HOT Spot (GHOST) reflectance model (Lacaze & Roujean, 2001) in combination with the POLarization and Directionality of the Earth Reflectances (POLDER) instrument data and statistically related the canopy clumping index to the directional spectral indices ('directional Hot-Dark Spot' – HDS index and 'Normalized Difference between Hotspot and Darkspot' – NDHD index). RT model inversions have proved that multi-angle spectroscopy measurements improve LAI retrieval results over those generated only from single-angle measurements (Knyazikhin et al., 1998).

## 2.4 Discussion on scaling by means of radiative transfer models

While the scale matters, radiative transfer, as the process based theory, is universally applicable through several spatial scales. Models at two levels, leaf and canopy, are traditionally constructed for the radiative transfer within vegetation. Leaf RT models like PROSPECT (Jacquemoud & Baret, 1990; Jacquemoud et al., 1996), or LIBERTY (Dawson et al., 1998) physically simulate directional-hemispherical reflectance and transmittance of plant leaves. These can be used in the canopy RT models to compute phase functions for the multiple scattering, thus both RT model types are often coupled into one, e.g. the PROSPECT with the SAILH model (Haboudane et al., 2002) or the LIBERTY with the FLIGHT model (Dawson, 2000). Indeed, this model coupling is the only way RT models can be inverted in order to retrieve information on the leaf anatomy or biochemical constituents (Demarez & Gastellu-Etchegorry, 2000; Gascon et al., 2004; Schaepman et al., 2005).

Current radiative transfer models generally use measured directional-hemispherical optical properties of the leaves that lack specific directional information. New instruments and measurement protocols and subsequently RT models are currently under development aiming to obtain the bidirectional optical properties. For instance, Combes et al. (2001) designed a goniophotometer combining many view directions at a high spectral resolution (sampling interval of 2 nm, spectral extent from 450 to 900 nm). The bidirectional leaf reflectance and transmittance are computed from the goniometer measurements by dividing the observed radiance by the radiance of a halon reference target measured in the same directional configuration, and by applying spectro-directional corrections accounting for the anisotropy of the reference reflectance (Bousquet et al., 2005). A deterministic RT model, based on diverse interactions of photons with a 3D plant leaf structure, was developed simultaneously with this measurement technique. A ray tracing code called RAYTRAN was introduced by

Govaerts et al. (1996) to calculate the bi-directional reflection distribution function (BRDF) along with the bidirectional transmission distribution function (BTDF) for any leaf representative assembled from the biologically-based 3D objects (cells of the epidermis layers, palisade parenchyma and spongy mesophyll) (Ustin et al., 2001). It is expected that future implementation of these bidirectional spectral properties will allow a full and more accurate scaling of the spectro-directional information from the leaf up to the canopy level.

Still, a basic question of interest about the scale of the spatial spectro-directional information is: *'Does higher resolution automatically increase the quality and accuracy of the results obtained from the optical remote sensing data?'* As shown, there is not a direct positive or negative answer because the overall resolution of the spectroscopy measurements is a complex function of spatial, spectral, directional, and temporal scale dimensions. In spite of this, the scaling abilities of the radiative transfer offer a systematic modelling of all these dimensions within a multi-conditional scenario, which can give hypothetical answers for the particular combinations of various dimensional resolutions.

Moreover, an analogous RT concept, up-scaling the spectroscopic information from leaf to canopy level, can potentially be adapted and functional on the higher observational level of the eco- and/or agro-systems. Following this idea, if one could produce the representative 'optical properties' of the whole ecosystem (e.g., deciduous, coniferous and mixed forest stand, alpine meadow, marshland, etc.), then a radiative transfer approach could be designed to physically scale spectro-directional information from ecosystem (regional scale) up to biome level (global scale). Such a radiative transfer model could also be inverted to retrieve physical quantitative variables of the ecosystems from the remote sensing data at a coarse spatial resolution, e.g. using VEGETATION sensor on board of the SPOT-4 satellite (spatial resolution of 1 km, swath 2250 km). Finally, the retrieved parameters could be used to parameterise global models for vegetation physiological processes like photosynthesis, respiration, or transpiration, which are connected to the CO<sub>2</sub> exchange fluxes and the general carbon cycle (Chen et al., 2003; Wang et al., 2004).

## 2.5 References

- Allen, W. A., Gayle, T. V., & Richardson, A. J. (1970), Plant-canopy irradiance specified by Duntley equations. *Journal of the Optical Society of America*, 60, 372-376.
- Asrar, G. (1989), Theory and applications of optical remote sensing. In A. K. Jin (Ed.), *Wiley series in remote sensing* (pp. 734). New York: John Wiley & Sons.
- Birky, A. K. (2001), NDVI and a simple model of deciduous forest seasonal dynamics. *Ecological Modelling*, 143, 43-58.
- Borel, C. C., Gerstl, S. A. W., & Powers, B. J. (1991), The radiosity method in optical remote sensing of structured 3-D surfaces. *Remote Sensing of Environment*, 36, 13-44.
- Bousquet, L., Lacherade, S., Jacquemoud, S., & Moya, I. (2005), Leaf BRDF measurements and model for specular and diffuse components differentiation. *Remote Sensing of Environment*, 98, 201-211.
- Briottet, X. (2004), Fundamentals of bi-directional reflectance and BRDF modelling: Concepts and definitions. Berlin: Wissenschaft und Technik Verlag, 31-38.
- Bruegge, C. J., Schaepman, M., Strub, G., Beisl, U., Demircan, A., Geiger, B., Painter, T. H., Paden, B. E., & Dozier, J. (2004), Field measurements of bi-directional reflectance. Berlin: Wissenschaft und Technik Verlag, 195-224.

- Bunnik, N. J. J. (1978), *The multispectral reflectance of shortwave radiation by agricultural crops in relation with their morphological and optical properties*. Wageningen: Wageningen UR - Veenman, pp. 178.
- Cao, C., & Lam, N. S.-N. (1997), Understanding the scale and resolution effects in remote sensing and GIS. In D. A. Quattrochi, & M. F. Goodchild (Ed.), *Scale in remote sensing and GIS* (pp. 406). Boca Raton CRC Press.
- Chandrasekhar, S. (1960), *Radiative Transfer* New York: Dover Publications Inc., pp.
- Chen, J. M., Li, X., Nilson, T., & Strahler, A. (2000), Recent advances in geometrical optical modelling and its applications. *Remote Sensing Reviews*, 18, 227-262.
- Chen, J. M., Liu, J., Leblanc, S. G., Lacaze, R., & Roujean, J.-L. (2003), Multi-angular optical remote sensing for assessing vegetation structure and carbon absorption. *Remote Sensing of Environment*, 84, 516-525.
- Cierniewski, J., & Verbrougghe, M. (1997), Influence of soil surface roughness on soil bidirectional reflectance. *International Journal of Remote Sensing* 18, 1277 - 1288.
- Combes, D., Moya, I., Andlauer, J., Jacquemoud, S., Sinoquet, H., & Varlet-Grancher, C. (2001), Un nouveau dispositif de mesure des propriétés optiques spectrales et bidirectionnelles de surfaces végétales. 8-12 January 2001, Aussois, France: CNES, 283-284.
- Daughtry, C. S. T., Walthall, C. L., Kim, M. S., de Colstoun, E., & Brown McMurtrey III, J. E. (2000), Estimating corn leaf chlorophyll concentration from leaf and canopy reflectance. *Remote Sensing of Environment*, 74, 229-239.
- Dawson, T. P. (2000), The potential for estimating chlorophyll content from a vegetation canopy using the Medium Resolution Imaging Spectrometer (MERIS). *International Journal of Remote Sensing*, 21, 2043-2051.
- Dawson, T. P., Curran, P. J., North, P. R. J., & Plummer, S. E. (1999), The propagation of foliar biochemical absorption features in forest canopy reflectance: A theoretical analysis. *Remote Sensing of Environment*, 67, 147-159.
- Dawson, T. P., Curran, P. J., & Plummer, S. E. (1998), LIBERTY - Modeling the effects of leaf biochemical concentration on reflectance spectra. *Remote Sensing of Environment*, 65, 50-60.
- Deering, D. E. (1989), Field measurements of bidirectional reflectance. New York: John Wiley & Sons, 734.
- Demarez, V., Gastellu-Etchegorry, J. P., Mougin, E., Marty, G., Proisy, C., Dufrene, E., & Le Dantec, V. (1999), Seasonal variation of leaf chlorophyll content of a temperate forest. Inversion of the PROSPECT model. *International Journal of Remote Sensing*, 20, 879-894.
- Despan, D., & Jacquemoud, S. (2004), Optical properties of soil nad leaf: Necessity and problems of modeling. Berlin: Wissenschaft und Technik Verlag, 39-70.
- Diner, D. J., Asner, G. P., Davies, R., Knyazikhin, Y., Muller, J. P., Nolin, A. W., Pinty, B., Schaaf, C. B., & Stroeve, J. (1999), New directions in earth observing: Scientific applications of multiangle remote sensing. *Bulletin of the American Meteorological Society*, 80, 2209-2228.
- Disney, M. I., Lewis, P., & North, P. R. J. (2000), Monte Carlo Ray tracing in optical canopy reflectance modelling. *Remote Sensing Reviews*, 18, 163-196.
- Dungan, J. L. (2001), Scaling up and scaling down: The relevance of the support effect on remote sensing of vegetation. In N. J. Tate, & P. M. Atkinson (Ed.), *Modelling scale in geographic information science* (pp. 277). Chichester John Wiley & Sons.
- Fassnacht, K. S., Gower, S. T., MacKenzie, M. D., Nordheim, E. V., & Lillesand, T. M. (1997), Estimating the leaf area index of North Central Wisconsin forests using the landsat thematic mapper. *Remote Sensing of Environment*, 61, 229-245.
- Forshaw, M. R. B., Haskell, A., Miller, P. F., Stanley, D. J., & Townshend, J. R. G. (1983), Spatial-resolution of remotely sensed imagery - a review paper. *International Journal of Remote Sensing*, 4, 497-520.
- Franklin, S. E. (2001), *Remote sensing for sustainable forest management*. Boca Raton: Lewis Publishers, pp. 407.



- Gascon, F., Gastellu-Etchegorry, J. P., Lefevre-Fonollosa, M. J., & Dufrene, E. (2004), Retrieval of forest biophysical variables by inverting a 3-D radiative transfer model and using high and very high resolution imagery. *International Journal of Remote Sensing*, 25, 5601-5616.
- Gastellu-Etchegorry, J. P., Demarez, V., Pinel, V., & Zagolski, F. (1996), Modeling radiative transfer in heterogeneous 3-D vegetation canopies. *Remote Sensing of Environment*, 58, 131-156.
- Gastellu-Etchegorry, J. P., Martin, E., & Gascon, F. (2004), DART: a 3D model for simulating satellite images and studying surface radiation budget. *International Journal of Remote Sensing*, 25, 73-96.
- Gobron, N., Pinty, B., Verstraete, M. M., & Govaerts, Y. (1997), A semidiscrete model for the scattering of light by vegetation. *Journal of Geophysical Research-Atmospheres*, 102, 9431-9446.
- Goel, N. S., & Grier, T. (1986), Estimation of canopy parameters for inhomogeneous vegetation canopies from reflectance data: 1. Two-dimensional row canopy. *International Journal of Remote Sensing*, 7, 665-681.
- Goel, N. S., Rozehnal, I., & Thompson, R. L. (1991), A computer graphics based model for scattering from objects of arbitrary shapes in the optical region. *Remote Sensing of Environment*, 36, 73-104.
- Goel, N. S., & Strebel, D. E. (1984), Simple beta distribution representation of leaf orientation in vegetation canopies. *Agronomy Journal*, 76, 800-802.
- Goodchild, M. F., & Quattrochi, D. A. (1997), Scale, multiscaling, remote sensing, and GIS. In D. A. Quattrochi, & M. F. Goodchild (Ed.), *Scale in remote sensing and GIS* (pp. 406). Boca Raton CRC Press.
- Govaerts, Y. M., Verstraete, M. M., Jacquemoud, S., & Ustin, S. L. (1996), Three-dimensional radiation transfer modeling in a dicotyledon leaf. *Applied Optics*, 35, 6585-6598.
- Gutschick, V. P., & Wiegand, F. W. (1984), Radiation transfer in vegetative canopies and other layered media: Rapidly solvable exact integral equation not requiring fourier resolution. *Journal of Quantitative Spectroscopy and Radiative Transfer*, 31, 71-82.
- Haboudane, D., Miller, J. R., Tremblay, N., Zarco-Tejada, P. J., & Dextraze, L. (2002), Integrated narrow-band vegetation indices for prediction of crop chlorophyll content for application to precision agriculture. *Remote Sensing of Environment*, 81, 416-426.
- Hapke, B. (1981), Bidirectional Reflectance Spectroscopy: 1. Theory. *Journal of Geophysical Research*, 86, 3039-3054.
- Hapke, B. (1984), Bidirectional reflectance spectroscopy: 3. Correction for macroscopic roughness. *Icarus*, 59, 41-59.
- Hapke, B. (1986), Bidirectional reflectance spectroscopy: 4. The extinction coefficient and the opposition effect. *Icarus*, 67, 264-280.
- Hapke, B. (1993), *Theory of reflectance and emittance spectroscopy*. New York: Cambridge University Press, pp. 455.
- Hapke, B., & Wells, E. (1981), Bidirectional Reflectance Spectroscopy: 2. Experiments and Observations. *Journal of Geophysical Research*, 86, 3055-3060.
- Irons James, R., Campbell Gaylon, S., Norman John, M., Graham David, W., & Kovalick William, M. (1992), Prediction and measurement of soil bidirectional reflectance. *IEEE Transactions on Geoscience and Remote Sensing*, 30, 249-260.
- Jacquemoud, S., & Baret, F. (1990), Prospect - a model of leaf optical properties spectra. *Remote Sensing of Environment*, 34, 75-91.
- Jacquemoud, S., Ustin, S. L., Verdebout, J., Schmuck, G., Andreoli, G., & Hosgood, B. (1996), Estimating leaf biochemistry using the PROSPECT leaf optical properties model. *Remote Sensing of Environment*, 56, 194-202.
- Jarvis, P. G. (1995), Scaling up. *Plant, Cell & Environment*, 1079-1089.
- Jordan, C. F. (1969), Deviation of leaf-area index from quality of light on the forest floor. *Ecology*, 50, 663-666.

- Kimes, D. S., & Kirchner, J. A. (1982), Radiative-transfer model for heterogeneous 3-D scenes. *Applied Optics*, 21, 4119-4129.
- Knyazikhin, Y., Martonchik, J. V., Diner, D. J., Myneni, R. B., Verstraete, M., Pinty, B., & Gobron, N. (1998), Estimation of vegetation canopy leaf area index and fraction of absorbed photosynthetically active radiation from atmosphere-corrected MISR data. *Journal of Geophysical Research D: Atmospheres*, 103, 32239-32256.
- Kuusik, A. (1994), A multispectral canopy reflectance model. *Remote Sensing of Environment*, 50, 75-82.
- Kuusik, A. (1995a), A Fast, Invertible Canopy Reflectance Model. *Remote Sensing of Environment*, 51, 342-350.
- Kuusik, A. (1995b), A Markov-Chain Model of Canopy Reflectance. *Agricultural and Forest Meteorology*, 76, 221-236.
- Lacaze, R., Chen, J. M., Roujean, J.-L., & Leblanc, S. G. (2002), Retrieval of vegetation clumping index using hot spot signatures measured by POLDER instrument. *Remote Sensing of Environment*, 79, 84-95.
- Lacaze, R., & Roujean, J.-L. (2001), G-function and HOt SpoT (GHOST) reflectance model: application to multi-scale airborne POLDER measurements. *Remote Sensing of Environment*, 76, 67-80.
- Lee, K.-S., Cohen, W. B., Kennedy, R. E., Maersperger, T. K., & Gower, S. T. (2004), Hyperspectral versus multispectral data for estimating leaf area index in four different biomes. *Remote Sensing of Environment*, 91, 508-520.
- Lenoble, J. (1985), *Radiative transfer in scattering and absorbing atmospheres: Standard computational procedures*. Hampton: A. Deepak Publishing, pp. 300.
- Lewis, P. (1999), Three-dimensional plant modelling for remote sensing simulation studies using the Botanical Plant Modelling System. *Agronomie*, 19, 185-210.
- Li-Cor (1983), *1800-12 Integrating sphere instruction manual*. Publication number 8305-0034.
- Liang, S. (2004), *Quantitative remote sensing of land surfaces*. Hoboken, New Jersey John Wiley & Sons, pp. 534.
- Liang, S., & Strahler, A., H. (1993), Calculation of the angular radiance distribution for a coupled atmosphere and canopy. *IEEE Transactions on Geoscience and Remote Sensing*, 31, 491-502.
- Liang, S., & Strahler Alan, H. (1994a), Four-stream solution for atmospheric radiative transfer over a non-Lambertian surface. *Applied Optics*, 33, 5745-5753.
- Liang, S., & Strahler Alan, H. (1994b), Retrieval of surface BRDF from multiangle remotely sensed data. *Remote Sensing of Environment*, 50, 18-30.
- Liang, S., & Townshend, J. R. G. (1996a), A modified hapke model for soil bidirectional reflectance. *Remote Sensing of Environment*, 55, 1-10.
- Liang, S., & Townshend, J. R. G. (1996b), A parametric soil BRDF model: A four stream approximation for multiple scattering. *International Journal of Remote Sensing*, 17, 1303-1315.
- Liang, S. L., & Strahler, A. H. (1995), An analytic radiative-transfer model for a coupled atmosphere and leaf canopy. *Journal of Geophysical Research-Atmospheres*, 100, 5085-5094.
- Lillesand, T. M., & Kiefer, R. W. (1994), *Remote sensing and image interpretation*. New York: John Wiley & Sons, Inc., pp. 724.
- Marceau, D. J., & Hay, G. J. (1999), Remote sensing contributions to the scale issue. *Canadian Journal of Remote Sensing*, 25, 357-366.
- Marchuk, G. I., & Lebedev, V. I. (1971), *The numerical methods in the neutron transport theory*. Moscow, (in Russian): Atomizdat.
- Mishchenko, M. I., Dlugach, J. M., Yanovitskij, E. G., & Zakharova, N. T. (1999), Bidirectional reflectance of flat, optically thick particulate layers: an efficient radiative transfer solution and applications to snow and soil surfaces. *Journal of Quantitative Spectroscopy and Radiative Transfer*, 63, 409-432.

- Myneni, R. B. (1991), Modeling Radiative-Transfer and Photosynthesis in 3-Dimensional Vegetation Canopies. *Agricultural and Forest Meteorology*, 55, 323-344.
- Myneni, R. B., & Asrar, G. (1991), Photon Interaction Cross-Sections for Aggregations of Finite-Dimensional Leaves. *Remote Sensing of Environment*, 37, 219-224.
- Myneni, R. B., Asrar, G., & Hall, F. G. (1992), A 3-dimensional radiative-transfer method for optical remote-sensing of vegetated land surfaces. *Remote Sensing of Environment*, 41, 105-121.
- Myneni, R. B., Asrar, G., & Kanemasu, E. T. (1987), Light scattering in plant canopies: The method of Successive Orders of Scattering Approximations (SOSA). *Agricultural and Forest Meteorology*, 39, 1-12.
- Myneni, R. B., & Ganapol, B. D. (1991), A Simplified Formulation of Photon Transport in Leaf Canopies with Scatterers of Finite Dimensions. *Journal of Quantitative Spectroscopy & Radiative Transfer*, 46, 135-140.
- Myneni, R. B., Gutschick, V. P., Asrar, G., & Kanemasu, E. T. (1988), Photon transport in vegetation canopies with anisotropic scattering Part IV. Discrete-ordinates/exact-kernel technique for two-angle photon transport in slab geometry. *Agricultural and Forest Meteorology*, 42, 101-120.
- Myneni, R. B., Marshak, A. L., & Knyazikhin, Y. V. (1991), Transport-Theory for a Leaf Canopy of Finite-Dimensional Scattering Centers. *Journal of Quantitative Spectroscopy & Radiative Transfer*, 46, 259-280.
- Myneni, R. B., & Ross, J. (1991), *Photon - vegetation interactions : applications in optical remote sensing and plant ecology*. Berlin Springer-Verlag, pp. 565.
- Myneni, R. B., Ross, J., & Asrar, G. (1989), A review on the theory of photon transport in leaf canopies. *Agricultural and Forest Meteorology*, 45, 1-153.
- Nicodemus, F. E., Richmond, J. C., Hsia, J. J., Ginsberg, I. W., & Limperis, T. (1977), Geometrical considerations and nomenclature for reflectance. *Natl Bur Stand (US) Monogr*, 52.
- Nilson, T. (1971), A theoretical analysis of the frequency of gaps in plant stands. *Agricultural and Forest Meteorology*, 8, 25-38.
- Nilson, T., & Peterson, U. (1991), A forest canopy reflectance model and a test case. *Remote Sensing of Environment*, 37, 131-142.
- Olea, R. A. (1991), *Geostatistical glossary and multilingual dictionary : members of the 1984 - 1989 IAMG Committee on Geostatistics*. New York Oxford University Press, pp. 177.
- Pinty, B., Gobron, N., Widlowski, J. L., Gerstl, A. W., Verstraete, M. M., Antunes, M., Bacour, C., Gascon, F., Gastellu, J. P., Goel, N., Jacquemoud, S., North, P., Qin, W., & Thompson, R. (2001), Radiation transfer model intercomparison (RAMI) exercise. *Journal of Geophysical Research D: Atmospheres*, 106, 11937-11956.
- Pinty, B., Widlowski, J. L., Taberner, M., Gobron, N., Verstraete, M. M., Disney, M., Lewis, P., Gascon, F., Gastellu, J. P., Jiang, L., Li, X., Su, L., Tang, S., Wang, H., Wang, J., Yan, G., Zang, H., Kuusk, A., Nilson, T., Ni-Meister, W., North, P., Qin, W., Thompson, R., & Verhoef, W. (2004), RADIATION Transfer Model Intercomparison (RAMI) exercise: Results from the second phase. *Journal of Geophysical Research D: Atmospheres*, 109, 1-19.
- Qin, W., & Gerstl, S. A. W. (2000), 3-D scene modeling of semidesert vegetation cover and its radiation regime. *Remote Sensing of Environment*, 74, 145-162.
- Qin, W., Gerstl, S. A. W., Deering, D. W., & Goel, N. S. (2002), Characterizing leaf geometry for grass and crop canopies from hotspot observations: A simulation study. *Remote Sensing of Environment*, 80, 100-113.
- Qin, W., & Xiang, Y. (1994), On the hotspot effect of leaf canopies: Modeling study and influence of leaf shape. *Remote Sensing of Environment*, 50, 95-106.
- Quattrochi, D. A. (1993), The need for a lexicon of scale terms in integrating remote-sensing data with geographic information-systems. *Journal of Geography*, 92, 206-212.

- Schaepman-Strub, G., Schaepman, M. E., Painter, T., Dangel, S., Martonchik, J. V., & Verstraete, M. (2004), Review of reflectance nomenclature used in optical remote sensing with quantitative comparisons. Zurich: Remote Sensing Laboratories, University of Zurich, 73-110.
- Schaepman, M. E., Koetz, B., Schaepman-Strub, G., & Itten, K. I. (2005), Spectrodirectional remote sensing for the improved estimation of biophysical and -chemical variables: two case studies. *International Journal of Applied Earth Observation and Geoinformation*, 6, 271-282.
- Schönermark, M. v., Geiger, B., & Roser, H. P. (2004), *Reflection properties of vegetation and soil*. Berlin: Wissenschaft und Technik Verlag, pp. 352.
- Shabanov, N. V., Knyazikhin, Y., Baret, F., & Myneni, R. B. (2000), Stochastic modeling of radiation regime in discontinuous vegetation canopies. *Remote Sensing of Environment*, 74, 125-144.
- Shultis, J. K., & Myneni, R. B. (1988), Radiative transfer in vegetation canopies with anisotropic scattering. *Journal of Quantitative Spectroscopy and Radiative Transfer*, 39, 115-129.
- Sobolev, V. V. (1975), *Light scattering in planetary atmospheres*. New York: Pergamon Press.
- Stamnes, K., Tsay, S. C., Wiscombe, W., & Jayaweera, K. (1988), Numerically Stable Algorithm for Discrete-Ordinate-Method Radiative-Transfer in Multiple-Scattering and Emitting Layered Media. *Applied Optics*, 27, 2502-2509.
- Steven, M. D. (1998), The sensitivity of the OSAVI vegetation index to observational parameters. *Remote Sensing of Environment*, 63, 49-60.
- Suits, G. H. (1971-1973), The calculation of the directional reflectance of a vegetative canopy. *Remote Sensing of Environment*, 2, 117-125.
- Tate, N. J., & Atkinson, P. M. (2001), *Modelling scale in geographical information science*. New York: John Wiley & Sons, Ltd.
- Tucker, C. J. (1979), Red and photographic infrared linear combinations for monitoring vegetation. *Remote Sensing of Environment*, 8, 127-150.
- Turner, D. P., Cohen, W. B., Kennedy, R. E., Fassnacht, K. S., & Briggs, J. M. (1999), Relationships between Leaf Area Index and Landsat TM Spectral Vegetation Indices across Three Temperate Zone Sites. *Remote Sensing of Environment*, 70, 52-68.
- Ustin, S. L., Jacquemoud, S., & Govaerts, Y. (2001), Simulation of photon transport in a three-dimensional leaf: Implications for photosynthesis. *Plant, Cell and Environment*, 24, 1095-1103.
- Verhoef, W. (1984), Light-scattering by leaf layers with application to canopy reflectance modeling - the Sail model. *Remote Sensing of Environment*, 16, 125-141.
- Wang, Q., Tenhunen, J., Falge, E., Bernhofer, C., Granier, A., & Vesala, T. (2004), Simulation and scaling of temporal variation in gross primary production for coniferous and deciduous temperate forests. *Global Change Biology*, 10, 37-51.
- Widlowski, J. L., Pinty, B., Lavergne, T., Verstraete, M. M., & Gobron, N. (2005), Using 1-D models to interpret the reflectance anisotropy of 3-D canopy targets: Issues and caveats. *Ieee Transactions on Geoscience and Remote Sensing*, 43, 2008-2017.
- Williams, J. (1995), *Geographic information from space. Processing and application of geocoded satellite images*. Chichester, etc.: John Wiley & Sons, pp. 210.
- Woodcock, C. E., & Strahler, A. H. (1987), The factor of scale in remote sensing. *Remote Sensing of Environment*, 21, 311-332.
- Zarco-Tejada, P. J., Miller, J. R., Noland, T. L., Mohammed, G. H., & Sampson, P. H. (2001), Scaling-up and model inversion methods with narrowband optical indices for chlorophyll content estimation in closed forest canopies with hyperspectral data. *Ieee Transactions on Geoscience and Remote Sensing*, 39, 1491-1507.

## CHAPTER 3

### **Applicability of the PROSPECT model for Norway spruce needles**

Reprint of:<sup>†</sup>

Malenovský, Z., Albrechtová, J., Lhotáková, Z., Zurita-Milla, R., Clevers, J.G.P.W., Schaepman, M.E., Cudlín, P.: Applicability of the PROSPECT model for Norway spruce needles. *International Journal of Remote Sensing*, in press.

---

<sup>†</sup> Reprinted with permission from Taylor & Francis © 2006. This article has been accepted for publication in a forthcoming issue of *International Journal of Remote Sensing*. IJRS is available online at <http://www.journalsonline.tandf.co.uk/openurl.asp?genre=journal&issn=0143-1161>.

## Abstract

---

The potential applicability of the leaf radiative transfer model PROSPECT (version 3.01) was tested for Norway spruce (*Picea abies* (L.) Karst.) needles collected from stress resistant and resilient trees. Direct comparison of the measured and simulated leaf optical properties between 450–1000 nm revealed the requirement to recalibrate the PROSPECT chlorophyll and dry matter specific absorption coefficients  $k_{ab}(\lambda)$  and  $k_m(\lambda)$ . The subsequent validation of the modified PROSPECT (version 3.01.S) showed close agreement with the spectral measurements of all three needle age-classes tested; the root mean square error (RMSE) of all reflectance ( $\rho$ ) values within the interval of 450–1000 nm was equal to 1.74%, for transmittance ( $\tau$ ) it was 1.53% and for absorbance ( $\alpha$ ) it was 2.91%. The total chlorophyll concentration, dry matter content, and leaf water content were simultaneously retrieved by a constrained inversion of the original PROSPECT 3.01 and the adjusted PROSPECT 3.01.S. The chlorophyll concentration estimated by inversion of both model versions was similar, but inversion accuracy of the dry matter and water content was significantly improved. Decrease in RMSE from 0.0079 g.cm<sup>-2</sup> to 0.0019 g.cm<sup>-2</sup> for dry matter and from 0.0019 cm to 0.0006 cm for leaf water content proved the better performance of the recalibrated PROSPECT version 3.01.S.

*Keywords:* PROSPECT model, Norway spruce needles, leaf optical properties, retrieval of biochemical properties.

### 3.1 Introduction

Norway spruce (*Picea abies* (L.) Karst.) is one of the most abundant tree species of natural montane forest ecosystems and is predominant in the Euro-Asian boreal biome (taiga), which represents about 20% of the world's landmass (Walker & Kenkel, 2000). Recent radiative transfer modelling of coniferous forests at the canopy (Kuusk & Nilson, 2000; Fang et al., 2003; Kotz et al., 2004; Smolander & Stenberg, 2005) as well as shoot level (Smolander & Stenberg, 2003; Rautiainen & Stenberg, 2005), along with current approaches in quantitative remote sensing (RS) (Fernandes et al., 2004; Gamon et al., 2004; Peddle et al., 2004; Schaepman et al., 2005) can provide biochemical and biophysical parameters of boreal forest stands. These quantitative characteristics, like leaf area index (LAI) or clumping of the vegetation foliage, are required as input into physiological models, for instance photosynthetic models used for estimation and mapping the net primary productivity (NPP) as an important component of the terrestrial carbon cycle (Lacaze et al., 2002; Chen et al., 2003). Retrieval of quantitative parameters from optical remote sensing data through radiative transfer modelling needs properly measured and/or simulated optical properties of the conifer assimilatory organs-needles (Nilson et al., 2003; Widen, 2004). Use of inappropriate leaf optical properties may directly lead to under- or over-estimation of the reflectance modelled by the radiative transfer models at the shoot and/or canopy level, especially within near- . Consequently, the estimation of quantitative parameters obtained through inversion of these radiative transfer models may lead to large uncertainties (Asner et al., 1998), rendering these variables useless for further parameterization of the vegetation physiological models.

Direct measurement of the optical properties of a coniferous leaf is a difficult task due to the small size and specific acicular shape of needles. One of the first methods was proposed by Daughtry et al. (2000a) and was subsequently improved by Middleton et al. (1997) and Mesarch et al. (1999). Improvements included mainly direct computation of the gap fraction (GF) between measured needles, placed one by one in the field of view, by means of image analysis. This approach allows the measurement of both sides of the same needles, and avoids the assumption of zero transmittance at 680 nm. Harron and Miller (1995a) designed a special carrier for conifer needles in order to avoid gaps between the needles, and thus the necessity of the GF estimation. This solid carrier was designed to suppress specular light scattered from the curved needle surface, which escapes from the integrating sphere during the reflectance measurement, and which is introduced into the sphere during the transmittance measurement. Considering all the mentioned difficulties and uncertainties related to the needle optical property measurements, it is worth thinking about a proper leaf radiative transfer model, e.g. the PROSPECT model, simulating leaf optical properties using measurable leaf structural characteristics and foliar chemistry.

PROSPECT is a radiative transfer model to simulate optical properties of individual leaves based on biophysical and biochemical parameters developed by Jacquemoud and Baret (1990). Nowadays, it is a widely used model in radiative transfer modelling (Jacquemoud et al., 2000; Pinty et al., 2001; Verhoef & Bach, 2003) and has become an important basis for quantitative RS approaches (Gastellu-Etchegorry & Bruniquel-Pinel, 2001; Combal et al., 2003; Zarco-Tejada et al., 2003b; Zarco-Tejada et al., 2004b). PROSPECT's base lies in the generalized "plate model" of Allen et al. (1970), which considers a compact theoretical plant leaf as a transparent plate. The original "plate model" had three input parameters: a refractive

index of material  $n$ , an incidence angle  $\alpha$ , and a transmission coefficient  $\theta$ . Allen et al.'s model had to be generalized, because its scheme of a unique compact layer did not work properly for case of dicotyledonous leaves. A leaf was assumed to be a pile of  $N$  homogeneous plates separated by  $N-1$  air spaces. Then the scattering within a leaf was described by the refractive index  $n$  alone with a leaf mesophyll structure parameter  $N$ .

The latest version of the PROSPECT model (3.01; from May 1998) allows the hemispherical reflectance and transmittance spectra from 400 to 2500 nm to be computed for different kinds of leaves using just four input variables: leaf mesophyll structure parameter  $N$ , chlorophyll concentration  $C_{ab}$ , water depth  $C_w$ , and the dry matter concentration  $C_m$ . A spectral absorption coefficient  $k_0(\lambda)$  of a fresh leaf for a given wavelength is modelled by the equation:

$$k_0(\lambda) = k_e(\lambda) + \left( \frac{C_{ab} \cdot k_{ab}(\lambda) + C_w \cdot k_w(\lambda) + C_m \cdot k_m(\lambda)}{N} \right) \quad (3.1)$$

where  $k_{ab}(\lambda)$ ,  $k_w(\lambda)$ , and  $k_m(\lambda)$  are the specific absorption coefficients of chlorophyll a+b, water, and dry matter, respectively.  $k_e(\lambda)$  explains the non-zero absorption of an albino leaf up to a wavelength of 480 nm. The specific absorption coefficient  $k_{ab}(\lambda)$  models absorption for wavelengths between 400–750 nm,  $k_w(\lambda)$  between 950–2500 nm, and  $k_m(\lambda)$  for the whole spectrum of 400–2500 nm. These coefficients might be deduced by means of optical spectral measurements of pure substances or by the measurement of the absorption coefficients  $k_0(\lambda)$  together with concentrations of the fresh leaf components (Jacquemoud et al., 1996).

To date, the PROSPECT model is widely used in numerous studies because of its simplicity, low number of inputs and inversion ability. It has been applied to simulate leaf optical properties of broadleaf canopies (Jacquemoud et al., 1995; Lelong et al., 1998; Demarez & Gastellu-Etchegorry, 2000; Combal et al., 2003) as well as coniferous trees (Kotz et al., 2004; Rautiainen et al., 2004; Zarco-Tejada et al., 2004a). The model was also used within calibration studies concerning requirements for airborne imaging spectrometers (Schaepman et al., 2002; Schläpfer & Schaepman, 2002). Most recently, PROSPECT served as a base to build the leaf part of an integrated vegetation fluorescence leaf-canopy model called FluorMOD (Miller et al., 2003; Miller et al., 2005).

PROSPECT validation for deciduous trees was carried out by le Maire et al. (2004). However, so far no validation of the PROSPECT model for Norway spruce needles has been reported (Jacquemoud, personal communication). Therefore, we have tested the ability of the PROSPECT model to correctly generate hemispherical reflectance and transmittance signatures of Norway spruce needles as the first objective of this study. It was subsequently found that the current PROSPECT version 3.01 is not fully applicable for Norway spruce needles. Hence, we proposed an update of the model as the second study objective, producing a new PROSPECT version signed 3.01.S. The update aimed to employ PROSPECT modifications enabling the accurate simulation of optical properties of the first three needle age-classes. This adjustment was meant to give a base for a PROSPECT version suitable for retrieval of the quantitative parameters of a spruce canopy from optical remote sensing data. It is important to mention that the PROSPECT update and validation was carried out for a limited range of wavelengths from 450–1000 nm. This limited spectral range was introduced by the use of a LI-COR spectroradiometer LI-1800-22, measuring optical properties only within the wavelengths from 400 to 1100 nm, and a high level of noise within the spectral intervals of 400–450 nm and 1000–1100 nm. The additional objective of the study was to



validate the PROSPECT up-date by: (i) direct comparison of the measured and PROSPECT simulated spectral signatures, and (ii) estimation of the biochemical leaf constituent concentrations from measured needle spectra through inversion of the original and newly updated PROSPECT.



Figure 3.1. General location of the study area at the Šumava Mts., Czech Republic (close to the Modrava village).

## 3.2 Material and Methods

### 3.2.1 Study site and sampling set-up

A dataset of measured leaf optical properties, along with biochemical and biophysical characteristics of spruce needles, was acquired for mountain forest stands of the Šumava Mts. (National Park, southern Czech Republic), close to the village Modrava (48° 59' N, 13° 28' E; figure 3.1). Fifteen stress resistant (RN) and fifteen stress resilient (RT) Norway spruce trees (*Picea Abies* (L.) Karst.) were selected at the study area. Crowns of the RN trees contain mainly original 'primary' shoots and less than 50% of proventitious 'secondary' shoots (Gruber, 1994), thus they are called resistant, non-transformed (Malenovský et al., 2006). The architecture of the RT crowns (resilient, transformed trees) was transformed by more than 50% of 'secondary' shoots, which were formed as a result of regeneration after increasing stress impact. The total defoliation of the production crown part for both stress categories varied between 30 and 35%, and so the microclimatic conditions inside the crowns were expected to be similar. Two branches were cut off by a tree-climber from the south side of each sample crown during the period 5–15 September 2002. The first branch was always taken from the top part of the crown (called the 'juvenile' part) and the second branch from the upper level of the most effective functional crown part, called the 'production' part (Malenovský et al., 2006). The architecture of each branch was described immediately after collection and shoots of the last three age-classes (current year = C, two growing periods old = C+1, and three growing periods old = C+2) were detached according to the sampling scheme in table 3.1. In total 221 shoot samples were placed into zip-lock plastic bags together

with a wet pulp paper and transferred to the laboratory in a dark portable cooler with frozen blue ice (about -4° C). There they were stored in a dark and cold chamber by -16° C, and processed within 24 hours.

Table 3.1. Sampling scheme applied on the selected Norway spruce trees and the average properties per homogeneous unit (values in parentheses are standard deviations).

Average sample parameters	RN <sup>♦</sup> trees		RT <sup>♦♦</sup> trees		
	Juvenile <sup>*</sup> Primary <sup>+</sup>	Production <sup>**</sup> Primary	Juvenile Primary	Production Primary	Secondary <sup>++</sup>
<b>C needles</b>					
No. of samples	15	15	15	14	15
Thickness [cm]	0.108 (0.010)	0.107 (0.011)	0.106 (0.009)	0.095 (0.012)	0.095 (0.010)
C <sub>w</sub> [cm] <sup>1</sup>	0.063 (0.006)	0.063 (0.007)	0.061 (0.008)	0.051 (0.015)	0.057 (0.009)
Hemispherical-surface [cm <sup>2</sup> ]	1.510 (0.311)	1.465 (0.332)	1.566 (0.299)	1.286 (0.197)	1.416 (0.254)
C <sub>m</sub> [mg/cm <sup>2</sup> ] <sup>2</sup>	25.4 (2.8)	26.0 (2.9)	24.7 (3.2)	24.3 (6.7)	21.7 (2.9)
C <sub>xc</sub> [µg/cm <sup>2</sup> ] <sup>3</sup>	6.62 (0.82)	6.67 (1.47)	5.95 (1.32)	5.54 (1.48)	5.22 (1.42)
C <sub>ab</sub> [µg/cm <sup>2</sup> ] <sup>4</sup>	51.80 (7.75)	50.04 (9.84)	43.3 (10.85)	39.19 (11.6)	38.85 (10.37)
<b>C+1 needles</b>					
No. of samples	15	15	15	14	14
Thickness [cm]	0.110 (0.014)	0.111 (0.009)	0.104 (0.011)	0.095 (0.015)	0.099 (0.010)
C <sub>w</sub> [cm]	0.062 (0.009)	0.064 (0.008)	0.056 (0.007)	0.049 (0.016)	0.056 (0.009)
Hemispherical-surface [cm <sup>2</sup> ]	1.615 (0.323)	1.468 (0.363)	1.457 (0.259)	1.334 (0.369)	1.401 (0.291)
C <sub>m</sub> [mg/cm <sup>2</sup> ]	28.4 (4.1)	28.4 (4.9)	27.1 (2.9)	25.3 (8.0)	24.8 (3.3)
C <sub>xc</sub> [µg/cm <sup>2</sup> ]	10.06 (2.16)	9.87 (2.14)	7.95 (1.75)	7.12 (2.11)	7.10 (1.87)
C <sub>ab</sub> [µg/cm <sup>2</sup> ]	72.32 (15.72)	67.71 (14.93)	55.11 (14.16)	48.74 (16.46)	50.41 (13.62)
<b>C+2 needles</b>					
No. of samples	15	15	15	14	15
Thickness [cm]	0.107 (0.012)	0.102 (0.011)	0.101 (0.010)	0.090 (0.013)	0.092 (0.009)
C <sub>w</sub> [cm]	0.056 (0.007)	0.054 (0.006)	0.053 (0.006)	0.047 (0.007)	0.050 (0.009)
Hemispherical-surface [cm <sup>2</sup> ]	1.388 (0.240)	1.241 (0.221)	1.252 (0.240)	1.241 (0.198)	1.230 (0.242)
C <sub>m</sub> [mg/cm <sup>2</sup> ]	29.3 (3.3)	28.4 (3.2)	28.1 (4.4)	23.4 (3.3)	24.9 (4.4)
C <sub>xc</sub> [µg/cm <sup>2</sup> ]	13.27 (1.74)	12.88 (2.20)	10.47 (1.90)	8.92 (1.87)	9.68 (2.84)
C <sub>ab</sub> [µg/cm <sup>2</sup> ]	89.56 (13.00)	86.75 (13.61)	70.70 (13.14)	59.14 (14.72)	65.49 (18.44)

♦ RN – multiple stress resistant trees

♦♦ RT – multiple stress resilient trees

\* Juvenile – upper juvenile part of the spruce crown (first 3-5 whorls)

\*\* Production – middle part of the spruce crown producing most of the assimilates

+ Primary – primary shoots growing from regular buds

++ Secondary – secondary shoots growing from proventitious buds

According to Gruber (1994).

<sup>1</sup> C<sub>w</sub> – thickness of water inside of needles

<sup>2</sup> C<sub>m</sub> – dry matter content

<sup>3</sup> C<sub>xc</sub> – concentration of the total carotenoids

<sup>4</sup> C<sub>ab</sub> – concentration of the chlorophylls a + b

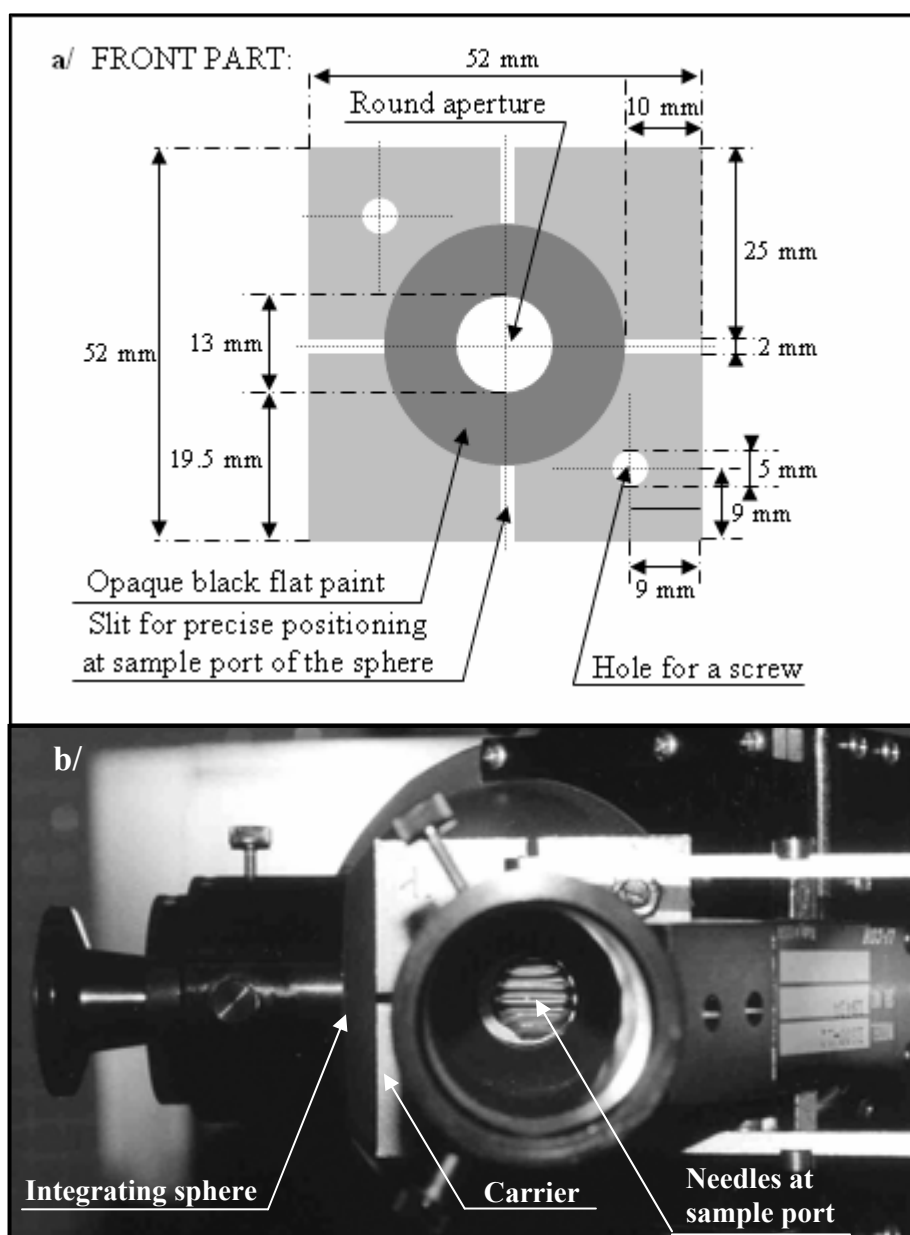


Figure 3.2. A universal carrier of conifer needles used for measurement of the directional hemispherical optical properties in a LI-COR integrating sphere LI-1800-12: a/ technical layout; b/ sample needles mounted in the universal carrier, placed at the sample port of the integrating sphere LI-1800-12 and illuminated in the reflectance measurement mode.

### 3.2.2 *Laboratory measurement of the foliar pigments*

The concentrations of the chlorophyll *a* and *b* ( $C_{ab}$ ) and the total amount of carotenoids ( $C_{xc}$ ) in spruce needles were determined spectrophotometrically (details in Soukupova et al., 2001). About 50 needles of each sampled age-class were cut off in the field from the same shoots as used for needle optical properties measurements. They were put into micro-tubes,

packed into a dark cloth and transported in a portable cooler with frozen blue ice (about -4°C) to the laboratory (Entcheva Campbell et al., 2004). There they were weighted and frozen at -70 C. On average, 0.5 g of sampled frozen needles was placed in 10 ml dimethylformamide (DMF) (Porra et al., 1989) and left in the dark at 8°C for five days until the needles were bleached. The absorbance of the extracts was then measured at wavelengths of 480 nm, 647 nm, and 664 nm using a Unicam Helio  $\alpha$  spectrophotometer (Helios alpha, Unicam Ltd., Cambridge, UK). Finally, chlorophyll and carotenoid concentrations were calculated according to the equations of Wellburn (1994).

### 3.2.3 *Measurement protocol of the optical and biophysical properties of spruce needles*

The original *Daughtry's method* (Daughtry et al., 2000a) was adapted to measure optical properties of the sampled Norway spruce needles. We used the LI-COR spectroradiometer LI-1800-22 (Li-Cor, Inc., Lincoln, NE, USA) coupled with an integrating sphere LI-1800-12 (Li-Cor, 1983) to measure spruce needle hemispherical reflectance and transmittance between 400-1100 nm with a wavelength interval of 5 nm. The diameter of the sample port of the integrating sphere LI-1800-12 is 14.5 mm. We found out that in some cases the spruce needles were shorter than the sample port diameter, and they were so thin that inner-element gaps between needles were unavoidable. Therefore, we designed a universal foliar element carrier for all lengths of spruce needles. A detailed technical description of the carrier is available in figure 3.2a. Mostly six needles, seven or even eight needles in case of extremely thin or short leaves, were cut off from each year-class shoot. Consequently, they were mounted between two identical frame pieces using both tips if they were longer than 13 mm, or mounted “zigzag” by only one tip when they were shorter than 13 mm. The carrier was precisely placed at the position of the sample port of the integrating sphere using four orienting slits and corresponding marks on the sphere shell, and reflectance and/or transmittance signatures were acquired (figure 3.2b). Consecutively, the carrier was precisely superposed by a black paper template mask with a 10.5 mm aperture in diameter for reflectance, and a 9 mm circular aperture for transmittance measurements, to compute the gap fraction (GF) between illuminated needles. They were scanned using a double lamp (to prevent the occurrence of needle object shadows in the taken pictures) desktop scanner HP ScanJet 5370C (Hewlett-Packard Company) at a resolution of 1200 dpi. Direct determination of the gap fraction was done by way of image processing, when the number of pixels of the total gap area between the sunlit needles was divided by the number of pixels of the total measured (illuminated) area. The maximal distance between sample elements was set equal to the width of the needles ( $GF < 0.50$ ); the gap fraction for all samples in reflectance mode was on average 0.40 and in transmittance mode it was 0.36.

Hemispherical reflectance and transmittance of sample needles was computed according to the following equations (Mesarch, et al., 1999):

$$\text{Reflectance} = \rho = \frac{\left( \frac{R_{\text{TOTAL}} - \text{STR}}{\text{REF} - \text{STR}} \right)}{(1 - \text{GF}_R)} \quad (3.2)$$

$$\text{Transmittance} = \tau = \left[ \left( \frac{T_{\text{TOTAL}}}{\text{REF} - \text{STR}} \right) - (\rho_w \text{GF}_T) \right] \frac{1}{(1 - \text{GF}_T)} \quad (3.3)$$

where  $R_{TOTAL}$  is the flux of radiation reflected from the sample in reflectance mode, STR is the flux of stray light radiation, REF is the flux of radiation reflected from a  $BaSO_4$  reference standard in reference mode,  $GF_R$  is the gap fraction of the sample in reflectance mode,  $T_{TOTAL}$  is the flux of radiation transmitted through the sample in transmittance mode,  $\rho_w$  is the reflectance of integrating sphere wall, and  $GF_T$  is the gap fraction of the sample in transmittance mode.

Stray light inside the integrating sphere was measured as a radiation flux of the empty illuminated sample port in reflectance mode. The reflectance of the integrating sphere wall  $\rho_w$  was assumed to be 0.955. Elimination of random noise within the reflectance and transmittance spectral signatures was carried out by a Savitzky-Golay smoothing filter (Savitzky & Golay, 1964) using a second order polynomial function with a bandwidth of 15 nm (Demetriades-Shah et al., 1990; Zarco-Tejada, 2000).

The biophysical characteristics required for leaf radiative transfer modelling were acquired simultaneously with the measurement of needle spectra (table 3.1). The surface of six sampled needles had been dried by pulp paper and their fresh matter was weighed before the spectral measurement. Then the needles were scanned using the HP double lamp desktop scanner at a resolution of 1200 dpi and the needle projections were computed from the greyscale images using an image processing technique. The total surface of needles was calculated as a projected area multiplied by a universal conversion factor of 2.57 derived experimentally for Norway spruce needles by Waring (1983). Finally, the total needle surface area was divided by two to acquire the hemispherical-surface projection of sample needles (Pokorny & Marek, 2000). After the spectral measurements, the thickness of the leaves was measured by a micrometer and the average thickness was computed for each sample. Finally, the needle samples were oven-dried at 60° C for 48 hours and their dry biomass was weighed.

#### 3.2.4 *Set-up of methodology for PROSPECT applicability analyses*

We present an overview of the basic methodological steps for testing the applicability of the PROSPECT model for Norway spruce needles in figure 3.3. In the first step, the suitability of the original PROSPECT model was verified using a training sample set. Since the current version of model was not found to be fully applicable for spruce leaves, a recalibration of the specific absorption coefficients was pursued. The validation of the updated model version was carried out using a set of samples for direct and inverse runs of the model.

#### 3.2.5 *Verification of PROSPECT for Norway spruce needles*

A first hypothesis considered the PROSPECT model version 3.01 being directly applicable for simulating optical properties of Norway spruce needles within the wavelength range 450-1000 nm. It is important to mention that the wavelength interval ranging from 400-450 nm and 1000-1100 nm were excluded from the analyses due to high contamination by random noise generated during the spectroradiometric measurements. Forward simulations were conducted for 110 needle samples randomly selected from the spectral dataset forming the 'training' dataset (36 of C, 36 of C+1, and 38 of C+2 needle samples). Simulation results were directly compared with the spectral signatures measured in the laboratory using a LICOR spectroradiometer. Measured and simulated average leaf reflectance, transmittance, and absorption and their standard deviation were plotted for each wavelength. Also the root mean square errors (RMSE) was computed separately for the individual spectral signatures for each observed wavelength and finally used to validate the PROSPECT performance.

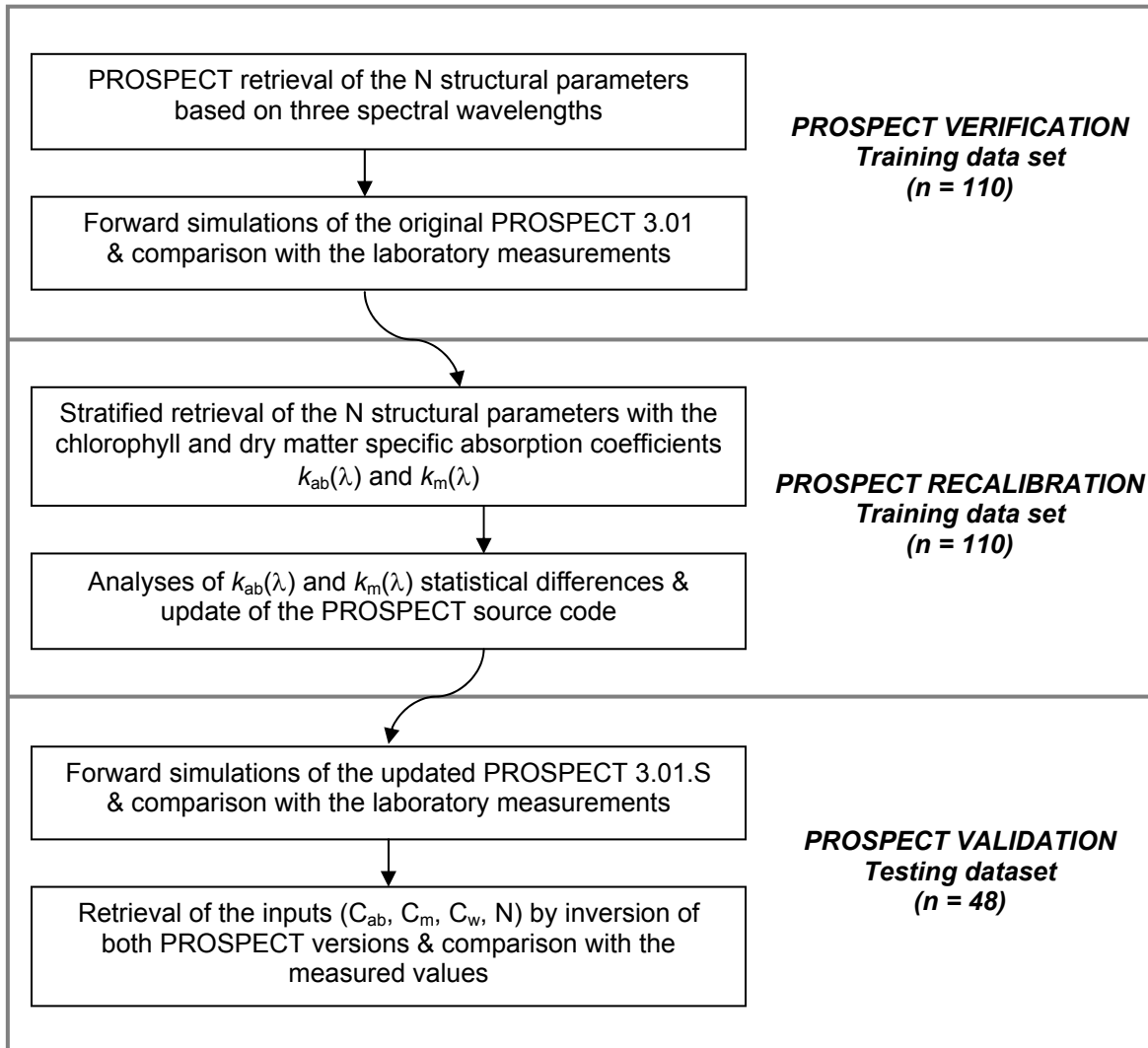


Figure 3.3. Flowchart of the basic methodological steps used in the study for verification, recalibration and validation of the original and updated PROSPECT source code (n is the number of the samples within each dataset).

All the PROSPECT input variables were obtained from the laboratory measurements except the structural parameter N. The wavelength independent empirical parameter N was retrieved for each Norway spruce sample through PROSPECT inversion as discussed in Demarez et al. (1999) and Zarco-Tejada et al. (2004a). The retrieval method was fully adopted from Jacquemoud et al. (1996), where three wavelengths corresponding to the maximum sample reflectance ( $\lambda_{\rho \max}$ ), transmittance ( $\lambda_{\tau \max}$ ), and absorption ( $\lambda_{\alpha \max}$ ) have been selected to determine the N parameter. These three wavelengths are located in the NIR plateau and may be confounded (Jacquemoud et al., 1996). The structural parameter N for each sample of the training dataset was retrieved by an iterative constrained nonlinear multivariable function

(Coleman & Li, 1996), searching the minimum of a root mean square error based merit function  $M_N$ :

$$M_N = \sqrt{\frac{\sum_{\lambda} [(\rho - \rho_{\text{PROSPECT}})_{\lambda}^2 + (\tau - \tau_{\text{PROSPECT}})_{\lambda}^2]}{n}} \quad (3.4)$$

where  $n = 3$  (three selected wavelengths  $\lambda$ ),  $\rho$  and  $\tau$ , and  $\rho_{\text{PROSPECT}}$  and  $\tau_{\text{PROSPECT}}$  are measured and PROSPECT generated sample reflectance and transmittance of the given wavelength  $\lambda$ . The N retrieval was constrained by a minimum and maximum value of 0.1 and 10.0 respectively.

### 3.2.6 *Stratified recalibration of PROSPECT specific absorption coefficients*

The necessity to recalibrate the original PROSPECT version for Norway spruce needles was identified during the first phase of the model verification process. A consecutive hypothesis proposed that parallel recalibration of the chlorophyll and dry matter specific absorption coefficients  $k_{\text{ab}}(\lambda)$  and  $k_{\text{m}}(\lambda)$  allows PROSPECT to simulate the spruce needle spectral characteristics with significant higher accuracy. A stratified approach was used to retrieve  $k_{\text{ab}}(\lambda)$  and  $k_{\text{m}}(\lambda)$  jointly with the N parameter from the optical properties of the training dataset. This approach was designed in three nested loops allowing for each needle sample (a first loop) the optimal N parameter (a second middle loop) and both of the specific absorption coefficients per investigated wavelengths (a third inner loop) to be obtained simultaneously. The N value was systematically varying between the lower and the higher limits, i.e. 1.5 and 3.0 respectively, in steps of 0.01. The  $k_{\text{ab}}(\lambda)$  and  $k_{\text{m}}(\lambda)$  values are optimized for each PROSPECT simulated wavelength  $\lambda$  between 450-1000 nm by the nonlinear multivariable function (Coleman & Li, 1996), searching for a local minimum of the following merit function  $M_{k_{\text{ab}}(\lambda), k_{\text{m}}(\lambda)}$ :

$$M_{k_{\text{ab}}(\lambda), k_{\text{m}}(\lambda)} = \sqrt{(\rho - \rho_{\text{PROSPECT}})_{\lambda}^2 + (\tau - \tau_{\text{PROSPECT}})_{\lambda}^2 + (\alpha - \alpha_{\text{PROSPECT}})_{\lambda}^2} \quad (3.5)$$

where  $\alpha$  is the measured needle absorption, and  $\alpha_{\text{PROSPECT}}$  is the simulated absorbance at a given wavelength  $\lambda$ . The upper and lower constraining limits of retrieved  $k_{\text{ab}}(\lambda)$  and  $k_{\text{m}}(\lambda)$  coefficients were defined by a 100% variation range of the original PROSPECT  $k_{\text{ab}}(\lambda)$  and  $k_{\text{m}}(\lambda)$  values. The specific absorption coefficients  $k_{\text{e}}(\lambda)$  and  $k_{\text{w}}(\lambda)$  as well as the refraction index  $n$  were assumed to be correct, and thus taken from the PROSPECT model. The concentrations of the required fresh leaf biochemical components were measured as input variables to the model. At the end of the third inner loop, the wavelength dependent sets of the specific spectral absorption coefficients were obtained by using 151 N values for all samples. The best fitting N value of each sample was found by minimizing equation 3.4 between three selected wavelengths of the optical properties measured and simulated using newly gained specific spectral absorption coefficients. The optimal  $k_{\text{ab}}(\lambda)$  and  $k_{\text{m}}(\lambda)$  values per sample were selected corresponding with the best fitting N parameter. Differences in mean  $k_{\text{ab}}(\lambda)$  and  $k_{\text{m}}(\lambda)$  computed for each needle year-class and stress class were assessed by a statistic paired *t*-test. A one-way ANOVA statistical test was performed to study significant differences of the retrieved N parameters in-between the three considered needle age-classes, the two functional crown parts, and the two spruce stress categories combined into the classes of shoot types. Finally, 'universal' N values were established by averaging and rounding the N values for

those needle classes, where the N parameters did not differ significantly according to the statistical test.

### 3.2.7 Validation of updated PROSPECT

The second collection of 48 measured needle optical properties (17 of C, 16 of C+1, and 15 of C+2 needles) was used as an independent ‘testing’ dataset to evaluate the accuracy of the up-dated PROSPECT labelled as 3.01.S. A PROSPECT database of the spruce specific absorption coefficients was produced for each needle year-class C, C+1, and C+2. First, a direct validation was performed by linear regression of all the wavelengths of measured and PROSPECT generated hemispherical  $\rho$ ,  $\tau$ , and  $\alpha$ , and computing the general RMSEs for all the wavelengths together. Then the average and standard deviation for each wavelength within the interval of interest (450-1000 nm) were compared by means of RMSE. The measured optical properties were also compared with simulations using the ‘universal’ N values, investigating the sensitivity of the PROSPECT output on the generalized structural parameter N.

The second part of the validation was dedicated to comparing the accuracy of the biochemical constituent quantities retrieved from the optical properties of the measured testing samples using the original 3.01 and the recalibrated 3.01.S PROSPECT models. All the PROSPECT inputs (total chlorophyll concentration  $C_{ab}$ , dry matter content  $C_m$ , water content  $C_w$ , and structural number N) were estimated concurrently using two different PROSPECT inversion approaches. The first (partially unconstrained) inversion used the  $M_j^{\text{spectral}}$  merit function based purely on the spectral (radiative) information of the samples:

$$M_j^{\text{spectral}} = \sqrt{\frac{\sum_{\lambda} [(\rho - \rho_{\text{PROSPECT}})_{\lambda}^2 + (\tau - \tau_{\text{PROSPECT}})_{\lambda}^2 + (\alpha - \alpha_{\text{PROSPECT}})_{\lambda}^2]}{n}}. \quad (3.6)$$

A rather complex merit function  $M_j^{\text{prior}}$ , also using measured ‘a priori’ information on the retrieved parameters, was applied as a second constrained PROSPECT inversion:

$$M_j^{\text{prior}} = \sqrt{\frac{\sum_{\lambda} [(\rho - \rho_{\text{PROSPECT}})_{\lambda}^2 + (\tau - \tau_{\text{PROSPECT}})_{\lambda}^2 + (\alpha - \alpha_{\text{PROSPECT}})_{\lambda}^2]}{n}} + \sqrt{\sum_j \left[ \frac{V_j - V_j^{\text{prior}}}{V_j^{\text{max}} - V_j^{\text{min}}} \right]} \quad (3.7)$$

where  $j$  are simultaneously retrieved variables  $C_{ab}$ ,  $C_m$ ,  $C_w$ , and N,  $V_j$  is the estimated value of the variable  $j$ ,  $V_j^{\text{prior}}$  is the measured prior value of the variable  $j$ , and  $V_j^{\text{max}}$  and  $V_j^{\text{min}}$  are the maximum and minimum values of the measured variable  $j$ . The iterative constrained nonlinear multivariable function (Coleman & Li, 1996) was again applied to find the lowest merit function values. The minimal and maximal input variable limits were in the case of  $M_j^{\text{spectral}}$  defined by an expert estimation based on literature references. In the case of  $M_j^{\text{prior}}$  they were computed from the measurements of the testing dataset samples (see table 3.2). Specification of the variable constraints is important to prevent a possibility of the so-called ‘ill-posed’ inversion problem (see Combal et al., 2003), especially if multiple variables are retrieved simultaneously. It is worth mentioning that all the variables were retrieved simultaneously, but from four different wavelength intervals, suitable for one particular variable only. The assessment of  $C_{ab}$  employed wavelengths of chlorophyll influence (i.e., 450-750 nm), the



estimation of  $C_m$  used all the wavelengths of interest of this study (450-1000 nm), water content  $C_w$  was estimated from the NIR wavelengths (950-1000 nm), and the parameter  $N$  was retrieved from three selected wavelengths of the maximal  $\rho$ ,  $\tau$ , and  $\alpha$ . The obtained results were plotted against the measured biochemical concentrations and compared by means of the RMSEs. The  $N$  parameters were compared with those retrieved for the direct PROSPECT simulations, in order to evaluate the  $N$  number stability.

### 3.3 Results

#### 3.3.1 Retrieved values of the $N$ parameter and PROSPECT suitability validation

Minimal, maximal, and mean values of the  $N$  structural parameters retrieved from the training dataset of the sampled Norway spruce needles were 1.72, 2.63, and 2.12, respectively. On the one hand the ANOVA statistical test did not show any significant difference between the  $N$  structural parameters of the three tested age-classes of needles. But on the other hand it showed a significantly lower  $N$  mean for needles from RT production crown part compared to needles from RN production crown part ( $\alpha = 0.005$ ). In particular, the needles from primary and secondary shoots of the RT trees ( $P_{RT}$ ,  $S_{RT}$  needles) had lower mean  $N$  values of 1.99 and 2.02 than primary needles from shoots of the RN trees ( $P_{RN}$  needles) with a mean  $N$  equal to 2.19. Mean  $N$  values of the juvenile crown parts of both stress response categories were similar and not significantly different from the other categories (see table 3.3).

Average hemispherical reflectance, transmittance, and absorption of the training samples and the PROSPECT simulations are depicted in figure 3.4abc. It is obvious that the spectral signatures are better matching within the visible part than within the near infrared part of the electromagnetic spectrum where a significant disagreement appeared. Figure 3.5a shows an average RMSE of  $\rho$  smaller than 2.0%, a RMSE for  $\tau$  smaller than 2.5%, and a RMSE of  $\alpha$  below 4.0%, for the spectral interval of 450-700 nm. For the wavelengths of 700-1000 nm the RMSE values of  $\rho$  and  $\tau$  varied between 5.0-8.0% and for  $\alpha$  the RMSE was for some wavelengths reaching almost 15.0%. The original PROSPECT model is systematically underestimating NIR values of  $\rho$  and  $\tau$  (figure 3.4ab), while  $\alpha$  was as a consequence overestimated (figure 3.4c). These results indicate unacceptable performance of the PROSPECT model for the case of Norway spruce needles.

Table 3.2. Boundary values for the biochemical and structural variables retrieved by means of the original and recalibrated PROSPECT inversions, using the  $M_j^{\text{spectral}}$  and  $M_j^{\text{prior}}$  retrieval functions.

Variable $j$	$M_j^{\text{spectral}}$		$M_j^{\text{prior}}$	
	<i>min</i>	<i>max</i>	<i>min</i>	<i>max</i>
$C_{ab}$ [ $\mu\text{g}/\text{cm}^2$ ]	10.0000	120.0000	25.5700	85.1000
$C_m$ [ $\text{mg}/\text{cm}^2$ ]	1.0000	100.0000	14.1000	41.9000
$C_w$ [cm]	0.0010	0.1000	0.0419	0.0701
$N$	0.5000	10.0000	0.5000	10.0000

### 3.3.2 *Adjusted specific absorption coefficients and new N parameters*

Based on a logical order, given later in the discussion part, it was decided to recalibrate PROSPECT by means of new specific absorption coefficients for dry matter  $k_m(\lambda)$  and simultaneously for chlorophyll  $k_{ab}(\lambda)$  by means of the stratified inversion retrieving also the N parameter. Figure 3.6a and figure 3.7a show that the retrieved  $k_m(\lambda)$  values are similar to the original values in the VIS wavelengths. However, strong differences were statistically proved between the three needle age-classes in the NIR part of the spectrum. The  $k_m(\lambda)$  differences for the shoot type stress-classes were insignificantly smaller and statistically negligible. Newly gained  $k_{ab}(\lambda)$  values were different for the needle age-classes as well as for some of the stress-classes within the spectral range of 450-700 nm (figure 3.6b and figure 3.7b).

New values of the structural parameter N were retrieved from the training samples by minimizing equation 3.5 during the stratified PROSPECT recalibration. New N numbers are in general lower than the originally estimated, especially for cases where values were higher than 2.00 (see figure 3.8). However, the ANOVA test yielded the same statistically significant differences for new as for old N values (table 3.3). It means that only the N numbers of stress resistant (RN) and stress resilient (RT) samples were statistically different. Concerning the stress-categories, only the mean N values of the P<sub>RN</sub> needles were significantly different from the mean N values of the P<sub>RT</sub> and S<sub>RT</sub> needles ( $\alpha$ -level = 0.005). The average 'universal' N parameters for each category were generated by rounding the newly retrieved N numbers (table 3.3).

Table 3.3. The values of the structural parameter N retrieved from optical properties of the training dataset by inversion of the original and recalibrated PROSPECT model. The universally identified (rounded) N values and statistically different categories (one-way ANOVA test;  $\alpha$ -level of significance = 0.005) are presented.

Category	<i>N</i> retrieved by PROSPECT 3.0I	<i>N</i> retrieved by PROSPECT 3.0I.S	Rounded 'universal' N (3.0I.S)	Statistically different from the category
Current needles (n=36)	2.1179	2.0681	2.07	-
Current+1 needles (n=36)	2.1510	2.1097	2.11	-
Current+2 needles (n=38)	2.0820	2.0618	2.06	-
RN <sup>♦</sup> (n=59)	2.1628	2.1232	2.12	RT
RT <sup>♦♦</sup> (n=51)	2.0626	2.0290	2.03	RN
J <sub>RN</sub> <sup>1</sup> (n=29)	2.1372	2.1013	2.10	-
P <sub>RN</sub> <sup>2</sup> (n=30)	2.1892	2.1459	2.15	P <sub>RT</sub> , S <sub>RT</sub>
J <sub>RT</sub> <sup>3</sup> (n=19)	2.1565	2.1147	2.12	-
P <sub>RT</sub> <sup>4</sup> (n=14)	1.9868	1.9579	1.96	P <sub>RN</sub>
S <sub>RT</sub> <sup>5</sup> (n=18)	2.0224	1.9939	1.99	P <sub>RN</sub>

♦ RN – multiple stress resistant trees

♦♦ RT – multiple stress resilient trees

(n = number of samples within the category)

<sup>1</sup> J<sub>RN</sub> – primary, stress resistant needle samples of the juvenile crown part

<sup>2</sup> P<sub>RN</sub> – primary, stress resistant needle samples of the production crown part

<sup>3</sup> J<sub>RT</sub> – primary, stress resilient needle samples of the juvenile crown part

<sup>4</sup> P<sub>RT</sub> – primary, stress resilient needle samples of the production crown part

<sup>5</sup> S<sub>RT</sub> – secondary (regenerative), stress resilient needle samples of the production crown part

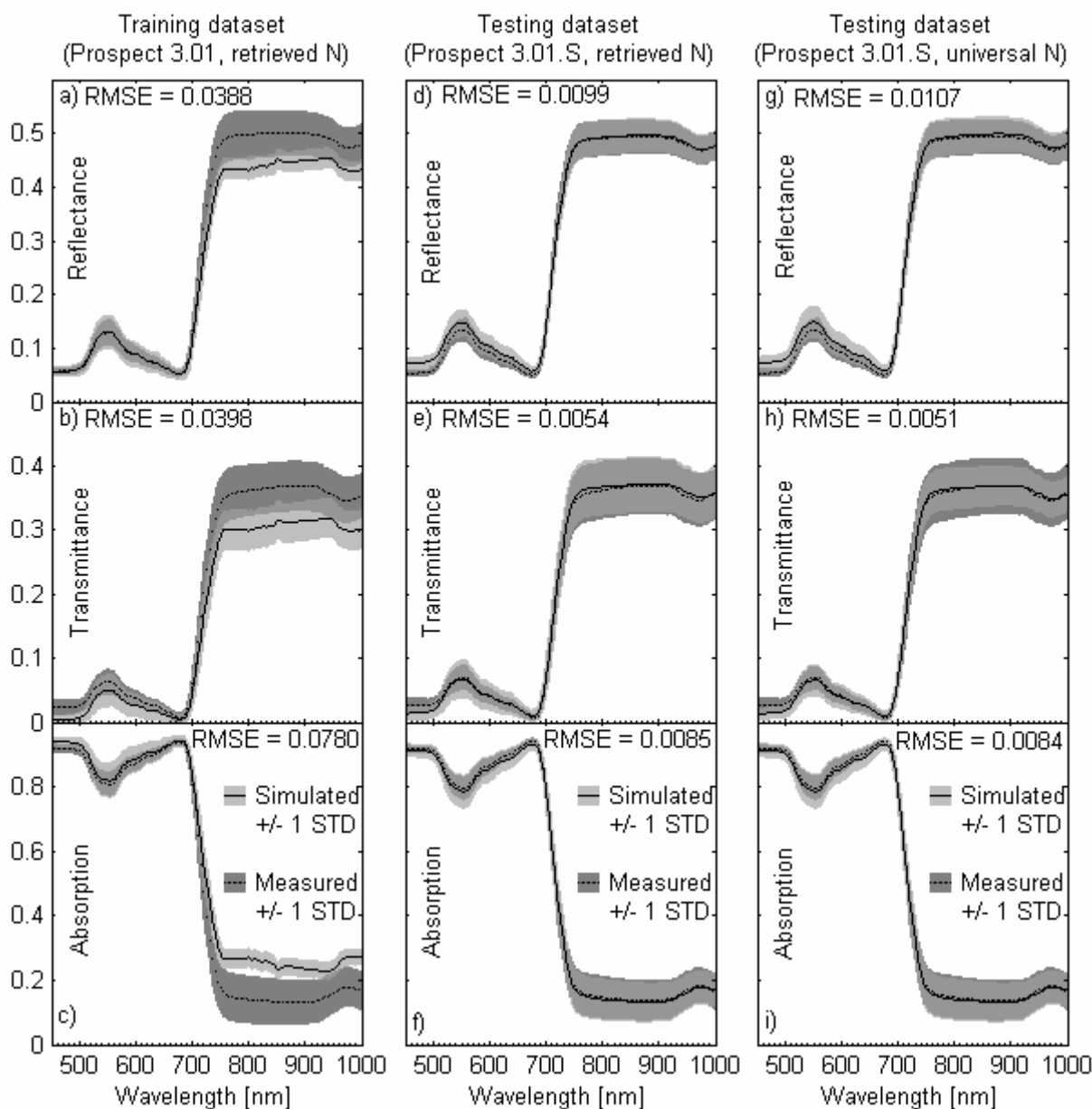


Figure 3.4. Direct comparison of the PROSPECT simulated and measured average optical properties of the training and testing dataset (solid grey areas represents +/- one standard deviation, RMSE = root mean square error). a), b), and c) show simulations of the original PROSPECT version 3.01 using the sample specific retrieved N values and inputs of the training sample set; d), e), and f) show results of the updated PROSPECT version 3.01.S using the sample specific retrieved N values; g), h), and i) show outputs of the updated PROSPECT version 3.01.S using the universally identified N values (see table 3.3).

### 3.3.3 Forward validation of the recalibrated PROSPECT model

The adjusted PROSPECT code was validated by forward simulations of the optical properties of the test dataset, using the retrieved (sample specific) as well as the ‘universal’ N

parameters. Figure 3.4def and 4ghi show means and standard deviations of simulated optical properties ( $\rho$ ,  $\tau$ , and  $\alpha$ ) that closely match the laboratory measurements. The simulations are comparable for both N parameters, the retrieved sample specific and ‘universal’ N. The average RMSEs computed for  $\rho$ ,  $\tau$ , and  $\alpha$  were equal or smaller than 1%. These positive results are supported also by the output of the linear regression computed between 5328 simulated and measured wavelengths of 48 test spectral signatures. Intercepts for the  $\rho$ ,  $\tau$ , and  $\alpha$  linear equations were about zero (0.016, -0.003 and -0.002, respectively), slopes were close to one (0.97, 1.02, and 0.99, respectively), and coefficients of determinations ( $R^2$ ) were in all three cases equal to 0.99. These results proved a close correlation between the new PROSPECT simulated and measured optical properties. Recalibration of the  $k_{ab}(\lambda)$  and  $k_m(\lambda)$  coefficients yielded comparable RMSE values within both the NIR and VIS wavelengths (see figure 3.9). The absorption RMSE values of the investigated spectral wavelengths were slightly above or below 3.0%. The RMSEs for the reflectance and transmittance signatures were even smaller (around or below 2.0% for the retrieved sample specific N parameter). As expected, the recalibrated PROSPECT model showed small sensitivity for the ‘universal’ N values generated from the training needle samples. The ‘universal’ N parameters did not influence the  $\alpha$  RMSE and slightly increased the RMSE of  $\rho$  and  $\tau$  compared to the retrieved sample specific N numbers (cf., figure 3.9a and b).

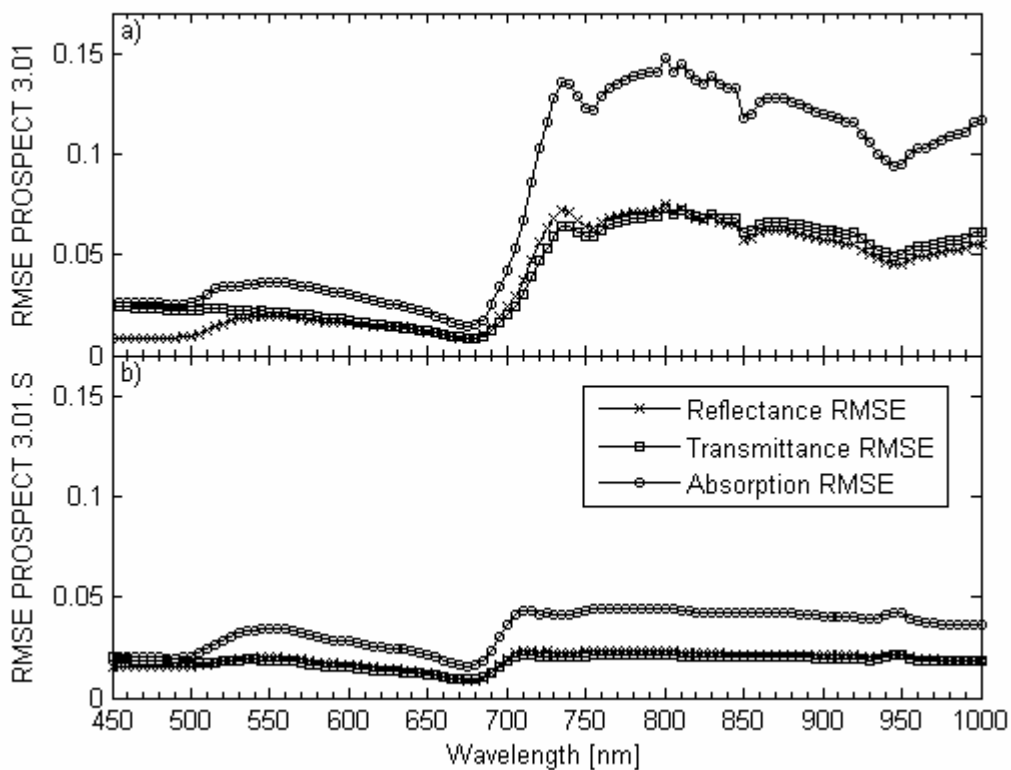


Figure 3.5. Mean root mean square errors (RMSE) for each of the investigated wavelength (450-1000 nm) computed between the reflectance, transmittance, and absorption values of the training dataset samples and values simulated by a) the original PROSPECT version 3.01; b) the recalibrated PROSPECT version 3.01.S.

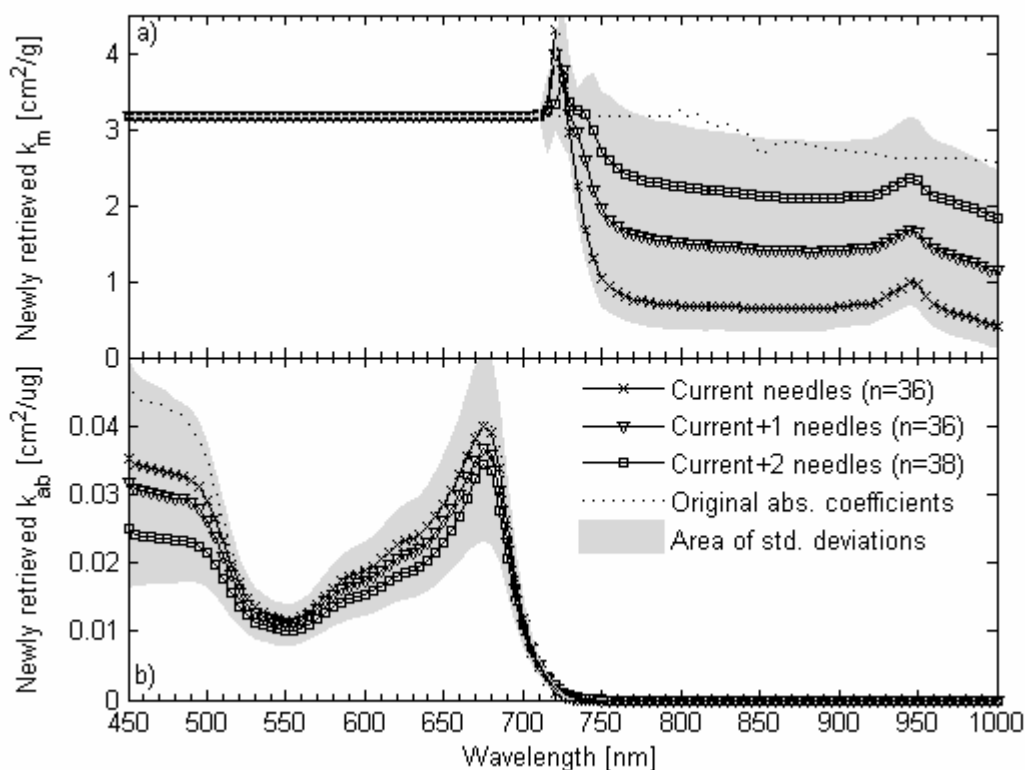


Figure 3.6 Comparison of the newly retrieved a) dry matter ( $k_m$ ) and b) chlorophyll ( $k_{ab}$ ) specific absorption coefficients used for the PROSPECT model update per three investigated Norway spruce needle age-classes ( $n$  = number of the samples; solid grey represents area of all the standard deviations of newly recalibrated  $k_{ab}$  and  $k_m$ ).

### 3.3.4 Multiple retrieval of the PROSPECT inputs

Both versions (original and recalibrated) of the PROSPECT model were run in the inversion mode to simultaneously retrieve all the input parameters. Comparison of the measured values with values retrieved by means of the minimizing equation 3.6 is given in figure 3.10. Comparing the scatterplots and the RMSE values, one can draw the conclusion that recalibration of the  $k_{ab}(\lambda)$  and  $k_m(\lambda)$  coefficients slightly decreased accuracy of the chlorophyll estimation. On the other hand the strong underestimation of dry matter and water content was corrected. Also the  $N$  parameters obtained from the multiple inversion were quite close to the values from the single retrieval. Still the overall chlorophyll, dry matter and water content RMSEs are too high. The RMSE for  $C_{ab}$  equal to  $17.25 \mu\text{g}\cdot\text{cm}^{-2}$  represents about 30% of the measured chlorophyll content range (min.  $C_{ab} = 25.57 \mu\text{g}\cdot\text{cm}^{-2}$ ; max.  $C_{ab} = 85.10 \mu\text{g}\cdot\text{cm}^{-2}$ ),  $C_m$  equal to  $0.007 \text{g}\cdot\text{cm}^{-2}$  represents about 25% of the measured dry matter range (min.  $C_m = 0.014 \text{g}\cdot\text{cm}^{-2}$ ; max.  $C_m = 0.042 \text{g}\cdot\text{cm}^{-2}$ ) and the RMSE for  $C_w$  equal to  $0.0155 \text{cm}$  represents about 55% of the measured water content range (min.  $C_w = 0.0419 \text{cm}$ ; max.  $C_w = 0.0701 \text{cm}$ ).

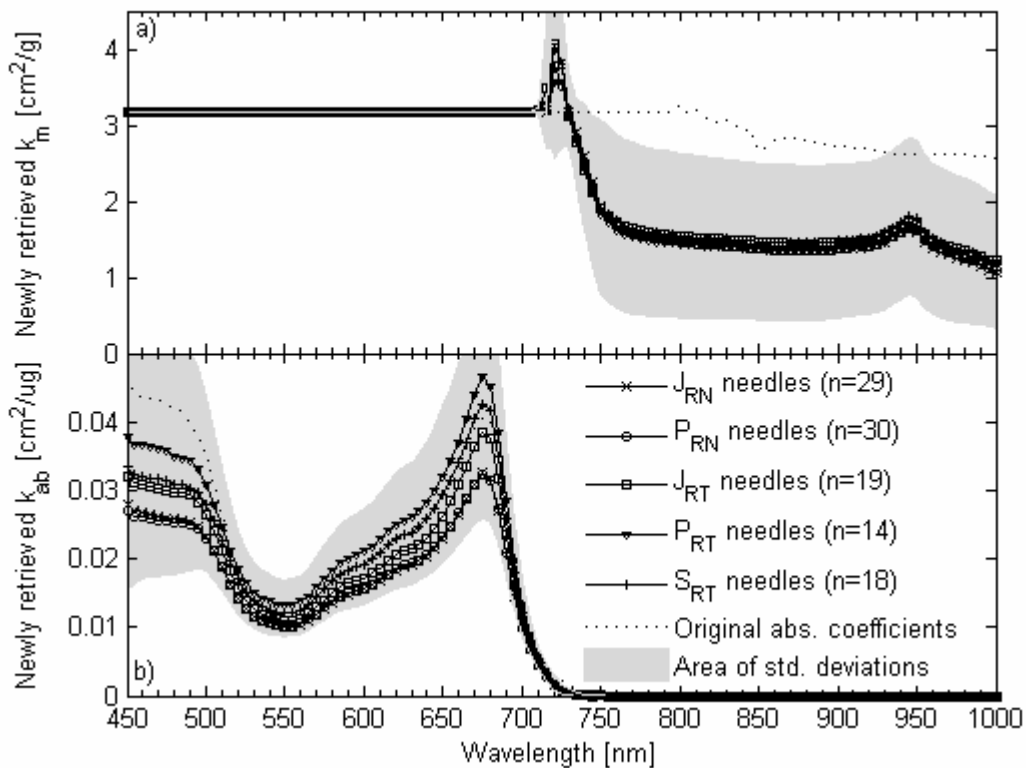


Figure 3.7 Comparison of the newly retrieved a) dry matter ( $k_m$ ) and b) chlorophyll ( $k_{ab}$ ) specific absorption coefficients sorted per stress shoot type classes of Norway spruce needles (JRN = primary stress resistant needle samples of the juvenile crown part, PRN = primary, stress resistant needle samples of the production crown part, JRT = primary, stress resilient needle samples of the juvenile crown part, PRT = primary stress resilient needle samples of the production crown part, SRT = regenerative secondary stress resilient needle samples of the production crown part;  $n$  = number of the samples; solid grey represents area of all the standard deviations of newly recalibrated  $k_{ab}$  and  $k_m$ ).

Results of the PROSPECT constrained inversions, using combined spectral and prior information, are plotted against the measurement results in figure 3.11. As expected, the prior knowledge about retrieved variables increased significantly the retrieval accuracy in cases where the spectral information was poor (i.e.,  $C_m$  and  $C_w$ ). The updated PROSPECT model 3.01.S was able to retrieve the  $C_{ab}$  concentration with an average RMSE of  $8.77 \mu\text{g}\cdot\text{cm}^{-2}$  (i.e., 14% of the measured chlorophyll concentration range), which is comparable to the RMSE of  $8.05 \mu\text{g}\cdot\text{cm}^{-2}$  resulting from the original PROSPECT code. A remarkable improvement was achieved for the dry matter content retrieval. Almost all the  $C_m$  values estimated by the original PROSPECT were underestimated (RMSE =  $0.0079 \text{g}\cdot\text{cm}^{-2}$ ), some of them even stroked the lowest specified  $C_m$  limit of  $0.0141 \text{g}\cdot\text{cm}^{-2}$ . But the  $C_m$  values inverted from the recalibrated PROSPECT follow the one-to-one relationship line with a mean RMSE of  $0.0021 \text{g}\cdot\text{cm}^{-2}$  (i.e., 8% of the measured dry matter range). The additional ‘a priori’ information improved also water content prediction, where the RMSE for  $C_w$  equal to  $0.0019 \text{cm}$ , computed from the retrieval of the original PROSPECT, was decreased in case of the updated

PROSPECT to 0.0006 cm (i.e., 7% and 2% of the measured water content range). Similarity between the N parameters obtained from the single and the multiple retrievals decreased, because no 'a priori' information concerning the N numbers was available and thus implemented in any of the retrieval algorithms. Nevertheless, the RMSE for N of 0.0335 for the recalibrated model remained acceptably small.

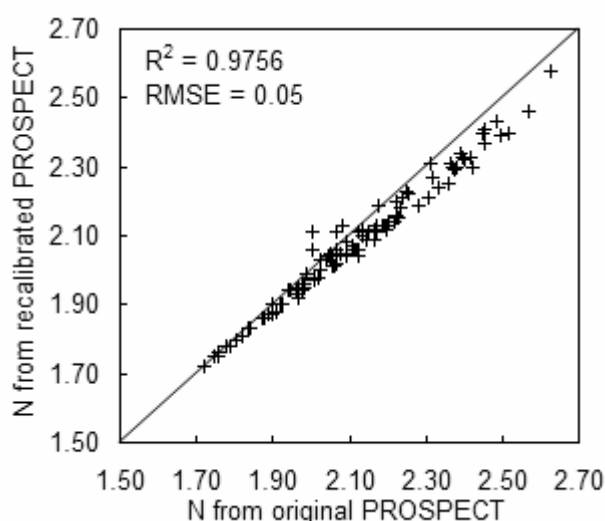


Figure 3.8. Relationship of the N structural parameters estimated for the samples of the training dataset (110 samples) by inversion of the original and the recalibrated PROSPECT model (solid line represents a one-to-one relationship,  $R^2$  = coefficient of determination, RMSE = root mean square error).

### 3.4 Discussion

Our verification tests did not reveal a direct applicability of the PROSPECT 3.01 model for Norway spruce needles in the wavelength range from 450 nm to 1000 nm. However, we assumed that the original 1-dimensional structure, designing the PROSPECT model as a pile of N homogeneous plates of mesophyll cells separated by N-1 air spaces (Jacquemoud & Baret, 1990), is an acceptably robust simplification of the inner leaf structure for a spruce needle (as well as others), which has a radial arrangement of inner cells around the vascular tissues in the centre. A new hypothesis was formulated under this assumption, proposing that a recalibration of the model specific coefficients will result in increased PROSPECT performance. It is implausible to presume that the values of the refraction index  $n$ , responsible for the internal scattering of photons inside the leaf, could be a cause of the observed spectral discrepancy in NIR, because  $n$  is a stable parameter with low variability within all the wavelengths ( $n$  at 500 nm = 1.4880, at 800 nm = 1.4345). Moreover, the highest spectral inaccuracies were found for the leaf absorption ( $\alpha$ ) driven by the spectral absorption coefficient  $k_0(\lambda)$ , which is computed out of the specific absorption coefficients of the main leaf constituents ( $k_e(\lambda)$ ,  $k_{ab}(\lambda)$ ,  $k_w(\lambda)$ , and  $k_m(\lambda)$ ). The absorption between 450-1000 nm is

formed by the specific chlorophyll and dry matter absorption coefficients  $k_{ab}(\lambda)$  and  $k_m(\lambda)$ . For this reason, both of these coefficients were recalibrated.

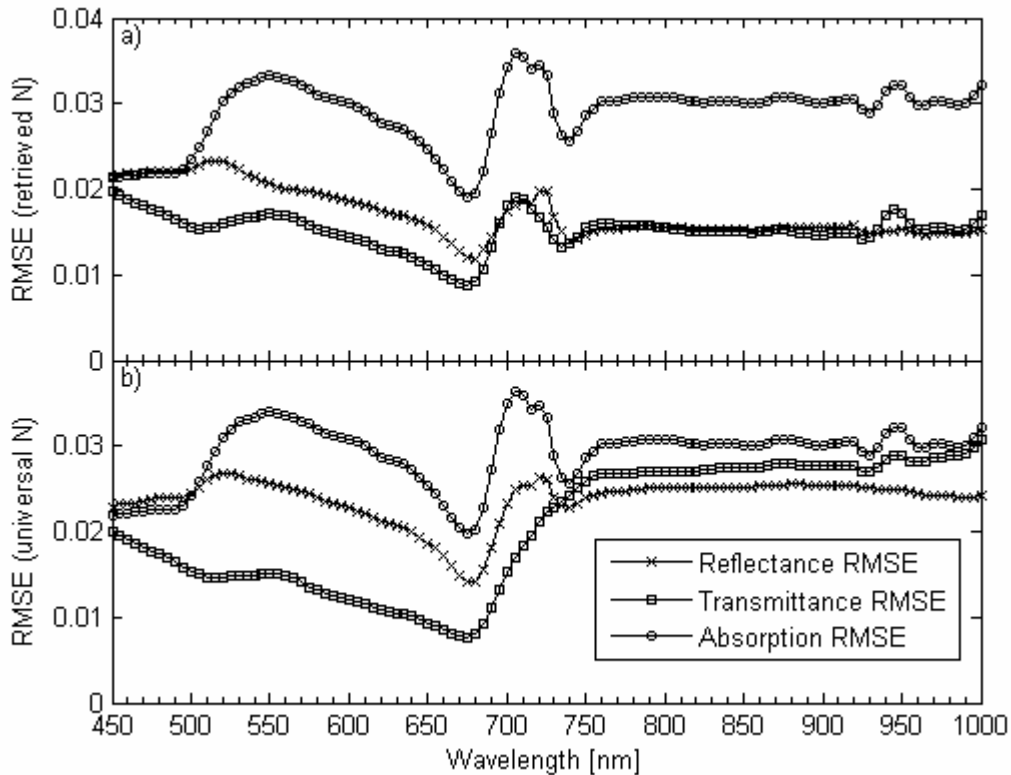


Figure 3.9. Mean root mean square errors (RMSE) for each of the investigated wavelength computed between the reflectance, transmittance, and absorption measurements of the independent testing dataset (48 samples) and the updated PROSPECT simulations using: a) the N numbers retrieved for each testing sample; and b) the ‘universal’ N values generated for each stress category from the training dataset samples (see table 3.3).

ANOVA analyses of the newly gained  $k_m(\lambda)$  values proved statistically significant ( $\alpha$ -level = 0.01) differences between all examined needle age-classes. The  $k_m(\lambda)$  values express the specific absorption of several complex organic molecules present in the leaf dry matter. O’Neill et al. (2002) determined average abundance of cellulose and lignin, main dry matter components of Sitka spruce (*Picea sitchensis* (Bong.) Carr.) needles, as being 20.5 % and 11.0 % respectively. Phenolic compounds, whose concentration increases with the needle age, represent another abundant component of spruce needles (Soukupova et al., 2001). It is logical that quality, and consequently the absorption ability of the spruce needle dry matter, changes with the needles aging. These compositional changes result in the lowest  $k_m$  (700-1000 nm) for C, higher for C+1, and the highest for C+2 needles. Furthermore, ageing seems to be more important for the absorbance properties of needles between 700-1000 nm than the needle origin (shoot type), because differences between the shoot type stress-classes were less significant (see figure 3.6a and figure 3.7a). The age-class and some stress shoot type differences were statistically proven also for  $k_{ab}(\lambda)$  between 450-700 nm (see figure 3.6b and



figure 3.7b). The  $k_{ab}(\lambda)$  represents a combined specific absorption of chlorophyll a+b, carotenoids and other plant pigments, thus these results suggest that the ratio of the needle pigments is changing per age-class and shoot type. It would be too complex and potentially insignificant to create PROSPECT databases for each combination of the age-classes and the stress shoot types. Therefore, finally, only three databases of the recalibrated specific absorption coefficients were released per needle year-class, as the needle age differences were statistically significant for both specific absorption coefficients  $k_{ab}(\lambda)$  and  $k_m(\lambda)$ . Validation of the newly recalibrated PROSPECT version was positive for direct as well as inverted use of the model. Consequently, a further recalibration, employing also the specific absorption coefficients  $k_e(\lambda)$  and  $k_w(\lambda)$ , was not proposed.

The structural parameter N did not statistically differ per needle age-class, but per stress-class of the shoot types (table 3.3). In view of the fact that the N parameter reflects quantitative information about leaf inner structure, we conclude that needles of the RN trees contain less mesophyll cell layers than needles of the RT trees (especially needles of the production crown parts). However, the inner arrangement of the mesophyll tissue inside the needles must be additionally investigated to confirm such a conclusion. As a result, the N parameter, retrieved from top of canopy imaging spectrometer data, could be hypothetically used as a biomarker indicating the presence of the chronic stress within the Norway spruce crowns. Physical retrieval of the N parameter for separate spruce crowns would be possible by coupling the PROSPECT model with an appropriate forest canopy radiative transfer model, e.g. the Analytic Radiative-Transfer Model for a Coupled Atmosphere and Leaf Canopy (Liang & Strahler, 1995), the DART model (Gastellu-Etchegorry et al., 1996; Gastellu-Etchegorry et al., 2004) or the INFORM model (Schlerf & Atzberger, 2006), and inverting this coupled model using optical remote sensing data at a very high spatial resolution (e.g., 0.5-1.0 m). However, a reachable accuracy of N estimation and the physiological relationship between N and needle stress state need further investigation.

On the one hand, the site specific structural parameter N can be retrieved through an iterative self-parameterized spectral inversion of PROSPECT. On the other hand, the ‘universal’ N values, representative for characteristic vegetation types or biological species, can be estimated from an extensive dataset of the measured leaf optical properties. The ‘universal’ N values, generated from our training dataset and applied in forward PROSPECT simulations of the testing dataset, produced results highly comparable with results using the sample specific N values. This finding makes both types of N parameter reconcilable.

The lowest achieved RMSE of about  $8.0 \mu\text{g}\cdot\text{cm}^{-2}$  in chlorophyll estimation at the leaf level is higher than the RMSE of approximately  $3.7 \mu\text{g}\cdot\text{cm}^{-2}$  obtained from the PROSPECT inversion by Jacquemoud and Baret (1990) or le Maire et al. (2004). Nevertheless, one has to take into account several unavoidable uncertainty sources originating from limitations of the needle shaped leaves.

As stated in the introduction, the protocol of the needle optical property measurement and consequent quality of the measurements might be improved. A systematic uncertainty is introduced mainly with the correction for the gap fraction (GF). This is a very sensitive correction that may cause a deviation of about 5% in reflectance values and even more in transmittance values. An individual quality check of each spectral signature ensured their standard quality and allowed for their use in a successful PROSPECT recalibration. Potential use of a new type of needle carrier could eliminate the need for GF correction and guarantee

required quality of the needle shaped leaf optical properties (Harron, 2000; Zarco-Tejada et al., 2004a).

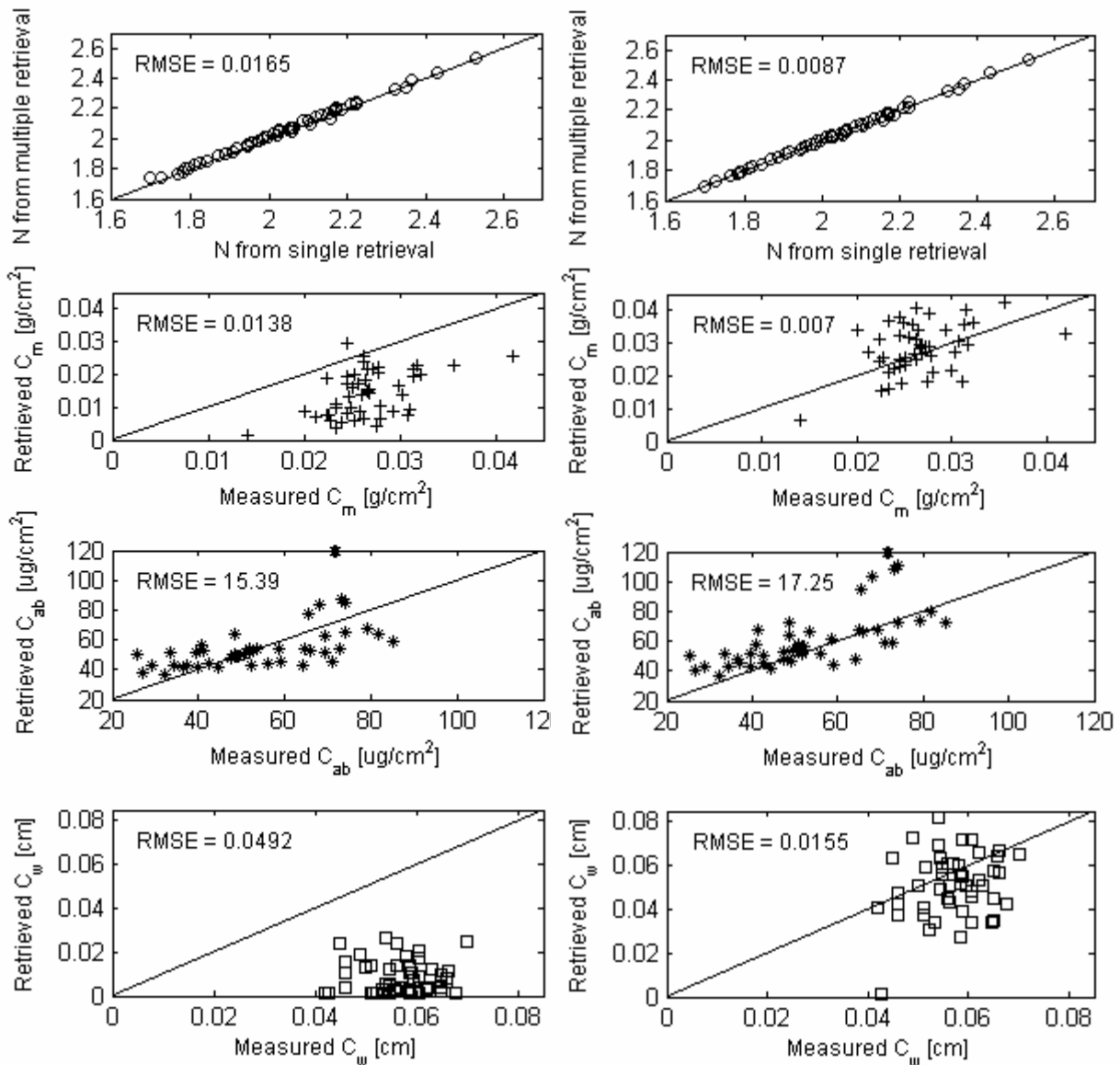


Figure 3.10 Results of the partially unconstrained inversion of the original (graphs in left column) and recalibrated (graphs in right column) PROSPECT, retrieving concurrently all the model inputs ( $C_{ab}$ ,  $C_m$ ,  $C_w$ , and  $N$ ) using 48 samples of the testing dataset. The merit function was based on the spectral information and expert knowledge on the variability limits of the retrieved parameters (see equation 3.6), (RMSE = root mean square error between measured and simulated values; solid line represents a one-to-one relationship function;  $N$  from single retrieval = structural parameters retrieved only for the purpose of direct PROSPECT simulations,  $N$  from multiple retrieval = structural parameters retrieved together with all other PROSPECT inputs for a verification purpose).

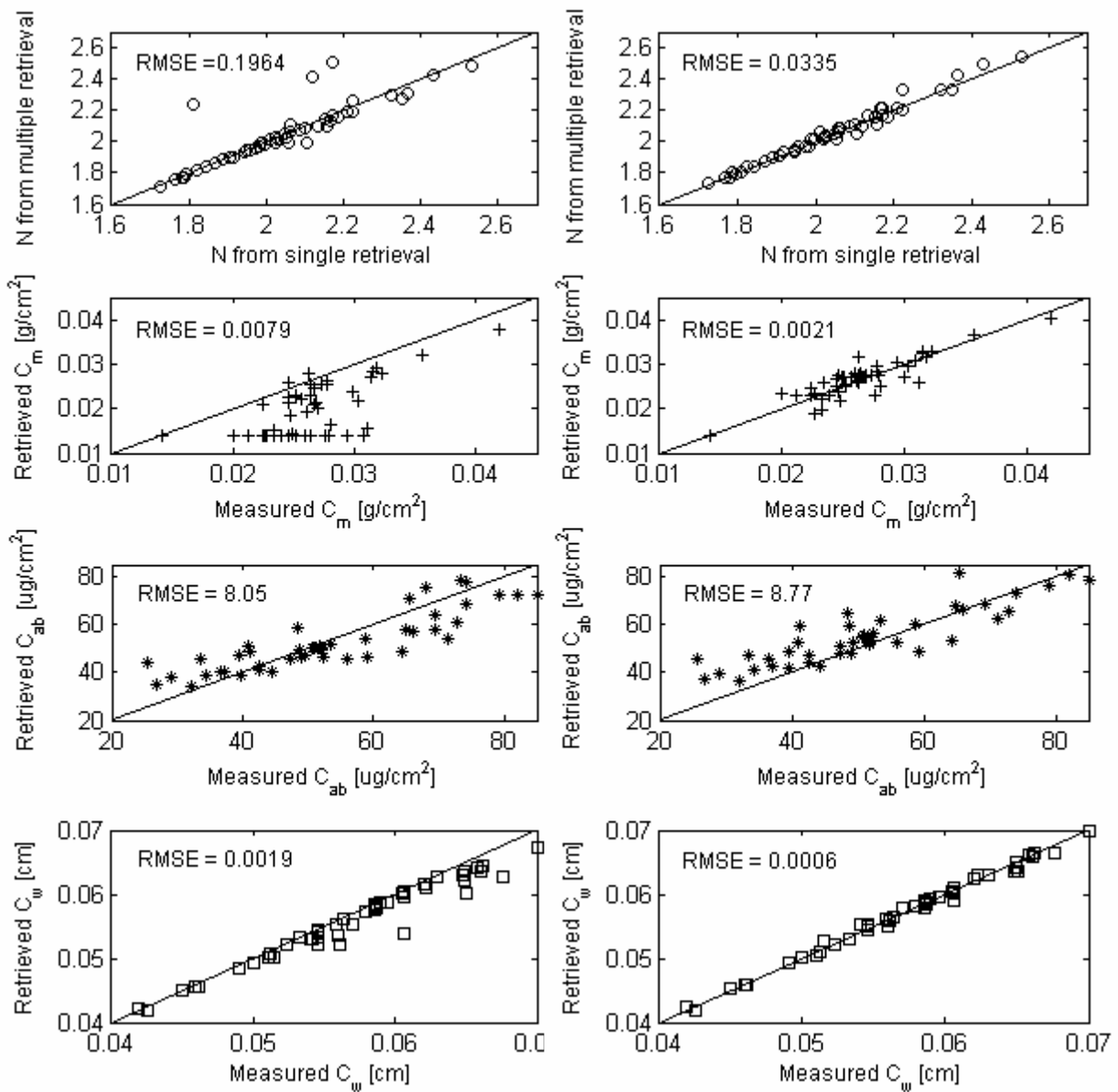


Figure 3.11 Results of the constrained inversion of the original (graphs in left column) and recalibrated (graphs in right column) PROSPECT retrieving concurrently all the model inputs ( $C_{ab}$ ,  $C_m$ ,  $C_w$ , and  $N$ ) using 48 samples of the testing dataset. The merit function was not based only on the spectral information, but it was constrained by measured ‘a priori’ knowledge on targeting values and variability limits of the retrieved parameters (see equation 3.7), (RMSE = root mean square error between measured and simulated values; solid line represents a one-to-one relationship function;  $N$  from single retrieval = structural parameters retrieved only for the purpose of direct PROSPECT simulations,  $N$  from multiple retrieval = structural parameters retrieved together with all other PROSPECT inputs for a verification purpose).

Unfortunately, the use of two separate within-shoot sample sets, one for determination of foliar pigments and a second one for spectral measurement, was practically unavoidable and causes a potential inaccuracy. The needle samples for laboratory analysis of the chlorophyll concentration must be kept in a cold dark environment, therefore their spectroscopic examination without risk of the chlorophyll disturbance is practically impossible.

A last factor influencing the accuracy of the results is represented by the necessity to transform the  $C_{ab}$  and  $C_m$  units from [ $\mu\text{g.g}$ ] and [ $\text{g}$ ] of dry matter to [ $\mu\text{g.cm}^{-2}$ ] and [ $\text{g.cm}^{-2}$ ] of needle hemispherical-surface projection. The transformation was carried out through the relation of the dry matter content [ $\text{g}$ ] to the hemispherical-surface area of the needles [ $\text{cm}^2$ ]. Unfortunately, the Norway spruce needle is not a flat leaf neither being monofacial or bifacial, but it has a square diagonal cross profile mostly with four facets. For this reason the projected leaf area has to be substituted by a so-called hemispherical-surface projection, which was computed using a universal conversion factor of 1.285 (i.e., 2.57 to obtain total needle surface area). The value of this conversion factor was obtained from the leaf cross-section widths (Pokorny & Marek, 2000), where a low value belongs to a flattened needle and a high value corresponds to a quadratic cross-section of the needle. Niinemets (1997) proved that needle thickness and width are statistically different for younger and older Norway spruce needles due to varying irradiance conditions within the crown. Further, Pokorny (unpublished data) found that the cross-section conversion factor, computed for spruce needles of the same whorl, was higher for older age-classes than for young needles. If we assume that a set of six average spruce needles has an average projection of  $1.1\text{cm}^2$  and dry matter weight of  $0.037\text{g}$ , then the unit conversion using the universal factor of 1.285 will result in a dry matter concentration of  $0.0262\text{g.cm}^{-2}$  (our real average). But if we use the lowest (1.115) and the highest (1.490) value of the conversion factor measured for Norway spruce needles by Pokorny (unpublished data), then the dry matter content of the same needle sample will result in  $0.0302\text{g.cm}^{-2}$  and  $0.0226\text{g.cm}^{-2}$ , respectively, which is a significant difference. Obviously the unit transformation is highly sensitive to the cross-section conversion factor. Finally, we conclude that using sample specific cross-section factors for each year-class would increase the reliability of the  $C_{ab}$  and  $C_m$  measurements related to the hemispherical-surface needle area, and subsequently support their closer correlations depicted in figure 3.10 and figure 3.11. Based on this reasoning, it is recommended for forthcoming studies that the cross-section conversion factor of each investigated needle set should be computed separately.

### 3.5 Conclusions

---

A comparison of the PROSPECT simulations with measured hemispherical spectral signatures of Norway spruce needles resulted in a model recalibration effort. We updated the specific absorption coefficient of chlorophyll  $k_{ab}(\lambda)$  and dry matter  $k_m(\lambda)$  of each needle year-class between 450-1000 nm. The  $k_{ab}(\lambda)$  and  $k_m(\lambda)$  readjustment improved the PROSPECT retrieval in such a way that the RMSE of the measured and PROSPECT simulated absorptions between 700-1000 nm decreased on average from 14% to 5%, and for the NIR reflectance and transmittance from about 6% to 2%. In general, the errors obtained were comparable to the PROSPECT validation performed by Jacquemoud and Baret (1990). It was also shown that

properly generated ‘universal’ values of the N structural parameter can plausibly substitute the sample specific N numbers.

The multiple variable retrievals, carried out for both PROSPECT versions (the original version 3.01 and the recalibrated version 3.01.S), revealed the credibility of the recalibration process. The most satisfactory results were achieved from a constrained spectral retrieval supported by ‘a priori’ information on retrieved variables. These results highlight the importance of prior knowledge for cases of inaccurate spectral information. However, the PROSPECT recalibration and validation was performed using the training and testing samples from the same geographic area. The same sample origins decrease the trustworthiness in universality of the recalibrated PROSPECT 3.01.S and increases the probability of the site specific character. Unquestionably, the new model version also has to be tested and optionally recalibrated on datasets collected from a broader variety of Norway spruces (trees growing in different environmental conditions) to validate and ensure its general applicability.

The findings of morphological, physiological and consequently spectroscopic differences among the age-classes of evergreen coniferous leaves (e.g., Malenovský et al., 2006) indicate that each of the needle generations has to be treated separately. Therefore, this study focused on the specialization of the PROSPECT model for specific cases of Norway spruce needle of different ages. Such recalibration reduces the broad applicability of the model, but secures a minimum required accuracy. Indeed, the application of specialized PROSPECT codes in remote sensing would require ancillary information on the plant physiological characteristics (e.g., forest inventory databases, plant functional types pre-classification, etc.) and remote sensing data of very high spatial resolution, where the individual tree species can be identified. The leaf optical properties of the whole coniferous canopy (e.g., Norway spruce crowns), used for a low spatial resolution remote sensing application dealing with mixed vegetation spectral information, can be modelled as the average of all present leaf age-classes, weighted by their abundance within the canopy.

Despite the fact that PROSPECT was recalibrated and applied to Norway spruce needles, this model was originally designed for bifacial leaves having two different mesophyll tissues arranged in parallel cell layers separated by air layers. The LIBERTY model (Dawson et al., 1998b) was designed specifically for the radiative transfer through a coniferous needle by attempting to mimic the inner needle structure. However, the LIBERTY model requires too many input parameters, which tentatively are unfeasible to collect simultaneously during a field validation campaign. Moreover, as shown by Moorthy et al. (2003), a proper parameterization of all the LIBERTY inputs is difficult and critical task to ensure overall accuracy of the resulting optical properties. Therefore, we conclude that design of a new robust needle-specific radiative transfer model, geometrically adapted to the needle inner structure while maintaining a reasonable number of input parameters, should be a research focus for further development.

### **3.6 Acknowledgements**

---

The authors acknowledge the provision of the source code of PROSPECT by S. Jacquemoud, and the financial support provided for Zbyněk Malenovský by the Ministry of Education, Youth and Sports of the Czech Republic within the Sabbatical Fellowship 1K04. This study was carried out within the Research Plan of the Institute of Systems Biology and

Ecology: AV0Z6087904 - Ecology of the Man-managed Landscape (Academy of Sciences of the Czech Republic), and contribution of co-authors from Charles University by the Grant Agency of the Academy of Sciences A600110507. The authors thank the anonymous reviewers for their comments and suggestions.

### 3.7 References

- Albrechtova, J., Rock, B. N., Soukupova, J., Entcheva, P., Solcova, B., & Polak, T. (2001), Biochemical, histochemical, structural and reflectance markers of damage in Norway spruce from Krusne hory Mts. used for interpretation of remote sensing data. *Journal of Forest Science*, 47, 26-33.
- Allen, W. A., Gausman, H. W., Richards, A. J., & Thomas, J. R. (1969), Interaction of isotropic light with a compact plant leaf. *Journal of the Optical Society of America*, 59, 1376-1379.
- Asner, G. P. (1998), Biophysical and biochemical sources of variability in canopy reflectance. *Remote Sensing of Environment*, 64, 234-253.
- Asner, G. P., Wessman, C. A., Schimel, D. S., & Archer, S. (1998), Variability in leaf and litter optical properties: Implications for BRDF model inversions using AVHRR, MODIS, and MISR. *Remote Sensing of Environment*, 63, 243-257.
- Bacour, C., Jacquemoud, S., Tourbier, Y., Dechambre, M., & Frangi, J.-P. (2002), Design and analysis of numerical experiments to compare four canopy reflectance models. *Remote Sensing of Environment*, 79, 72-83.
- Chen, J. M., Liu, J., Leblanc, S. G., Lacaze, R., & Roujean, J.-L. (2003), Multi-angular optical remote sensing for assessing vegetation structure and carbon absorption. *Remote Sensing of Environment*, 84, 516-525.
- Coleman, T. F., & Li, Y. (1996), An interior trust region approach for nonlinear minimization subject to bounds. *SIAM Journal on Optimization*, 6, 418-445.
- Combal, B., Baret, F., & Weiss, M. (2002), Improving canopy variables estimation from remote sensing data by exploiting ancillary information. Case study on sugar beet canopies. *Agronomie*, 22, 205-215.
- Combal, B., Baret, F., Weiss, M., Trubuil, A., Mace, D., Pragnere, A., Myneni, R., Knyazikhin, Y., & Wang, L. (2003), Retrieval of canopy biophysical variables from bidirectional reflectance: Using prior information to solve the ill-posed inverse problem. *Remote Sensing of Environment*, 84, 1-15.
- Cudlin, P., Novotny, R., Moravec, I., & Chmelikova, E. (2001), Retrospective evaluation of the response of montane forest ecosystems to multiple stress. *Ekologia-Bratislava*, 20, 108-124.
- Daughtry, C. S. T., Biehl, L. L., & Ranson, K. J. (1989), A new technique to measure the spectral properties of conifer needles. *Remote Sensing of Environment*, 27, 81-91.
- Dawson, T. P., Curran, P. J., & Plummer, S. E. (1998), LIBERTY- Modeling the effects of leaf biochemical concentration on reflectance spectra. *Remote Sensing of Environment*, 65, 50-60.
- Demarez, V., & Gastellu-Etchegorry, J. P. (2000), A modeling approach for studying forest chlorophyll content. *Remote Sensing of Environment*, 71, 226-238.
- Demarez, V., Gastellu-Etchegorry, J. P., Mougou, E., Marty, G., Proisy, C., Dufrene, E., & Le Dantec, V. (1999), Seasonal variation of leaf chlorophyll content of a temperate forest. Inversion of the PROSPECT model. *International Journal of Remote Sensing*, 20, 879-894.
- Demetriades-Shah, T. H., Steven, M. D., & Clark, J. A. (1990), High resolution derivative spectra in remote sensing. *Remote Sensing of Environment*, 33, 55-64.
- Entcheva Campbell, P. K., Rock, B. N., Martin, M. E., Neefus, C. D., Irons, J. R., Middleton, E. M., & Albrechtova, J. (2004), Detection of initial damage in Norway spruce canopies using hyperspectral airborne data. *International Journal of Remote Sensing*, 25, 5557-5583.

- Fang, H., Liang, S., & Kuusk, A. (2003), Retrieving leaf area index using a genetic algorithm with a canopy radiative transfer model. *Remote Sensing of Environment*, 85, 257-270.
- Fernandes, R. A., Miller, J. R., Chen, J. M., & Rubinstein, I. G. (2004), Evaluating image-based estimates of leaf area index in boreal conifer stands over a range of scales using high-resolution CASI imagery. *Remote Sensing of Environment*, 89, 200-216.
- Gamon, J. A., Huemmrich, K. F., Peddle, D. R., Chen, J., Fuentes, D., Hall, F. G., Kimball, J. S., Goetz, S., Gu, J., & McDonald, K. C. (2004), Remote sensing in BOREAS: Lessons learned. *Remote Sensing of Environment*, 89, 139-162.
- Gastellu-Etchegorry, J. P., & Bruniquel-Pinel, V. (2001), A modeling approach to assess the robustness of spectrometric predictive equations for canopy chemistry. *Remote Sensing of Environment*, 76, 1-15.
- Gastellu-Etchegorry, J. P., Demarez, V., Pinel, V., & Zagolski, F. (1996), Modeling radiative transfer in heterogeneous 3-D vegetation canopies. *Remote Sensing of Environment*, 58, 131-156.
- Gastellu-Etchegorry, J. P., Martin, E., & Gascon, F. (2004), DART: a 3D model for simulating satellite images and studying surface radiation budget. *International Journal of Remote Sensing*, 25, 73-96.
- Gruber, F. (1994), Morphology of coniferous trees: possible effects of soil acidification on the morphology of Norway spruce and Silver fir., New York: Wiley-Liss, 265-324.
- Harron, J. W. (2000), Optical properties of phytoelements in conifers. *MSc Thesis*, Toronto, Canada: York University, 193.
- Harron, J. W., & Miller, J. R. (1995), An alternative methodology for reflectance and transmittance measurements of conifer needles. 1995, Saskatchewan: Saskatoon, 654-661.
- Jacquemoud, S., Bacour, C., Poilve, H., & Frangi, J.-P. (2000), Comparison of four radiative transfer models to simulate plant canopies reflectance: direct and inverse mode. *Remote Sensing of Environment*, 74, 471-481.
- Jacquemoud, S., & Baret, F. (1990), Prospect - a model of leaf optical properties spectra. *Remote Sensing of Environment*, 34, 75-91.
- Jacquemoud, S., Baret, F., Andrieu, B., Danson, F. M., & Jaggard, K. (1995), Extraction of vegetation biophysical parameters by inversion of the PROSPECT + SAIL models on sugar beet canopy reflectance data. Application to TM and AVIRIS sensors. *Remote Sensing of Environment*, 52, 163-172.
- Jacquemoud, S., Ustin, S. L., Verdebout, J., Schmuck, G., Andreoli, G., & Hosgood, B. (1996), Estimating leaf biochemistry using the PROSPECT leaf optical properties model. *Remote Sensing of Environment*, 56, 194-202.
- Kotz, B., Schaepman, M., Morsdorf, F., Bowyer, P., Itten, C., & Allgower, B. (2004), Radiative transfer modelling within a heterogeneous canopy for estimation of forest fire fuel properties. *Remote Sensing of Environment*, in press.
- Kuusk, A., & Nilson, T. (2000), A directional multispectral forest reflectance model. *Remote Sensing of Environment*, 72, 244-252.
- Lacaze, R., Chen, J. M., Roujean, J.-L., & Leblanc, S. G. (2002), Retrieval of vegetation clumping index using hot spot signatures measured by POLDER instrument. *Remote Sensing of Environment*, 79, 84-95.
- le Maire, G., Francois, C., & Dufrene, E. (2004), Towards universal broad leaf chlorophyll indices using PROSPECT simulated database and hyperspectral reflectance measurements. *Remote Sensing of Environment*, 89, 1-28.
- Lelong, C. C. D., Pinet, P. C., & Poilve, H. (1998), Hyperspectral imaging and stress mapping in agriculture: A case study on wheat in Beauce (France). *Remote Sensing of Environment*, 66, 179-191.
- Li-Cor (1983), *1800-12 Integrating sphere instruction manual*. Publication number 8305-0034. pp.

- Liang, S. L., & Strahler, A. H. (1995), An Analytic Radiative-Transfer Model for a Coupled Atmosphere and Leaf Canopy. *Journal of Geophysical Research-Atmospheres*, 100, 5085-5094.
- Mesarch, M. A., Walter-Shea, E. A., Asner, G. P., Middleton, E. M., & Chan, S. S. (1999), A revised measurement methodology for conifer needles spectral optical properties: Evaluating the influence of gaps between elements. *Remote Sensing of Environment*, 68, 177-192.
- Middleton, E. M., Walter-Shea, E. A., Mesarch, M. A., Chan, S. S., & Rusin, R. J. (1997), Optical properties of Black spruce and Jack pine needles at BOREAS sites in Saskatchewan, Canada. *Canadian Journal of Remote Sensing*, 23, 109-119.
- Miller, J. R., Berger, M., Alonso, L., Cerovic, Z., Goulas, Y., Jacquemoud, S., Louis, J., Mohammed, G., Moya, I., Pedrós, R., Moreno, J., Verhoef, W., & Zarco-Tejada, P. J. (2003), Progress on the Development of an Integrated Canopy Fluorescence Model. 21-25 July 2003, France: Toulouse, 601-603.
- Miller, J. R., Berger, M., Goulas, Y., Jacquemoud, S., Louis, J., Mohammed, G., Moise, N., Moreno, J., Moya, I., Pedrós, R., Verhoef, W., & Zarco-Tejada, P. J. (2005), Development of a Vegetation Fluorescence Canopy Model. *Final Report*, April 2005, European Space Agency ESA-ESTEC, 138.
- Moorthy, I., Miller, J. R., Zarco-Tejada, P. J., & Noland, T. L. (2003), Needle chlorophyll content estimation: A comparative study of PROSPECT and LIBERTY. 21-25 July 2003, France: Toulouse: IEEE International, 1676-1678.
- Niinemets, U. (1997), Acclimation to low irradiance in *Picea abies*: Influences of past and present light climate on foliage structure and function. *Tree Physiology*, 17, 723-732.
- Nilson, T., Kuusk, A., Lang, M., & Lukk, T. (2003), Forest reflectance modeling: Theoretical aspects and applications. *Ambio*, 32, 535-541.
- O'Neill, A. L., Kupiec, J. A., & Curran, P. J. (2002), Biochemical and reflectance variation throughout a Sitka spruce canopy. *Remote Sensing of Environment*, 80, 134-142.
- Peddle, D. R., Johnson, R. L., Cihlar, J., & Latifovic, R. (2004), Large area forest classification and biophysical parameter estimation using the 5-Scale canopy reflectance model in Multiple-Forward-Mode. *Remote Sensing of Environment*, 89, 252-263.
- Pokorny, R., & Marek, M. V. (2000), Test of accuracy of LAI estimation by LAI-2000 under artificially changed leaf to wood area proportions. *Biologia Plantarum*, 43, 537-544.
- Porra, R. J., Thompson, W. A., & Kriedemann, P. E. (1989), Determination of accurate extinction coefficients and simultaneous equations for assaying chlorophylls a and b extracted with four different solvents: verification of the concentration of chlorophyll standards by atomic absorption spectroscopy. *Biochimica and Biophysica Acta*, 975, 384-394.
- Rautiainen, M., & Stenberg, P. (2005), Application of photon recollision probability in coniferous canopy reflectance simulations. *Remote Sensing of Environment*, 96, 98-107.
- Rautiainen, M., Stenberg, P., Nilson, T., & Kuusk, A. (2004), The effect of crown shape on the reflectance of coniferous stands. *Remote Sensing of Environment*, 89, 41-52.
- Savitzky, A., & Golay, M. J. E. (1964), Smoothing and differentiation of data by simplified least squares procedures. *Analytical Chemistry*, 36, 1627-1637.
- Schaepman, M. E., Koetz, B., Schaepman-Strub, G., & Itten, K. I. (2005), Spectrodirectional remote sensing for the improved estimation of biophysical and -chemical variables: two case studies. *International Journal of Applied Earth Observation and Geoinformation*, 6, 271-282.
- Schaepman, M. E., Schläpfer, D., & Müller, A. (2002), Performance requirements for airborne imaging spectrometers. *Proceedings of SPIE - The International Society for Optical Engineering*, 4480, 23-31.
- Schläpfer, D., & Schaepman, M. (2002), Modeling the noise equivalent radiance requirements of imaging spectrometers based on scientific applications. *Applied Optics*, 41, 5691-5701.



- Schlerf, M., & Atzberger, C. (2006), Inversion of a forest reflectance model to estimate structural canopy variables from hyperspectral remote sensing data. *Remote Sensing of Environment*, 100, 281-294.
- Smolander, S., & Stenberg, P. (2003), A method to account for shoot scale clumping in coniferous canopy reflectance models. *Remote Sensing of Environment*, 88, 363-373.
- Smolander, S., & Stenberg, P. (2005), Simple parameterizations of the radiation budget of uniform broadleaved and coniferous canopies. *Remote Sensing of Environment*, 94, 355-363.
- Soukupova, J., Rock, B. N., & Albrechtova, J. (2001), Comparative study of two spruce species in a polluted mountainous region. *New Phytologist*, 150, 133-145.
- Verhoef, W., & Bach, H. (2003), Simulation of hyperspectral and directional radiance images using coupled biophysical and atmospheric radiative transfer models. *Remote Sensing of Environment*, 87, 23-41.
- Walker, D. J., & Kenkel, N. C. (2000), The adaptive geometry of boreal conifers. *Community Ecology*, 1, 13-23.
- Waring, R. H. (1983), Estimating forest growth and efficiency in relation to canopy leaf-area. *Advances in Ecological Research*, 13, 327-354.
- Wellburn, A. R. (1994), The spectral determination of chlorophyll a and chlorophyll b, as well as total carotenoids, using various solvents with spectrophotometers of different resolution. *Journal of Plant Physiology*, 144, 307-313.
- Widen, N. (2004), Assessing the accuracy of land surface characteristics estimated from multi-angular remotely sensed data. *International Journal of Remote Sensing*, 25, 1105-1117.
- Zarco-Tejada, P. J. (2000), Hyperspectral remote sensing of closed forest canopies: Estimation of chlorophyll fluorescence and pigment content. *PhD Thesis*, Toronto, Canada: York University, 224.
- Zarco-Tejada, P. J., Miller, J. R., Harron, J., Hu, B., Noland, T. L., Goel, N., Mohammed, G. H., & Sampson, P. (2004a), Needle chlorophyll content estimation through model inversion using hyperspectral data from boreal conifer forest canopies. *Remote Sensing of Environment*, 89, 189-199.
- Zarco-Tejada, P. J., Miller, J. R., Morales, A., Berjon, A., & Aguera, J. (2004b), Hyperspectral indices and model simulation for chlorophyll estimation in open-canopy tree crops. *Remote Sensing of Environment*, 90, 463-476.
- Zarco-Tejada, P. J., Rueda, C. A., & Ustin, S. L. (2003), Water content estimation in vegetation with MODIS reflectance data and model inversion methods. *Remote Sensing of Environment*, 85, 109-124.



---

**CHAPTER 4****Differences in leaf optical properties of environmentally stressed Norway spruce (*Picea abies* (L.) Karst.) crowns**

Reprint of:

Malenovský, Z., Lhotáková, Z., Albrechtová, J., Clevers, J.G.P.W., Schaepman, M.E., Cudlín, P.: Differences in leaf optical properties of environmentally stressed Norway spruce (*Picea abies* [L.] Karst.) crowns. *Trees – Structure and Function*, in preparation.

## **Abstract**

---

We investigated the optical variability among Norway spruce (*Picea abies*) needle categories defined as relevant combinations of the following criteria: i) tree stress response class – stress resistant or stress resilient trees, ii) functional crown part – juvenile or production crown part and iii) shoot type – primary or secondary shoots.

The needle hemispherical-directional reflectance, transmittance and absorption differences were tested in the wavelength range from 505-800 nm. Spectral analysis was supported with measurements of foliar pigment concentration, dry matter content and anatomical analysis.

Significant quantitative optical differences were discovered at red edge and green wavelengths, when comparing needles of primary shoots of two stress response classes. Qualitative spectral differences were found at wavelengths in the far-red and green fluorescence emissions.

Needle samples of a specific age-class collected from a randomly selected branch within two crown parts were representative for both of them. However, spectroscopic approaches at a spatial resolution broader than the crown size should take the leaf spectral differences between the stress resistant and stress resilient spruce trees into consideration.

*Keywords:* environmental stress, leaf optical properties, needle structure, *Picea abies* (Norway spruce), remote sensing.

## 4.1 Introduction

An adequate understanding of the leaf optical properties is an important precondition to comprehend the radiative transfer through a complex vegetation canopy (Combal et al., 2003). The leaf optical properties, defined as the reflectance  $\rho(\lambda)$ , transmittance  $\tau(\lambda)$ , and absorbance  $\alpha(\lambda)$  of the photons by and/or within the leaf tissues (Gates et al., 1965), are indicating the leaf actual physiological status, influenced by complex environmental conditions including stress agents. Hence, the plant optical properties were soon recognized as reliable indicators of early plant stress occurrence (Horler et al., 1980).

Stress is usually defined as a significant deviation from the optimal living conditions of a plant, which negatively affects function, growth or development of the organism (Larcher, 1995). Stress tolerance of the plant is manifested either as stress resistance (capacity of a system to maintain certain structures and functions despite disturbance leading to over-compensation or hardening) and/or as stress resilience (ability of the system to return to its former state after it has been disturbed) (Chapin et al., 2002) what is also called restabilization or adjustment (Larcher, 1995). However, if the phase of resistance lasts too long the plant may enter the phase of exhaustion leading to permanent damage or plant death. Usually no single causal factor is responsible for the plant decline, but it is rather a synergistic effect of several natural and anthropogenic stressors called multiple environmental stress (Mooney et al., 1991).

The response of plant leaves to changing environmental factors involves both short-term physiological and long-term structural and morphological modifications (Dickson & Isebrands, 1991). Early plant reactions on stressors are detectable as changes in the leaf biochemistry (e.g., foliar pigment concentration). Lower concentration of photosynthetic pigments was detected by Gowin and Goral (1977) in needles of conifers growing in areas polluted by SO<sub>2</sub> and by Polle et al. (1993) in areas polluted by ozone. Secondly, specific changes in leaf anatomy can develop. Albrechtová et al. (2006) observed an increase of intercellular spaces in mesophyll tissues of Norway spruce (*Picea abies*) needles growing at SO<sub>2</sub> polluted sites in the Krušné Hory Mts. (Czech Republic). General changes in needle morphology like reduction of leaf dry mass content per leaf area due to urban air pollution were indicating a defective development of internal leaf tissues (Nakatani et al., 2004).

Long-term responses to environmental stresses at the canopy level are represented by changes in a plant structure. Development of Norway spruce crown architecture is facilitated by three modes of shoot formation classified as: i) proleptic (from embryonal buds initiated during the same season), ii) regular (from one year old winter buds), and iii) proventitious, called secondary by Lesinski (1989), (from proventitious dormant buds, which were developed minimally two years before shoot formation). The secondary shoot formation is a non-specific tree response to environmental change, as well as an integrating response to environmental stress (Nicolini et al., 2001; Malenovský et al., 2006). The upper part of the crown (named *juvenile* part) is colonizing new space above the forest canopy by means of regular (primary) shoots. The middle crown part (called *production* part) consists of the prevailing primary structure in case of stress resistant (RN) crowns, while the secondary shoots are formed within stress resilient (RT) crowns at a different rate according to the ratio of degradation and regeneration. Finally, for adult trees the basal crown part with insufficient irradiance is almost completely formed by secondary shoots (Gruber, 1994). This part is

unimportant for tree production so it was excluded from our experiment. All the combinations created out of two functional crown parts, stress response classes and shoot formations result in the following examined needle categories: i) primary-juvenile-stress resistant (J\_RN), ii) primary-production-stress resistant (P\_RN), iii) primary-juvenile-stress resilient (J\_RT), iv) primary-production-stress resilient (P\_RT), and v) secondary-production-stress resilient (S\_RT) needles.

The interaction of solar radiation with plant leaf tissues is characterized by the following processes (Fukshansky, 1981): i) specular reflection with changes in polarisation, ii) multiple scattering (diffuse component) iii) refraction, iv) absorption, and v) fluorescence emissions. The specular component of the radiation comes mainly from the leaf surface (cuticle waxes), while the isotropic diffuse component arises from the leaf interior (Brakke, 1994). Bousquet et al. (2005) showed that specular reflection of a leaf with a thick smooth cuticle was almost constant within the wavelengths from 480-880 nm. The multiple scattering is induced by the refraction of two discontinuities, expressed by the refraction index ( $n \approx 1$  for air,  $n \approx 1.44$  for hydrated cell walls) (Allen et al., 1969). Most scattering occurs at the cell walls at the air-tissue interfaces, whereas the foliar pigments contribute little to internal scattering (Fukshansky et al., 1993). The leaf absorption is, in general, a function of changes in spin and angular momentum of electrons, transitions between orbital states of electrons in atoms and vibration-rotational modes within the molecules (Hodanova, 1985). The foliar pigments (chlorophylls  $a+b$ , carotenoids, etc.) are major absorbers of the visible solar radiation. They also play an important role in the leaf fluorescence emissions, which exhibit their maximum in the green (520-530 nm), red (690 nm) and far-red (735-740 nm; red edge) part of the electromagnetic spectrum (Lichtenthaler et al., 1998).

A number of studies have been focused on the leaf spectral properties in relation to their biochemical content and anatomical structure (Fourty et al., 1996; O'Neill et al., 2002). The findings of these studies provided the basis for leaf radiative transfer modelling (Jacquemoud & Baret, 1990; Dawson et al., 1998b) which in turn allows estimation of the leaf biochemistry (Demarez et al., 1999). Leaf optical properties, being the inputs of vegetation canopy radiative transfer models (Pinty et al., 2004), facilitate estimations of the biochemical vegetation parameters from airborne or spaceborne image data (Gastellu-Etchegorry & Bruniquel-Pinel, 2001).

The remote sensing approaches developed to estimate the leaf biochemical concentrations have been based on the assumption that the leaf optical properties vary little with their location in the canopy. Considering possible physiological (anatomical) variability in Norway spruce needles, a detailed study investigating spatial variability of the leaf optical properties within the tree crowns is required to confirm or reject this assumption. Therefore, the first objective of this study was to examine the quantitative and qualitative differences in leaf optical properties of five Norway spruce needle categories as defined above, measured at the visible (VIS) and the near-infrared (NIR) part of the electromagnetic spectrum. Next objective was to statistically explore the relation between spectral differences and quantitative characteristics of the needle biochemistry and anatomy, i.e. concentrations of the basic foliage pigments, chlorophyll  $a+b$  ( $C_{ab}$ ) and total carotenoids ( $C_{xc}$ ), dry matter content ( $C_m$ ), and for a limited number of samples the relation with the volume of the needle internal structures (total needle volume, volume of mesophyll tissue, dermal tissues, central cylinder containing the vascular bundle and intercellular air spaces). It is important to highlight that spectral differences for needle age classes, already explored in previous studies (e.g., Hoshizaki et al., 1988; Rock et al., 1994), were not tested within this work. Nevertheless, a balanced number

of needle samples of the last three age classes was used, so that the variability caused by leaf ageing was considered.

## 4.2 Materials and methods

---

### 4.2.1 *Study site and sampling set-up*

A dataset of measured leaf optical properties along with biochemical and biophysical characteristics of spruce needles was acquired at the Šumava Mts. (National Park in the south of the Czech Republic), situated close to the village Modrava (48° 59' N, 13° 28' E) (Malenovský et al., 2006). Fifteen stress resistant (RN) and fifteen stress resilient (RT) Norway spruce trees were selected through the mountain forest stands at the study area. Two branches were cut off by a tree-climber from the south side of each sample crown between September 5<sup>th</sup> and September 15<sup>th</sup>, 2002. The first branch was taken from the *juvenile* crown part and the second branch from the upper level of the *production* crown part. Only sunlit shoots of the last three age classes (current year C, one to two year old C+1, and two to three year old C+2) were detached for further analysis according to the sampling scheme published in Malenovský et al. (2006). The shoot samples were placed into zip-lock plastic bags with a wet pulp paper and transferred to the laboratory in a dark cooler with frozen blue ice (about -4°C). There they were stored in a dark cold freezer (-16°C) and spectrally measured within 24 hours.

### 4.2.2 *Laboratory determination of the foliar pigments*

Parallel needle sets as for the spectroscopic examination were collected in the field. After transportation in a dark cooler, samples were preserved at -70°C until being processed. The foliar pigments were extracted in dimethylformamide (DMF) according to Porra et al. (1989). The amount of photosynthetic pigments ( $C_{ab}$  – chlorophyll *a*, chlorophyll *b* and  $C_{xc}$  – total carotenoids) was determined spectrophotometrically according to equations by Wellburn (1994). The concentration of pigment expressed as weight of pigment per gram of needle dry mass was transformed into micro-grams per needle hemispherical-surface projection [ $\mu\text{g cm}^{-2}$ ] in order to work with units commonly used in remote sensing applications.

### 4.2.3 *Analysis of the needle anatomy*

Cross-sections from frozen needles were obtained using the principle of systematic uniform random sampling (SURS) (Howard & Reed, 1998). Five sections (50  $\mu\text{m}$  thick) 2 mm apart were made along the longitudinal needle axis with the first position determined at random within 2 mm interval from the apex.

For all C+2 needles (10 samples per category), images of the cross-sections were acquired using an Olympus Camedia 5050 digital camera combined with a Olympus BX 50 light transmission microscope equipped by a dry objective Olympus (4x, N.A. = 0.1). The area of the cross-sections and of the various tissues was determined using image analysis software (Lucia G: LIM, Prague). The total needle volume and volumes of individual tissues were determined by the Cavalieri method (Howard & Reed, 1998).

Sections of needles acquired with the SURS principle were examined also with a Bio-rad MRC600 confocal laser scanning microscope with a NIKON water immersion objective (60x,

N.A. = 1.2), using an excitation wavelength at 488 nm. The autofluorescence of chlorophyll in chloroplasts and of phenolic compounds in cell walls was exploited in order to detect the area of mesophyll cells and intercellular air spaces for individual sampling frames with the point-counting method using the Ellipse software (ViDiTo, Slovakia). The volume of intercellular spaces was determined by the Cavalieri method (Howard & Reed, 1998) for C+2 needles of the production crown part (30 samples in total).

#### 4.2.4 *Measurement of the spruce needles optical and biophysical properties*

The hemispherical-directional reflectance and transmittance of the sampled Norway spruce needles were measured between 400-1100 nm with a wavelength interval of 5 nm using a LI-COR spectroradiometer LI-1800-22 (Li-Cor, Inc., Lincoln, NE, USA) coupled with an integrating sphere LI-1800-12. The method proposed by Daughtry (2000a) and extended by Mesarch et al. (1999) was adapted for the Norway spruce needles. Technical details of the improved measurement method are described in Malenovský et al. (2006). The hemispherical-directional reflectance and transmittance signatures of needle samples were computed according to the equations of Mesarch et al. (1999). Elimination of random noise was done by a Savitzky-Golay smoothing filter, applying a second order polynomial function with a bandwidth of 15 nm (Demetriades-Shah et al., 1990). Very noisy spectral signatures were excluded, establishing the size of the final spectral dataset on 143 samples (48 of C, 46 of C+1, and 49 of C+2 needle samples representing 30 of J\_RN, 30 of J\_RT, 30 of P\_RN, 24 of P\_RT, and 29 of S\_RT needle category). The leaf absorption  $\alpha(\lambda)$  was then computed from the measured reflectance  $\rho(\lambda)$  and transmittance  $\tau(\lambda)$ :  $\alpha(\lambda) = 1 - \rho(\lambda) - \tau(\lambda)$ .

The needle projections were measured simultaneously with the spectral measurements using a threshold technique applied on the greyscale images of needle silhouettes (obtained by scanning with a resolution of 1200 dpi) (Malenovský et al., 2006). The total surface of needles was calculated as the projected area multiplied by a universal conversion factor of 2.57, derived experimentally for Norway spruce needles by Waring (1983) and divided by two to acquire the hemispherical-surface projection. Finally, the needle samples were oven-dried at 60°C for 48 hours and weighted. The weight of dry biomass was divided by the needle hemispherical-surface projection in order to obtain the dry matter concentration ( $C_m$ ) in [mg cm<sup>-2</sup>].

#### 4.2.5 *Methods of needle optical properties assessment*

Assessment of the leaf optical properties has been carried out in two ways: i) a quantitative evaluation looking at the intensity (magnitude) of the reflectance, transmittance, and absorption within specific wavelength intervals, and ii) a qualitative assessment, evaluating the pattern and changes in shapes of the measured spectral signatures.

##### *Quantitative evaluation*

The wavelengths of the spectral signatures were divided into four spectral intervals: green (505-600 nm), red (600-685 nm), red edge (RE; 685-760 nm), and near-infrared (NIR; 760-800 nm). The wavelength intervals 400-505 nm and 800-1100 nm were excluded from the analyses because of the high contamination by random sensor noise. The area under the reflectance, transmittance, and absorption curve ( $AUC(\rho, \tau, \alpha)$ ) was integrated within the specified wavelengths according to:



$$AUC(\rho, \tau, \alpha) = \sum_{i=1}^n f(\lambda_i^*)(\lambda_i - \lambda_{i-1}) \text{ where } f(\lambda_i^*) = (h(\lambda_i) + h(\lambda_{i-1}))/2, \quad (4.1)$$

$f(\lambda_i^*)$  is a mean height  $h$  of the spectral signature at two successive wavelengths ( $\lambda_i$  and  $\lambda_{i-1}$ ), and  $n$  is number of integrated wavelengths within the defined spectral interval. The integrated  $AUC$  was providing robust quantitative proportions of the reflected, transmitted, and absorbed light, which were statistically tested for significant differences between the needle categories. Secondly, a more detailed statistical validation of the differences between the needle categories and their relations to the needle anatomical characteristics was carried out for the  $\rho$ ,  $\tau$  and  $\alpha$  values per measured wavelength between 505-800 nm.

#### Qualitative evaluation

A technique called *continuum removal* (Curran et al., 2001) was applied to investigate qualitative changes in needle optical properties between the wavelengths of 505-800 nm. Kokaly and Clark (1999) applied this technique on absorption features of the reflectance measured over dried and ground leaves to estimate the concentrations of nitrogen, lignin, and cellulose. Lately, the continuum removal technique has been used in hyperspectral remote sensing for instance by Underwood et al. (2003) or by Huang et al. (2004).

The continuum line was linearly interpolated between the spectral values at 505 and 800 nm (Kokaly & Clark, 1999). Then, the continuum removal ( $CR(\lambda)$ ) of needle reflectance, transmittance and absorption, respectively, was computed according to the following formula:

$$CR(\lambda) = 1 - \left( \frac{\rho(\lambda)}{R(\lambda)} \right), \quad (4.2)$$

where  $\rho(\lambda)$  is the reflectance at the wavelength  $\lambda$  and  $R(\lambda)$  is a corresponding value at the interpolated continuum line (Curran et al., 2001). The continuum removed spectral signatures ( $\rho$ ,  $\tau$ , and  $\alpha$ ) of all samples were statistically examined per wavelength for significant differences and relationships with the measured biochemical and internal structural properties.

#### 4.2.6 Statistical tests

The statistical significance of the quantitative and qualitative differences between the needle categories was assessed by a one-way analysis of variance (ANOVA) combined with a Tukey-Kramer multiple comparison test in case of a normal distribution of the input dataset. The Kruskal-Wallis (Bonferroni) multiple comparison test, was employed in case of datasets without normal distribution of the inputs. Relationships between the spectral variables and the needle pigment concentrations, dry matter content and volumes of the needle internal structures (tissues) were investigated by correlation (Pearson correlation coefficient  $R$ ) and linear regression tests (coefficient of determination  $r^2$ ).

### 4.3 Results

---

#### 4.3.1 Differences in biochemical and anatomical parameters of the needle categories

The concentrations of photosynthetic pigments ( $C_{ab}$  and  $C_{xc}$ ) did not significantly differ between needles from the juvenile and the production functional parts of the RN crowns. The

same was observed for the stress resilient (RT) trees. However, a significant difference ( $P = 0.0005$ ) in concentration of the examined photosynthetic pigments was found between the RN samples (J\_RN, P\_RN) and the RT samples (J\_RT, P\_RT, and S\_RT), as illustrated in figure 4.1a. The dry matter content ( $C_m$ ) was statistically different between J\_RN, P\_RN and P\_RT, S\_RT categories, but J\_RT samples did not significantly differ from any of those classes (figure 4.1a).

The ANOVA test results of the C+2 anatomical properties described in figure 4.1b revealed that the total needle volume of the J\_RN samples was different from the P\_RT, S\_RT samples and the volume of the P\_RT category was also different from the P\_RN and J\_RT needle categories. The total needle volume of P\_RN, J\_RT, and S\_RT did not differ significantly. The volume of mesophyll tissue (including the intercellular air spaces) in the J\_RN, P\_RN, and J\_RT samples was higher than in the P\_RT and S\_RT samples. A similar situation was found for the volumes of dermal tissue, except that the volumes for the S\_RT samples did not differ from any of the other needle categories. The central cylinder volumes differed only between the J\_RN and P\_RT needle categories. Finally, the P\_RN volume of the mesophyll cells as well as intercellular air spaces appeared to be significantly higher than these volumes for the P\_RT and S\_RT categories.

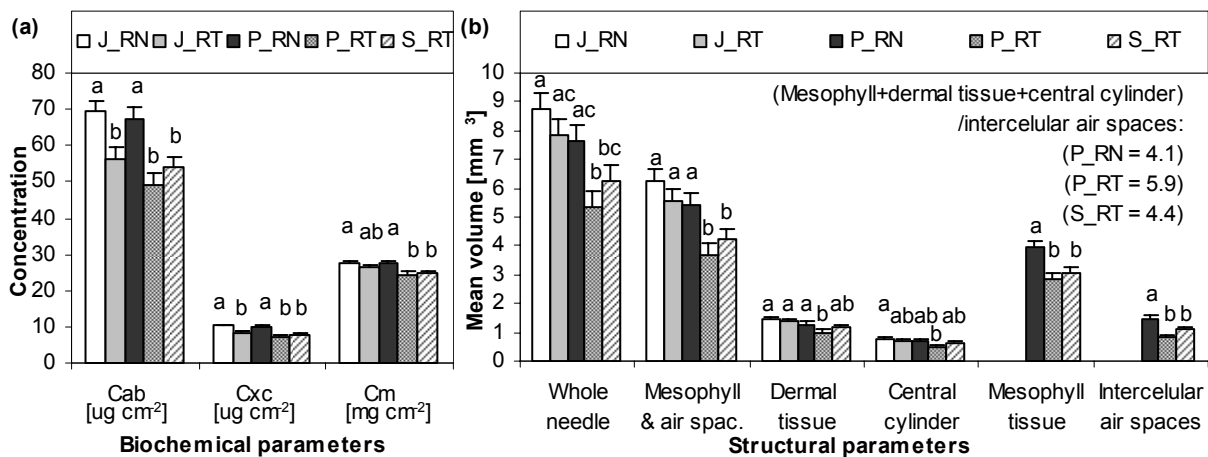


Figure 4.1. Results of the one-way ANOVA analysis for (a) the concentrations of the measured needle biochemical compounds ( $C_{ab}$  – concentration of the chlorophylls a+b,  $C_{xc}$  – concentration of the total carotenoids,  $C_m$  – dry matter content) and (b) the mean volumes of the whole needles and basic needle internal structures for selected three years old samples (10 samples per category). Bar represents one standard error. Columns with different superscripts represent a statistically significant difference between the categories ( $P = 0.05$ ). Values in parenthesis represent the volume ratio of the mesophyll, dermal and central cylinder tissue against the intercellular air spaces.

Needle categories:

- J\_RN – primary needles from the stress resistant juvenile crown part,
- J\_RT – primary needles from the stress resilient juvenile crown part,
- P\_RN – primary needles from the stress resistant production crown part,
- P\_RT – primary needles from the stress resilient production crown part,
- S\_RT – secondary needles from the stress resilient production crown part.

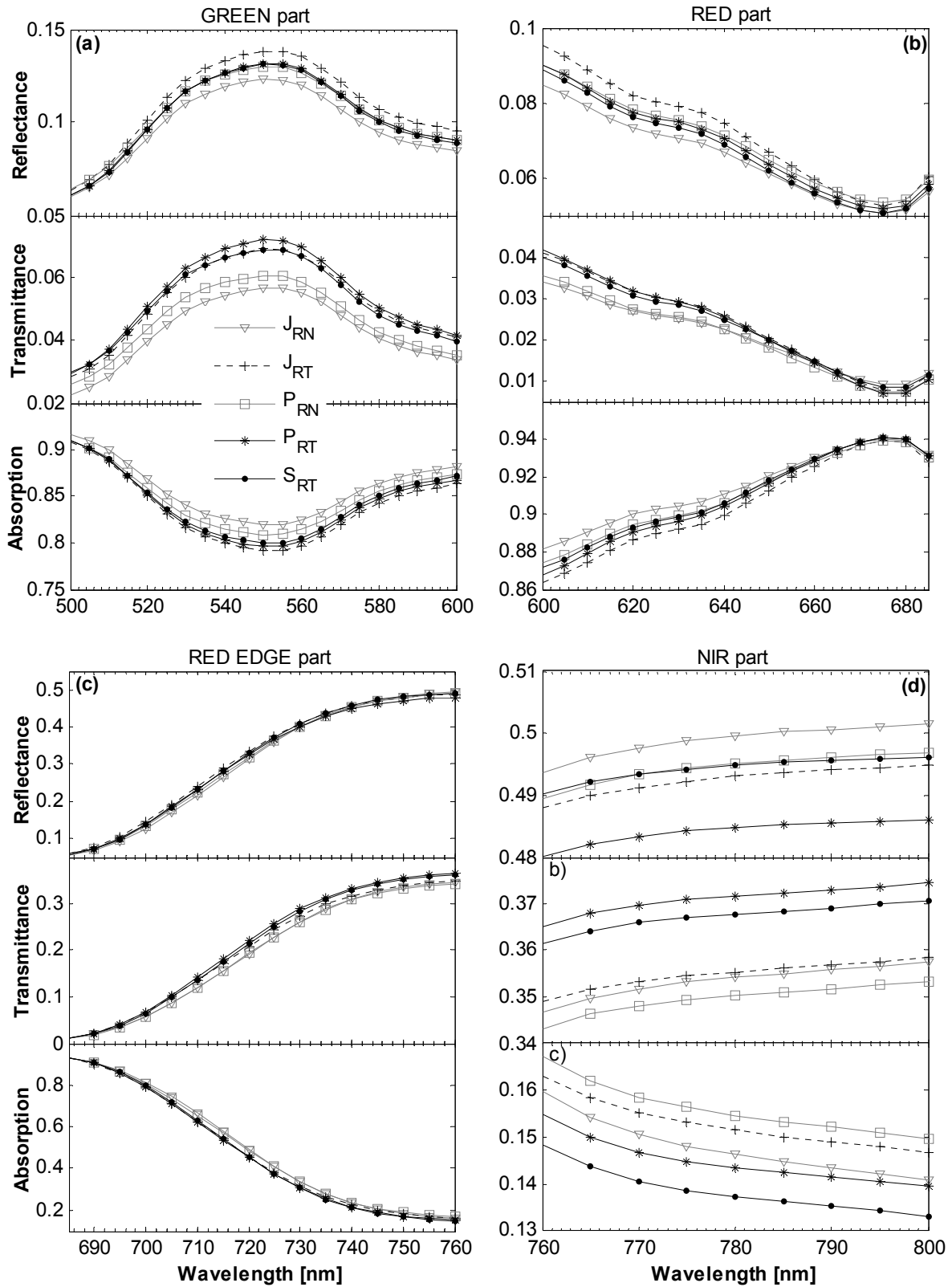


Figure 4.2. The average measured optical properties of the needle categories in (a) green, (b) red, (c) red edge (RE) and (d) near infrared (NIR) part of the electromagnetic spectrum. For description of needle categories: JRN, JRT, PRN, PRT and SRT see legend of figure 4.1.

#### 4.3.2 Differences in optical properties of spruce needles and statistical relations to biochemical and biophysical parameters

The averaged optical properties of investigated needle categories are depicted in Figure 4.2. It is obvious that the RN reflectance, transmittance and absorption signatures systematically differed from the RT signatures within the green, red, and RE part of the electromagnetic spectrum (lower in case of  $\rho$  and  $\tau$ , and higher in case of  $\alpha$ ). Spectral signatures in the NIR spectral region are quite similar and their order is less systematic.

##### Quantitative evaluation

Most of the significant quantitative differences between optical properties of the needle categories were identified within green and red wavelengths (505-655 nm). Some differences were discovered within short wavelengths of the RE part (690-720 nm) and no statistically significant difference was revealed in the NIR part. Concerning the integrated AUC, differences were found for green  $\rho$  ( $P = 0.1$ ), green  $\alpha$  ( $P = 0.03$ ) and also red  $\rho$  ( $P = 0.06$ ) AUC of the J\_RN and J\_RT categories (figure 4.3a,c). Similarly, evidence of a statistical difference was found for the AUC of green J\_RN and P\_RT transmittances and between the AUC of RE J\_RN, P\_RN and P\_RT transmittances ( $P = 0.06$ ) (figure 4.3b). Detailed analysis per measured wavelength showed that reflectances for J\_RN samples at 570-655 nm and 690-710 nm are statistically lower than for J\_RT samples ( $P = 0.08$ ). More complex results were found for the transmittance values of the needle categories. Transmittances of the J\_RN samples differed (were lower at  $P = 0.01$ ) at 535-570 nm and 715-720 nm from P\_RT samples, at 505-510 nm and 525-530 nm from both P\_RT and S\_RT samples, and at 515-520 nm from all the stress resilient needle categories, i.e. J\_RT, P\_RT and S\_RT. Finally, the absorption values at 505-615 nm were higher ( $P = 0.06$ ) for J\_RN than for J\_RT samples.

As shown in table 4.1, several green, red, and RE wavelengths were significantly related to the  $C_{ab}$  and  $C_{xc}$  leaf concentrations (Pearson coefficient  $R > 0.70$ ,  $r^2$  coefficient = 0.46-0.65). A positive correlation was observed for the needle absorption and a negative one for the reflectance and transmittance at visible and red edge wavelengths. The strongest statistically significant linear regressions were obtained for the relation between the foliage pigments and  $\rho$ ,  $\tau$ , and  $\alpha$  at 550 nm and 710 nm ( $r^2 > 0.50$ ). The correlation and regression relationships between spectral values and dry matter content were weak ( $r^2 = 0.12-0.43$ ).

##### Qualitative evaluation

Statistically significant differences between the continuum removed (CR) hemispherical reflectances, transmittances and absorptions of the needle categories within the 505-800 nm region are given in table 4.2. A stable spectral difference was observed between J\_RN and J\_RT needle categories for green CR ( $\rho$ ,  $\tau$ , and  $\alpha$ ) and red CR ( $\rho$ ). However, more significant differences were discovered between the CR ( $\rho$ ,  $\tau$ , and  $\alpha$ ) of the red edge wavelengths. Special attention concerning the high separability of the examined stress response classes should be paid to the CR reflectance at 725-745 nm, the CR transmittance at 725-740 nm, and the CR absorption at 725-730 nm. No significant differences in CR spectral signatures of the NIR part were found, except for the CR reflectance at 760 nm and 765 nm where P\_RN samples were different from S\_RT samples. All the observed differences were consistent in the way that the stress resistant CR values were always different only from the stress resilient CR values, so no mutual difference in-between RN samples or in-between RT samples was recorded.

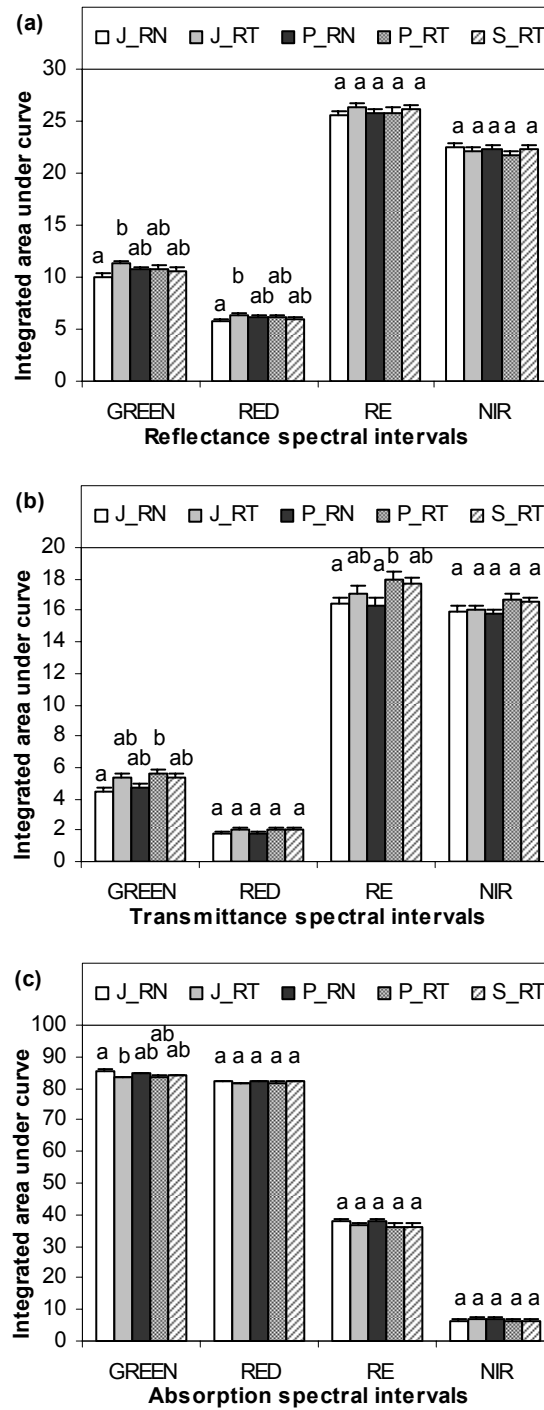


Figure 4.3. Statistical one-way ANOVA differences of the integrated areas under the (a) reflectance, (b) transmittance and (c) absorption curve of the green (505-600 nm), red (600-685 nm), red edge (RE, 685-760 nm) and near infrared (NIR, 760-800 nm) spectral intervals. Bar represents one standard error. Columns with different superscripts represent a statistically significant difference between the categories ( $P = 0.1$ ). For needle categories see legend of figure 4.1.

Table 4.1. The coefficients of determination ( $r^2$ ) for linear regressions between needle hemispherical optical properties (reflectance, transmittance, and absorption) per wavelength and biochemical needle characteristics.

$\lambda$ * [nm]	$r^2$ for REFLECTANCE			$r^2$ for TRANSMITTANCE			$r^2$ for ABSORPTION		
	$C_m^{**}$ [g cm <sup>-2</sup> ]	$C_{xc}^{**}$ [ $\mu$ g cm <sup>-2</sup> ]	$C_{ab}^{**}$ [ $\mu$ g cm <sup>-2</sup> ]	$C_m$ [g cm <sup>-2</sup> ]	$C_{xc}$ [ $\mu$ g cm <sup>-2</sup> ]	$C_{ab}$ [ $\mu$ g cm <sup>-2</sup> ]	$C_m$ [g cm <sup>-2</sup> ]	$C_{xc}$ [ $\mu$ g cm <sup>-2</sup> ]	$C_{ab}$ [ $\mu$ g cm <sup>-2</sup> ]
515							0.21	0.49	0.52
520							0.22	0.55	0.57
525	0.13	0.49	0.50				0.23	0.58	0.60
530	0.13	0.51	0.52				0.24	0.59	0.61
535	0.14	0.52	0.53	0.29	0.46	0.49	0.24	0.60	0.62
540	0.14	<b>0.53</b> #	<b>0.54</b> #	0.29	0.48	0.51	0.24	0.60	0.62
545	0.14	<b>0.53</b> #	<b>0.54</b> #	0.30	0.49	0.52	0.24	0.60	0.62
550	0.14	<b>0.53</b> #	<b>0.54</b> #	0.30	0.50	0.54	0.24	<b>0.60</b> #	<b>0.63</b> #
555	0.14	0.52	0.54	0.30	<b>0.51</b> #	<b>0.54</b> #	0.23	<b>0.60</b> #	<b>0.63</b> #
560	0.13	0.52	0.53	0.29	<b>0.51</b> #	<b>0.54</b> #	0.23	0.59	0.62
565	0.13	0.50	0.52	0.28	<b>0.51</b> #	<b>0.54</b> #	0.22	0.58	0.61
570	0.12	0.48	0.51	0.27	0.50	0.53	0.21	0.57	0.60
575	0.12	0.46	0.49	0.26	0.48	0.51	0.20	0.55	0.58
580				0.25	0.47	0.50	0.20	0.54	0.57
585				0.25	0.47	0.50	0.19	0.53	0.56
590				0.24	0.47	0.49	0.19	0.52	0.55
595				0.24	0.47	0.49	0.18	0.51	0.55
600				0.23	0.47	0.49	0.18	0.51	0.54
605				0.23	0.46	0.48	0.18	0.50	0.53
610							0.18	0.49	0.52
615							0.17	0.48	0.51
620							0.17	0.47	0.50
625							0.17	0.47	0.50
630							0.17	0.46	0.49
695				0.24	0.50	0.51	0.20	0.53	0.56
700	0.14	0.49	0.52	0.29	0.55	0.57	0.23	0.58	0.61
705	0.15	0.53	0.55	0.32	0.58	0.60	0.25	0.61	0.64
710	0.15	<b>0.54</b> #	<b>0.55</b> #	0.35	0.60	0.62	0.27	0.64	0.65
715	0.14	0.53	0.53	0.38	<b>0.62</b> #	<b>0.63</b> #	0.28	<b>0.65</b> #	<b>0.65</b> #
720	0.13	0.50	0.48	0.41	0.61	0.62	0.29	0.64	0.63
725				0.42	0.60	0.59	0.29	0.61	0.59
730				0.43	0.57	0.55	0.27	0.56	0.52
735				0.42	0.53	0.51	0.25	0.49	0.45
740				0.41	0.50	0.47			

\* Only wavelengths ( $\lambda$ ) with a Pearson correlation coefficient ( $R$ )  $\geq 0.70$  for at least one independent variable are listed.

\*\*  $C_m$  – dry matter content,  $C_{xc}$  – carotenoid concentration and  $C_{ab}$  – chlorophyll concentration.

# The highest significant coefficients of determination within the examined spectral regions.

Table 4.2. Result of the one-way ANOVA combined with the Tukey-Kramer and Kuskal-Wallis test appointing statistically significant differences among continuum removed (CR) hemispherical optical properties between 505-800 nm: (a) reflectance, (b) transmittance, and (c) absorption.

(a)		<i>Statistical differences in CR REFLECTANCE per wavelength [nm] (<math>\alpha</math>-level = 0.01)</i>														
Needle cat.*	510 to 660	685 to 700	705	710	715	720	725	730	735	740	745	750	755	760	765	
J <sub>RN</sub>	J <sub>RT</sub>	J <sub>RT</sub>	J <sub>RT</sub> P <sub>RT</sub>	J <sub>RT</sub> P <sub>RT</sub>	J <sub>RT</sub> P <sub>RT</sub>	J <sub>RT</sub> P <sub>RT</sub>	J <sub>RT</sub> P <sub>RT</sub>	J <sub>RT</sub> P <sub>RT</sub>	J <sub>RT</sub> P <sub>RT</sub>	J <sub>RT</sub> P <sub>RT</sub>	J <sub>RT</sub> P <sub>RT</sub>	J <sub>RT</sub> P <sub>RT</sub>	J <sub>RT</sub> P <sub>RT</sub>	J <sub>RT</sub> P <sub>RT</sub>	J <sub>RT</sub> P <sub>RT</sub>	
J <sub>RT</sub>	J <sub>RN</sub>	J <sub>RN</sub>	J <sub>RN</sub>	J <sub>RN</sub>	J <sub>RN</sub>	J <sub>RN</sub>	J <sub>RN</sub>	J <sub>RN</sub>	J <sub>RN</sub>	J <sub>RN</sub>	J <sub>RN</sub>	J <sub>RN</sub>	J <sub>RN</sub>	J <sub>RN</sub>	J <sub>RN</sub>	
P <sub>RN</sub>								J <sub>RT</sub> P <sub>RT</sub>	J <sub>RT</sub> P <sub>RT</sub>	P <sub>RT</sub>	P <sub>RT</sub>	P <sub>RT</sub>	P <sub>RT</sub>	P <sub>RT</sub>	P <sub>RT</sub>	
P <sub>RT</sub>		J <sub>RN</sub>	J <sub>RN</sub>	J <sub>RN</sub>	J <sub>RN</sub>	J <sub>RN</sub>	J <sub>RN</sub>	J <sub>RN</sub>	J <sub>RN</sub>	J <sub>RN</sub>	J <sub>RN</sub>	J <sub>RN</sub>	J <sub>RN</sub>	J <sub>RN</sub>	J <sub>RN</sub>	
S <sub>RT</sub>			J <sub>RN</sub>	J <sub>RN</sub>	J <sub>RN</sub>	J <sub>RN</sub>	J <sub>RN</sub>	J <sub>RN</sub>	J <sub>RN</sub>	J <sub>RN</sub>	J <sub>RN</sub>	J <sub>RN</sub>	J <sub>RN</sub>	J <sub>RN</sub>	J <sub>RN</sub>	
(b)		<i>Statistical differences in CR TRANSMITTANCE per wavelength [nm] (<math>\alpha</math>-level = 0.03)</i>														
Needle cat.	550 to 580	710	715	720	725	730	735	740	745							
J <sub>RN</sub>	J <sub>RT</sub>		J <sub>RT</sub>	J <sub>RT</sub> P <sub>RT</sub>	J <sub>RT</sub> P <sub>RT</sub>	J <sub>RT</sub> P <sub>RT</sub>	J <sub>RT</sub> P <sub>RT</sub>	J <sub>RT</sub> P <sub>RT</sub>	J <sub>RT</sub> P <sub>RT</sub>	J <sub>RT</sub> P <sub>RT</sub>	J <sub>RT</sub> P <sub>RT</sub>					
J <sub>RT</sub>	J <sub>RN</sub>		J <sub>RN</sub>	J <sub>RN</sub>	J <sub>RN</sub>	J <sub>RN</sub>	J <sub>RN</sub>	J <sub>RN</sub>	J <sub>RN</sub>	J <sub>RN</sub>	J <sub>RN</sub>					
P <sub>RN</sub>											P <sub>RT</sub>					
P <sub>RT</sub>			J <sub>RN</sub>	J <sub>RN</sub>	J <sub>RN</sub>	J <sub>RN</sub>	J <sub>RN</sub>	J <sub>RN</sub>	J <sub>RN</sub>	J <sub>RN</sub>	J <sub>RN</sub>					
S <sub>RT</sub>					J <sub>RN</sub>	J <sub>RN</sub>	J <sub>RN</sub>	J <sub>RN</sub>	J <sub>RN</sub>	J <sub>RN</sub>	J <sub>RN</sub>					
(c)		<i>Statistical differences in CR ABSORPTION per wavelength [nm] (<math>\alpha</math>-level = 0.03)</i>														
Needle cat.	510 to 575	715	720	725	730											
J <sub>RN</sub>	J <sub>RT</sub>		J <sub>RT</sub>	J <sub>RT</sub> P <sub>RT</sub>	J <sub>RT</sub> P <sub>RT</sub>	J <sub>RT</sub> P <sub>RT</sub>										
J <sub>RT</sub>	J <sub>RN</sub>		J <sub>RN</sub>	J <sub>RN</sub>	J <sub>RN</sub>	J <sub>RN</sub>										
P <sub>RN</sub>																
P <sub>RT</sub>			J <sub>RN</sub>	J <sub>RN</sub>	J <sub>RN</sub>											
S <sub>RT</sub>				J <sub>RN</sub>	J <sub>RN</sub>											

\* For needle categories see legend of figure 4.1.

Table 4.3. The coefficients of determination ( $r^2$ ) for linear regressions between continuum removed (CR) values of the reflectance, transmittance, and absorption per wavelength and biochemical needle properties.

CR $\lambda$ * [nm]	$r^2$ for CR REFLECTANCE			$r^2$ for CR TRANSMITTANCE			$r^2$ for CR ABSORPTION		
	$C_m$ ** [g cm <sup>-2</sup> ]	$C_{xc}$ ** [ $\mu$ g cm <sup>-2</sup> ]	$C_{ab}$ ** [ $\mu$ g cm <sup>-2</sup> ]	$C_m$ [g cm <sup>-2</sup> ]	$C_{xc}$ [ $\mu$ g cm <sup>-2</sup> ]	$C_{ab}$ [ $\mu$ g cm <sup>-2</sup> ]	$C_m$ [g cm <sup>-2</sup> ]	$C_{xc}$ [ $\mu$ g cm <sup>-2</sup> ]	$C_{ab}$ [ $\mu$ g cm <sup>-2</sup> ]
510	0.13	0.48	0.52						
515	0.13	0.50	0.54				0.16	0.48	0.51
520	0.14	0.52	0.55				0.18	0.51	0.55
525	0.15	0.53	0.56	0.22	0.49	0.50	0.19	<b>0.53</b> #	<b>0.56</b> #
530	0.15	<b>0.53</b> #	<b>0.57</b> #	0.23	<b>0.49</b> #	<b>0.51</b> #	0.19	<b>0.53</b> #	<b>0.56</b> #
535	0.15	0.53	0.56	0.22	<b>0.49</b> #	<b>0.51</b> #	0.18	0.52	0.55
540	0.15	0.51	0.55	0.21	<b>0.49</b> #	<b>0.51</b> #	0.17	0.50	0.54
545	0.15	0.50	0.55	0.21	<b>0.49</b> #	<b>0.51</b> #	0.16	0.48	0.52
550	0.15	0.49	0.54	0.20	<b>0.49</b> #	<b>0.51</b> #	0.15	0.45	0.50
555	0.14	0.48	0.53	0.20	0.48	0.51			
560	0.14	0.46	0.51	0.18	0.47	0.50			
565	0.13	0.44	0.49	0.17	0.45	0.48			
700				0.17	0.45	0.49			
705				0.19	0.48	0.53			
710	0.16	0.45	0.51	0.21	0.51	0.55			
715	0.17	0.48	0.54	0.23	0.53	0.57			
720	0.19	0.51	0.56	0.25	0.55	0.59			
725	0.21	0.54	0.59	0.26	0.57	0.61			
730	0.23	0.58	0.62	0.28	0.59	0.62	0.27	0.56	0.60
735	0.26	0.61	0.64	0.30	0.61	0.63	0.33	<b>0.64</b> #	<b>0.63</b> #
740	0.30	<b>0.64</b> #	<b>0.66</b> #	0.32	<b>0.63</b> #	<b>0.64</b> #	0.31	0.56	0.53
745	0.33	0.64	0.64	0.34	0.64	0.62			
750	0.35	0.60	0.57	0.36	0.61	0.57			
755	0.32	0.49	0.45	0.34	0.51	0.45			

\* Only wavelengths ( $\lambda$ ) with a Pearson correlation coefficient (R)  $\geq 0.70$  for at least one independent variable are listed.

\*\*  $C_m$  – dry matter content,  $C_{xc}$  – carotenoid concentration and  $C_{ab}$  – chlorophyll concentration.

# The highest significant coefficients of determination within the examined spectral regions.

The coefficients of determination ( $r^2$ ) between CR  $\rho$ ,  $\tau$ , and  $\alpha$  at measured wavelengths and biochemical concentrations for cases where the Pearson correlation coefficient of at least one relation exceeded 0.70 are given in table 4.3. It is worth mentioning that the strongest relationships with pigments for the visible spectral part were obtained for the wavelengths at about 530 nm ( $r^2 = 0.49-0.56$ ), and concerning the red edge spectral part for the wavelengths at 735 nm and 740 nm ( $r^2 = 0.63-0.66$ ). Similarly to the spectral intensities, the correlations and regressions of the CR spectral wavelengths with the dry matter content were rather poor ( $r^2 = 0.13-0.36$ ).

#### 4.3.3 Spectral differences and relationships with anatomical features of C+2 needles

The quantitative differences in AUC of C+2 needle optical properties within the four defined spectral regions were consistent with the results obtained for all three age classes according to the ANOVA test (see figure 4.3). Additional significant differences were



identified for green absorption, where the AUC of the J\_RN samples was higher than the AUC of the P\_RT samples ( $P = 0.03$ ). Also the AUC of transmittance in red and RE intervals was larger for P\_RT needles than for J\_RN and P\_RN needles ( $P = 0.02$ ). The same difference was found for the AUC of RE absorption ( $P = 0.02$ ), except that the P\_RT AUC was smaller than the AUC of J\_RN and P\_RN samples.

The significance of the qualitative differences in continuum removed (*CR*) spectral signatures of the C+2 needle categories was investigated only for wavelengths with a strong relationship to the measured needle anatomical parameters. Strong correlations and regressions were found for the *CR* reflectance at 740-750 nm and *CR* transmittance at 735-745 nm with the volumes of the intercellular air spaces (Pearson coefficient  $R \geq 0.66$ ,  $r^2 = 0.43-0.51$ ), and also between the *CR* reflectance at 745-750 nm and the volumes of the mesophyll tissue (Pearson coefficient  $R \geq 0.65$ ,  $r^2 = 0.43-0.44$ , cf., table 4.4). The correlations with the volumes of the other structural parameters were not significant. As one can see in Table 4.4, the wavelengths where the *CR*  $\rho$  and  $\tau$  strongly correlate with the intercellular air spaces and with the foliar pigment concentrations ( $C_{ab}$  and  $C_{xc}$ ) are similar. The *CR* absorption at 740 nm was only strongly correlated with foliar pigments. The one-way ANOVA showed that the *CR* reflectance and absorption of the C+2 RN samples at 740 nm were, except the S\_RT category, statistically different from the RT samples. This was in agreement with the differences in pigment concentrations and also intercellular air spaces (cf., figure 4.1). A similar pattern was also found for the *CR* transmittance at 745 nm, but significantly different was only the J\_RN category from J\_RT and P\_RT, and P\_RN from P\_RT.

## 4.4 Discussion

### 4.4.1 *Understanding the quantitative differences in optical properties of needle categories*

Our results about the variability in optical properties of Norway spruce crowns were consistent with the findings of O'Neill et al. (2002), investigating reflectance variation throughout a Sitka spruce (*Picea sitchensis*) canopy. Spectral variability between needles of the same age coming from different parts of the same crown was relatively small. All the samples were taken from sun-lit branches, which may explain the lack of differences in pigment content between juvenile and production crown parts. The optical differences in the visible and the red edge wavelengths, found between the needles of the RN and RT trees, fully corresponded with the differences found in their foliar pigment concentrations. All the sampled trees were growing under the same environmental conditions and they did not display any visible symptoms of severe damage (they differed only by the proportion of secondary shoots in the production crown part). Thus, the lower concentrations of foliar pigments detected in needles of the resilient trees may indicate that they are more sensitive to multiple stress than the resistant trees. Similarly to Gitelson and Merzlyak (1996) the strongest regressions between chlorophyll or carotenoid concentrations and optical properties were established at the red edge (710-715 nm). The second highest ones were found between pigments and spectral signatures at the green wavelengths (540-565 nm). The red wavelengths of strong photosynthetic pigment's absorption (665-680 nm) did not reveal a significant correlation with the  $C_{ab}$  and  $C_{xc}$  concentrations. This can be explained by the presumption that

these wavelengths become saturated and consequently less sensitive to the changes in the quantity of pigments (Daughtry et al., 2000a).

Table 4.4. Pearson correlation coefficients (R) and coefficients of determination ( $r^2$ ) for linear regressions between continuum removed (CR) values of the reflectance and transmittance per wavelength and biochemical and anatomical properties of 30 selected three years old needle samples.

$\lambda$ [nm]*	Biochemical concentrations [ $\mu\text{g cm}^{-2}$ ]				Structural parameters – Volumes [ $\text{mm}^3$ ]				
	$C_{xc}$ **		$C_{ab}$ **		Mesophyll tissue		Intercellular spaces		
	R	$r^2$	R	$r^2$	R	$r^2$	R	$r^2$	
<i>Continuum Removed (CR) REFLECTANCE of C+2 needle samples (n = 30)</i>									
740	<b>0.78</b> #	<b>0.60</b> #	<b>0.77</b> #	<b>0.59</b> #	0.61	0.37	<b>0.69</b> #	<b>0.47</b> #	
745	<b>0.77</b> #	<b>0.59</b> #	<b>0.73</b> #	<b>0.54</b> #	<b>0.65</b> #	<b>0.43</b> #	<b>0.72</b> #	<b>0.51</b> #	
750	<b>0.71</b> #	<b>0.50</b> #	<b>0.64</b> #	0.41	<b>0.67</b> #	<b>0.44</b> #	<b>0.69</b> #	<b>0.48</b> #	
<i>Continuum Removed (CR) TRANSMITTANCE of C+2 needle samples (n = 30)</i>									
735	<b>0.74</b> #	<b>0.54</b> #	<b>0.75</b> #	<b>0.57</b> #	0.58	0.36	<b>0.66</b> #	<b>0.43</b> #	
740	<b>0.74</b> #	<b>0.54</b> #	<b>0.74</b> #	<b>0.54</b> #	0.60	0.38	<b>0.67</b> #	<b>0.44</b> #	
745	<b>0.72</b> #	<b>0.52</b> #	<b>0.70</b> #	<b>0.49</b> #	0.62	0.38	<b>0.67</b> #	<b>0.45</b> #	

\* Only wavelengths ( $\lambda$ ) with a Pearson correlation coefficient (R)  $\geq 0.65$  for the relation with the intercellular air spaces or mesophyll tissue volume are listed.

\*\*  $C_{xc}$  – carotenoid concentration and  $C_{ab}$  – chlorophyll concentration.

# The highest significant coefficients of determination within the examined spectral regions.

In a parallel study (Malenovský et al., 2006) we have shown statistical differences in the leaf empirical structural parameter N of the PROSPECT model (Jacquemoud & Baret, 1990), which appeared to be lower ( $N < 2.0$ ) for the P\_RT and S\_RT samples and higher ( $N > 2.1$ ) for the J\_RN, P\_RN and J\_RT samples. According to Jacquemoud and Baret (1990) a low N parameter corresponds with a compact mesophyll tissue causing a decrease in multiple scattering of light and consequently decreasing the leaf reflectance while increasing the transmittance. A high N value represents a mesophyll with more intercellular air cavities and a higher amount of cell walls, resulting in more multiple scattering, which increases the reflectance while decreasing the leaf transmittance. Our results of the C+2 needle's interior showed an almost six times higher volume of the central cylinder with mesophyll and dermal tissues than the volume of the intercellular spaces for the P\_RT samples (figure 4.1b), which corresponds with the low value of the N structural parameter in PROSPECT. The lower density of the intercellular air spaces in needles of P\_RT samples contributed probably to their low NIR reflectance and their high NIR transmittance within all the needle categories (Figure 4.2d). The reverse spectral effect was observed for the P\_RN needle category containing more intercellular air spaces and exhibiting a higher N structural parameter. The volume of the central cylinder with mesophyll and dermal tissues proved to be only four times higher than the volume of the intercellular spaces for the P\_RN C+2 samples.

In contrast to our results, Rock et al. (1994) described an opposite relationship when observing needles of two age classes of Red spruce (*Picea rubens* Sarg.). Needles with a lower percentage of intercellular air spaces exhibited a slight increase of NIR reflectance and a significant decrease of NIR transmittance. However, the changes in NIR reflectance and transmittance were due to higher NIR absorption, enlarged by an increase in cell size and consequently total amount of needle biomass. Thus, internal structures (amount of cell wall-air interfaces) played a less important role in these spectral differences.

Although we have proved statistical differences between RN and RT needle categories with regard to volumes of whole needles, mesophyll tissue and intercellular air spaces (figure 4.1b), the NIR reflectances and transmittances remained statistically invariant for all the examined needle categories and were also not found to be statistically related to these volumetric changes. A statistically lower dry matter content of the needles from the RT trees was expected to decrease their NIR absorption. The NIR absorption of the P\_RT and S\_RT samples was actually lower compared to other samples (Figure 4.2d); however, this difference was rather small and statistically not significant.

#### 4.4.2 Interpretation of the qualitative differences in relation to the needle properties and processes

Surprisingly, the highly significant regressions between the concentrations of foliar pigments and the continuum removed spectral signatures were spectrally shifted compared to the spectral intensities. The strongest relationship was found at the wavelengths around 740 nm corresponding with the wavelength of far-red chlorophyll fluorescence (Buschmann et al., 2000). As for the visible part the strongest regressions were observed at wavelengths at about 530 nm (table 4.3) where the fluorescence emission raises by the photo-chemical protective reaction of the xanthophylls (Lichtenthaler, 1998). Besides, the continuum removed reflectance and transmittance at 740 nm were statistically different for the defined needle categories (table 4.2), which might have been caused by their different fluorescence due to environmental stresses (Lichtenthaler et al., 1998). However, the fluorescence fluxes of the examined samples were not measured. An evidence supporting this hypothesis was shown by Zarco-Tejada et al. (2003a), revealing that the first derivative (a technique of a similar kind as continuum removal) applied on the canopy reflectance between 600-800 nm was capable of tracking the steady-state fluorescence changes.

The continuum removed reflectances and transmittances between 735-750 nm were strongly correlated with the concentrations of foliar pigments, but also with the amount of intercellular air spaces. This finding suggests a concurrent effect of the biochemical and internal structural parameters on the leaf optical properties at these wavelengths. A higher amount of intercellular air spaces increases the number of cell wall-air interfaces and may enhance the multiple scattering, but it also changes the spatial distribution of the chloroplasts, which may influence the needle optical properties. Therefore, further detailed needle anatomical 3D analysis should be performed to better understand the interaction of light with the heterogeneously distributed leaf cells.

## **4.5 Conclusions**

---

In this study we have found no significant measurable optical differences between needles originating from the juvenile and the production crown parts for either stress resistant or stress resilient Norway spruce trees. Therefore, we conclude that needles of a specific age-class sampled from a randomly selected branch within the juvenile or production crown parts can be considered as being representative for all needles of the same age-class throughout both functional crown parts of the tree. Nevertheless, statistical comparison of the optical properties of needles from stress resistant and stress resilient trees showed significant spectral differences at red edge, green and partially red wavelengths of the electromagnetic spectrum.

The spectral differences found at red edge and green spectral regions were statistically related to the variability in concentration of the observed foliar pigments, responding to the magnitude of environmental stressors. Therefore, we can conclude that remote sensing approaches, designed to estimate Norway spruce foliar pigment concentrations, should take into consideration the spectral differences between the actual tree stress response classes (resistant vs. resilient), because they might have an impact on both: i) calibration and parameterisation of statistical or physical models, and ii) validation of their results.

The observed differences in continuum removed reflectance and transmittance between the stress resistant and stress resilient trees suggest that this transformation may potentially trace changes in plant fluorescence processes. Yet, detection of small fluorescence emissions from the reflectance of a natural forest canopy measured by airborne or satellite spectroradiometers will be complicated by several negative factors, e.g. the angular anisotropy of the canopy reflectance, the complexity of the canopy structure, disturbance by the atmosphere and an insufficient signal to noise ratio. Therefore, we suggest focusing more on fluorescence monitoring in further analysis.

#### 4.6 Acknowledgements

---

This study was supported by the Sabbatical Fellowship 1K04 provided to Zbyněk Malenovský by the Ministry of Education, Youth and Sports of the Czech Republic, by the Research Plan of the Institute of Systems Biology and Ecology (AVOZ60870520) and the project IAA600110507 of the Grant Agency of the Academy of Sciences of Czech Republic (Charles University).

#### 4.7 References

---

- Albrechtová J, Rock BN, Soukupová J, Entcheva P, Šolcová B, Polák T. 2001. Biochemical, histochemical, structural and reflectance markers of damage in Norway spruce from Krušné hory Mts. used for interpretation of remote sensing data. *Journal of Forest Science* 47: 26-33.
- Bousquet L, Lacherade S, Jacquemoud S, Moya I. 2005. Leaf BRDF measurements and model for specular and diffuse components differentiation. *Remote Sensing of Environment* 98: 201-211.
- Brakke TW. 1994. Specular and diffuse components of radiation scattered by leaves. *Agricultural and Forest Meteorology* 71: 283-295.
- Buschmann C, Langsdorf G, Lichtenthaler HK. 2000. Imaging of the blue, green, and red fluorescence emission of plants: An overview. *Photosynthetica* 38: 483-491.
- Chapin FS, Matson PA, Mooney HA. 2002. *Principles of terrestrial ecosystem ecology*. New York, Berlin: Springer.
- Cudlin P, Novotny R, Moravec I, Chmelikova E. 2001. Retrospective evaluation of the response of montane forest ecosystems to multiple stress. *Ekologia-Bratislava* 20: 108-124.
- Curran PJ, Dungan JL, Peterson DL. 2001. Estimating the foliar biochemical concentration of leaves with reflectance spectrometry: Testing the Kokaly and Clark methodologies. *Remote Sensing of Environment* 76: 349-359.
- Daughtry CST, Biehl LL, Ranson KJ. 1989. A new technique to measure the spectral properties of conifer needles. *Remote Sensing of Environment* 27: 81-91.

- Daughtry CST, Walthall CL, Kim MS, de Colstoun EB, McMurtrey III JE. 2000. Estimating corn leaf chlorophyll concentration from leaf and canopy reflectance. *Remote Sensing of Environment* 74: 229-239.
- Dawson TP, Curran PJ, Plummer SE. 1998. LIBERTY- Modeling the effects of leaf biochemical concentration on reflectance spectra. *Remote Sensing of Environment* 65: 50-60.
- Demarez V, Gastellu-Etchegorry JP, Mougou E, Marty G, Proisy C, Dufrene E, Le Dantec V. 1999. Seasonal variation of leaf chlorophyll content of a temperate forest. Inversion of the PROSPECT model. *International Journal of Remote Sensing* 20: 879-894.
- Demetriades-Shah TH, Steven MD, Clark JA. 1990. High resolution derivative spectra in remote sensing. *Remote Sensing of Environment* 33: 55-64.
- Dickson RE, Isebrands JG. 1991. Leaves as regulators of stress response. In: Mooney HA, Winner WE and Pell EJ, eds. *Response of plants to multiple stresses*. San Diego, New York, London: Academic Press, p. 4-34.
- Fourty T, Baret F, Jacquemoud S, Schmuck G, Verdebout J. 1996. Leaf optical properties with explicit description of its biochemical composition: Direct and inverse problems. *Remote Sensing of Environment* 56: 104-117.
- Fukshansky L. 1981. Optical properties of plants. In: Smith H, eds. *Plants and the daily spectrum*. London: Academic Press, p. 21-42.
- Fukshansky L, Remisowsky AMv, McClendon J, Ritterbusch A, Richter T, Mohr H. 1993. Absorption-spectra of leaves corrected for scattering and distributional error - a radiative-transfer and absorption statistics treatment. *Photochemistry and Photobiology* 57: 538-555.
- Gastellu-Etchegorry JP, Bruniquel-Pinel V. 2001. A modeling approach to assess the robustness of spectrometric predictive equations for canopy chemistry. *Remote Sensing of Environment* 76: 1-15.
- Gates DM, Keegan HJ, Schleter JC, Weidner VR. 1965. Spectral properties of plants. *Applied Optics* 4: 11-20.
- Gausman HW, Allen WA, Escobar DE. 1974. Refractive-index of plant-cell walls. *Applied Optics* 13: 109-111.
- Gitelson AA, Merzlyak MN. 1996. Signature analysis of leaf reflectance spectra: Algorithm development for remote sensing of chlorophyll. *Journal of Plant Physiology* 148: 494-500.
- Gowin T, Goral I. 1977. Chlorophyll and pheophytin content in needles of different age of trees growing under conditions of chronic industrial pollution. *Acta Societatis Botanicorum Poloniae* 46: 151-159.
- Gruber F. Morphology of coniferous trees: possible effects of soil acidification on the morphology of Norway spruce and Silver fir. In: *Effects of acid rain on forest processes*, edited by Godbold DL and Hüttermann A. New York: Wiley-Liss, 1994, p. 265-324.
- Hodanova D. 1985. Leaf optical properties. In: Sestak Z, eds. *Photosynthesis during leaf development*. Prague, Czech Republic: Academia Praha, p. 396.
- Horler DNH, Barber J, Barringer AR. 1980. Effects of heavy metals on the absorbance and reflectance spectra of plants. *International Journal of Remote Sensing* 1: 121-136.
- Hoshizaki T, Rock BN, Wong SKS. 1988. Pigment analysis and spectral assessment of spruce trees undergoing forest decline in the NE United States and Germany. *GeoJournal* 17: 173-178.
- Howard CV, Reed MG. 1998. *Unbiased Stereology*. Oxford, UK: BIOS Scientific Publishers.
- Huang Z, Turner BJ, Dury SJ, Wallis IR, Foley WJ. 2004. Estimating foliage nitrogen concentration from HYMAP data using continuum removal analysis. *Remote Sensing of Environment* 93: 18-29.
- Jacquemoud S, Baret F. 1990. Prospect - a model of leaf optical properties spectra. *Remote Sensing of Environment* 34: 75-91.
- Kokaly RF, Clark RN. 1999. Spectroscopic determination of leaf biochemistry using band-depth analysis of absorption features and stepwise multiple linear regression. *Remote Sensing of Environment* 67: 267-287.

- Larcher W. 1995. *Physiological plant ecology*. Berlin, Heidelberg: Springer Verlag.
- Lesinski JA. 1989. Morphological vigour indicators in Norway spruce. *Ecological Monitoring in Forestry*, Usti n. L., Czech Republic. Lesprojekt, Brandys n. L., p. 38-46.
- Lichtenthaler HK. 1998. The stress concept in plants: An introduction. *Annals New York Academy of Sciences* 851: 187-198.
- Lichtenthaler HK, Wenzel O, Buschmann C, Gitelson A. 1998. Plant stress detection by reflectance and fluorescence. *Annals New York Academy of Sciences* 851: 271-285.
- Malenovský Z, Albrechtová J, Lhotáková Z, Zurita-Milla R, Clevers JGPW, Schaepman ME, Cudlín P. 2006. Applicability of the PROSPECT model for Norway spruce needles. *International Journal of Remote Sensing*: in press.
- Mesarch MA, Walter-Shea EA, Asner GP, Middleton EM, Chan SS. 1999. A revised measurement methodology for conifer needles spectral optical properties: Evaluating the influence of gaps between elements. *Remote Sensing of Environment* 68: 177-192.
- Mooney HA, Winternal WE, Pell EJ. 1991. *Response of plants to multiple stresses*. San Diego, New York, London: Academic Press.
- Myneni RB, Ross J. 1991. *Photon - vegetation interactions: Applications in optical remote sensing and plant ecology*. Berlin Springer-Verlag.
- Nakatani N, Kume A, Kobayashi T, Hirakawa T, Sakugawa H. 2004. Needle morphology related to chemical contents in the needles of Japanese fir (*Abies firma*) trees subjected to acidic depositions at Mt. Oyama, eastern Japan. *Water, Air, and Soil Pollution* 152: 97-110.
- Nicolini E, Chanson B, Bonne F. 2001. Stem growth and epicormic branch formation in understorey beech trees (*Fagus sylvatica* L.). *Annals of Botany* 87: 737-750.
- O'Neill AL, Kupiec JA, Curran PJ. 2002. Biochemical and reflectance variation throughout a Sitka spruce canopy. *Remote Sensing of Environment* 80: 134-142.
- Pinty B, Widlowski JL, Taberner M, Gobron N, Verstraete MM, Disney M, Lewis P, Gascon F, Gastellu JP, Jiang L, Li X, Su L, Tang S, Wang H, Wang J, Yan G, Zang H, Kuusk A, Nilson T, Ni-Meister W, North P, Qin W, Thompson R, Verhoef W. 2004. RADIATION Transfer Model Intercomparison (RAMI) exercise: Results from the second phase. *Journal of Geophysical Research D: Atmospheres* 109: 1-19.
- Polle A, Pfirrmann T, Chakrabarti S, Rennenberg H. 1993. The effects of enhanced ozone and enhanced carbon-dioxide concentrations on biomass, pigments and antioxidative enzymes in spruce needles (*Picea abies* L.). *Plant Cell and Environment* 16: 311-316.
- Porra RJ, Thompson WA, Kriedemann PE. 1989. Determination of accurate extinction coefficients and simultaneous equations for assaying chlorophylls a and b extracted with four different solvents: verification of the concentration of chlorophyll standards by atomic absorption spectroscopy. *Biochimica and Biophysica Acta* 975: 384-394.
- Rock BN, Williams DL, Moss DM, Lauten GN, Kim M. 1994. High-spectral-resolution field and laboratory optical reflectance measurements of Red spruce and Eastern hemlock needles and branches. *Remote Sensing of Environment* 47: 176-189.
- Underwood E, Ustin S, DiPietro D. 2003. Mapping nonnative plants using hyperspectral imagery. *Remote Sensing of Environment* 86: 150-161.
- Waring RH. 1983. Estimating forest growth and efficiency in relation to canopy leaf-area. *Advances in Ecological Research* 13: 327-354.
- Wellburn AR. 1994. The spectral determination of chlorophyll a and chlorophyll b, as well as total carotenoids, using various solvents with spectrophotometers of different resolution. *Journal of Plant Physiology* 144: 307-313.
- Zarco-Tejada PJ, Pushnik JC, Dobrowski S, Ustin SL. 2003. Steady-state chlorophyll a fluorescence detection from canopy derivative reflectance and double-peak red-edge effects. *Remote Sensing of Environment* 84: 283-294.

**CHAPTER 5****Influence of woody elements of a Norway spruce canopy on nadir reflectance simulated by the DART model at very high spatial resolution**

Reprint of:<sup>‡</sup>

Malenovský, Z., Martin, E., Homolová, L., Gastellu-Etchegorry, J.-P., Zurita-Milla, R., Schaepman, M.E., Pokorný, R., Clevers, J.G.P.W., Cudlín P.: Influence of woody elements of a Norway spruce canopy on nadir reflectance simulated by the DART model at very high spatial resolution. *Remote Sensing of Environment*, accepted.

---

<sup>‡</sup> Reprinted with permission from Elsevier © 2006.

## **Abstract**

---

A detailed sensitivity analysis investigating the effect of woody elements introduced into the Discrete Anisotropic Radiative Transfer (DART) model on the nadir bidirectional reflectance factor (BRF) for a simulated Norway spruce canopy was performed at a very high spatial resolution (modelling resolution 0.2 m, output pixelsize 0.4 m). We used such a high resolution to be able to parameterize DART in an appropriate way and subsequently to gain detailed understanding of the influence of woody elements contributing to the radiative transfer within heterogeneous canopies. Three scenarios were studied by modelling the Norway spruce canopy as being composed of i) leaves, ii) leaves, trunks and first order branches, and finally iii) leaves, trunks, first order branches and small woody twigs simulated using mixed cells (i.e., cells approximated as composition of leaves and/or twigs turbid medium, and large woody constituents). The simulation of each scenario was performed for 10 different canopy closures (CC = 50-95%, in steps of 5%), 25 leaf area index (LAI = 3.0-15.0 m<sup>2</sup>m<sup>-2</sup>, in steps of 0.5 m<sup>2</sup>m<sup>-2</sup>), and in four spectral bands (centred at 559, 671, 727, and 783 nm, with a FWHM of 10 nm). The influence of woody elements was evaluated separately for both, sunlit and shaded parts of the simulated forest canopy respectively. The DART results were verified by quantifying the simulated nadir BRF of each scenario with measured Airborne Imaging Spectroradiometer (AISA) Eagle data (pixel size 0.4m). These imaging spectrometer data were acquired over the same Norway spruce stand that was used to parameterise the DART model.

The Norway spruce canopy modelled using the DART model consisted of foliage as well as foliage including robust woody constituents (i.e., trunks and branches). All results showed similar nadir BRF for the simulated wavelengths. The incorporation of small woody parts in DART caused the canopy reflectance to decrease about 4% in the near-infrared (NIR), 2% in the red edge (RE) and less than 1% in the green band. The canopy BRF of the red band increased by about 2%. Subsequently, the sensitivity on accounting for woody elements for two spectral vegetation indices, the normalised difference vegetation index (NDVI) and the angular vegetation index (AVI), was evaluated. Finally, we conclude on the importance of including woody elements in radiative transfer based approaches and discuss the applicability of the vegetation indices as well as the physically based inversion approaches to retrieve the forest canopy LAI at very high spatial resolution.

*Keywords:* woody elements, radiative transfer, DART, Norway spruce canopy, high spatial resolution, LAI, AISA



## 5.1 Introduction

---

Leaf Area Index (LAI) is a basic structural vegetation parameter mainly controlled by canopy biophysical and morphological processes. LAI is proportionally related to the rate of canopy photosynthesis and consequently to the CO<sub>2</sub> fixation and the net primary production (Liang & Strahler, 1995; Huang et al., 2004; Kotz et al., 2004). A number of studies have successfully demonstrated the effect of physiological vegetation characteristics on climate state (Hoffmann & Jackson, 2000; Zeng & Neelin, 2000; Zhang et al., 2001). In this respect, LAI is acknowledged to be one of the key input parameter for many eco-physiological and climate models describing land surface processes (Kucharik et al., 2000; Arora, 2002). The retrieval of biochemical and biophysical canopy properties, based on radiative transfer methods, represents a universal method that can be applied to both, airborne and satellite imagery (Tian et al., 2002; Fang et al., 2003; Schaepman et al., 2005; Schlerf & Atzberger, 2006). Quasi operational LAI products are, therefore, made available very early and achieve currently significant interest from the scientific communities (Knyazikhin et al., 1998; Tian et al., 2002; Combal et al., 2003; Shabanov et al., 2003; Shabanov et al., 2005). However, the retrieval models developed for coarse spatial resolution spaceborne sensors are not directly applicable to airborne imaging spectrometers with very high spatial resolution (Gastellu-Etchegorry et al., 2004).

LAI represents a biophysical structural parameter describing amount of the forest canopy foliage biomass (Monteith & Unsworth, 1990). The structural heterogeneity of a Norway spruce (*Picea abies* (L.) Karst.) canopy foliage is typically increasing with increasing age of the stand due to senescence and the influence of environmental stress agents (Remphrey & Davidson, 1992; Ishii & McDowell, 2002b). When the tree crowns become older, irregular structures within the canopy emerge due to the variation in solar irradiation caused by shadowing effects of the neighbouring trees and due to the effect of environmental multiple stress (Dehaan & Taylor, 2003). The foliage distribution (i.e., leaf density and clumping) within a spruce crown is usually a result of such a morphological transformation, starting with specific defoliation processes often followed by systematic regeneration (Gruber, 1994; Nicolini et al., 2001). These physiological processes cause a unique three-dimensional (3D) pattern, resulting in a significant spatially heterogeneous distribution of the leaves and/or shoots (needle sets of one generation) (Ishii et al., 2002a). In particular the proportion of woody elements (e.g., trunks, branches, and small twigs) is larger during the defoliation stage resulting in a decrease of LAI. Current research on Norway spruce eco-physiological processes demonstrates possibility to describe mathematically distribution of the canopy foliage and woody structures (Kuuluvainen & Sprugel, 1996; Dzierzon et al., 2003). Consequently, such simplified structural relations can be incorporated into radiative transfer (RT) models, used for estimation of forest canopy bio-chemical and bio-physical parameters. Prerequisite for such an approach is that the existing models can be run at a very high spatial resolution, typically with a spatial resolution in the order of a few decimetres, allowing a detailed modelling of all relevant forest canopy structural features.

Destructive ground measurements on 16 Norway spruce trees of our experimental forest stand revealed that brown woody biomass represents about 13% and assimilating green biomass about 87% of canopy surface. The influence of woody elements within a forest canopy have systematically been considered in ground measurements of forest LAI (Kucharik

et al., 1998; Gamon et al., 2004; Jonckheere et al., 2004), but has not been largely included in forest RT modelling. Some of the existing RT models consider trunks and branches as solid geometrical objects, for instance the 4-Scale RT model (Broge & Leblanc, 2001; Gamon et al., 2004), but in general the clumps of small woody particles, irregularly dispersed within the forest canopies, are ignored. Myneni et al. (2003) modelled the trunks and branches as dark objects with a red reflectance equalling to 3.79% and a near infra-red reflectance equalling to 10.02%. However, according to our field measurements of the hemispherical-directional reflectance (HDRF) (Schaepman-Strub et al., 2005), the Norway spruce bark may reflect as much as 20-25% between 600-700 nm and even 40-50% between 800-900 nm, resulting in a significantly higher contribution of the woody parts than previously reported. Thus, detailed knowledge of the effect of woody elements on the forest canopy reflectance is essential for designing a refined method retrieving the forest structural parameters (e.g., LAI).

The main objective of this study is to investigate the influence of woody elements (trunks, branches, and tiny twigs) at nadir top of canopy (TOC) reflectance of a Norway spruce stand at very high spatial resolution. The TOC reflectance expressed as bidirectional reflectance factor (BRF) will be simulated using a 3D Discrete Anisotropic Radiative Transfer (DART) model (Gastellu-Etchegorry et al., 1996). In order to validate reliability of the DART images modelled within this study, the forest canopy reflectance of all scenarios is compared against atmospherically corrected hyperspectral images captured by the AISA Eagle airborne sensor. Finally, the sensitivity of two vegetation indices (i.e., Normalized Difference Vegetation Index – NDVI, and Angular Vegetation Index – AVI) and the impact of woody elements therein are discussed as well as their influence on the retrieval of the leaf area index (LAI).

## 5.2 Material and Methods

---

### 5.2.1 Test site

The study test site is a montane Norway spruce stand located at the Bily Kriz experimental research site in the Moravian-Silesian Beskydy Mountains (figure 5.1), in the eastern part of the Czech Republic bordering with Slovakia (18.54°E, 49.50°N; altitude 936 m above sea level) (Kratochvilová et al., 1989). The geological bedrock of the area is sandstone originating the Mesozoic era. The soil type is a humic podzol combined with loamy sand soil. The humic horizon depth is between 60-80 cm with the gravel fraction of 30-40% and clay fraction of 15-38%. The average annual air temperature is about 5.5°C, the average annual precipitation amounts to 1000-1400 mm. The snow cover is present in average 160 days per year. The forest stand is made of a regularly spaced plantation of Norway spruce (*Picea abies* (L.) Karst.) trees established with three years old spruce seedlings in 1981. The trees of the monoculture are currently 27 years old (in the year 2005) with an average tree height of 10.6 m, and average diameter at breast height (DBH) of 12.8 cm. Further, the Bily Kriz research site (Pavelka et al., 2003) is also part of the MODIS ASCII Subset project (Oak Ridge National Laboratory Distributed Active Archive Center, 2005b), as well as part of the FLUXNET Global Network (Oak Ridge National Laboratory Distributed Active Archive Center, 2005a) having a flux tower equipped with the typical eddy covariance system measuring the exchanges of carbon dioxide (CO<sub>2</sub>), water vapour, and energy between the forest stand and the atmosphere.



Figure 5.1. Location of the experimental research site Bily Kriz at the Moravian-Silesian Beskydy Mountains (East border between Czech Republic and Slovakia).

### 5.2.2 *Methodological concept*

The overall methodological concept of the study is illustrated in figure 5.2. The DART model was parameterized based on detailed field observations in order to simulate the spectral response of the 27 years old Norway spruce stand. Three scenarios, summarized in table 5.1, were applied: i) ‘scenario F’ – the canopy is only represented by Foliage (leaf elements), ii) ‘scenario FW’ – the canopy is represented by Foliage and robust Woody parts, i.e. trunks and first order branches (main branches growing directly from the trunk), and iii) ‘scenario FWT’ – the canopy is represented by Foliage, robust Woody parts, and tiny Twigs, i.e. small branches with a diameter smaller than one cm. DART modelled images (DMI) were generated for each scenario and used to evaluate the influence of the woody elements on nadir spruce canopy BRF at the following wavelengths: 559 (green), 671 (red), 727 (red edge), and 783 nm (near-infrared). The measured spruce BRF signatures were extracted from pre-processed high spatial resolution images acquired by AISA Eagle and subsequently a comparison of the DART modelled BRF and AISA measured BRF spectral signatures was carried out. Finally, the sensitivity of two vegetation indices (NDVI, AVI) for LAI was investigated for three different model scenarios. The hypothesis of this study is that the combination of a carefully parameterized DART model supported by extensive ground measurements allows quantifying the influence of the woody parts on TOC BRF of a tree canopy at very high spatial resolution.

### 5.2.3 *The DART model*

The DART model simulates radiative transfer in complex 3D scenes, i.e. urban and natural Earth landscapes possibly with the topography and the atmosphere present. It uses several simulation approaches (e.g., ray tracing, exact kernel and/or discrete ordinate techniques)

covering the whole solar reflective and emissive part of the electromagnetic spectrum. Since its first release (Gastellu-Etchegorry et al., 1996), its accuracy, range of applications and graphic user interface were significantly improved (Pinty et al., 2001; Gastellu-Etchegorry et al., 2004). The latest DART version has two functioning modes: i) mode *R* (reflective) and ii) mode *T* (thermal). Mode *R* simulates the reflectance of direct sun and/or atmosphere radiation while mode *T* simulates a scene's thermal emission, jointly with a solar emission scenario (e.g., modelling the spectral domain 3-4  $\mu\text{m}$ ). In mode *R*, DART is able to make use of a Monte Carlo based simulation approach, capable of modelling very accurately multiple scattering effects. The two major outputs of the DART model are either remotely sensed optical images as well as a 3D radiation budget. The remotely sensed images can be modelled for any urban and natural landscape, atmosphere, wavelength, sun/view direction, altitude and spatial resolution ( $> 0.1$  m). DART simulates also directional reflectance factors and brightness temperatures, albedo and also images directly related to the leaf mesophyll, with or without the use of a sensor transfer function.

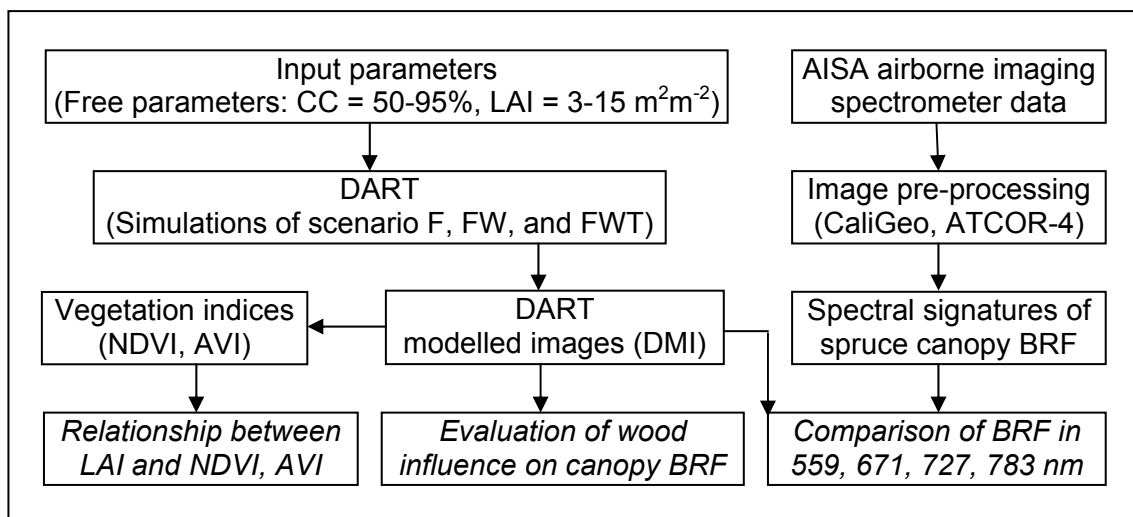


Figure 5.2 Flowchart of the methodological approach (scenario F – only foliage elements were simulated; scenario FW – the foliage elements together with trunk and first order branches were simulated; scenario FWT – foliage elements with trunk and first order branches plus small twigs were simulated; CC = canopy closure, LAI = leaf area index, NDVI = normalised difference vegetation index, AVI = angular vegetation index, BRF = bidirectional reflectance factor).

Any landscape can be simulated using DART as a function of rectangular matrices of parallelepiped cells of any size. These are the building blocks for simulating infinite large scenes. These scenes are usually repetitive in all three spatial dimensions, or partially repetitive for ensuring continuity in the vertical dimension as well as in the infinite slopes. Any scene element is simulated with the help of cells that are composed of turbid media (e.g., a leaf, grass, twigs, air, etc.), plane opaque surfaces of triangles and parallelograms based on parametric reflectance models (e.g., soil, roads, tree trunks and branches of first order, buildings walls and roofs, as well as rivers), or a mixture of all mentioned. The scenes can be very simple (e.g., a layered turbid medium) or rather complex (e.g., urban and natural

landscapes) created directly from ancillary digital information such as land cover maps, spectral databases of Earth elements, atmospheric physical and spectral vertical profiles, etc. In addition, the operator can define specific atmospheric quantities, accurately describing the state of the atmosphere (e.g., atmospheric water vapour, aerosol optical depth, urban pollution, etc.). The radiative transfer is tracked by an iterative procedure where one iteration (i) scatters radiation that is intercepted at further iterations (i+1). In order to decrease the computational load, the geometric origin of rays may always belong to a predefined grid of points within the sampled cells, or are directly located on the cell facets. Specular and diffuse scattering as well as emissivity of the vegetation and the urban elements are also accounted for. Since DART aims at very high accuracy, also the hot spot phenomenon, multiple scattering, and Earth surface-atmosphere coupling mechanisms are accurately modelled for any sun or viewing direction as well as the afore mentioned atmospheric conditions. To maintain modelling consistency, Kirchoffs law ( $\epsilon_d = 1 - \rho_{hd}$ ) as well as the reciprocity law ( $\rho_{hd} = \rho_{dh}$ ) are verified for simulated turbid media. DART has been successfully tested and validated against field measurements and has also been compared with other models within the RAMI experiment (Pinty et al., 2004). Recently, the DART model was patented (PCT/FR 02/01181) and the industrial version was jointly developed by Magellium Corporation and the Centre National d'Etudes Spatiales (CNES, France).

Table 5.1 Description of the three DART modelled scenarios.

<i>Name of scenario</i>	<i>Building units (canopy elements)</i>
F – Foliage	Cells of uniform turbid medium (leaves)
FW – Foliage, Wood	Cells of uniform turbid medium (leaves) Opaque surfaces of geometrical objects (trunks and first order branches <sup>1</sup> )
FWT – Foliage, Wood, Twigs	Cells of uniform turbid medium (leaves or tiny twigs <sup>2</sup> ) Opaque surfaces of geometrical objects (trunks and first order branches) Mixed cells of turbid media and opaque surfaces <sup>3</sup>

<sup>1</sup>Branches growing directly from the trunk.

<sup>2</sup>Branches smaller than one cm in diameter.

<sup>3</sup>Mixed cells can be composed as following combinations: i) diverse mixed turbid media (leaves + tiny twigs), or ii) uniform or mixed turbid media with opaque surfaces (leaves + tiny twigs + first order branches, or leaves + first order branches, or tiny twigs + first order branches).

#### 5.2.4 *Parameterization of the spruce forest stand in the DART model*

New forest canopy structural features had to be incorporated into a new DART model in order to allow the parameterization of woody elements. The purpose of this innovation was to increase model reliability and accuracy of the woody forest species simulation at high spatial scales. The Norway spruce architecture in DART comprises a trunk (superimposing parallelepipeds) with branches and a conical crown. The crown is filled with scattering elements distributed in structures of five hierarchical levels: i) trunk, ii) branches, iii) twigs, iv) leaves, and v) empty space. Trunk (i) building within a crown accounts for its heterogeneous structure, i.e. trunk optical and geometrical parameters can vary per defined crown level (l). First order branches (ii) are simulated using four triangles centered along a pre-defined axis at specified zenith and azimuth angles. Tiny woody twigs, i.e. branches

smaller than one cm in diameter, (iii) are represented by turbid medium cells with specific optical properties, a pre-defined twig density ( $\mu_t$ ) or the twig area index (TAI), and the twig angle distribution (TAD) (Centre d'Etudes Spatiales de la Biosphère, 2005). The leaf volume density (iv) ( $\mu_f$ ) or LAI within a crown vary in vertical as well as horizontal direction following physical distribution functions. Additionally, the mixed cells, containing mixed turbid media (leaves and tiny twigs) and also the geometrical objects (trunk and main branches), can be modeled. The specific LAI of coniferous species is implemented as defined by Chen & Black (2004), proposing the LAI of non-flat leaves to be half the total intercepting leaf area per unit ground surface area. The TAI definition is adapted similarly as the LAI, being half the total area of woody branches in a diameter smaller than one centimetre per unit ground surface area. Finally, crowns are filled with empty spaces (v) (air gaps) simulating defoliation and clumping of the branches. The defoliation of the canopy is spatially distributed in accordance with recent eco-physiological knowledge of Norway spruce growing strategies (Gruber, 1994). Details about the canopy structural parameters, the design of woody elements, and the radiative transfer through complex forest canopies as implemented in DART are described in the literature published by the Centre d'Etudes Spatiales de la Biosphère (2005) and Malenovský et al. (2006).

Table 5.2. Input parameters for the DART scenes used to generate multispectral images for all three study scenarios.

<i>Sun position</i>		/Real solar noon/	
Zenith angle	$\theta_s$	[°]	47.80
Azimuth angle (from North clockwise)	$\phi_s$	[°]	176.50
<i>Spectral bands</i>		/Full-width-half-maximum – FWHM = 10 nm/	
Green central wavelength	$\lambda_{\text{green}}$	[nm]	559
Red central wavelength	$\lambda_{\text{red}}$	[nm]	671
Red-edge central wavelength	$\lambda_{\text{RE}}$	[nm]	727
Near-infrared central wavelength	$\lambda_{\text{NIR}}$	[nm]	783
<i>Scene parameters</i>		/representing a 25 year old Norway spruce forest stand/	
Cell size		[m]	0.20
Horizontal dimensions	x, y	[m]	6.00, 6.00
Number of trees			3-8
Canopy closure (varied parameter)	CC	[%]	50-95 /in steps of 5/
Leaf area index (varied parameter)	LAI	[m <sup>2</sup> m <sup>-2</sup> ]	3-15 /in steps of 0.5/

Detailed parameterization of the DART model was based on field measurements of the Norway spruce stand at the Bily Kriz research site in September 2004. Ancillary allometric and eco-physiological data of the tree crowns were collected during a field campaign carried out at the same research site in summer 1997 (Pokorný & Marek, 2000). Summary of the DART parameters used for the three scenario simulations is given in table 5.2. A repetitive 3D rectangular matrix with a basic cell resolution of 0.2 m represented the forest stand. The total amount of trees and their position within the scene varied according to the simulated canopy closure (CC) category in following way: three trees for the CC of 50% and 55%, four trees for the CC of 60% (figure 5.3a) and 65%, five trees for the CC of 70%, 75% and 80%, six trees for the CC of 85%, seven trees for the CC of 90%, and eight trees for the CC of 95%.

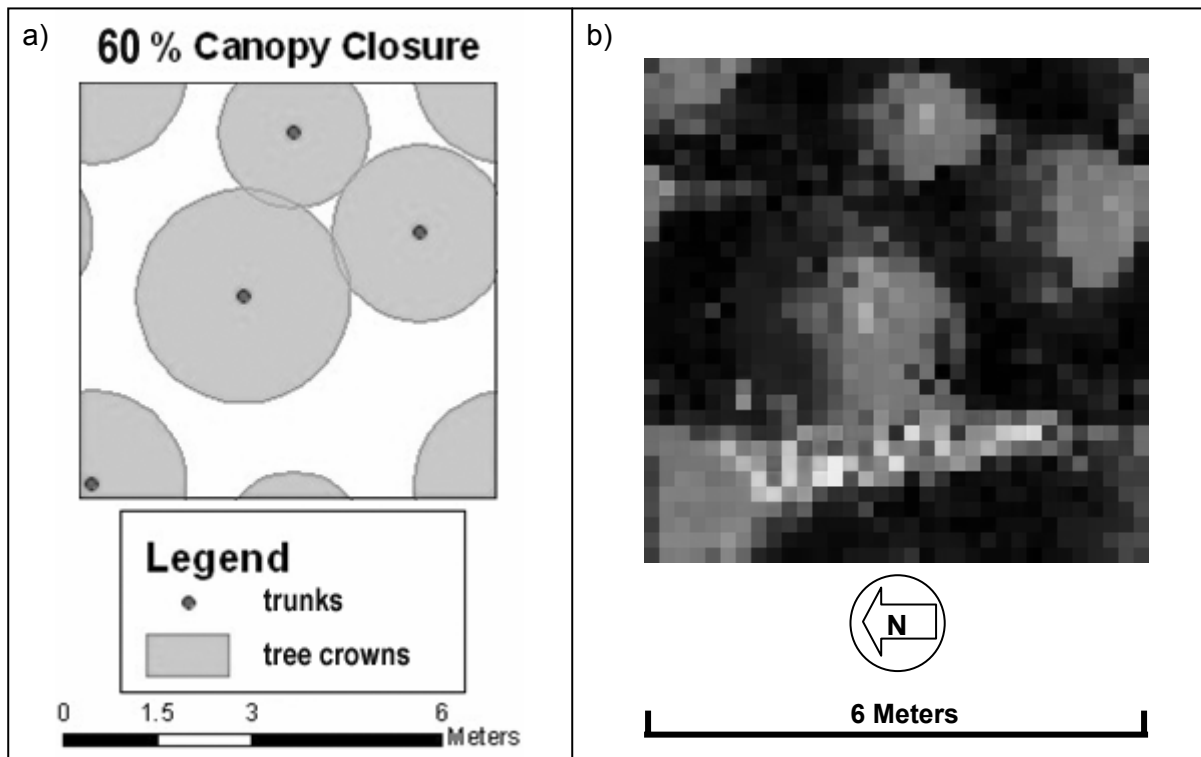


Figure 5.3 a) Vertical projection of the DART Norway spruce stand representation with canopy closure of 60% (four representative trees); b) DART output – greyscale image of three spectral band composition (NIR, red, and green band; white = sunlit background, light grey = sunlit crowns, dark grey = shaded crowns, black = deeply shaded crowns and background).

The basic allometric parameters (e.g., tree and crown height, bottom crown radius, etc.) reflect the current growing stage of the observed forest stand (table 5.3). For each within crown level  $l$ , the LAI horizontal distribution is characterized by four parameters:  $\alpha(l)$ ,  $\beta(l)$ ,  $\gamma(l)$  and  $\kappa(l)$ . The leaf volume density  $\mu_f(r) = 0$  and  $r < \alpha(l)$  with  $r > \kappa(l)$ , while  $\mu_f(r)$  is constant for  $r \in [\gamma(l) \ \kappa(l)]$ , where  $r$  is the horizontal distance from the tree trunk. The horizontal distribution of holes is defined by two parameters:  $a(l)$  and  $b(l)$ , where total defoliation (i.e., 100% empty cells) is defined for distances of  $r < a$  and  $r > b$ , and the specific proportion of leaf/empty cells is defined for  $r \in [a(l) \ b(l)]$ . The horizontal distribution of needles was derived from the analysis of 24 sample branches cut off from the bottom, middle and top part of the eight sample tree crowns. This analysis also provided information on branch foliage clumping, i.e. spatial distribution of empty spaces (air gaps) among shoots (so called random mosaic defoliation), and also location of the 100% defoliated zones (so called inner crown defoliation) (Cudlin et al., 2001). The vertical distribution of green biomass (apparent leaf volume density  $\mu_f$ ) is parameterized by crown foliage destructive measurements carried out on 16 trees of the same age during summer 1997. The leaf angle distribution (LAD) was defined as ellipsoidal (Irons et al., 1992), computed from the crown level specific average leaf angle (ALA) of  $25^\circ$  for two upper crown levels,  $30^\circ$  for two middle upper crown levels,  $35^\circ$  for two middle lower crown levels, and  $40^\circ$  for last four bottom crown levels. ALA values were derived through a combination of the needle angular distribution within the

shoot and shoot angular distribution within the crown. Trunks were defined as the superimposition of parallelepipeds with different height and side size for each vertical crown level *l*. The thickness of the trunk within crown is computed based on the trunk diameter out of crown (e.g., DBH) multiplied by a relative trunk diameter specific for each vertical crown level *l* (table 5.3). Two whorls of first order branches, defined for each distinct vertical crown level, consisted of 4-6 branches. Small woody twigs, treated as uniform turbid cells of fine wood or cells mixed with foliage and first order branch triangles, were specified in a radius of 0.2 m around the first order branches. The ellipsoidal twig angle distribution (TAD) is equal to the average shoot angle, which was measured to be on average 35° for the whole canopy.

Table 5.3. Measured parameters of the trees modelled in DART for simulation of all three study scenarios. Values in parenthesis stand for standard deviation (STDEV).

<i>Tree parameters</i>	/Mean parameters derived for eight individual tree/	
Trunk height below crown	[m]	0.38 (0.13)
Trunk height within crown	[m]	8.08 (0.76)
Trunk diameter below crown	[m]	0.17 (0.02)
Relative trunk diameter within crown	[relative]	0.41 (0.03)
Crown type		Conical
Crown height	[m]	10.08 (0.76)
Crown bottom radius	[m]	1.60 (0.24)
Living crown bottom radius	[m]	1.54 (0.24)
Crown top radius	[m]	0.00
Total tree height	[m]	10.45 (0.88)
Average leaf angle	ALA [°]	34 (7)
Mean twig area index	TAI [m <sup>2</sup> m <sup>-2</sup> ]	0.082 (0.017)
Average twig angle	ATA [°]	35
Number of crown levels		10
Relative height of one tree level	[relative]	0.09
$\alpha$ parameter of horizontal leaf distr.	$\alpha$ [relative]	0.00
$\beta$ parameter of horizontal leaf distr.	$\beta$ [relative]	0.34
$\gamma$ parameter of horizontal leaf distr.	$\gamma$ [relative]	0.63
$\kappa$ parameter of horizontal leaf distr.	$\kappa$ [relative]	1.00
<i>a</i> parameter of horizontal hole distr.	<i>a</i> [relative]	0.15
<i>b</i> parameter of horizontal hole distr.	<i>b</i> [relative]	1.00
Percentage of full leaf cells within crown	[%]	48.00

The optical properties, i.e. integrated hemispherical-directional reflectance and transmittance, of the canopy elements (leaves and bark of the woody parts) and background elements (litter and bare soil) were obtained from laboratory measurements. These were performed under artificial illumination in an integrating sphere LI-1800-12 (Li-Cor, Inc., Lincoln, NE, USA) (Li-Cor, 1983) coupled with a laboratory/field spectroradiometer ASD FieldSpec Pro FR (Analytical Spectral Devices, ASD Inc., USA) in September 2004. The needle samples of last three generations from the sunlit crown part (3<sup>rd</sup> branch whorl from the top) and the shaded crown part (7<sup>th</sup> branch whorl from the top, inside a crown) were collected from ten selected trees of the experimental forest stand. The needle optical properties were measured according to the improved methodology proposed by Daughtry et al. (2000a) and revised later by Middleton et al. (1999) and Mesarch et al. (1999). The laboratory spectral



measurements range between 350-2500 nm in steps of 1 nm. Determination of the needle optical properties representative for each distinct crown level is based on a percentage distribution of the needle age classes and an appropriate ratio of the sunlit and shaded needles within seven vertical crown zones (figure 5.4a). The reflectance properties of the trunks within the scene are computed as the average of five bark HDRF measurements. It was unfeasible to measure optical properties of the tiny twig bark due to the too small cylindrical shape of fine twigs. Therefore, the bark optical properties of first order branches are assumed to be similar to the twig bark properties (cf., figure 5.4b). Due to the absence of the vegetation understory the HDRF of the background is specified by an equal proportion of litter (senescent needles) and bare soil reflectance given in figure 5.4b. Because the used integrating sphere LI-1800-12 was not designed to measure specular and diffuse reflectance separately, the optical properties of all the modelled elements represent an integration of both values, and subsequently had to be assumed and defined in DART as being of lambertian nature.

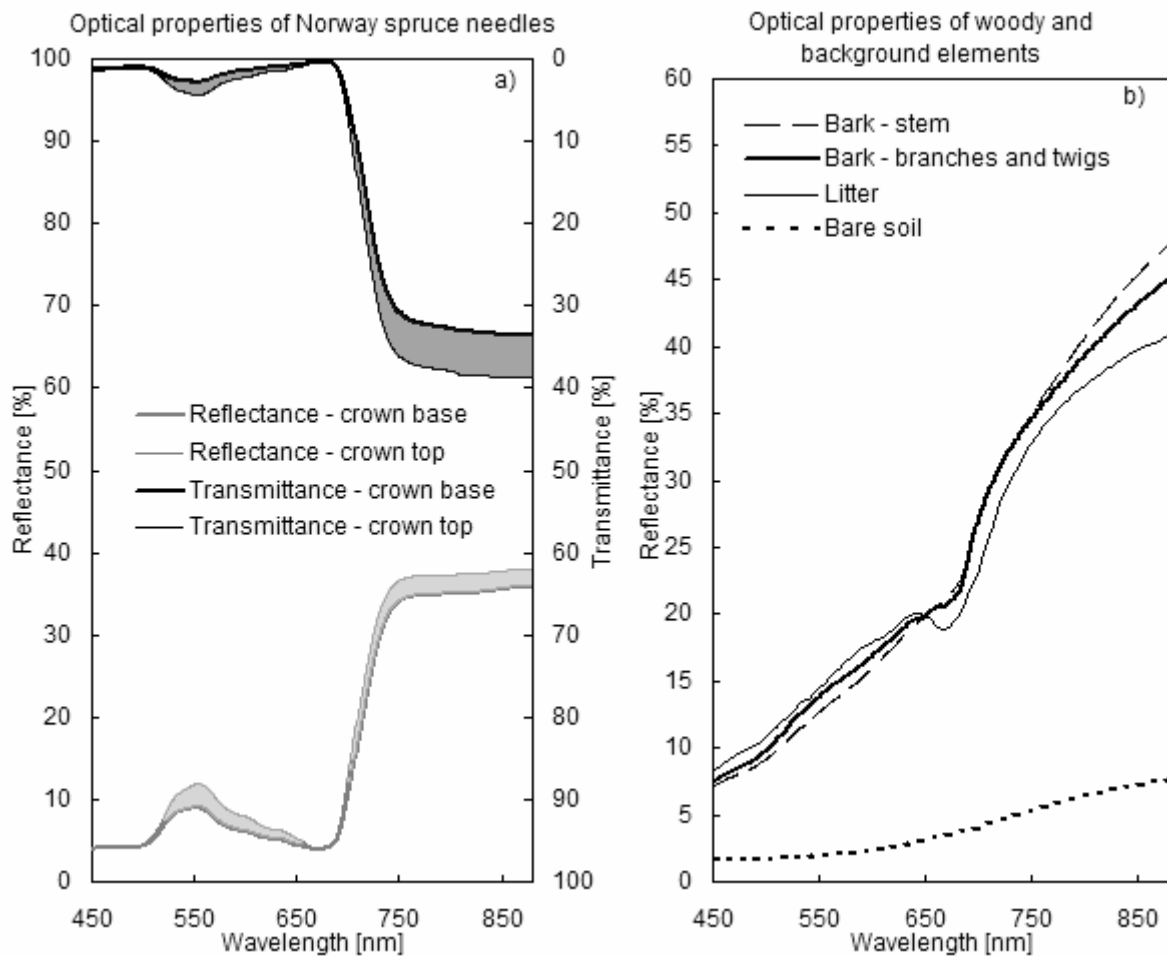


Figure 5.4. Measured optical properties (hemispherical-directional reflectance and transmittance) of the surfaces used to parameterize the DART simulations: a) ranges of the Norway spruce needle optical properties defined from base to top of the crown, b) optical properties of woody elements (bark of stem, branches and twigs) and background (litter and bare soil).

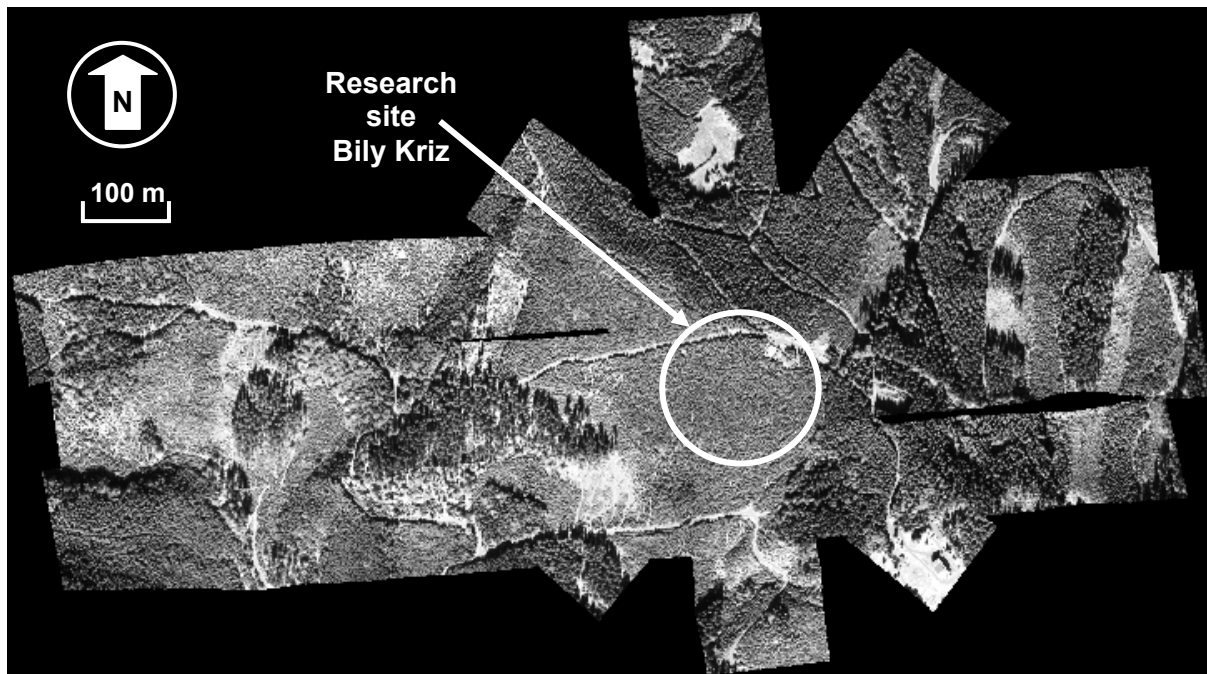


Figure 5.5. Six ortho-rectified flight lines acquired by the airborne AISA Eagle imaging spectroradiometer in a multi-directional pattern with the pixel size of 0.4 m over the permanent experimental research site Bily Kriz (Beskydy Mts., Czech Republic; 18.54°E, 49.50°N, altitude 936 m above sea level; greyscale image of NIR, red, and green band composition).

### 5.2.5 *DART modelled images*

In total 250 simulations per scenario were performed for four spectral bands, each using DART 2005. These simulations are the result of all possible combinations of CC between 50–95% (in steps of 5%) and LAI from 3.0–15.0  $\text{m}^2\text{m}^{-2}$  (in steps of 0.5  $\text{m}^2\text{m}^{-2}$ ). The ranges of the CC and LAI were set according to the minimal and maximal values measured within the spruce stand at Bily Kriz research site. The diffuse hemispherical irradiation was not simulated within the scenes, resulting the DART to simulate spectral images representing top of canopy bidirectional reflectance factor (BRF). BRF is defined as being a function of the solar illumination direction ( $\theta_s, \phi_s$ ), surface reflection direction ( $\theta_r, \phi_r$ ), and spectral wavelength  $\lambda$  (Schaepman et al., 2005). DART modelled images at 0.2 m spatial resolution (e.g., figure 5.3b) were aggregated by means of a bilinear resampling to a pixel size of 0.4 m in order to match the AISA Eagle image resolution. The very high spatial resolution allowed the selection of pure spruce canopy pixels, avoiding potential disturbing effects of sunlit as well as of shaded background of litter and soil. Therefore, sunlit and shaded pixels of the tree crowns were delineated from the DART simulated nadir BRF images and an average reflectance of these pixels was separately extracted. The sunlit crown parts are in this study defined as the spruce canopy surface being insolated directly by the sun, i.e. the crown turbid cells interacting with direct solar irradiation. The sunlit crown pixels were easily distinguishable by means of high BRF intensity (mainly in the NIR). The area of the shaded crown is defined by the crown turbid cells not interacting with direct solar irradiation, i.e. the

spruce canopy surfaces at the dark side of crowns or shaded by the tree crowns in their neighbourhood. Since spatial resolution of the DART leaf turbid cell was set to 0.2x0.2 m, an aggregated image (pixel size of 0.4 m) composed of sunlit pixels may contain a minor ineffective fraction of shaded leaf turbid cells. Finally, we have defined the overall canopy reflectance as mean BRF of all sunlit and shaded spruce crown pixels. The effect of the woody elements on the BRF, as well as on the vegetation indices, was evaluated from the DMI of the three scenarios separately for the sunlit and shaded crown parts, and also for the overall spruce canopy.

#### 5.2.6 AISA Eagle airborne image data

Several flight lines above the montane Norway spruce forest stands of the Bily Kriz experimental research site were acquired using the Airborne Imaging Spectroradiometer (AISA) Eagle pushbroom VNIR airborne scanner (Spectral Imaging, SPECIM Ltd., Finland) starting 11:50 a.m. (GMT) on September 18<sup>th</sup> 2004 (figure 5.5). 64 spectral bands with a Full-Width-Half-Maximum (FWHM) of about 10 nm and a spatial resolution of 0.4 m were acquired in the spectral range from 398.39–983.06 nm. The AISA images were acquired under the clear sky conditions (no clouds, visibility > 30 km) implying a low portion of diffusely scattered light compared to the direct solar illumination. Radiometric correction to radiance values was performed using the CaliGeo software (Spectral Imaging, SPECIM Ltd., Finland), parameterized by the sensor specific calibration coefficients. The atmospheric correction was performed in two steps. First we used the empirical line method (Smith & Milton, 1999) to convert at-sensor radiances to surface reflectance (HDRF). The concept of the HDRF is similar to the BRF definition except that illumination is coming from the entire upper hemisphere (Schaeppman-Strub et al., 2005). For the empirical line correction we used a set of five lambertian calibration panels (each 2.5 x 2.5m large in size, placed on the flat ground) with a flat response curve ranging from 5% to 70% within the visible and NIR wavelengths (Malenovský et al., 2006). Their nadir reflectance (HDRF) was measured in a field with the ASD FieldSpec Pro spectroradiometer during the AISA image acquisition. The quality control of the data revealed a brightness gradient within the airborne images in across-track direction, mainly due to the large field of view (FOV = 29.9°). Therefore, a nadir normalisation method was applied to convert HDRF to BRF using ATCOR-4 (Fukshansky et al., 1993). The resultant radiometric quality of the data was verified with the reflectance of three independent calibration targets (i.e., clay, gravel, and homogeneous grass cover). Three spots of each target, clearly visible on the AISA images, were measured during the flight with the FieldSpec Pro spectroradiometer (50 scans per one measurement) and averaged. The size of the measured calibration sites extends far beyond the AISA pixel size, allowing for selection of pure reflectance spectra uncontaminated by the adjacency effects. Finally, the AISA BRF images were geo-orthorectified using the Universal Transverse Mercator (UTM) geographic projection (zone 34 North) in combination with a digital elevation model having 2 m vertical resolution and 0.4 m horizontal resolution. The geo-referencing was accomplished also using ancillary data about the aircraft position recorded during the image acquisition by the Aerocontrol IIB system (Ingenieur-Gesellschaft für Interfaces, IGI GmbH, Germany) composed of an Inertial Measurement Unit (IMU) combined with a Global Positioning System (GPS). The achieved positional accuracy is about 1.2 m (3 pixels) in the horizontal directions.

### 5.2.7 Comparison of DART and AISA Eagle BRF's

The results of the DART simulations were validated with BRF of the AISA image. A regular network of 14 x 3 points (at distances of 5 m) was established within the experimental forest stand (figure 5.6). Precise geographic position of the points in UTM geographic projection (zone 34 North) was measured with a Differential Global Positioning System (DGPS) using TRIMBLE 4700 and 4800 receivers (Trimble Navigation Limited, USA) in combination with an Impulse 200 Laser Rangefinder and a MapStar electronic compass (Laser Technology Inc., USA), controlled by a Field Map data collecting system (Institute of Forest Ecosystem Research, IFER Ltd., Czech Republic). A set of hemispherical photographs was taken at each sampling point with a Nikon Coolpix 8700 digital camera (Nikon Corporation, Japan) equipped with a fish-eye lens (FOV = 180°). Hemispherical images were processed by the CAN EYE software (Combal et al., 2003) to extract LAI of the spruce canopy for 12 matrices of 3x3 points (10x10 m). The vector file containing the 12 matrices was superimposed on the geo-rectified AISA Eagle image as shown in figure 5.6 to locate the observation points. A maximum likelihood (MLH) supervised classification (Liang & Strahler, 1995) of the AISA image was used to distinguish the categories of sunlit and shaded spruce canopy and sunlit and shaded ground within each matrix. The MLH classification of the matrices was applied to create masks of sunlit and shaded crown parts. Subsequently, the percentage of sunlit and shaded canopy pixels in each matrix was used to estimate the canopy closure (CC). CC was calculated as the ratio of the number of pixels classified as sunlit or shaded (i.e., pixels of overall spruce canopy) against the total number of pixel within a matrix. The combination of measured LAI and image derived CC of each matrix was used as the primary key to search through the DMI and retrieve corresponding overall canopy BRF of each simulated scenario. Finally, the AISA image derived spruce canopy BRF of four selected bands was compared with the canopy BRF values of corresponding DART modelled images.

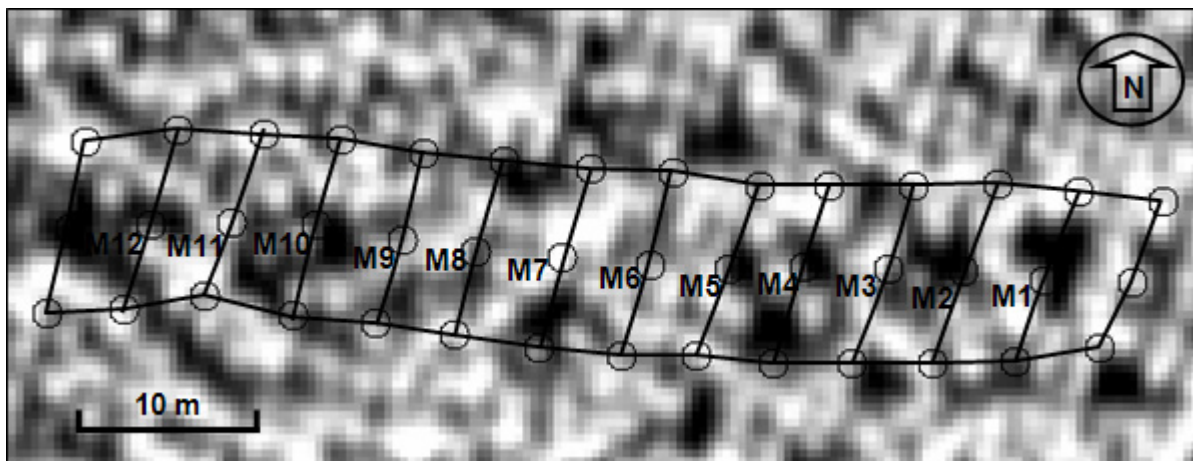


Figure 5.6. BRF validation matrices, used also for the measurement of the forest stand leaf area index (LAI), plotted over the grey-scale AISA Eagle band (738 nm). M1-M12 stands for centres of 12 validation matrices of 3x3 points (10x10 m; one circle represents one sampling point).

### 5.2.8 *NDVI and AVI vegetation indices*

The vegetation indices are specifically designed to detect changes in physical or chemical properties of the observed objects from their reflected radiation (Bannari et al., 1995). Physically based radiative transfer models offer the flexibility to design, test and vary spectral vegetation indices computed at different spatial, spectral and directional resolution (Broge & Leblanc, 2001; Haboudane et al., 2002). We use two vegetation indices to demonstrate independently the sensitivity of them to the presence of woody elements simulated in three DART scenarios at the very high spatial resolution. The Normalized Difference Vegetation Index (NDVI) was designed to distinguish vegetation from other objects (bare soil, snow, water, clouds) (Rouse et al., 1973). It is a traditional index based on reflectance differences at visible and NIR wavelengths:

$$NDVI = \frac{(\rho_{NIR} - \rho_{red})}{(\rho_{NIR} + \rho_{red})}, \quad (5.1)$$

where  $\rho_{NIR}$  is the near-infrared reflectance and  $\rho_{red}$  is the red reflectance. Early research indicated a close statistical relationship between the NDVI and the LAI (Jordan, 1969; Tucker, 1979), but several more recent studies reported low correlation of these two variables in dense canopies (Fassnacht et al., 1997; Turner et al., 1999; Lee et al., 2004), as well as for spectral data at high spatial resolution (Gastellu-Etchegorry et al., 2004). The second index, called the Angular Vegetation Index (AVI), is based on a geometric concept of the angle defined between reflectances at green, red, and near-infrared wavelength (Dawson et al., 1998a):

$$AVI = \frac{2 \left( \pi - \left( \left( \frac{\pi}{2} - \tan^{-1} \frac{(\lambda_{red}(\rho_{NIR} - \rho_{red}))}{(\lambda_{NIR} - \lambda_{red})} \right) + \left( \frac{\pi}{2} - \tan^{-1} \frac{(\lambda_{red}(\rho_{green} - \rho_{red}))}{(\lambda_{red} - \lambda_{green})} \right) \right) \right)}{\pi}, \quad (5.2)$$

where  $\rho_{NIR}$  is the near-infrared reflectance at the wavelength  $\lambda_{NIR}$ ,  $\rho_{red}$  is the red reflectance at the wavelength  $\lambda_{red}$ , and  $\rho_{green}$  is the green reflectance at the wavelength  $\lambda_{green}$ . The spectral bands used for the AVI computation in this study were selected from the available simulated wavelengths as following:  $\rho_{green} = 559$  nm,  $\rho_{red} = 671$  nm, and  $\rho_{NIR} = 783$  nm. This angular index was designed in order to eliminate the influence of soil background and atmospheric aerosols (North, 2002). However, the sensitivity of the index for presence of woody elements in a canopy has not been previously investigated.

## 5.3 Results

### 5.3.1 *Effect of non-photosynthetic woody elements on nadir spruce canopy BRF*

In general, the DART modelled images of all three scenarios show a negative relationship between LAI and BRF of all four bands (figure 5.7). This general trend of descending reflectance can be explained by a larger photon absorbance ability of the forest canopy with higher foliage density  $\mu_f$  composed in more leaf layers. In other words, as leaf foliage density increases, the crown absorption increases and simultaneously the crown transmittance

decreases. This limits the amount of photons available for scattering at crown elements of lower canopy levels and the background (soil). Final canopy BRF is composed of radiation reflected directly from the insolate crown elements (radiation of specular and diffuse nature) and radiation scattered back from the lower crown parts and background (radiation of only diffuse nature). The results in figure 5.7 suggest that intensity increase of the first mentioned canopy BRF components are smaller with growing leaf density (LAI) than the decrease of the second diffuse component.

The reflectance of sunlit crown parts and specified CC for scenario F ranged between 5-6% in the green, around 2% in the red, 19-23% in the RE, and 29-35% in the NIR band. As expected the reflectance of shaded pixels was lower, gaining about 1-3% in the green, 0-1% in the red, 5-12% in the RE, and 5-20% in the NIR. The overall canopy reflectance, computed as being the mean of the sunlit and shaded crown pixels, was approximately 3-5% in the green, 1-2% in the red, 11-18% in the RE, and 20-27% in the NIR band, respectively (cf., figure 5.7abcd). The spectral variability between the CC steps at all LAI classes was quite low. In scenario FW, after the introduction of the trunks and first order branches, the relationship between LAI and BRF did not change significantly (figure 5.7efgh). Only nadir reflectances of sunlit crowns at 783 nm decreased about 2-3%. All the other cases showed only negligible change, less than 1%. Finally, strong changes were observed for the FWT scenario (figure 5.7ijkl). The introduction of accurate modelling of small twigs by means of the mixed cells increased the canopy spectral heterogeneity, which resulted in higher variability and irregularity within the CC spectral responses per LAI (mainly sunlit crown parts). The BRF of the sunlit pixels in the green slightly decreased down to 4-6%, in the red increased up to 3-5%, and in the RE and NIR band decreased down to 15-20% and 20-30%, respectively. The BRF of the shaded pixels remained more stable, meaning that there was minor change of about 1% for the CC reflectances at the RE and about 3% at the NIR wavelengths. The BRF of the green band increased above 3%, and BRF of the red band increased up to 1-3%. Finally, the overall canopy reflectance for the FWT scenario remained almost unchanged for the 559 nm wavelength, decreased slightly for longer wavelengths at 727 and 783 nm, and increased at 671 nm wavelength by means of about 2-3%.

Closer investigation of the nadir reflectances simulated at 783 nm (figure 5.8) revealed that the BRF values for higher sunlit CC signatures (CC > 55%) of scenario F and FW display a non-monotonic, skewed Gaussian-like, behaviour. It is obvious that more than one LAI value produces the same TOC reflectance as illustrated in figure 5.8ac. For example a LAI of 4 m<sup>2</sup>m<sup>-2</sup> at CC = 95% resulted in a similar BRF compared to a LAI value of about 10 m<sup>2</sup>m<sup>-2</sup>. The same phenomenon was observed also for the other bands of green (559 nm), red edge (727 nm), and near infrared wavelengths (736, 745, 755, and 764 nm), except the red (671 nm) band, which is strongly driven by the chlorophyll absorption. However, the introduction of mixed cells decreased the overall nadir NIR BRF and reduced the intensity of this phenomenon by compensating an increase of BRF values for low LAI (figure 5.8e). This is most probably due to higher NIR refraction of twig bark being propagated through sparse canopies. figure 5.8bdf show a stronger monotypic negative correlation between LAI and NIR BRF of the shaded crown pixels for all CC categories. Shaded canopy signatures were less affected by the mixed cells, because the results of scenario F and FW appeared to be almost similar and only a minor shift of BRF (about 1-2%) was observed for scenario FWT. Similarly, the signal of the overall canopy reflectance remained monotonic, with descending BRF for increasing LAI values.

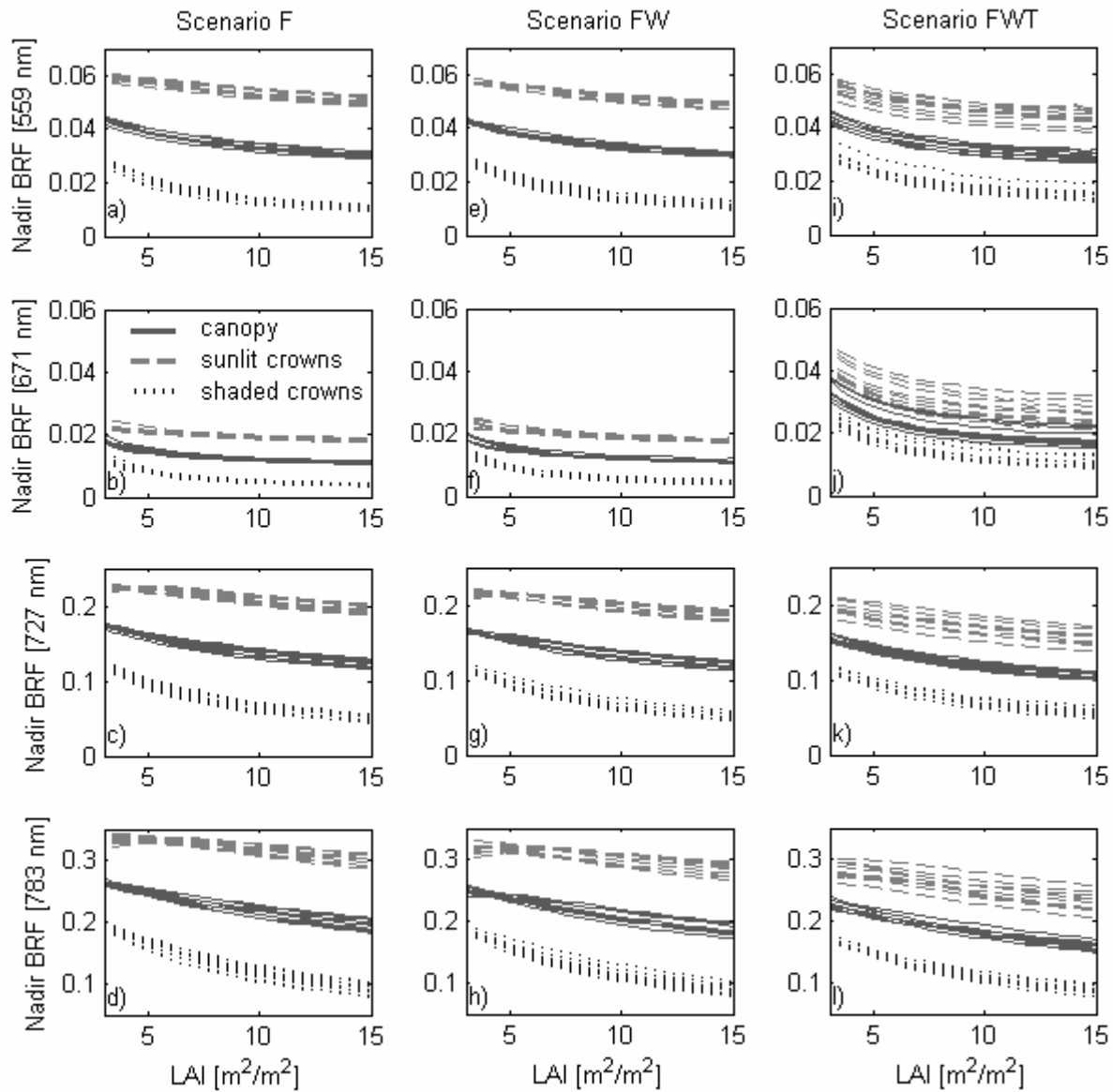


Figure 5.7. Relation of DART nadir bidirectional reflectance factor (BRF) and LAI simulated at 559, 671, 727, and 783 nm within the Norway spruce canopy composed of i) only foliage (scenario F: a-d), ii) leaves and major woody parts (scenario FW: e-h), and iii) leaves, trunks, branches of first order, and twigs smaller than one cm in diameter (scenario FWT: i-l). Light grey dashed lines represent BRF of sunlit crown pixels of 10 canopy closures (CC = 50-95% with step of 5%), black dotted lines represent BRF of shaded crown pixels of 10 canopy closures, and dark grey full lines represents BRF of 10 canopy closures of the whole spruce crowns.

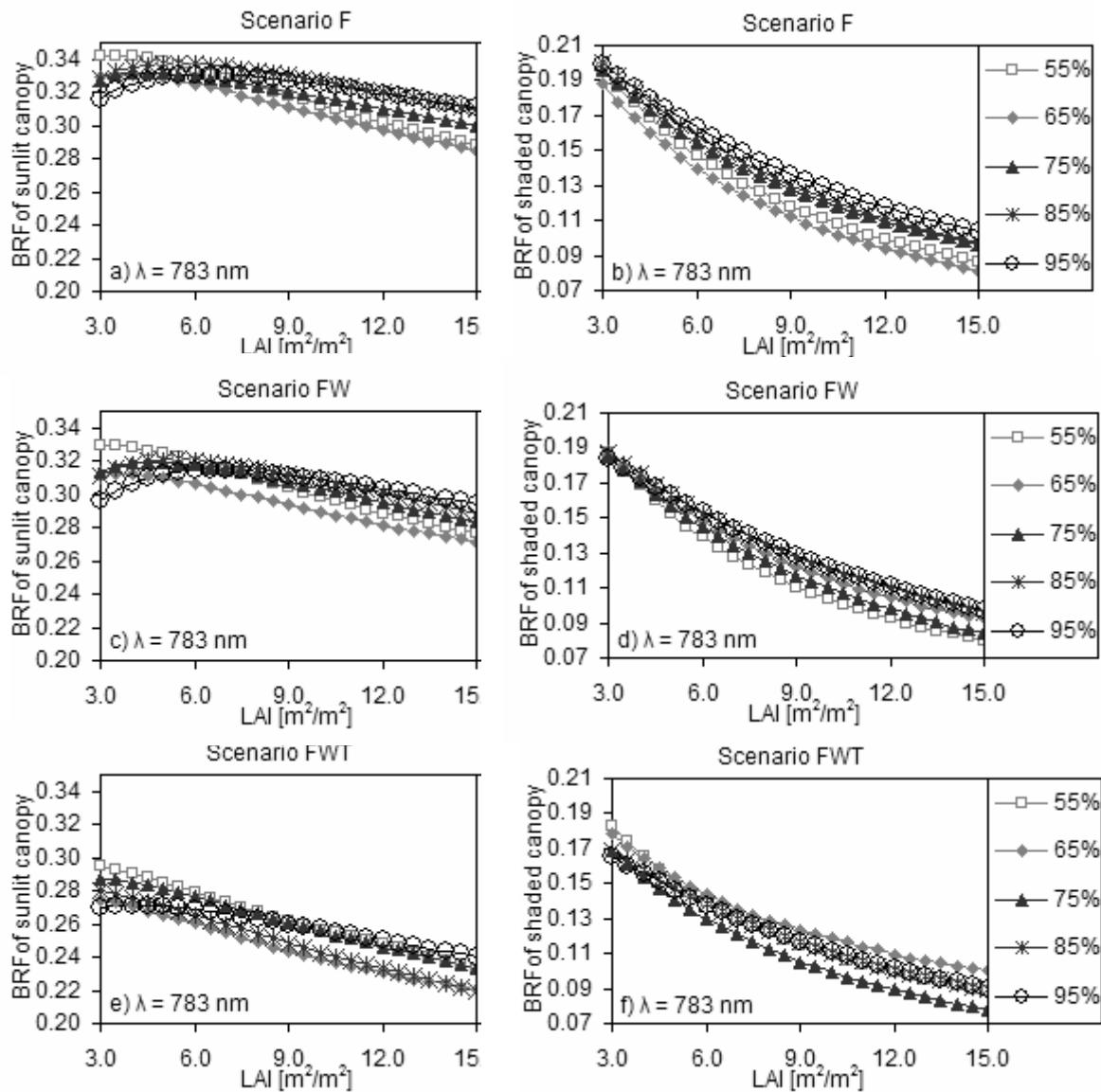


Figure 5.8. Detailed relationship of the canopy leaf area index (LAI) and the bidirectional reflectance factor (BRF) of the sunlit and shaded crown parts at 783 nm simulated by the DART model for five different canopy closures (CC = 55, 65, 75, 85, and 95%) for each of the three scenarios: i) scenario F – only foliage (a, b), ii) scenario FW – leaves and major woody parts (c, d), and iii) scenario FWT – leaves, trunks, main branches, and small twigs (e, f).



### 5.3.2 *Validation of the DART scenarios against the AISA BRF measurements*

The cross-comparison of the atmospherically corrected AISA BRF and ground measured nadir reflectance of three selected natural targets was used to validate the reliability of the AISA image processing procedures (figure 5.9). The reflectance of the calibration targets was measured using an ASD FieldSpec Pro spectroradiometer at nadir view. Given the centre positioning of the calibration targets and the nadir ground measurements, we approximate for this comparison HDRF  $\approx$  BRF. The high spatial resolution of AISA and the size of the reflectance panels allow the selection of pure calibration pixels. In addition, both natural calibration surfaces, i.e. clay and gravel, showed a close match between the ground and AISA airborne measurements with a reflectance root mean square error (RMSE) of 0.23% for clay and 0.18% for gravel, computed for 39 spectral bands between 450-800 nm (figure 5.9abcd). A higher RMSE of 3.16% was obtained for the grass surface. A discrepancy of about 5% appeared between the ground and airborne data for the grassland at NIR wavelengths (figure 5.9ef). Because the grass stand was quite uniform concerning the height and biodiversity, this discrepancy may be caused by the angular effects raised from structural differences (e.g., LAI and LAD) within the grass canopy measured by the ASD FieldSpec Pro spectroradiometer and the AISA scanner.

Table 5.4. Root mean square errors (RMSE) computed for BRF of four spectral bands of the experimental spruce canopy obtained from 12 matrices (10 x 10 m) placed over the AISA Eagle image and corresponding DART simulated BRF for all three considered scenarios.

	<i>Spectral bands</i>			
	<i>559 [nm]</i>	<i>671 [nm]</i>	<i>727 [nm]</i>	<i>783 [nm]</i>
<i>RMSE of canopy BRF [%]</i>				
Scenario F	0.35	0.21	2.67	3.50
Scenario FW	0.27	0.23	2.08	2.31
Scenario FWT	0.27	0.77	0.83	1.35
<i>RMSE of sunlit BRF [%]</i>				
Scenario F	1.05	0.09	4.57	5.35
Scenario FW	0.84	0.10	3.62	3.71
Scenario FWT	0.39	1.08	1.15	1.23
<i>RMSE of shaded BRF [%]</i>				
Scenario F	0.61	0.43	1.41	2.26
Scenario FW	0.60	0.42	1.24	1.79
Scenario FWT	0.55	0.48	1.17	1.89

Figure 5.10 shows the modelled DART scenarios in relation to the AISA BRF measurements extracted from the 12 sample matrices depicted in figure 5.6. The fractions of sunlit and shaded crown pixels of both sources were comparable due to the similar canopy closure of the DMI and AISA matrices. The smallest BRF differences were found for the shaded canopy pixels for all three scenarios (figure 5.10cfi). The computed RMSE between DART modelled and AISA measured BRF for the shaded canopy was nearly constant in green, red, and RE wavelengths, and it differed only in the NIR for scenario F (RMSE = 2.26%) (table 5.4). In spite of this, the variability of the shaded BRF was higher than variability of the sunlit BRF. Sunlit canopy reflectances demonstrated the best fit in three bands for scenario FWT. DART simulations for scenario F and FW systematically

overestimated the BRF at 559, 727, and 783 nm (figure 5.10beh), while scenario FWT overestimated reflectances in the 671 nm band. The RMSE of sunlit BRF for scenario FWT was computed to be smaller than 1.24% including all four spectral bands. RMSE values of sunlit BRF up to 3.71% were obtained for scenario FW, and even up to 5.35% for scenario F. On the other hand, these scenarios demonstrated a BRF RMSE of only 0.09 and 0.10% for the 671 nm wavelength, while the RMSE was equal to 1.08% for the FWT scenario (table 5.4). A similar pattern of BRF signatures and RMSE values was also obtained for the whole spruce canopy, mainly due to the contribution of the sunlit crown parts having a higher reflectance than the shaded parts (figure 5.10adg). In general, the best agreement between DART simulations and AISA Eagle measurements was obtained for the FWT scenario for all the tested spectral bands except the band at 671 nm wavelength.

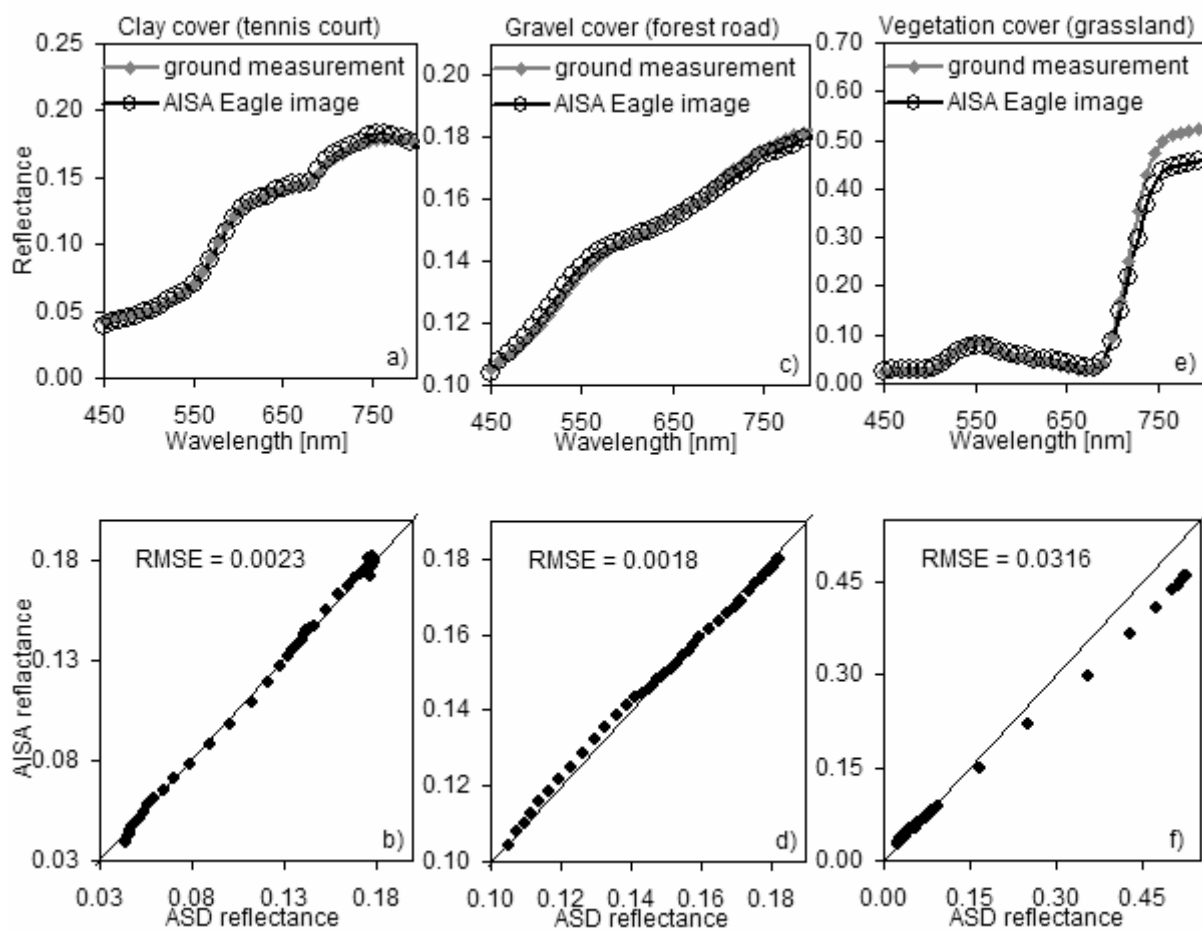


Figure 5.9. Validation of the AISA Eagle image radiometric and atmospheric corrections by comparison with ground measured ASD reflectance of three natural surfaces (50 scans per spot, three spots per surface): clay cover (tennis court – a, b), gravel cover (forest road – c, d), and homogeneous vegetation cover (grassland – e, f). The upper graphs show the reflectance signatures of both instruments, the lower graphs represent the relationship between the ground measured reflectances (HDRF) and the image-derived reflectances in the spectral range of 450-800 nm (RMSE = root mean square error).

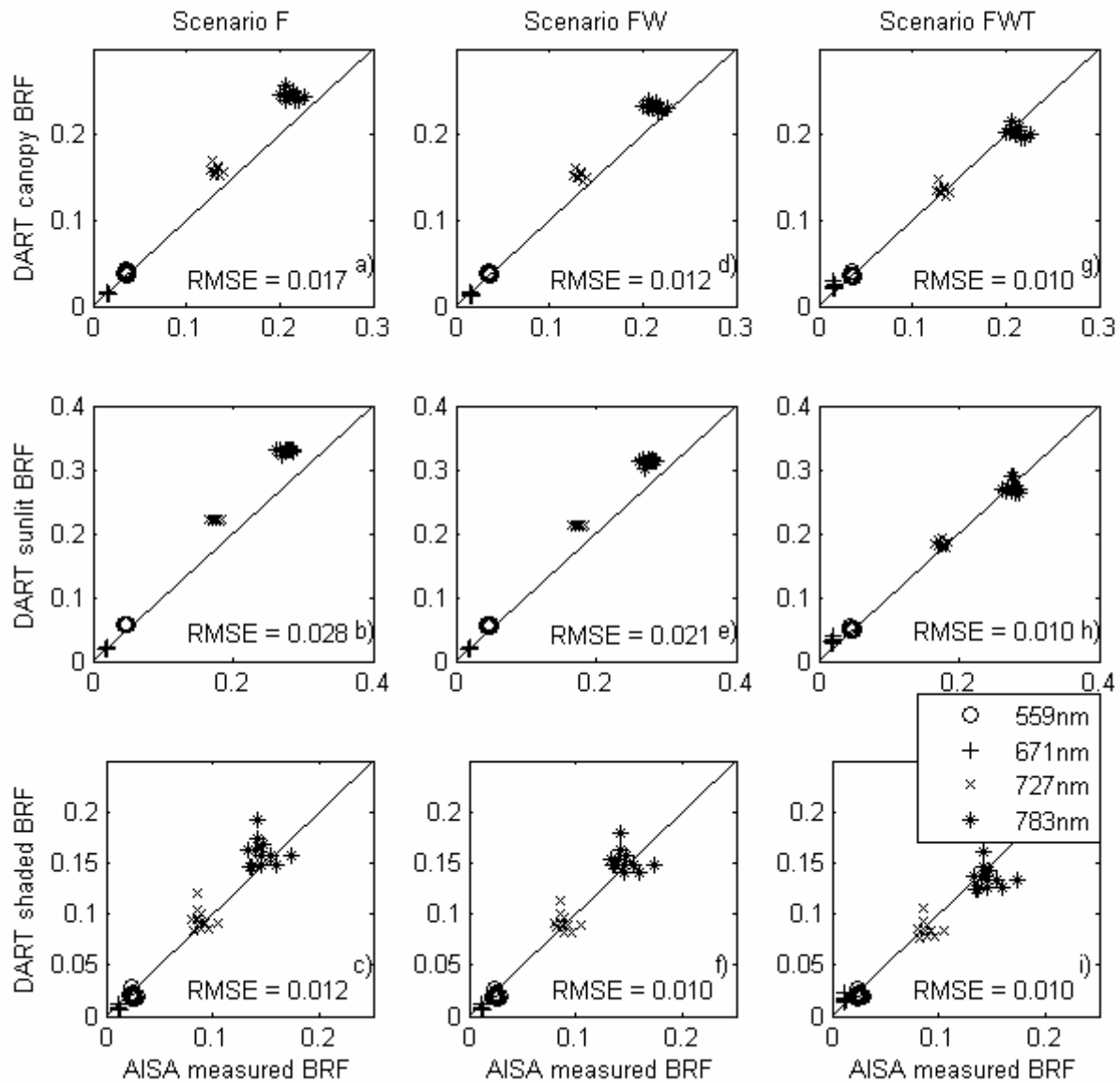


Figure 5.10. Direct comparison of the AISA Eagle bidirectional reflectance factor (BRF) obtained from 12 sample areas (10x10 m) and corresponding DART simulated BRF for comparable fraction of sunlit and shaded crown parts, as well as whole spruce canopy for three scenarios: i) scenario F – only foliage (a, b, c), ii) scenario FW – leaves and major woody parts (d, e, f), and iii) scenario FWT – leaves, trunks, main branches, and small twigs (g, h, i) (RMSE = root mean square error).

### 5.3.3 *Relation of vegetation indices with LAI at high spatial resolution*

Two vegetation indices, NDVI and AVI, were computed for each DART modelled image. Design of the DMI allowed us to evaluate changes in the vegetation indices with increasing LAI for 10 subsequent canopy closures per scenario. figure 5.11 illustrates the relationship between the NDVI and LAI values. All the plots showed that the NDVI saturates for an LAI

between 5–8  $\text{m}^2\text{m}^{-2}$ . Graphs for scenario F and FW have a very similar pattern, only the variability with the CC categories increased by introduction of the trunks and main branches and NDVI values are slightly lower (figure 5.11abcdef). A stronger decrease in NDVI values and even higher variability within the CC categories was noticed for scenario FWT (figure 5.11ghj). However, the NDVI values computed for the sunlit, shaded, and overall spruce canopy have a comparable range. It seems that this index is less sensitive to shadows within the canopy. Differences between the sunlit and shaded NDVI for the FWT scenario were almost negligible. In case of scenario F and FW, the sunlit NDVI was lower than the shaded NDVI, mainly for higher values of LAI, but still the absolute NDVI difference was quite small (about 0.10).

Sensitivities of the AVI index for canopy LAI are depicted in figure 5.12. The relationships are more complex than for the NDVI and they differ more between sunlit and shaded crown parts. The relationship for the sunlit AVI values appeared nearly flat, but for lower LAI values (3–7  $\text{m}^2\text{m}^{-2}$ ) they show indications of a non-monotonic (Gaussian-like) behaviour. AVI values for the shaded crown parts exhibited an almost linear decrease within increasing LAI. The canopy AVI values were also gradually decreasing with increasing LAI, but they were levelled off by the strong influence of the sunlit pixels in case of low LAI (3–5  $\text{m}^2\text{m}^{-2}$ ). Graphs for scenario F and FW showed a similar trend with lower AVI values for sunlit and consequently whole canopy simulations (figure 5.12abcdef). Resulting AVI values for the scenario FWT were systematically lowered by the mixed cells presence and their variability within the CC classes increased, especially for the sunlit crown parts (figure 5.12ghj).

## 5.4 Discussion

---

### 5.4.1 *Influence of the woody elements on simulated reflectance*

The results of our modelling experiment demonstrate that the woody elements, being still a minor contributor of a pixel's reflectance compared to the total amount of green foliage, influence noticeably the transfer of photons within the forest canopy. The DART modelled scenarios revealed that small woody twigs introduced into the leaf canopy play a more important role in forest RT than the robust woody parts like trunks and main branches. These robust woody parts caused only minor changes in the overall simulated canopy BRF (even for a forest stand with low LAI; cf., figure 5.7), whereas the introduction of the mixed cells in DART clearly influenced the BRF at all investigated wavelengths. The total absence of photon transmittance and high photon absorbance by the woody elements decreased the NIR canopy reflectance, despite of the relatively high bark reflectance at NIR wavelengths. These findings are in agreement with results of Myneni et al. (2003). An opposite effect was observed at the red wavelength, where the mixed cells increased canopy reflectance by approximately 2%. This difference results from a high reflectance of the twig bark (about 25%; figure 5.4) that, combined with a strong absorption of the foliage pigments, increased the red canopy BRF. Nadir BRF of the shaded parts was less influenced by the introduction of the mixed cells of the turbid media and opaque surfaces than nadir BRF of the sunlit parts, most probably due to lower signal level in the shade. The latter were more sensitive especially at NIR wavelengths, the wavelengths mostly influenced by the canopy structural characteristics including the woody element properties.

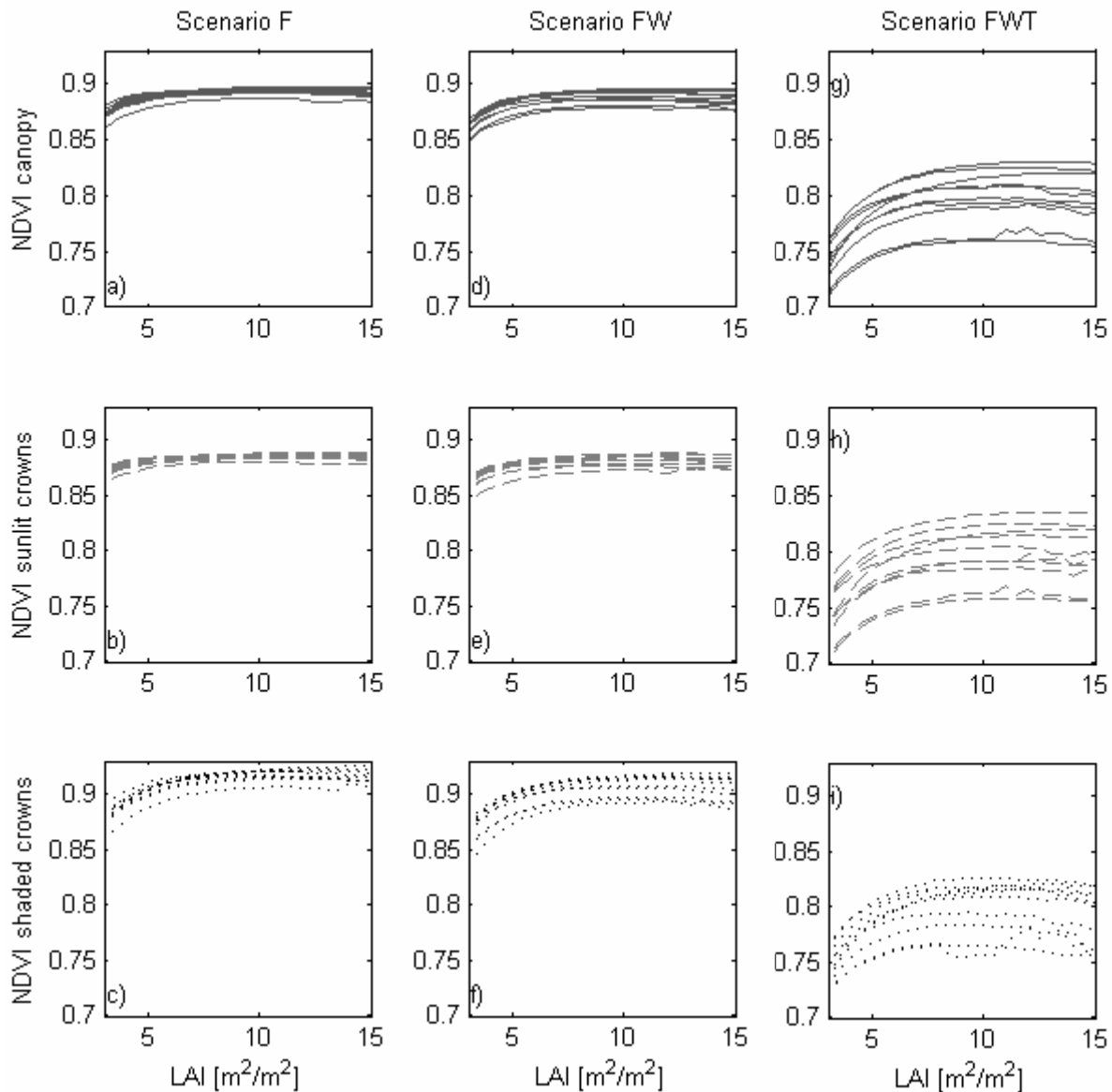


Figure 5.11. Relationship between spruce canopy leaf area index (LAI) and normalised difference vegetation index (NDVI) displayed for sunlit, shaded, and total canopy reflectance simulated by the DART model within three scenarios: i) scenario F – only foliage (a, b, c), ii) scenario FW – leaves and major woody parts (d, e, f), and iii) scenario FWT – leaves, trunks, main branches, and small twigs (g, h, i). Each line represents one of ten simulated canopy closure categories (CC = 50, 55, 60, 65, 70, 75, 80, 85, 90, and 95%).

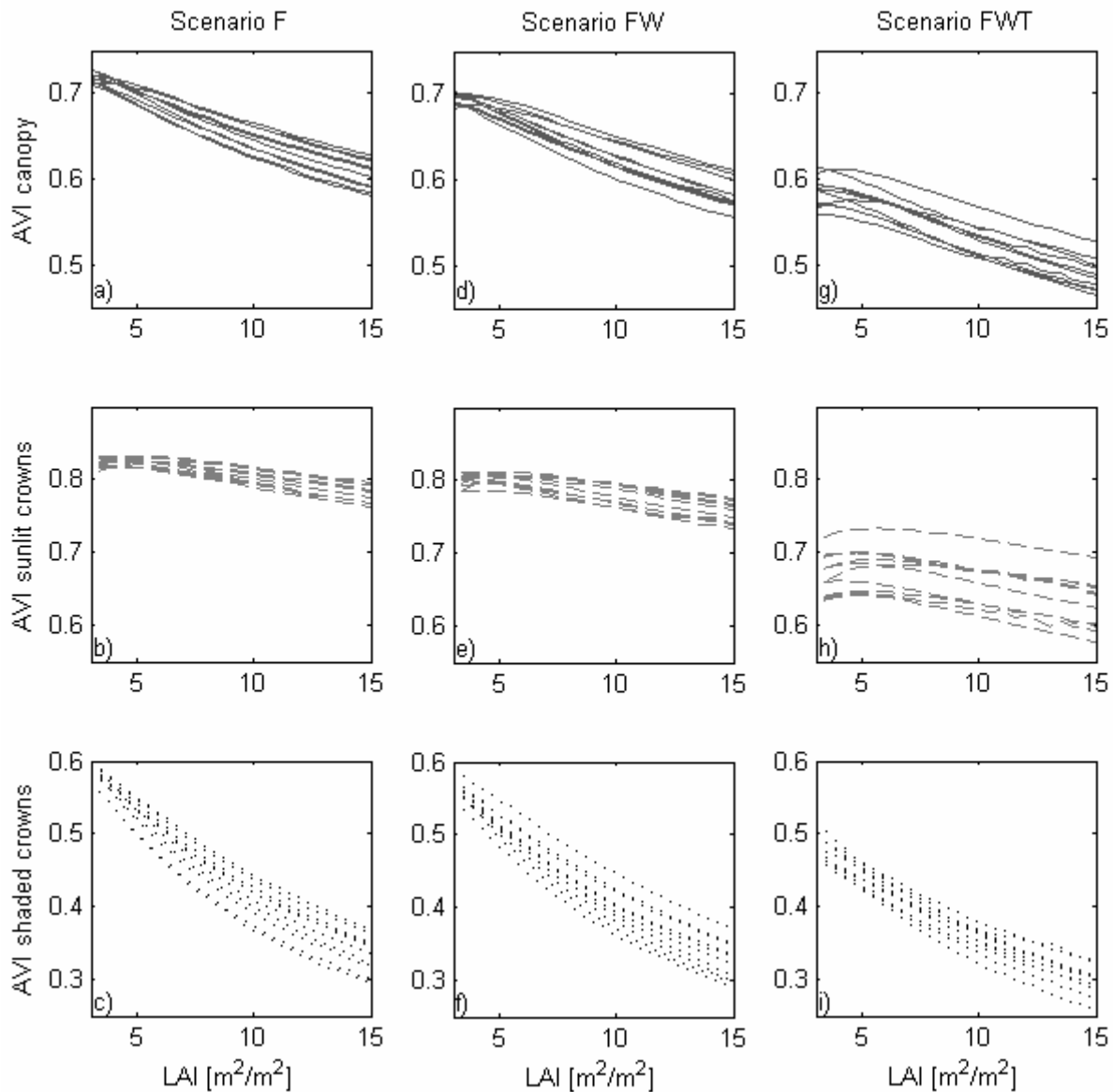


Figure 5.12. Relationship between spruce canopy leaf area index (LAI) and angular vegetation index (AVI) plotted for sunlit, shaded, and total canopy reflectance simulated by the DART model within three scenarios: i) scenario F – only foliage (a, b, c), ii) scenario FW – leaves and major woody parts (d, e, f), and iii) scenario FWT – leaves, trunks, main branches, and small twigs (g, h, i). Each line represents one of ten simulated canopy closure categories (CC = 50, 55, 60, 65, 70, 75, 80, 85, 90, and 95%).

Smolander & Stenberg (2003; 2005) introduced a within-shoot multiple scattering mechanism named the photon recollision probability (Panferov et al., 2001), which was later nested by Disney et al. (2004) into a Monte Carlo ray tracing model of a pine coniferous canopy. It has been shown by Rautiainen & Stenberg (2005) that the multiple scattering shoot correction, included in a semi-physical forest reflectance model named PARAS, increased the accuracy of a simulated coniferous canopy radiometric response. The within-shoot scattering decreased slightly the red and significantly the NIR BRF of the modelled forest canopy. The approach using mixed cells, as tested in this study, is aiming at the improvement of multiple scattering simulations within the forest canopy in general. However, it is not modelling coniferous shoot and within-shoot needle clumping in full geometrical detail. The mixed cells concept was not designed as a feature specific for the coniferous crowns, but as a universal parameter common for any woody forest canopy. Its physical and mathematical background is differing from the photon recollision probability (Combal et al., 2003) and will be discussed in scientific literature as well (Martin & Gastellu-Etchegorry, personal communication). Still, the results of both of these approaches are not contradictory, but are showing similar general trends of decreasing coniferous canopy reflectance mainly in NIR part of the electromagnetic spectrum.

#### *5.4.2 Reliability of the DART simulations*

The comparison of the DART modelled nadir BRF and the atmospherically corrected AISA Eagle BRF for 12 specific forest patches (figure 5.6) showed the best agreement for the scenario FWT. However, the results of the other two scenarios were also close to the AISA measurements (the highest BRF RMSE was about 5% in the NIR). It must also be assumed that some uncertainties in the airborne image due to atmospheric and radiometric corrections remain. However, they were minimized by a vicarious calibration approach and validated using three calibration targets (clay, gravel, and grass surface), which demonstrate the high accuracy of the AISA image calibration and correction. The only discrepancy in the data was found to be in the NIR plateau of the grass spectral target, which has been explained by the angular differences in the measured grass canopy.

The DART simulations of the scenario FWT suffered from a BRF overestimation in the red spectral band, most probably due to inaccurate parameterisation of the twig optical properties. These were assumed to be similar to the bark of large branches and uniform within the whole crown. Epiphytic green algae and lichens, dispersed irregularly throughout the canopy, often populate the bark of the spruce branches and twigs. The microstructure of their thalli should not interfere the NIR optical properties of the woody element bark, but some of them contain chlorophyll pigments, which increase red absorption and lower red reflectance of the bark. Consequently, the spatially distributed effect of epiphytic green algae and lichens, included into the twig and branch optical properties, could possibly reduce the red reflectance overestimation.

#### *5.4.3 Consequences on LAI retrieval and vegetation indices*

The most important wavelength with respect to the retrieval of forest LAI, are at the NIR plateau between 730-900 nm (considering the spectral range being confined to  $\lambda = 400-1000$  nm). Wavelengths of  $\lambda = 400-730$  nm are strongly influenced by the specific absorption of plant pigments (chlorophyll, carotenoids, etc.), and wavelengths of  $\lambda > 900$  nm by the specific absorption of water (Gates et al., 1965; Fukshansky, 1991). Higher concentration of these

plant leaf components rule the reflectance and transmittance at the mentioned wavelengths and thus these are less sensitive, and consequently less suitable, for inversion of the structural canopy properties, including LAI. The DART modelled images showed a minimum influence of simulated woody elements on the reflectance between 730-900 nm for shaded crown parts, but a regular reflectance decrease within these wavelengths for the sunlit canopy parts. The average decline of the overall spruce canopy NIR BRF of about 4% represents a strong argument to include the small woody elements into the radiative transfer model targeting the forest LAI inversion.

One can observe the increase of the BRF heterogeneity within the CC categories of the same LAI values after inclusion of the mixed cells into the DART simulations (cf., figure 5.7). This effect can potentially disturb the overall accuracy of the LAI retrieved for a forest canopy. Therefore, any LAI retrieving algorithm specifically designed for high spatial resolution image data should take into account the canopy closure as being a sensitive parameter driving the inversion quality.

With respect to the vegetation indices, the NDVI was found to be sensitive to tiny twig appearance within the simulated canopy. This can be explained by the fact that presence of the mixed cells caused a negatively correlated shift between the NIR and red canopy reflectance. Consequently, the ratios of the differences and sums of these bands decreased the NDVI values. However, minor irregularities were observed for the lower CC of the FWT scenario (figure 5.11ghj). These irregularities appeared due to the higher heterogeneity of canopy BRF after small twig introduction. Additionally, the results of all the DART simulations showed that NDVI is not a suitable tool for LAI inversion at very high spatial resolution, due to the fast saturation of the LAI-NDVI relationship. Nevertheless, figure 5.11 implies that this relationship for the FWT scenario saturates at higher LAI values than for the other scenarios.

The AVI values decreased with increasing LAI for simulations of the third FWT scenario. This originates from a reflectance decrease in the green and NIR and an increase in the red part. Such a spectral behaviour caused a widening of the angle between the lines connecting green with red and red with NIR reflectance and consequently a drop of the index value. The relation between canopy LAI and AVI disclosed a linearly decreasing function, but only for LAI values larger than  $5.0 \text{ m}^2 \text{ m}^{-2}$ . This fact makes AVI not to be fully suitable for the canopy LAI retrieval either. However, no quantification of the effect on LAI retrieval was carried out, because the index computation is based on two wavelengths strongly influenced by the chlorophyll concentration, which was used in the DART modelling as a fixed parameter.

## 5.5 Conclusions

---

In this study we have investigated the influence of woody elements, i.e. trunks additionally composed of main branches and tiny twigs, on the TOC reflectance of a Norway spruce canopy at very high spatial resolution. The inclusion of trunks including first order branches into the DART model had a minor impact on the nadir reflectance of the simulated canopy. However, the introduction of mixed cells (table 5.1) noticeably reduced nadir TOC reflectance at NIR wavelengths. This TOC BRF reduction can mainly be observed in the sunlit part of the simulated canopy, whereas the reflectance of the shaded canopy part remained almost unchanged. These findings were confirmed by the direct comparison of the



DART modelled images with atmospherically corrected airborne hyperspectral data. The study findings particularly highlighted the importance of sensitivity analyses dealing with the radiative transfer through complex forest canopies. The introduction of additional input parameters results in an increase of the RT model complexity, but also in a decrease of its invertability (Combal et al., 2003). Nevertheless, if sound a priori knowledge on the model input parameters is used, it may reduce the ill-posed inverse problem and increase the accuracy of the retrieved parameters.

More specifically, the inclusion and distribution of wood abundance in RT based approaches targeting at LAI retrieval at very high spatial resolution is a prerequisite when analyzing individual tree crowns. In particular the spatial distribution of small twig elements within the leaf canopy, being an important photon absorbing and scattering mechanism, significantly improves the retrieval. Also the findings on using two vegetation indices (NDVI, AVI) favour the physical LAI retrieval based inversion of the RT model rather than using empirical inversion based on establishing a statistical relationship between LAI and these indices.

Significant relevance will be attributed in the future to (3D) radiative transfer based inversion approaches for the retrieval of biophysical and biochemical variables. Where current approaches already rely on biome or ecosystem specific parameterization of the RT, future approaches will increasingly rely on more detailed parameterization of vegetation specific properties, such as plant functional types, species composition and the like. The inclusion of woody trunks, main branches and tiny twigs in DART demonstrated in a Norway spruce canopy in this paper confirm this trend.

## 5.6 Acknowledgements

---

This study was carried out within the ESA/PECS project No. 98029 and the Research Plan AV0Z6087904 of the Institute of System Biology and Ecology, Academy of Sciences of the Czech Republic. Zbyněk Malenovský likes to acknowledge financial support from the Sabbatical Fellowship 1K04 provided by the Ministry of Education, Youth and Sports of the Czech Republic.

## 5.7 References

---

- Ahl, D. E., Gower, S. T., Mackay, D. S., Burrows, S. N., Norman, J. M., & Diak, G. R. (2004), Heterogeneity of light use efficiency in a northern Wisconsin forest: implications for modeling net primary production with remote sensing. *Remote Sensing of Environment*, 93, 168-178.
- Arora, V. K. (2002), Modeling vegetation as a dynamic component in soil-vegetation-atmosphere transfer schemes and hydrological models. *Reviews of Geophysics*, 40, 3-1.
- Atzberger, C. (2004), Object-based retrieval of biophysical canopy variables using artificial neural nets and radiative transfer models. *Remote Sensing of Environment*, 93, 53-67.
- Bannari, A., Morin, D., Bonn, F., & Huete, A. R. (1995), A review of vegetation indices. *Remote Sensing Reviews*, 13, 95-120.
- Broge, N. H., & Leblanc, E. (2001), Comparing prediction power and stability of broadband and hyperspectral vegetation indices for estimation of green leaf area index and canopy chlorophyll density. *Remote Sensing of Environment*, 76, 156-172.

- Campbell, G. S. (1990), Derivation of an angle density function for canopies with ellipsoidal leaf angle distributions. *Agricultural & Forest Meteorology*, 49, 173-176.
- Centre d'Etudes Spatiales de la Biosphère (CESBIO) (2005), DART (Discrete Anisotropic Radiative Transfer). *Web page available on-line on <http://www.cesbio.ups-tlse.fr/us/dart0.htm>*, CESBIO, France, Accessed November 30, 2005.
- Chen, J. M., & Black, T. A. (1991), Measuring leaf area index of plant canopies with branch architecture. *Agricultural & Forest Meteorology*, 57, 1-12.
- Chen, J. M., & Black, T. A. (1992), Defining leaf area index for non-flat leaves. *Plant, Cell and Environment*, 15, 421-429.
- Chen, J. M., & Leblanc, S. G. (1997), A four-scale bidirectional reflectance model based on canopy architecture. *Ieee Transactions on Geoscience and Remote Sensing*, 35, 1316-1337.
- Clevers, J. G. P. W. (1988), Multispectral Aerial-Photography as a New Method in Agricultural Field Trial Analysis. *International Journal of Remote Sensing*, 9, 319-332.
- Combal, B., Baret, F., Weiss, M., Trubuil, A., Mace, D., Pragnere, A., Myneni, R., Knyazikhin, Y., & Wang, L. (2003), Retrieval of canopy biophysical variables from bidirectional reflectance: Using prior information to solve the ill-posed inverse problem. *Remote Sensing of Environment*, 84, 1-15.
- Cudlín, P., Novotný, R., Moravec, I., & Chmeliková, E. (2001), Retrospective evaluation of the response of montane forest ecosystems to multiple stress. *Ekologia-Bratislava*, 20, 108-124.
- Daughtry, C. S. T., Biehl, L. L., & Ranson, K. J. (1989), A new technique to measure the spectral properties of conifer needles. *Remote Sensing of Environment*, 27, 81-91.
- Disney, M., Lewis, P., & Saich, P. (2006), 3D modelling of forest canopy structure for remote sensing simulations in the optical and microwave domains. *Remote Sensing of Environment*, 100, 114-132.
- Dzierzon, H., Sievanen, R., Kurth, W., Perttunen, J., & Sloboda, B. (2003), Enhanced possibilities for analyzing tree structure as provided by an interface between different modelling systems. *Silva Fennica*, 37, 31-44.
- Fang, H., & Liang, S. (2005), A hybrid inversion method for mapping leaf area index from MODIS data: Experiments and application to broadleaf and needleleaf canopies. *Remote Sensing of Environment*, 94, 405-424.
- Fassnacht, K. S., Gower, S. T., MacKenzie, M. D., Nordheim, E. V., & Lillesand, T. M. (1997), Estimating the leaf area index of North Central Wisconsin forests using the landsat thematic mapper. *Remote Sensing of Environment*, 61, 229-245.
- Fukshansky, L. (1991), Photon Transport in Leaf Tissue: Applications in Plant Physiology. In R. B. Myneni, & J. Ross (Ed.), *Photon - vegetation interactions : applications in optical remote sensing and plant ecology* (pp. 253-302). Berlin Springer-Verlag.
- Gascon, F., Gastellu-Etchegorry, J. P., Lefevre-Fonollosa, M. J., & Dufrene, E. (2004), Retrieval of forest biophysical variables by inverting a 3-D radiative transfer model and using high and very high resolution imagery. *International Journal of Remote Sensing*, 25, 5601-5616.
- Gascon, F., Gastellu-Etchegorry, J. P., & Lefevre, M. J. (2001), Radiative transfer model for simulating high-resolution satellite images. *Ieee Transactions on Geoscience and Remote Sensing*, 39, 1922-1926.
- Gastellu-Etchegorry, J. P., Demarez, V., Pinel, V., & Zagolski, F. (1996), Modeling radiative transfer in heterogeneous 3-D vegetation canopies. *Remote Sensing of Environment*, 58, 131-156.
- Gastellu-Etchegorry, J. P., Martin, E., & Gascon, F. (2004), DART: a 3D model for simulating satellite images and studying surface radiation budget. *International Journal of Remote Sensing*, 25, 73-96.
- Gates, D. M., Keegan, J. C., & Prentice, K. C. (1965), Spectral properties of plants. *Applied Optics*, 4, 11-20.
- Gower, S. T. (2003), Patterns and mechanisms of the forest carbon cycle. *Annual Review of Environment and Resources*, 28, 169-204.

- Gower, S. T., Krankina, O., Olson, R. J., Apps, M., Linder, S., & Wang, C. (2001), Net primary production and carbon allocation patterns of boreal forest ecosystems. *Ecological Applications*, 11, 1395-1411.
- Gruber, F. (1994), Morphology of coniferous trees: possible effects of soil acidification on the morphology of Norway spruce and Silver fir. In D. L. Godbold, & A. Hüttermann (Ed.), *Effects of acid rain on forest processes* (pp. 265-324). New York: Wiley-Liss.
- Haboudane, D., Miller, J. R., Tremblay, N., Zarco-Tejada, P. J., & Dextraze, L. (2002), Integrated narrow-band vegetation indices for prediction of crop chlorophyll content for application to precision agriculture. *Remote Sensing of Environment*, 81, 416-426.
- Hoffmann, W. A., & Jackson, R. B. (2000), Vegetation-climate feedbacks in the conversion of tropical savanna to Grassland. *Journal of Climate*, 13, 1593-1602.
- Ishii, H., Ford, E. D., Boscolo, M. E., Manriquez, A. C., Wilson, M. E., & Hinckley, T. M. (2002a), Variation in specific needle area of old-growth Douglas-fir in relation to needle age, within-crown position and epicormic shoot production. *Tree Physiology*, 22, 31-40.
- Ishii, H., & McDowell, N. (2002b), Age-related development of crown structure in coastal Douglas-fir trees. *Forest Ecology and Management*, 169, 257-270.
- Jonckheere, I., Fleck, S., Nackaerts, K., Muys, B., Coppin, P., Weiss, M., & Baret, F. (2004), Review of methods for in situ leaf area index determination Part I. Theories, sensors and hemispherical photography. *Agricultural and Forest Meteorology*, 121, 19-35.
- Jordan, C. F. (1969), Deviation of leaf-area index from quality of light on the forest floor. *Ecology*, 50, 663-666.
- Knyazikhin, Y., Marshak, A., & Myneni, R. (2005), Three-dimensional radiative transfer in vegetation canopies. In A. Davis, & A. Marshak (Ed.), *Three-dimensional radiative transfer in the cloudy atmosphere* (pp. 617-651). New York: Springer-Verlag.
- Knyazikhin, Y., Martonchik, J. V., Diner, D. J., Myneni, R. B., Verstraete, M., Pinty, B., & Gobron, N. (1998), Estimation of vegetation canopy leaf area index and fraction of absorbed photosynthetically active radiation from atmosphere-corrected MISR data. *Journal of Geophysical Research-Atmospheres*, 103, 32239-32256.
- Koetz, B., Baret, F., Poilvé, H., & Hill, J. (2005), Use of coupled canopy structure dynamic and radiative transfer models to estimate biophysical canopy characteristics. *Remote Sensing of Environment*, 95, 115-124.
- Kratochvilová, I., Janouš, D., Marek, M. V., Barták, M., & Říha, L. (1989), Production activity of mountain cultivated Norway spruce stands under the impact of air pollution. *Ekologia-Bratislava*, 8, 407-419.
- Kucharik, C. J., Foley, J. A., Delire, C., Fisher, V. A., Coe, M. T., Lenters, J. D., Young-Molling, C., Ramankutty, N., Norman, J. M., & Gower, S. T. (2000), Testing the performance of a Dynamic Global Ecosystem Model: Water balance, carbon balance, and vegetation structure. *Global Biogeochemical Cycles*, 14, 795-825.
- Kucharik, C. J., Norman, J. M., & Gower, S. T. (1998), Measurements of branch area and adjusting leaf area index indirect measurements. *Agricultural and Forest Meteorology*, 91, 69-88.
- Kuuluvainen, T., & Sprugel, D. G. (1996), Examining age- and altitude-related variation in tree architecture and needle efficiency in Norway spruce using trend surface analysis. *Forest Ecology and Management*, 88, 237-247.
- Leblanc, S. G., Bicheron, P., Chen, J. M., Leroy, M., & Cihlar, J. (1999), Investigation of directional reflectance in boreal forests with an improved four-scale model and airborne POLDER data. *IEEE Transactions on Geoscience and Remote Sensing*, 37, 1396-1414.
- Lee, K.-S., Cohen, W. B., Kennedy, R. E., Maiersperger, T. K., & Gower, S. T. (2004), Hyperspectral versus multispectral data for estimating leaf area index in four different biomes. *Remote Sensing of Environment*, 91, 508-520.
- Li-Cor (1983), *1800-12 Integrating sphere instruction manual*. Publication number 8305-0034. pp.

- Malenovský, Z., Martin, E., Gastellu-Etchegorry, J. P., Cudlín, P., & Clevers, J. G. P. W. (2003), Heterogeneity description improvements of spruce crown architecture simulated using the 3D radiative transfer model DART. *Proceedings of the 2nd SPECTRA Workshop*, 28. - 30. October 2003, ESTEC, Noordwijk, The Netherlands: European Space Agency.
- Martonchik, J. V., Bruegge, C. J., & Strahler, A. H. (2000), A review of reflectance nomenclature used in remote sensing. *Remote Sensing Reviews*, 19, 9-20.
- Mesarch, M. A., Walter-Shea, E. A., Asner, G. P., Middleton, E. M., & Chan, S. S. (1999), A revised measurement methodology for conifer needles spectral optical properties: Evaluating the influence of gaps between elements. *Remote Sensing of Environment*, 68, 177-192.
- Middleton, E. M., Walter-Shea, E. A., Mesarch, M. A., Chan, S. S., & Rusin, R. J. (1997), Optical properties of Black spruce and Jack pine needles at BOREAS sites in Saskatchewan, Canada. *Canadian Journal of Remote Sensing*, 23, 109-119.
- Monteith, J. L., & Unsworth, M. H. (1990), *Principles of Environmental Physics*. London: 2nd edn. Edward Arnold, pp. 291.
- Myneni, R. B., Hoffman, S., Knyazikhin, Y., Privette, J. L., Glassy, J., Tian, Y., Wang, Y., Song, X., Zhang, Y., Smith, G. R., Lotsch, A., Friedl, M., Morisette, J. T., Votava, P., Nemani, R. R., & Running, S. W. (2002), Global products of vegetation leaf area and fraction absorbed PAR from year one of MODIS data. *Remote Sensing of Environment*, 83, 214-231.
- Myneni, R. B., Nemani, R. R., & Running, S. W. (1997), Estimation of global leaf area index and absorbed par using radiative transfer models. *Ieee Transactions on Geoscience and Remote Sensing*, 35, 1380-1393.
- Nicolini, E., Chanson, B., & Bonne, F. (2001), Stem growth and epicormic branch formation in understorey beech trees (*Fagus sylvatica* L.). *Annals of Botany*, 87, 737-750.
- North, P. R. J. (2002), Estimation of fAPAR, LAI, and vegetation fractional cover from ATSR-2 imagery. *Remote Sensing of Environment*, 80, 114-121.
- Oak Ridge National Laboratory Distributed Active Archive Center (ORNL DAAC) (2005a), FLUXNET A Global Network Integrating Worldwide CO<sub>2</sub> Flux Measurements. *Web page available on-line on <http://www.fluxnet.ornl.gov/fluxnet/index.cfm>*, Oak Ridge, Tennessee, USA, Accessed November 30, 2005.
- Oak Ridge National Laboratory Distributed Active Archive Center (ORNL DAAC) (2005b), MODIS ASCII Subsets. *Web page available on-line on <http://www.modis.ornl.gov/modis/index.cfm>*, Oak Ridge, Tennessee, USA, Accessed November 30, 2005.
- Panferov, O., Knyazikhin, Y., Myneni, R. B., Szarzynski, J., Engwald, S., Schnitzler, K. G., & Gravenhorst, G. (2001), The role of canopy structure in the spectral variation of transmission and absorption of solar radiation in vegetation canopies. *Ieee Transactions on Geoscience and Remote Sensing*, 39, 241-253.
- Pavelka, M., Janouš, D., Urban, O., Acosta, M., Pokorný, R., Havránková, K., & Formánek, P. (2003), Carbon sources in vertical profile of a norway spruce stand. *Folia Oecologica*, 30, 199-206.
- Pinty, B., Widlowski, J. L., Taberner, M., Gobron, N., Verstraete, M. M., Disney, M., Gascon, F., Gastellu, J. P., Jiang, L., Kuusk, A., Lewis, P., Li, X., Ni-Meister, W., Nilson, T., North, P., Qin, W., Su, L., Tang, S., Thompson, R., Verhoef, W., Wang, H., Wang, J., Yan, G., & Zang, H. (2004), Radiation Transfer Model Intercomparison (RAMI) exercise: Results from the second phase. *Journal of Geophysical Research-Atmospheres*, 109, -.
- Plummer, S. E., North, P. R., & Briggs, S. A. (1994), The Angular Vegetation Index: an atmospherically resistant index for the second along track scanning radiometer (ATSR-2). *Proceedings of the 6th Symposium on Physical Measurements and Spectral Signatures in Remote Sensing*, 17-21 January 1994, Toulouse, France: CNES, 717-722.
- Pokorný, R., & Marek, M. V. (2000), Test of accuracy of LAI estimation by LAI-2000 under artificially changed leaf to wood area proportions. *Biologia Plantarum*, 43, 537-544.
- Rautiainen, M., & Stenberg, P. (2005), Application of photon recollision probability in coniferous canopy reflectance simulations. *Remote Sensing of Environment*, 96, 98-107.

- Remphrey, W. R., & Davidson, C. G. (1992), Spatiotemporal Distribution of Epicormic Shoots and Their Architecture in Branches of *Fraxinus-Pennsylvanica*. *Canadian Journal of Forest Research-Revue Canadienne De Recherche Forestiere*, 22, 336-340.
- Richter, R., & Schlapfer, D. (2002), Geo-atmospheric processing of airborne imaging spectrometry data. Part 2: atmospheric/topographic correction. *International Journal of Remote Sensing*, 23, 2631-2649.
- Rouse, J. W., Haas, R. H., Schell, J. A., & Deering, D. W. (1973), Monitoring vegetation systems in the great plains with ERTS. *Third ERTS Symposium*, NASA SP-351 I, 309-317.
- Shabanov, N. V., Huang, D., Yang, W., Tan, B., Knyazikhin, Y., Myneni, R. B., Ahl, D. E., Gower, S. T., Huete, A. R., Aragão, L. E. O. C., & Shimabukuro, Y. E. (2005), Analysis and optimization of the MODIS leaf area index algorithm retrievals over broadleaf forests. *IEEE Transactions on Geoscience and Remote Sensing*, 43, 1855-1865.
- Shabanov, N. V., Wang, Y., Buermann, W., Dong, J., Hoffman, S., Smith, G. R., Tian, Y., Knyazikhin, Y., & Myneni, R. B. (2003), Effect of foliage spatial heterogeneity in the MODIS LAI and FPAR algorithm over broadleaf forests. *Remote Sensing of Environment*, 85, 410-423.
- Schaepman-Strub, G., Schaepman, M., Dangel, S., Painter, T., & Martonchik, J. (2005), About the use of reflectance terminology in imaging spectroscopy. *EARSeL eProceedings*, 4, 191-202.
- Schaepman, M. E., Koetz, B., Schaepman-Strub, G., & Itten, K. I. (2005), Spectrodirectional remote sensing for the improved estimation of biophysical and -chemical variables: Two case studies. *International Journal of Applied Earth Observation and Geoinformation*, 6, 271-282.
- Smith, G. M., & Milton, E. J. (1999), The use of the empirical line method to calibrate remotely sensed data to reflectance. *International Journal of Remote Sensing*, 20, 2653-2662.
- Smolander, S., & Stenberg, P. (2003), A method to account for shoot scale clumping in coniferous canopy reflectance models. *Remote Sensing of Environment*, 88, 363-373.
- Smolander, S., & Stenberg, P. (2005), Simple parameterizations of the radiation budget of uniform broadleaved and coniferous canopies. *Remote Sensing of Environment*, 94, 355-363.
- Strahler, A. H. (1980), The Use of Prior Probabilities in Maximum-Likelihood Classification of Remotely Sensed Data. *Remote Sensing of Environment*, 10, 135-163.
- Taylor, G. E. J. (1998), Forest ecosystems and air pollution: the importance of multiple stress interaction on a regional and global scale. In J. C. Cech, B. W. Wilson, & D. B. Crosby (Ed.), *Multiple stress in ecosystems* (pp. 23-40). Boca Raton: Lewis Publishers.
- Tian, Y., Woodcock, C. E., Wang, Y., Privette, J. L., Shabanov, N. V., Zhou, L., Zhang, Y., Buermann, W., Dong, J., Veikkanen, B., Häme, T., Andersson, K., Ozdogan, M., Knyazikhin, Y., & Myneni, R. B. (2002a), Multiscale analysis and validation of the MODIS LAI product I. Uncertainty assessment. *Remote Sensing of Environment*, 83, 414-430.
- Tian, Y., Woodcock, C. E., Wang, Y., Privette, J. L., Shabanov, N. V., Zhou, L., Zhang, Y., Buermann, W., Dong, J., Veikkanen, B., Häme, T., Andersson, K., Ozdogan, M., Knyazikhin, Y., & Myneni, R. B. (2002b), Multiscale analysis and validation of the MODIS LAI product II. Sampling strategy. *Remote Sensing of Environment*, 83, 431-441.
- Tucker, C. J. (1979), Red and photographic infrared linear combinations for monitoring vegetation. *Remote Sensing of Environment*, 8, 127-150.
- Turner, D. P., Cohen, W. B., Kennedy, R. E., Fassnacht, K. S., & Briggs, J. M. (1999), Relationships between Leaf Area Index and Landsat TM Spectral Vegetation Indices across Three Temperate Zone Sites. *Remote Sensing of Environment*, 70, 52-68.
- Turner, D. P., Ritts, W. D., Cohen, W. B., Gower, S. T., Zhao, M. S., Running, S. W., Wofsy, S. C., Urbanski, S., Dunn, A. L., & Munger, J. W. (2003), Scaling Gross Primary Production (GPP) over boreal and deciduous forest landscapes in support of MODIS GPP product validation. *Remote Sensing of Environment*, 88, 256-270.
- Turner, D. P., Ritts, W. D., Cohen, W. B., Maelersperger, T. K., Gower, S. T., Kirschbaum, A. A., Running, S. W., Zhao, M. S., Wofsy, S. C., Dunn, A. L., Law, B. E., Campbell, J. L., Oechel,

- W. C., Kwon, H. J., Meyers, T. P., Small, E. E., Kurc, S. A., & Gamon, J. A. (2005), Site-level evaluation of satellite-based global terrestrial gross primary production and net primary production monitoring. *Global Change Biology*, 11, 666-684.
- Weiss, M. (2004), Review of methods for in situ leaf area index (LAI) determination Part II. Estimation of LAI, errors and sampling. *Agricultural and Forest Meteorology*, 121, 37-53.
- Zeng, N., & Neelin, J. D. (2000), The role of vegetation-climate interaction and interannual variability in shaping the African Savanna. *Journal of Climate*, 13, 2665-2670.
- Zhang, L., Dawes, W. R., & Walker, G. R. (2001), Response of mean annual evapotranspiration to vegetation changes at catchment scale. *Water Resources Research*, 37, 701-708.

**CHAPTER 6****A new hyperspectral index for chlorophyll estimation of a forest canopy: Area under curve Normalised to Maximal Band depth between 650-725 nm**

Reprint of:<sup>§</sup>

Malenovský, Z, Ufer, C., Lhotáková, Z., Clevers, J.G.P.W., Schaepman, M.E., Albrechtová, J., Cudlín, P.: Area under curve Normalized to Maximal Band depth between 650-725 nm: A new hyperspectral index for chlorophyll estimation of a forest canopy. *EARSeL eProceedings*, 5(2), 161-172.

---

<sup>§</sup> Reprinted with permission from EARSeL and BIS © 2006.

## Abstract

Total chlorophyll ( $C_{ab}$ ) content of a forest canopy is used as indicator for the current state of a forest stand, and also as an input for various physiological vegetation models (i.e., models of photosynthesis, evapo-transpiration, etc.). Recent hyperspectral remote sensing allows retrieving the  $C_{ab}$  concentration of vegetation using the appropriate optical indices, and/or by means of biochemical information, scaled up from leaf to canopy level within radiative transfer (RT) models. Plenty of chlorophyll optical indices can be found in literature for the leaf level, nevertheless, only some of them were proposed for a complex vegetation canopy like a forest stand. A robust chlorophyll optical index at the canopy level should be driven by the  $C_{ab}$  concentration without negative influence of other factors represented by soil background or understory, canopy closure, canopy structure (e.g., leaf area index - LAI, clumping of leaves), etc.

A new optical index named Area under curve Normalized to Maximal Band depth between 650-725 nm ( $ANMB_{650-725}$ ) is proposed to estimate chlorophyll content of a Norway spruce (*Picea abies*, (L.) Karst.) crown. This index was designed to exploit modifications of a vegetation reflectance signature invoked within the red-edge wavelengths mainly by the changes in leaf chlorophyll content.  $ANMB_{650-725}$  is based on the reflectance continuum removal of the chlorophyll absorption feature between wavelengths of 650-725 nm. Suitability of the index and sensitivity on disturbing factors was tested using a 3D Discrete Anisotropic Radiative Transfer (DART) model coupled with a leaf radiative transfer model PROSPECT adjusted for spruce needles. The results of the  $ANMB_{650-725}$  abilities within a coniferous forest canopy were compared with the performance of the chlorophyll indices ratio TCARI/OSAVI.

Test results, carried out with the DART model simulating hyperspectral data with 0.9 m pixel size, showed a strong linear regression of the  $ANMB_{650-725}$  on spruce crown  $C_{ab}$  concentration ( $R^2=0.9798$ ) and its quite strong resistance against varying canopy structural features such as LAI and canopy closure. The root mean square error (RMSE) between real and the  $ANMB_{650-725}$  estimated  $C_{ab}$  concentrations was only  $9.53 \mu\text{g}/\text{cm}^2$  while the RMSE generated from prediction of the TCARI/OSAVI was two times higher ( $18.83 \mu\text{g}/\text{cm}^2$ ). Chlorophyll retrieval using the  $ANMB_{650-725}$  index remained stable also after introduction of two reflectance signal disturbing features: a) 20% of the spectral information of epiphytic lichen (*Pseudevernia* sp.) regularly distributed within the spruce canopy, and b) simulation of the sensor noise (computed for a signal to noise ratio equal to 5). RMSE of predicted  $C_{ab}$  concentration after the lichens introduction appeared to be  $10.51 \mu\text{g}/\text{cm}^2$  and the combined influence of lichen presence and sensor noise in the image caused an increase of the RMSE to  $12.13 \mu\text{g}/\text{cm}^2$ .

**Keywords:** hyperspectral quantitative remote sensing, chlorophyll optical index  $ANMB_{650-725}$ , DART, radiative transfer model.



## 6.1 Introduction

Current approaches of quantitative remote sensing allow to estimate the concentration of biochemical constituents spatially using fine spectral resolution (hyperspectral) image data in combination with radiative transfer models (Adams et al., 1985; Broge & Leblanc, 2001; Gamon et al., 2004; Peddle et al., 2004). One of the most important biochemical parameters of the vegetation canopy is the total concentration of the green foliar pigments, chlorophyll *a* and *b* ( $C_{ab}$ ). Chlorophyll concentration of the forest canopy can be used as a biomarker for an acute environmental stress (Malenovský et al., 2006), as well as an input for physiological ecosystem models, for instance models estimating the photosynthetic efficiency (Curran, 1994).

A number of optical indices for estimating the leaf  $C_{ab}$  content was proposed (le Maire et al., 2004), but not all of them are suitable to be used on the level of the complex forest canopy. A forest canopy is rather a spatially heterogeneous system, assembled from a certain amount of leaves and woody twigs (shoots in case of conifer species), branches of several orders, stems, and other components, arranged in the 3D space in a specific way. Therefore, any optical index, designed for estimation of the biochemical parameter, should be preferably driven only by the concentration of this biochemical constituent, and be independent of the other structural and biochemical characteristics of the canopy (e.g., density and distribution of leaves, canopy closure, etc.) including surrounding environment (e.g., influence of understory and soil on background).

Radiative transfer (RT) models represent an ideal tool to design and test such biochemical optical indices. Haboudane et al. (2002) gave a typical example how the RT models can be used for development of an optical index performing optimally on the canopy scale. They employed the leaf RT model PROSPECT coupled with the SAILH canopy RT model to establish and test the ratio of two optical indices TCARI (Daughtry et al., 2000a) and OSAVI (Steven, 1998) as an appropriate vegetation index for estimation of agriculture canopy  $C_{ab}$  content from hyperspectral imagery. The TCARI/OSAVI ratio, simulated for a corn field, was shown to be a robust chlorophyll biomarker, minimally influenced by the reflectance of the underlying soil and the variation in the canopy LAI (Zarco-Tejada et al., 2004b).

A similar technique, employing the RT models PROSPECT and DART (Discrete Anisotropic Radiative Transfer), was applied in our study to develop and test the sensitivity of a robust chlorophyll estimating optical index for a heterogeneous coniferous forest canopy. A newly proposed index named Area under curve Normalized to Maximal Band depth between 650-725nm ( $ANMB_{650-725}$ ) is based on the method called continuum removal of reflectance spectra (Broge & Leblanc, 2001), using advantages of fine spectral resolution and sampling band interval of the hyperspectral images acquired with a very small pixel-size. The continuum removal technique was lately used over aerial hyperspectral data by Underwood et al. (2003) for mapping of specific invasive plants, and by Kokaly et al. (2003) for discriminating different vegetation cover types in the Yellowstone National Park, as well as by Schmidt and Skidmore (2001) to differentiate saltmarsh vegetation types of the Dutch Waddenzee wetland. Already in 1999, Kokaly and Clark used normalised band depths calculated from specific continuum-removed absorption features of reflectance, measured over dried and ground leaves, to estimate the concentrations of nitrogen, lignin, and cellulose. Curran et al. (2001) refined the Kokaly and Clark methodologies combining band depths

normalised to the wavelength at the centre of the absorption feature (BNC) or the area of the absorption feature (BNA) with stepwise multiple linear regression. They used these spectral parameters to assess concentrations of  $C_{ab}$  within two absorption features: 408-518nm, and 588-750nm.

## 6.2 Methods

### 6.2.1 Design of the $ANMB_{650-725}$ index

The new chlorophyll estimating optical index  $ANMB_{650-725}$  is based on the continuum removal of the chlorophyll absorption feature at the red-edge part of the spectrum, i.e. between the wavelengths of 650-725 nm. The logic behind this spectral index is exploiting well known changes of a vegetation reflectance signature shape invoked within these wavelengths mainly by the changes in leaf chlorophyll content (figure 6.1). An increase in the chlorophyll concentration causes the chlorophyll absorption feature to deepen at the red-edge of reflectance with the absorption maximum at approximately 675-680 nm (see figure 6.1a). The reflectance at maximum chlorophyll absorption becomes saturated with increasing  $C_{ab}$  concentration (Daughtry et al., 2000a), but the adjacent wavebands (especially of longer wavelengths) remain very sensitive to these changes. Therefore, the area under a continuum-removed reflectance curve from 650 to 725 nm is getting significantly smaller with chlorophyll decline, and the maximal band depth of this area is systematically changing too (see figure 6.1b).

Based on this observation, the continuum removal procedure (Kokaly & Clark, 1999) is applied on the canopy bidirectional reflectance factor (BRF) of wavelengths between 650 to 725 nm as first step of the  $ANMB_{650-725}$  computation. Secondly, the area under the continuum-removed reflectance curve between 650 and 725 nm ( $AUC_{650-725}$ ) is integrated according to the equation:

$$AUC_{650-725} = \frac{1}{2} \sum_{j=1}^{n-1} (\lambda_{j+1} - \lambda_j) (\rho_{j+1} + \rho_j), \quad (6.1)$$

where  $\rho_j$  and  $\rho_{j+1}$  are values of the continuum-removed reflectance at the  $j$  and  $j+1$  bands,  $\lambda_j$  and  $\lambda_{j+1}$  are wavelengths of the  $j$  and  $j+1$  bands, and  $n$  is number of the used spectral bands. Finally, the  $ANMB_{650-725}$  index is computed as:

$$ANMB_{650-725} = \frac{AUC_{650-725}}{MBD_{650-725}}, \quad (6.2)$$

where  $MBD_{650-725}$  is a maximal band depth of the continuum-removed reflectance, placed at one of the spectrally stable wavelengths of strongest chlorophyll absorption about 675-680 nm. Normalisation of  $AUC_{650-725}$  by  $MBD_{650-725}$  is a crucial step ensuring a strong relationship between  $ANMB_{650-725}$  and the chlorophyll content at higher concentrations. The dependence relation of  $AUC_{650-725}$  on the  $C_{ab}$  concentration saturates for  $C_{ab} > 60 \mu\text{g}/\text{cm}^2$ , while values of the  $MBD_{650-725}$  above this  $C_{ab}$  concentration start to systematically decrease. This disproportional non-linear relationship between the  $AUC_{650-725}$  and the  $MBD_{650-725}$  makes

their ratio, i.e. the  $ANMB_{650-725}$  index, sensitive to not only low and average, but also to high concentrations of  $C_{ab}$ .

### 6.2.2 Radiative transfer models

The PROSPECT model, adopted for Norway spruce (*Picea Abies* (L.) Karst.) needles, and the canopy radiative transfer model DART were combined to simulate airborne very high spatial resolution hyperspectral images of a mature spruce forest stand, and subsequently to generate the BRF database of sunlit crown spectral signatures (see flowchart in figure 6.2).

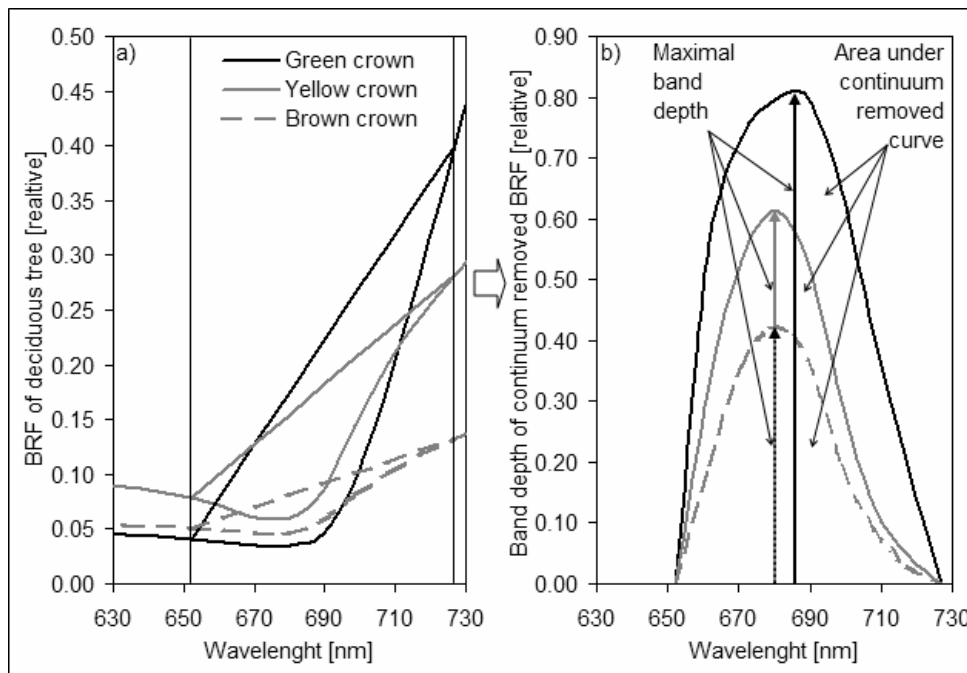


Figure 6.1. Description of continuum removal and band depth calculation to generate the  $ANMB_{650-725}$  index from sunlit vegetation spectral signatures of a “green” (high  $C_{ab}$ ), “yellow” (very low  $C_{ab}$ ), and “brown” (dead tree without  $C_{ab}$ ) coloured crown of a deciduous tree extracted from an AISA Eagle atmospherically corrected hyperspectral image: a) delineation of the reflectance feature at the chlorophyll absorption between 650 and 725 nm; b) maximal band depth ( $MBD_{650-725}$ ) and area under reflectance continuum-removed curve ( $AUC_{650-725}$ ).

The PROSPECT model (Jacquemoud & Baret, 1990) simulates leaf hemispherical reflectance and transmittance signatures from 400 to 2500 nm as a function of leaf structural parameters and leaf biochemical components. Scattering is described by a specific refractive index ( $n$ ) and a parameter characterising the leaf mesophyll structure ( $N$ ). Absorption is modelled using pigment concentration ( $C_{ab}$ ), water content ( $C_w$ ), dry matter content ( $C_m$ ) and the corresponding specific spectral absorption coefficients ( $k_{ab}$ ,  $k_w$ , and  $k_m$ ). PROSPECT was adjusted to simulate properly spectral properties of the Norway spruce needles by means of the measured leaf hemispherical directional optical, biochemical and structural characteristics (Malenovský et al., 2006). PROSPECT outputs were directly used in the DART model to simulate the bidirectional reflectance factor (BRF) (Schaeppman et al., 2005) at the top of the canopy (TOC).

DART is a 3D radiative transfer model, based on the discrete ordinance method and an iterative approach. A simulated landscape scene is represented as a rectangular solid medium of adjacent cells forming a 3D matrix. Each cell of the matrix is identified with the x, y and z coordinates at the centre point. Cells can create different types of scene elements, classified as opaque or solid cells (e.g., soil or water) and semi-opaque or turbid cells (e.g., leaves of vegetation), which can vary in spatial dimensions. Each of them requires specific optical and structural characteristics, for instance leaf area index, leaf angle distribution, and optical reflectance/transmittance functions in case of vegetation foliage. The 3D radiation regime and the canopy BRF are realistically generated by considering topography, major physical mechanisms (e.g., hotspot effect), surface optical properties and four types of scattering. A detailed description of the DART algorithm and functions is available in Gascon et al. (2004), Gastellu-Etcheberry et al. (1996), and Gastellu-Etcheberry et al. (2004).

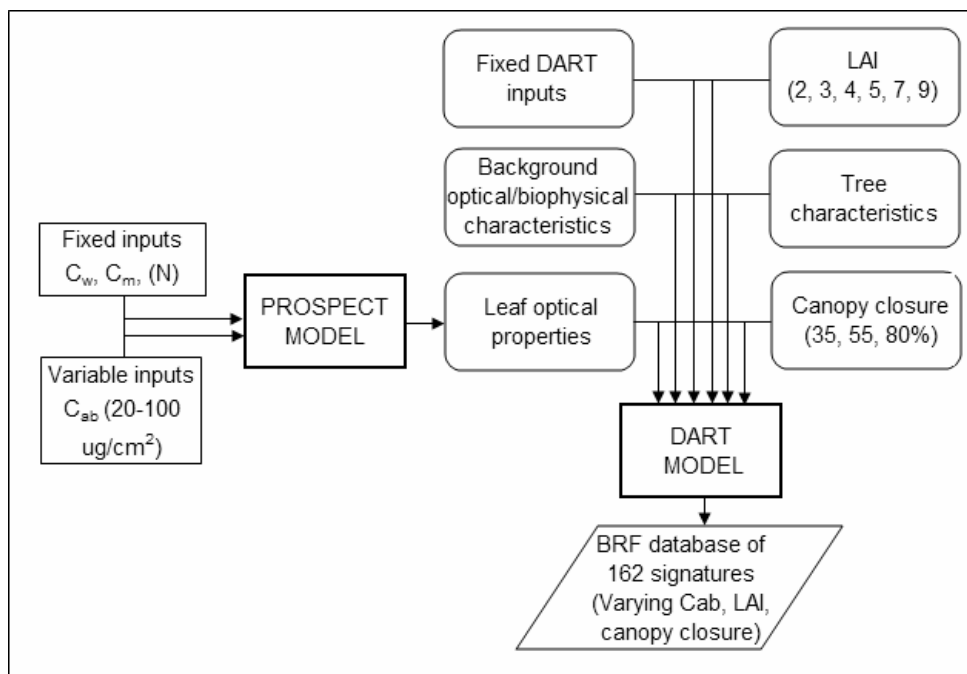


Figure 6.2. Flowchart illustrating the creation of the BRF database used to develop the ANMB<sub>650-725</sub> index, and to establish its statistical relationship with chlorophyll content.

### 6.2.3 Parameterization of the RT models and generation of the BRF database

The RT models were parameterized using the data acquired during September 2003 within the field survey of the Norway spruce forest stands situated near the village Modrava (48°59'N, 13°28'E), at the Sumava Mts. National Park (Czech Republic). The main information collected in the frame of this field campaign is shown in table 6.1. Heterogeneous representative 3D scenes of three canopy closures were generated out of averages and standard deviations of the tree field measurements. Clumping of the foliage within the branches was simulated as a combination of systematic and random propagation of the “gaps” (empty “air” cells) within the tree canopy. This calibration was based on the visual

observation of the crown defoliation and laboratory destruction of 16 representative branches. Ground surface was represented by a flat surface (digital elevation model was not included) covered by the most frequent mountain grass *Calamagrostis villosa*. Mean allometric characteristics of the examined representative trees used for the BRF database simulation are described in table 6.2. Leaf optical properties were generated in the adjusted PROSPECT model as weighted averages of spectral properties of the last three needle generations (age weights were calculated from the branch destruction). 78 needle samples from 13 selected trees were analyzed in this respect to obtain the following average input values:  $C_w = 0.06$  cm,  $C_m = 0.026$  g/cm<sup>2</sup>,  $N = 2.15$ .

Table 6.1. Basic inputs acquired for the radiative transfer simulation of the Norway spruce stands of Sumava Mts. in Czech Republic.

<i>Thematic class</i>	<i>Measured variables</i>	<i>Measuring methods and devices</i>
Bio-metric parameters of sampled trees	Tree positions, total trunk height, height of crown, horizontal crown projection, vertical crown profile, trunk diameters, length of live and dead crown, etc.	Digital forest mapping system FieldMap connected to the Impulse 200 Laser Rangefinder and the MapStar electronic compass.
Bio-physical parameters of crown	Leaf area index (LAI) per crown. Foliage density distribution – clumping of the leaves within crown.	Li-Cor plant canopy analyser (PCA) LAI-2000. Laboratory destruction of 16 sample branches.
Spectral properties	Hemispherical-directional optical properties of major forest stand surfaces (trunk bark, branch bark, understory, bare soil, rock, etc.)	Li-Cor spectroradiometer LI-1800-22 coupled with an integrating sphere LI-1800-12.

Table 6.2. Universal tree characteristics used for building the BRF database.

<i>Length of trunk [m]</i>		<i>Trunk diameter [m]</i>		<i>Length of crown [m]</i>	<i>Crown radius [m]</i>	
Outside of crown	Inside of crown	Outside of crown	Inside of crown		Lower part	Upper part
7.75	9.20	0.36	0.19	13.50	2.70	0.00

Finally, 162 DART simulations were performed to obtain the top of the canopy BRF database of the virtual Norway spruce stands through all possible combinations of the following varying inputs: LAI (2, 3, 4, 5, 7 and 9),  $C_{ab}$  content (20, 30, 40, 50, 60, 70, 80, 90, 100  $\mu\text{g}/\text{cm}^2$ ), and % of canopy closure (CC) (35, 55, and 80%). The solar illumination direction was defined by the azimuth angle of 181.2° and zenith angle of 42.2° (real solar noon on September 15<sup>th</sup>). Outputs were reproducing the hyperspectral images as potentially captured by the AISA airborne sensor (Specim Ltd., Finland) in the ‘spatial’ acquisition mode. This mode of the first AISA generation allowed very high spatial resolution of 0.9 m, compulsory for separation of the individual tree crowns, but only for a limited number of the equally spaced spectral bands. Thus 18 spectral bands meeting the AISA standards in full-width-half-maximum (FWHM) and spectral sampling interval were simulated (table 6.3). In the final step only spectral signatures of sunlit crown pixels of spectral bands from 648-726

nm were extracted to build the BRF database necessary for the chlorophyll ANMB<sub>650-725</sub> establishment. The BRF of sunlit crowns at 552 and 800 nm was additionally stored in the database for computing the chlorophyll predicting index TCARI/OSAVI (Haboudane et al., 2002), used in performance validation. The sunlit crown pixels were selected based on the reflectance thresholds of three channels (552, 671, and 800 nm). These thresholds were determined visually on limited number of crowns and then applied automatically within the remaining crowns. Unfortunately, this approach caused a slight misclassification at the border of both classes, resulting in inclusion of a few shaded pixels into the class of sunlit. Hence, this approach should be in future exchanged for an automatic segmentation algorithm with higher accuracy.

Table 6.3. Spectral description of simulated AISA bands.

<i>Band No.</i>	<i>Central λ [nm]</i>	<i>FWHM [nm]</i>	<i>Band No.</i>	<i>Central λ [nm]</i>	<i>FWHM [nm]</i>
1	452.6	7.3	10	671.3	7.6
2	474.5	7.3	11	700.2	7.6
3	496.4	7.3	12	726.0	7.6
4	524.0	7.3	13	748.8	7.6
5	551.7	7.3	14	780.7	7.6
6	576.5	7.3	15	800.4	7.6
7	601.2	7.3	16	844.5	7.6
8	624.6	7.3	17	861.2	7.6
9	648.5	7.6	18	870.3	7.6

#### 6.2.4 *ANMB650-725 validation and sensitivity analysis*

Three real forest research plots, selected within the mature Norway spruce stands at the Sumava Mts. National Park, were modelled in the DART model for validation of the ANMB<sub>650-725</sub>. DART landscape representatives were prepared using a FieldMap digital forest mapping system (IFER Ltd., Czech Republic) coupled with the Laser Rangefinder Impulse 200 and the MapStar electronic compass (Laser Technology Inc., USA) (for example of a forest input map see figure 6.3). Realistic scenes contained 13 sample trees, several neighbourhood adult and young trees, lying dead wood, and vegetation understory combined with litter of senescent spruce needles and bare soil. Hemispherical directional optical properties of needles and major scene surfaces were measured with the Li-Cor spectroradiometer LI-1800-22 connected to an integrating sphere LI-1800-12 (Li-Cor Inc., USA) (Li-Cor, 1983). Structural parameters of the forest stands were set in a similar way as for the BRF database scenes.

The total concentrations of the chlorophyll *a* and *b* ( $C_{ab}$ ) for 99 collected samples of current, two and three year old needles were determined spectrophotometrically in the laboratory. A Unicam Helios  $\alpha$  spectrophotometer (Unicam Ltd., UK) was used according to the methodology of Porra et al. (1989) and Wellburn (1994) for this purpose. The proper needle age-class ratio of chlorophyll concentrations was up-scaled by the adjusted PROSPECT-DART model into the TOC BRF AISA hyperspectral images of observed spruce stands (figure 6.4). ANMB<sub>650-725</sub> was derived from spectral signatures of sunlit crown pixels of 13 sample trees (see table 6.4). The equation of linear regression, established between

ANMB<sub>650-725</sub> and C<sub>ab</sub> concentration from the BRF database, was applied to estimate their C<sub>ab</sub> values. Finally, the root mean square error (RMSE) was computed between retrieved and true C<sub>ab</sub> concentrations to assess the accuracy of the ANMB<sub>650-725</sub> estimation.

Table 6.4. Biophysical and biochemical properties of 13 sample spruce crowns simulated in DART for the sensitivity analyses of ANMB<sub>650-725</sub>.

<i>ID of sample tree</i>	<i>% of crown defoliation</i>	<i>Leaf area index (LAI)</i>	<i>Chlorophyll content [<math>\mu\text{g}/\text{cm}^2</math>]</i>
24	35	9.18	81.79
25	45	8.87	68.99
11	45	7.24	43.41
21	45	6.59	93.55
16	45	6.32	74.15
29	50	7.26	55.13
22	50	4.85	81.74
10	55	5.82	63.16
5	60	4.37	60.40
15	60	3.94	47.96
8	60	3.73	27.56
6	60	1.16	58.94
17	65	3.43	77.90

The performance of the ANMB<sub>650-725</sub> optical index was also compared with C<sub>ab</sub> prediction abilities of the optical ratio TCARI/OSAVI. Haboudane et al. (2002) proposed the ratio of the Transformed Chlorophyll Absorption in Reflectance Index (TCARI) and the Optimized Soil-Adjusted Vegetation Index (OSAVI) (Rondeaux et al., 1996) as strongly sensitive to chlorophyll concentration and highly resistant to the variations of LAI (Leaf Area Index) and solar zenith angle at the canopy level. The TCARI is a transformed variant of the chlorophyll index MCARI (Modified Chlorophyll Absorption in Reflectance Index) (Daughtry et al., 1989), defined as follows:

$$\text{TCARI} = 3 \left[ (\rho_{700} - \rho_{670}) - 0.2(\rho_{700} - \rho_{550}) \left( \frac{\rho_{700}}{\rho_{670}} \right) \right] \quad (6.3)$$

The OSAVI index, belonging to the family of soil line vegetation indices (Steven, 1998), can be computed by the equation:

$$\text{OSAVI} = \frac{(1 + 0.16)(\rho_{800} - \rho_{670})}{(\rho_{800} + \rho_{670} + 0.16)}, \quad (6.4)$$

where  $\rho_j$  is the reflectance value at the  $j$ -th wavelength in nanometres;  $j \in (550, 670, 700, 800)$ .

Finally, a sensitivity analysis of the ANMB<sub>650-725</sub> C<sub>ab</sub> predictability on the presence of epiphytic lichens within the canopy (scenario #1) and added sensor noise (scenario #2) was performed. Scenario #1 was realised by changing the optical properties of the trees of interest in the DART model. Based on visual observation, 20% of the measured hemispherical optical properties of most common lichen at the Sumava spruce forests, *Pseudevernia* sp., were spectrally mixed with 80% of the original needle optical properties. Scenario #2 was

simulated by adding a certain level of noise to the simulated image of scenario #1. The noise simulated in this work tries to resemble only the noise caused by a detector. The fact that each hyperspectral system is recording an image by counting photons allows the assumption that this noise can be modeled with an independent, additive model: the noise  $n(i,j)$  has a zero-mean Gaussian distribution described by its standard deviation and/or variance. This means, that each pixel in the noisy image is the sum of the true pixel value and the random Gaussian distributed noise value ( $\sigma_n^2$ ). The intensity of sensor noise in an image is described by the signal to noise ratio (SNR), which is given by:

$$SNR = \sqrt{\frac{\sigma_f^2}{\sigma_n^2}} - 1 \quad (6.5)$$

where,  $\sigma_f^2$  is the variance of the real recorded image (in our case the image of scenario #1 plus noise) and  $\sigma_n^2$  is the variance of the zero-mean noise image (Fisher et al., 1994). The SNR value was set to five to simulate noise with a standard deviation  $\sigma_n \sim 20\%$  of the true image standard deviation  $\sigma_s$ . Then the  $\sigma_n$  was computed from:

$$\sigma_n = \frac{\sigma_s}{SNR} \quad (6.6)$$

The IDL function 'gen\_image\_doit' was used to generate an image with zero-mean noise of  $\sigma_n$  distributed by the Gaussian function per each spectral band. Then the appropriate noisy images were summed up with the image spectral bands of scenario #1.

### 6.3 Results

Figure 6.5a shows the exponential regression of the integrated area under continuum-removed reflectance curve between 650 and 725 nm ( $AUC_{650-725}$ ) on the canopy chlorophyll concentration computed out of the BRDF database. The  $AUC_{650-725}$  values saturate for a  $C_{ab}$  concentration above  $60 \mu\text{g}/\text{cm}^2$  which means  $AUC_{650-725}$  is not able to resolve a  $C_{ab}$  content higher than  $60 \mu\text{g}/\text{cm}^2$ . On the other hand, the maximal band depth of continuum-removed canopy reflectance between 650-725 nm ( $MBD_{650-725}$ ) is steeply growing with an increase of the  $C_{ab}$  concentration up to  $60 \mu\text{g}/\text{cm}^2$ , gains the maximal values at this  $C_{ab}$  concentration, and decreases for a  $C_{ab}$  content above  $60 \mu\text{g}/\text{cm}^2$  (figure 6.5b). Consequently, the proposed reciprocal ratio of these two optical parameters ( $ANMB_{650-725}$ ) exhibits a strong linear relationship with the total canopy chlorophyll concentration. The variability in  $ANMB_{650-725}$  due to varying LAI and canopy closure is rather low. One can see in figure 6.6a that the  $ANMB_{650-725}$  values for the specified  $C_{ab}$  concentration levels with a basic step of  $10 \mu\text{g}/\text{cm}^2$  did not overlap, except for three outliers. This suggests a low sensitivity of the  $ANMB_{650-725}$  index on the structural parameters of the simulated spruce canopy. The three outliers result from misclassification of the sunlit crown pixels. Some of the crown shaded pixels with higher portion of noise were included into the sunlit crown signature causing a non-systematic shift of the  $ANMB_{650-725}$  values.



The statistical relation of the  $C_{ab}$  content and  $ANMB_{650-725}$  obtained from the BRF database is highly significant ( $r^2 = 0.9798$ ) and comparable with the relationship between  $C_{ab}$  concentration and the ratio TCARI/OSAVI ( $r^2 = 0.9731$ ) (cf., figure 6.6ab). However, the final  $C_{ab}$  concentration for 13 sample trees estimated by means of both optical indices differs in accuracy. Plots of figure 6.7 and RMSE values computed between assessed and measured  $C_{ab}$  concentrations show considerably higher prediction accuracy for the  $ANMB_{650-725}$  (RMSE =  $9.53 \mu\text{g}/\text{cm}^2$ ) than for the TCARI/OSAVI index (RMSE =  $18.83 \mu\text{g}/\text{cm}^2$ ). Subsequently, the coefficient of determination for a linear regression, established between measured and estimated  $C_{ab}$ , is high for  $ANMB_{650-725}$  ( $r^2 = 0.7178$ ) and quite low for TCARI/OSAVI ( $r^2 = 0.1695$ ). These results suggest an appropriate and generally acceptable accuracy of the  $ANMB_{650-725}$  chlorophyll content prediction from sunlit forest canopy pixels of very high spatial resolution.

The introduction of 20% of an epiphytic lichen spectral signature into the canopy optical properties of the sample spruce trees did not result in a significant decrease of the  $ANMB_{650-725}$  estimation accuracy (RMSE =  $10.51 \mu\text{g}/\text{cm}^2$ ;  $r^2 = 0.6689$ ). As expected, simulated combined influence of the lichen occurrence within the crowns with the computer-generated sensor noise (SNR = 5) caused a decline in the  $ANMB_{650-725}$  prediction accuracy (RMSE =  $12.13 \mu\text{g}/\text{cm}^2$ ;  $r^2 = 0.5325$ ), but the accuracy was still higher than for the TCARI/OSAVI estimation without any disturbing effects. However, it has to be stressed that the  $ANMB_{650-725}$  index is computed as a BRF shape parameter through the wavelengths of the high  $C_{ab}$  absorption feature, which means within a quite low reflectance signal. Any noise significantly weakening the signal and disturbing the shape of the reflectance curve will cause a decrease of the chlorophyll prediction ability. Hence, sunlit crown pixels with a strong reflectance signal must be separated from noisy shadowed pixels and only these can be used for  $ANMB_{650-725}$  computation, otherwise index predictability is reduced (see outliers in figure 6.6a). Therefore, further testing and more sensitivity analyses, including other kinds of noise, more variations of spectral resolution and band sampling interval, and also lower spatial resolution, are required in order to show stability and full reliability of the  $ANMB_{650-725}$  hyperspectral index for  $C_{ab}$  concentration estimation.

## 6.4 Conclusions

A new optical index  $ANMB_{650-725}$  for estimating the canopy chlorophyll concentration from hyperspectral remote sensing data of a very high spatial resolution was proposed and causally explained. The  $ANMB_{650-725}$  is based on qualitative (shape) information of the vegetation reflectance curve rather than on the quantitative changes of reflectance intensity driven by the total chlorophyll content. First tests and a sensitivity analysis of the  $ANMB_{650-725}$  proved its robustness and acceptable prediction accuracy for heterogeneous spruce crowns contrary to the TCARI/OSAVI index, which was originally designed for agricultural crops. Computation of the index, using only four wavebands with the  $MBD_{650-725}$  always at channel of 671.3 nm due to the low spectral sampling interval, did not reduce the  $ANMB_{650-725}$  estimation capability. Even the introduction of two disturbing effects, occurrence of spruce epiphytic lichen *Pseudevernia* sp., and simulation of a low signal to noise ratio 5:1 within the hyperspectral image data did not change radically the index performance.

Nevertheless, further sensitivity analyses of this new chlorophyll optical index are recommended to be carried out on real hyperspectral imagery of higher spectral sampling interval. The results of estimation should be verified against real ground truth measurements of canopy chlorophyll concentrations.

Finally, the ANMB<sub>650-725</sub> index was developed and so far applied only on the Norway spruce stands. Therefore, it must also be tested and validated for the other plant species and functional plant types, especially broad-leaved species with different leaf interior and architecture of the canopy.

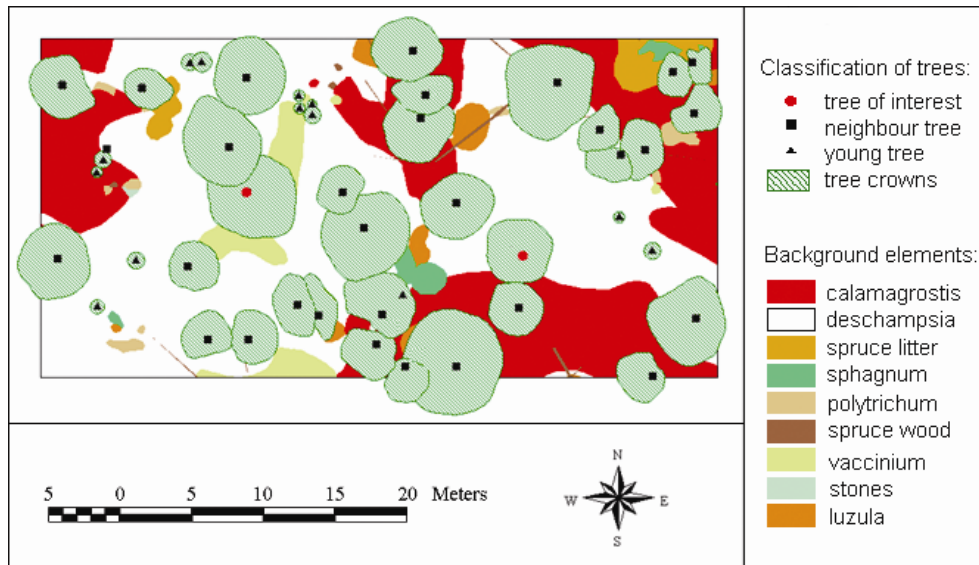


Figure 6.3. Map of one research plot at the Sumava Mts. National Park (Czech Republic) used in DART to generate hyperspectral images for accuracy assessment of the ANMB<sub>650-725</sub> index.

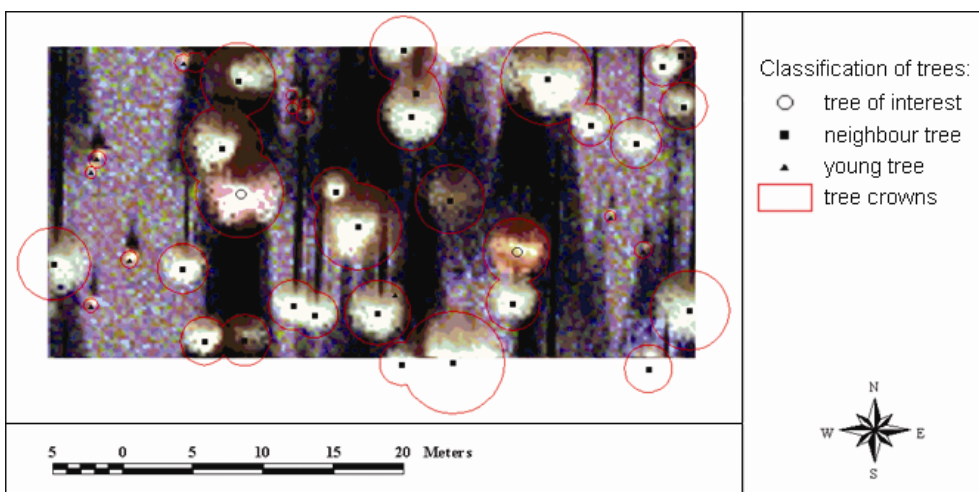


Figure 6.4. A false colour RGB composition of DART simulated nadir AISA bands (R = 800, G = 552 and B = 681 nm) for the research plot depicted in figure 6.3.

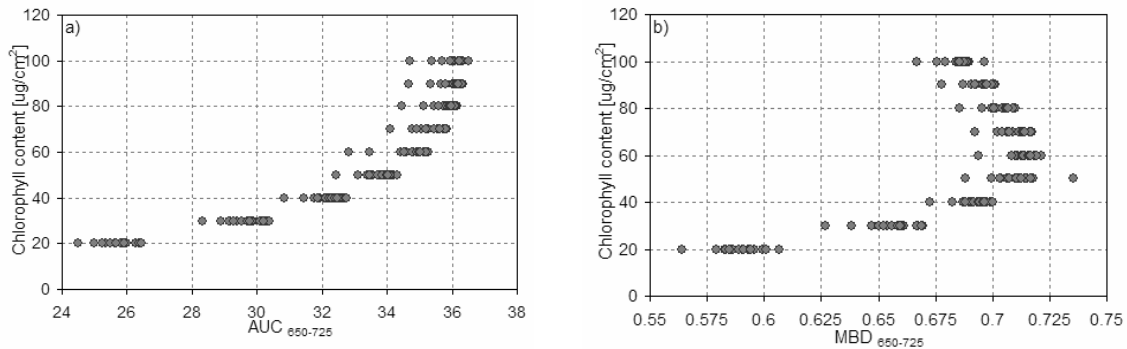


Figure 6.5. Relationship of the optical parameters and canopy chlorophyll concentration computed from the BRF database: a) Integrated area under continuum-removed reflectance between 650-725 nm (AUC<sub>650-725</sub>); b) Maximal band depth of continuum-removed reflectance between 650-725 nm (MBD<sub>650-725</sub>).

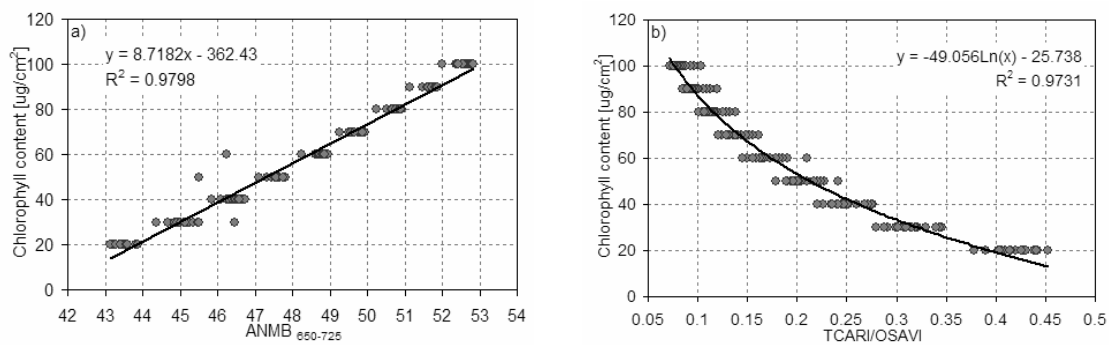


Figure 6.6. Statistical relationships between chlorophyll concentration and chlorophyll optical indices generated from the BRF database: a) Linear regression of canopy Cab concentration on the area under curve normalised to maximal band depth between 650-725 nm (ANMB<sub>650-725</sub>); b) Logarithmic statistical relationship of Cab concentration and the optical indices ratio TCARI/OSAVI.

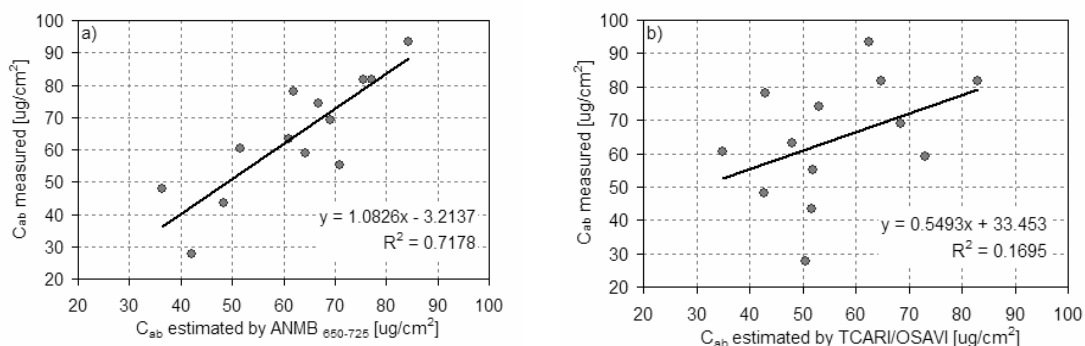


Figure 6.7. One-to-one relationship and linear regression of chlorophyll concentration measured for 13 sample spruce crowns and estimated by the optical index: a) ANMB<sub>650-725</sub>; b) TCARI/OSAVI.

## 6.5 Acknowledgements

---

Authors are grateful to Jean-Philippe Gastellu-Etchegorry and Emmanuel Martin from the CESBIO Laboratory (France) for the opportunity to use the DART model for this study. They are also thankful for the PROSPECT model source code provided by Stephane Jacquemoud (Universite Paris 7, France). Zbyněk Malenovský acknowledges financial support provided by the Czech Ministry of Education, Youth and Sports in frame of the Sabbatical fellowship 1K04. The study was carried out within the Research Plan of the Institute of Systems Biology and Ecology: AVOZ60870520.

## 6.6 References

---

- Broge, N. H., & Leblanc, E. (2001), Comparing prediction power and stability of broadband and hyperspectral vegetation indices for estimation of green leaf area index and canopy chlorophyll density. *Remote Sensing of Environment*, 76, 156-172.
- Curran, P. J. (1994), Attempts to drive ecosystem simulation models at local to regional scales. Chichester: Wiley & Sons 149-166.
- Curran, P. J., Dungan, J. L., & Peterson, D. L. (2001), Estimating the foliar biochemical concentration of leaves with reflectance spectrometry: Testing the Kokaly and Clark methodologies. *Remote Sensing of Environment*, 76, 349-359.
- Daughtry, C. S. T., Walthall, C. L., Kim, M. S., de Colstoun, E., & Brown McMurtrey III, J. E. (2000), Estimating corn leaf chlorophyll concentration from leaf and canopy reflectance. *Remote Sensing of Environment*, 74, 229-239.
- Fisher, B., Perkins, S., Walker, A., & Erik Wolfart, E. (1994), Hypermedia Image Processing Reference. 22.4.2005, Department of Artificial Intelligence, University of Edinburgh, UK.
- Gamon, J. A., Huemmrich, K. F., Peddle, D. R., Chen, J., Fuentes, D., Hall, F. G., Kimball, J. S., Goetz, S., Gu, J., & McDonald, K. C. (2004), Remote sensing in BOREAS: Lessons learned. *Remote Sensing of Environment*, 89, 139-162.
- Gascon, F., Gastellu-Etchegorry, J. P., Lefevre-Fonollosa, M. J., & Dufrene, E. (2004), Retrieval of forest biophysical variables by inverting a 3-D radiative transfer model and using high and very high resolution imagery. *International Journal of Remote Sensing*, 25, 5601-5616.
- Gastellu-Etchegorry, J. P., Demarez, V., Pinel, V., & Zagolski, F. (1996), Modeling radiative transfer in heterogeneous 3-D vegetation canopies. *Remote Sensing of Environment*, 58, 131-156.
- Gastellu-Etchegorry, J. P., Martin, E., & Gascon, F. (2004), DART: a 3D model for simulating satellite images and studying surface radiation budget. *International Journal of Remote Sensing*, 25, 73-96.
- Haboudane, D., Miller, J. R., Tremblay, N., Zarco-Tejada, P. J., & Dextraze, L. (2002), Integrated narrow-band vegetation indices for prediction of crop chlorophyll content for application to precision agriculture. *Remote Sensing of Environment*, 81, 416-426.
- Jacquemoud, S., & Baret, F. (1990), Prospect - a model of leaf optical properties spectra. *Remote Sensing of Environment*, 34, 75-91.
- Johnson, L. F., Hlavka, C. A., & Peterson, D. L. (1994), Multivariate analysis of AVIRIS data for canopy biochemical estimation along the oregon transect. *Remote Sensing of Environment*, 47, 216-230.
- Kokaly, R. F., & Clark, R. N. (1999), Spectroscopic determination of leaf biochemistry using band-depth analysis of absorption features and stepwise multiple linear regression. *Remote Sensing of Environment*, 67, 267-287.

- Kokaly, R. F., Despain, D. G., Clark, R. N., & Livo, K. E. (2003), Mapping vegetation in Yellowstone National Park using spectral feature analysis of AVIRIS data. *Remote Sensing of Environment*, 84, 437-456.
- le Maire, G., Francois, C., & Dufrene, E. (2004), Towards universal broad leaf chlorophyll indices using PROSPECT simulated database and hyperspectral reflectance measurements. *Remote Sensing of Environment*, 89, 1-28.
- Li-Cor (1983), 1800-12 Integrating sphere instruction manual. Publication number 8305-0034.
- Malenovský, Z., Albrechtová, J., Lhotáková, Z., Zurita-Milla, R., Clevers, J. G. P. W., Schaepman, M. E., & Cudlín, P. (2006), Applicability of the PROSPECT model for Norway spruce needles. *International Journal of Remote Sensing*, accepted.
- Malenovský, Z., Clevers, J. G. P. W., Arkimaa, H., Kuosmanen, V., Cudlín, P., & Polák, T. (2003), Spectral differences of the functional crown parts and status of Norway spruce trees studied using remote sensing. *Ekologia (Bratislava)*, 22, 207-210.
- Peddle, D. R., Johnson, R. L., Cihlar, J., & Latifovic, R. (2004), Large area forest classification and biophysical parameter estimation using the 5-Scale canopy reflectance model in Multiple-Forward-Mode. *Remote Sensing of Environment*, 89, 252-263.
- Porra, R. J., Thompson, W. A., & Kriedemann, P. E. (1989), Determination of accurate extinction coefficients and simultaneous equations for assaying chlorophylls a and b extracted with four different solvents: verification of the concentration of chlorophyll standards by atomic absorption spectroscopy. *Biochimica and Biophysica Acta*, 975, 384-394.
- Rondeaux, G., Steven, M., & Baret, F. (1996), Optimization of soil-adjusted vegetation indices. *Remote Sensing of Environment*, 55, 95-107.
- Schaepman-Strub, G., Schaepman, M., Dangel, S., Painter, T., & Martonchik, J. (2005), About the use of reflectance terminology in imaging spectroscopy. *EARSeL eProceedings*, 4, 191-202.
- Schmidt, K. S., & Skidmore, A. K. (2003), Spectral discrimination of vegetation types in a coastal wetland. *Remote Sensing of Environment*, 85, 92-108.
- Steven, M. D. (1998), The sensitivity of the OSAVI vegetation index to observational parameters. *Remote Sensing of Environment*, 63, 49-60.
- Underwood, E., Ustin, S., & DiPietro, D. (2003), Mapping nonnative plants using hyperspectral imagery. *Remote Sensing of Environment*, 86, 150-161.
- Wellburn, A. R. (1994), The spectral determination of chlorophyll a and chlorophyll b, as well as total carotenoids, using various solvents with spectrophotometers of different resolution. *Journal of Plant Physiology*, 144, 307-313.
- Zarco-Tejada, P. J., Miller, J. R., Morales, A., Berjon, A., & Agüera, J. (2004), Hyperspectral indices and model simulation for chlorophyll estimation in open-canopy tree crops. *Remote Sensing of Environment*, 90, 463-476.



---

## CHAPTER 7

### Synthesis

## 7.1 Conclusions on spectroscopy of Norway spruce canopies

To recall, this work emphasizes four initial research questions, defined as follows:

- I. How and to what extent can the RT model PROSPECT be used to simulate leaf optical properties of Norway spruce needles?
- II. What are the statistically significant differences in leaf optical properties of Norway spruce needles within and in-between crowns of two different environmental stress responses, with regard to their use in quantitative remote sensing methods?
- III. What is the influence of the presence of woody elements on the reflectance of a Norway spruce canopy simulated using the DART model?
- IV. On what basis can a robust, operational and reliable chlorophyll concentration retrieval approach be designed for a heterogeneous Norway spruce canopy at very high spatial resolution?

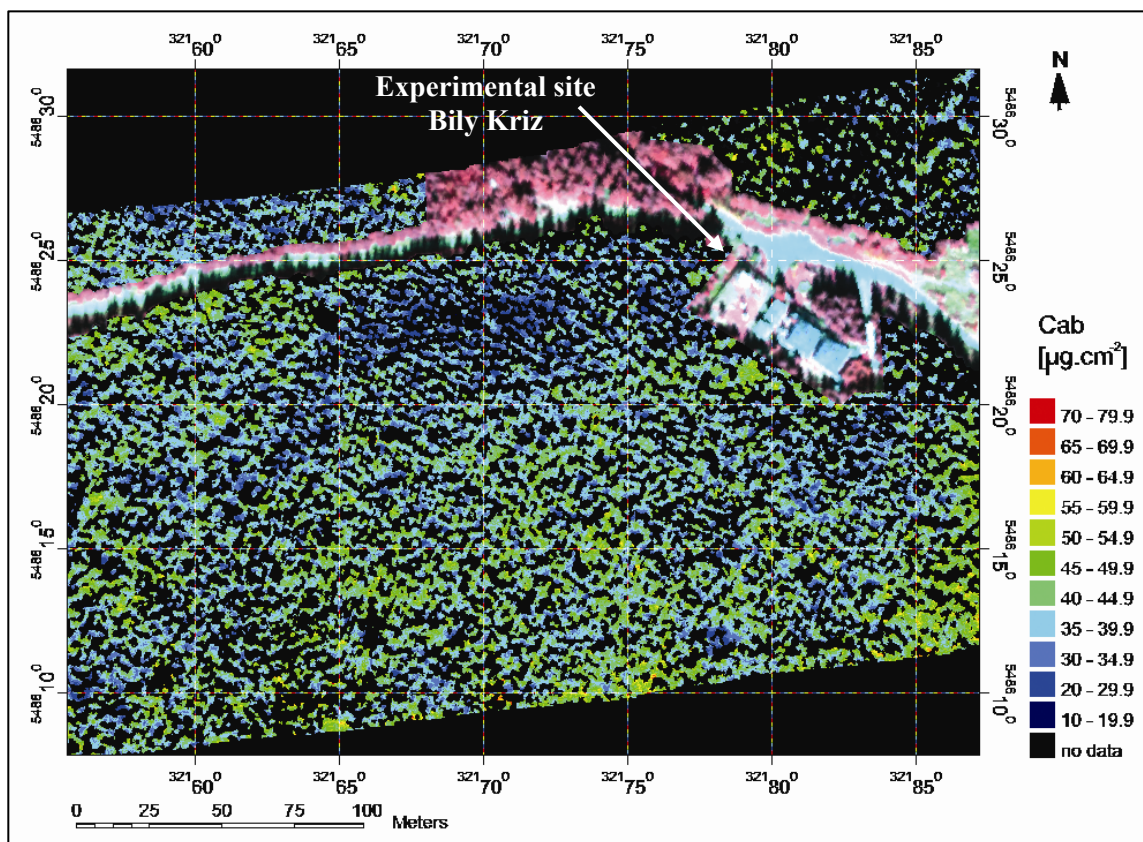


Figure 7.1. Chlorophyll concentration map of a sunlit Norway spruce canopy located around the experimental research site Bily Kriz at the Moravian-Silesian Beskydy Mts. (Czech Republic). The map was generated using four AISA spectral bands selected to compute the  $ANMB_{650-725}$  chlorophyll index (see text for details,  $C_{ab}$  represents the concentration of chlorophyll  $a+b$ ; the map projection is set to Universal Transverse Mercator, zone 34N).



Following the sequence of this work, the four research questions are dealt with as described in the next few paragraphs.

As shown in Chapter 3, the original version of the PROSPECT RT model was capable to simulate the Norway spruce leaf optical properties with the required accuracy only when the specific absorption coefficients were recalibrated. Because the absorption of the needles was changing with needle aging, the recalibration of the model resulted in being age-class specific. By doing so, three separate PROSPECT versions are proposed, one for each spruce needle generation. On one hand, this specialization of the PROSPECT model per age-class reduces its broad applicability, but on the other hand it significantly increases the accuracy of the modelled needle optical properties. This has turned out to be inevitable, since PROSPECT was originally not designed to model coniferous leaves. Consequently, the PROSPECT model is expected to be applicable also for leaves of other conifers. However, the recalibration and validation of the model before its use should be carried out for each coniferous species separately and, if necessary, also per individual age-class. Specialization of the PROSPECT model absorption coefficients is one way to increase its modelling accuracy. Another way is to increase the model's complexity by introducing new parameters and variables. For instance, the introduction of specific absorption coefficients and input concentrations for foliage pigments might be done separately (e.g., for chlorophyll, carotenoids, xanthophylls, etc.). By doing so, it will further increase the model precisions in the visible and red edge wavelength ranges and allows simultaneous inversion per defined pigment.

The only statistically significant differences in Norway spruce needle optical properties occurred in-between crowns of two different environmental stress responses (stress resistant vs. stress resilient). These spectral differences were related to the concentration of chlorophyll  $a+b$ , which was statistically lower for leaves of stress resilient crowns than for leaves of stress resistant crowns. No significant variability in leaf optical properties of sunlit needles was found within one spruce crown taking into account the last three needle age-classes. This implies that age-specific samples of sunlit needles, collected for spectrometric measurements, can be detached from any branch of the juvenile and production part of a Norway spruce crown. Nevertheless, as stated in Chapter 4, any sampling or sensing method applied, might deal with the fact that even within a Norway spruce forest canopy two neighbouring crowns of different environmental stress responses can occur, having statistically significant differences in their needle optical properties. This presence of different stress responses requires specially for imaging spectroscopy based approaches special attention, when collecting the ground information (e.g., leaf optical properties or concentrations of the biochemical constituents) targeting at the mapping of, for instance, foliar pigments. Wrongly collected calibration/validation field data will result in errors and discrepancies between the imaging spectroscopy estimates and ground truth measurements.

The sensitivity analysis, carried out as described in Chapter 5, showed an acceptable performance of the DART model for the simulation of Norway spruce top of canopy reflectance. The effect of robust woody elements (i.e., trunks and branches of first order) on simulated nadir canopy reflectance was negligible within all tested wavelengths (559, 671, 727, and 783 nm). The introduction of small woody twigs into the radiative transfer approach through a forest canopy increased the accuracy of the reflectance simulated at very high spatial resolution, especially within near infrared wavelengths of the sunlit canopy. These results point at the important role which tiny woody parts (or wooden parts of shoots) play when using physically based remote sensing approaches designed for a spruce forest stand. Again, in particular when employing radiative transfer models, the consideration of increased

level of detail remains an important issue. Additionally, the results of the sensitivity analysis showed a preference of using physically based methods of LAI retrieval over empirical methods based on optical indices. This need became obvious, in particular, when using imaging spectrometer data of very high spatial resolution.

Finally in Chapter 6, a hybrid method (i.e., a combined physical-statistical quantitative model) was proposed and tested for the estimation of total canopy chlorophyll concentration in sunlit Norway spruce crown pixels. The results were achieved with particularly high spatial resolution (40 cm pixel size), allowing a separation of the canopy into sunlit and shaded crown parts. The approach base lies on using the optical index  $ANMB_{650-725}$  (Area under curve Normalized to Maximal Band depth between 650-725 nm), generated using RT models and statistically related to the concentration of chlorophyll pigments. The index is computed as being the continuum removal of the canopy reflectance between wavelengths of strong chlorophyll absorption at 650-725 nm, and subsequently normalised by the maximal band depth of the removed continuum. The  $ANMB_{650-725}$  computation is minimizing the 'negative' influence of structural properties of the canopy (i.e., variability in crown structural heterogeneity, fractional cover, LAI, etc.) on the chlorophyll estimation. On the other hand, the  $ANMB_{650-725}$  index was proposed for hyperspectral images of very high spatial resolution, containing only a pure spectral response of the vegetation. The use of mixed pixels, containing a mixture of vegetative and non-vegetative parts, results in an erroneous (over- or under-estimated) estimation of chlorophyll concentration.

Even though the four research questions as indicated at the beginning of this paragraph were all treated in sufficient detail, research continues, in the respective chapters of this work, to derive spatially explicit maps of biochemical and biophysical properties of Norway spruce canopies.

## **7.2 Recent advances in the retrieval of biochemical and -physical properties in Norway spruce canopies**

---

An initial objective of this work was to prepare appropriate algorithms for the retrieval of biochemical and biophysical properties of Norway spruce canopies from airborne hyperspectral data at very high spatial resolution. In this chapter, the progress of the previously described work is continued and illustrated in certain detail.

Two particular quantitative characteristics of interest, namely chlorophyll concentration ( $C_{ab}$ ) and leaf area index (LAI) were retrieved on the same Norway spruce canopy as acquired by an AISA imaging spectrometer over the Bily Kriz experimental test site (Czech Republic). For these retrievals, combination of the PROSPECT and DART models was inverted. Although the preliminary results are very promising, the inversion routines still need to be improved and optimized. Nevertheless, the ultimate goal of this activity is a more frequent temporal mapping of these quantitative properties for the status assessment of mountain and/or boreal Norway spruce ecosystems from space-borne image data.

### ***7.2.1 Mapping the chlorophyll concentration of spruce crowns***

Retrieval of the chlorophyll concentration using the  $ANMB_{650-725}$  optical index (Malenovský et al., 2006) was recently performed using a subset of an AISA image acquired over the Bily Kriz experimental site (18.54°E, 49.50°N) on September 18<sup>th</sup>, 2004

(Malenovský et al., 2006). The images were geocoded and orthorectified as well as atmospherically corrected to represent top of canopy bidirectional reflectance factor (BRF). The montane spruce forest stands were selected around the experimental site, and their sunlit crown pixels were classified using an automated classification approach. The Norway spruce canopy adjusted DART model in combination with the PROSPECT model were used to simulate 432 BRF spectral images as being combinations of two distributions of trees (regular and clumped), three canopy closures (CC = 75, 85, and 95%) occurring the most frequently at the test site, six leaf area indices (LAI = 4, 5, 6, 7, 8, and 9) representing minimal to maximal field measured LAI, and six chlorophyll concentrations ( $C_{ab} = 10, 25, 40, 55, 70,$  and  $85 \mu\text{g}\cdot\text{cm}^{-2}$ ) again derived from representative field measurements of  $C_{ab}$  for the test site. The  $\text{ANMB}_{650-725}$  index was computed using four and then nine DART simulated bands with central wavelengths as closely located to the AISA bands (652.08, 661.41, 670.74, 680.06, 689.39, 698.72, 708.07, 717.41, and 726.76 nm with a Full-Width-Half-Maximum ranging from 9.33-9.35 nm). The statistical relationship between chlorophyll concentration and the  $\text{ANMB}_{650-725}$  was established and applied only to sunlit spruce crown parts of the AISA image (cf., figure 7.1).

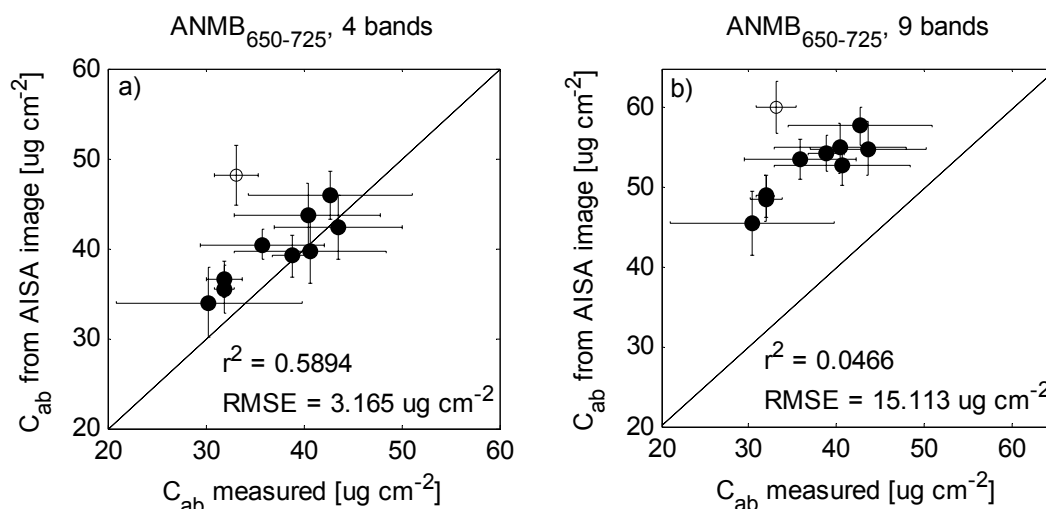


Figure 7.2. Accuracy assessment of the chlorophyll  $a+b$  concentrations ( $C_{ab}$ ) measured in the laboratory and estimated from the AISA image for ten spruce crowns using the  $\text{ANMB}_{650-725}$  computed from: a) four spectral bands, and b) nine spectral bands. Each circle represents a tree crown, full circles are crowns used for validation, and the empty circle is an outlier which was excluded from the validation process (horizontal bars represent two standard deviations in  $C_{ab}$  measured within the vertical crown levels; vertical bars represent two standard deviations of  $C_{ab}$  estimation within sunlit AISA pixels;  $r^2$  is coefficient of determination for a linear regression  $y = a x$ ; RMSE represents the root means square error computed between measured and estimated  $C_{ab}$ ).

The accuracy assessment of the  $\text{ANMB}_{650-725}$  based chlorophyll estimation was carried out for ten selected spruce trees. Their crowns were systematically (destructively) sampled by measuring three needle age-classes from two vertical crown levels. They were analyzed for  $C_{ab}$  content in the laboratory after clipping. The errors were generally acceptable except for one tree that happens to grow next to an iron meteorological tower (see outliers in figure

7.2ab). The reflectance of this crown was a mixture of foliage and iron signal that resulted in an overestimation of the  $C_{ab}$  concentration from the AISA image. Surprisingly, the validation revealed that the ANMB<sub>650-725</sub> based chlorophyll estimation using only four spectral bands (652.08, 670.74, 708.07, and 726.76 nm) was more accurate than the  $C_{ab}$  estimation using nine spectral bands located between 650-725 nm (cf., figure 7.2ab).

There are several potential explanations for this discrepancy (e.g., inaccurate ground truth and/or DART simulations, hidden sensitivity of the ANMB<sub>650-725</sub> to an unknown forest stand constituent, etc.) that will need closer investigation. Also the applicability of the ANMB<sub>650-725</sub> for other biologic plant species or functional plant types will be tested for its broader use in future. Finally, the whole retrieval procedure needs to be automated and optimized to make it more user-friendly and eventually converge to a (semi-) operational system.

### 7.2.2 Spatial estimation of forest stand leaf area index

A routine for inverting a DART simulated image for spatial estimation of Norway spruce canopy LAI from airborne AISA images has been developed already in 2005 (Malenovský et al., 2006). This retrieval method is purely physical-based, using a minimization merit function or an artificial neural network to invert the extensive database of DART simulated BRDF spectral bands for LAI of a spruce canopy within a moving image window of 6x6 meters.

Exploration of the DART simulated reflectance signatures revealed that the shaded crown parts have a stronger relationship to varying LAI than the sunlit crown pixels. The near infrared signal of the sunlit crowns saturated already at LAI = 5, while the reflectance signal of the shaded crown pixel was almost linearly decreasing with increasing LAI (Malenovský et al., 2006). Therefore, a proposed inversion algorithm was based on a spectral ratio of the shaded crown pixels divided by the sunlit ones within a defined moving window. The first results of spatial LAI mapping for the experimental site Bily Kriz matched the range of the ground measured LAI, but the spatial pattern of the retrieved LAI values was not fully correct. Consecutive sensitivity analyses discovered insufficiencies concerning the distribution and the deepness of the canopy shadows simulated with DART. Since the NIR reflectance of the shadowed crown pixels is used in this retrieval approach as being a primary key to forest stand LAI estimates, the shape of the spruce crowns and their spatial distribution in 3D space were identified as being the crucial parameter for a correct simulation of shadows within a forest stand.

Concluding from the above mentioned results, our following steps will focus on an appropriate representation of the digital elevation model (DEM) used in the DART virtual landscapes and the adjustments concerning variability in spruce crown shapes, dimensions, and positions. Improved parameterization of these features will allow the generation of a more reliable database of DART modelled images, supporting the production of acceptable accurate LAI patterns.

### 7.2.3 Scaling up to coarser spatial resolution of satellite data

The currently operated and future proposed hyperspectral and/or superspectral sensors onboard satellite platforms will play an increasing role in monitoring the terrestrial ecosystems at regional scale. The lessons learned during this work about refinement of the representation of Norway spruce leaf optical properties in models and enhancing the inversion routines used for airborne imaging spectrometer data represent essential knowledge for up-scaling spectral information from local to regional scale of forest canopies.

This knowledge base may serve as an important foundation for designing new algorithms retrieving quantitative parameters of Norway spruce ecosystems derived from spaceborne imaging spectrometer data with coarser spatial resolution. The use of this approach will be demonstrated in a continuation of this work, which has been accepted for funding by ESA (ESA-PECS, 2004). When listing recent satellite missions, the spectro-directional instrument CHRIS (Compact High Resolution Imaging Spectrometer) operating on the satellite platform PROBA (PROject for On-Board Autonomy) (Barnsley et al., 2004) is one of the most suitable systems for up-scaling the findings of this study. Considering future missions, the GMES (Global Monitoring for Environment and Security) superspectral land imaging system Sentinel-2 (Rast, 2004), expected to be launched by the European Space Agency (ESA) in 2008, will also be able to use the presented findings. In addition to these, two future satellite missions represent a further opportunity to implement the findings from this work. The first system is represented by joint Israeli-French micro-satellite named Venus (Vegetation and Environment monitoring on a New Micro Satellite) (CNES, 2006), with a planned launch in June 2009. The second one is a new satellite borne imaging spectrometer having LANDSAT type spatial resolution called EnMAP (Kayser-Threde, 2006), which is being proposed by the GFZ (Germany's National Research Centre for Geosciences) with support from the DLR (German Aerospace Centre (Deutsches Zentrum für Luft- und Raumfahrt)) with a launch date planned in 2010-2011.

Outcomes of this work have demonstrated the preparedness and availability of methods for spatially distributed retrieval of biophysical and biochemical variables at unprecedented accuracy in a timely fashion for the release of the next generation of imaging spectrometers.

### 7.3 General synopsis and outlook

---

The scientific contribution of this work can be categorized in several domains of fundamental and applied research. These are in particular the measurements and modelling of Norway spruce leaf optical properties, the validation of the use of the complex radiative transfer model DART for spruce canopies, the use of imaging spectroscopy in coniferous crowns at very high spatial resolution, the mapping of forest stress bio-indicators, and finally outlook onto the up-scaling of spectral information from high spatial resolution to a lower spatial resolution.

The here proposed protocol for the measurement of leaf optical properties of conifers, having the typical non-round shaped needle leaves, remains not to all extends accurate. Improvements to the presented method or even a completely new and more accurate approach may still be needed (e.g., designing an improved type of needle carrier (Harron & Miller, 1995b)). However, whatever approach will be designed, the fundamental issue to overcome the tiny size and the narrow shape of coniferous needles will always remain. It is therefore recommended, to focus on measurements of shoot level optical properties (i.e., shoot spectral phase functions) rather than on separate needles. Correspondingly, focus of the modelling of coniferous optical properties should also be shifted towards the shoot level. For example Smolander & Stenberg (2003; 2005) are stressing the importance of shoot geometry investigations for multiple scattering and absorption of the photons.

Concerning the modelling of radiative transfer through a complex coniferous canopy, this work pointed out on the role of tiny woody twigs within Norway spruce crowns. The presence

of woody elements was currently implemented in the DART model, but its physical description and mathematical implementation can be further improved and developed in a more reliable way. Consequently, this development should also integrate a shoot as being a unique modelling element of a coniferous canopy rather than as being a conjugation of two separate turbid mediums (i.e., a 'green' leaf medium combined with a 'brown' turbid medium of twigs). Nevertheless, DART is currently the only radiative transfer model allowing the modelling of not only robust, but also of fine woody elements. This DART feature is offering unique opportunities for modelling a forest canopy with a sparse leaf distribution and low leaf area due to the advancing pheno-phases or influence of the environmental stressors.

Data acquired with very high spatial resolution allowed for separate exploring the role of the sunlit and shaded Norway spruce crown parts for the retrieval of biochemical and structural canopy properties. We have learned that the sunlit crown pixels with a strong reflectance signal are very useful for accurate estimation of the total chlorophyll concentration, but they are less useful for retrieval of the total (not only green) canopy leaf area index. For the latter, the pixels of shaded crowns were carrying the main information facilitating prediction of the canopy LAI from nadir spectroscopic image data.

This work also demonstrated the potential of imaging spectroscopy and quantitative remote sensing for spatial environmental stress assessment of Norway spruce crowns. We have proved that needles of stress resilient crowns have significantly different optical properties from needles of stress resistant crowns, due to a systematically lower concentration of chlorophyll *a+b*. Accurate chlorophyll estimation, retrieved from hyperspectral image data per spruce crown, can serve as indicator of current crown status to forest managers. Moreover, the combination of several quantitative bio-indicators (e.g.,  $C_{ab}$ , LAI, foliage clumping, leaf angle distribution, etc.) could create a systematic tool for complex evaluation of the overall forest stand condition at very high spatial resolution.

Finally, the findings and methods of this work have a potential to produce information useful for parameterization or validation of physiological models of vegetation processes at local scale (e.g., big-leaf models for photosynthesis, stomatal conductance, etc. (Dai et al., 2004)). Additionally, in combination with an up-scaling method they could be employed by dynamic vegetation models running at higher (regional or global) scales (e.g., the Lund-Potsdam-Jena dynamic vegetation model (Sitch et al., 2003)), or could become a part of a forest ecosystem monitoring system using Earth observing satellite image data as input (e.g., Global Monitoring for Environment and Security (GENACS, 2005)).

This activity will facilitate a regular temporal monitoring of the ecosystems, validating status (rate and quality) of their services. The natural and anthropogenic precipitous changes in ecosystems services play, according to the Millennium Ecosystem Assessment findings (Millennium, 2005b), one of the key roles in evolution and stability of the whole biosphere, creating the basic environmental conditions for the Earth living planet including the human society.

## 7.4 References

---

- Barnsley, M. J., Settle, J. J., Cutter, M. A., Lobb, D. R., & Teston, F. (2004), The PROBA/CHRIS mission: A low-cost smallsat for hyperspectral multiangle observations of the earth surface and atmosphere. *Ieee Transactions on Geoscience and Remote Sensing*, 42, 1512-1520.

- CNES (2006), VENUS - Vegetation and Environment monitoring on a New Micro-Satellite. <http://smc.cnes.fr/VENUS/>, June 27th, 2006.
- Dai, Y. J., Dickinson, R. E., & Wang, Y. P. (2004), A two-big-leaf model for canopy temperature, photosynthesis, and stomatal conductance. *Journal of Climate*, 17, 2281-2299.
- ESA-PECS (2004), ESA Science and Technology - PRODEX. <http://www.sci.esa.int/science-e/www/object/index.cfm?fobjectid=35683>, July 10th, 2006.
- GENACS Consortium (2005), GMES - Global Monitoring for Environment and Security. <http://www.gmes.info>, June 29th, 2006.
- Harron, J. W., & Miller, J. R. (1995), An alternative methodology for reflectance and transmittance measurements of conifer needles. *17th Canadian Symposium on Remote Sensing*, 1995, Saskatchewan: Saskatoon, 654-661.
- Kayser-Threde GmbH (2006), EnMAP - Environmental Mapping and Analysis Program. <http://www.enmap.de>, July 10th, 2006.
- Malenovský, Z., Homolová, L., Martin, E., Gastellu-Etchegorry, J. P., Pokorný, R., Kaplan, V., Zurita-Milla, R., & Schaepman, M. E. (2006a), Mapping the chlorophyll concentration of Norway spruce canopy using high spatial resolution imaging spectroscopy. *Remote Sensing of Environment*, in preparation.
- Malenovský, Z., Martin, E., Homolová, L., Gastellu-Etchegorry, J. P., Zurita-Milla, R., Schaepman, M. E., Pokorný, R., Clevers, J. G. P. W., & Cudlin, P. (2006b), Influence of woody elements of a Norway spruce canopy on nadir reflectance simulated by the DART model at very high spatial resolution. *Remote Sensing of Environment*, accepted.
- Malenovský, Z., Martin, E., Homolová, L., Pokorný, R., Schaepman, M. E., Gastellu-Etchegorry, J. P., Zurita-Milla, R., Clevers, J. G. P. W., & Cudlin, P. (2005), Influence of forest canopy structure simulated using the Discrete Anisotropic Radiative Transfer (DART) model on the retrieval of spruce stand LAI. In S. Liang, J. Liu, X. Li, R. Liu, & M. E. Schaepman (Ed.), *The 9th International Symposium on Physical Measurements and Signatures in Remote Sensing* (pp. 846-848). Beijing, China: ISPRS XXXVI(7/W20).
- Malenovský, Z., Ufer, C. M., Lhotáková, Z., Clevers, J. G. P. W., Schaepman, M. E., Albrechtová, J., & Cudlin, P. (2006c), A new hyperspectral index for chlorophyll estimation of a forest canopy: Area under curve Normalized to Maximal Band depth between 650-725 nm *EARSel eProceedings*, 161-172.
- Millennium Ecosystem Assessment (2005), Living beyond our means - Natural assets and human well-being. <http://www.millenniumassessment.org>, June 9th, 2006.
- Rast, M. and GMES Sentinel-2 Mission Team (2004), *GMES Sentinel-2 Mission Requirements Document*. ESA, pp. 32.
- Sitch, S., Smith, B., Prentice, I. C., Arneth, A., Bondeau, A., Cramer, W., Kaplan, J. O., Levis, S., Lucht, W., Sykes, M. T., Thonicke, K., & Venevsky, S. (2003), Evaluation of ecosystem dynamics, plant geography and terrestrial carbon cycling in the LPJ dynamic global vegetation model. *Global Change Biology*, 9, 161-185.
- Smolander, S., & Stenberg, P. (2003), A method to account for shoot scale clumping in coniferous canopy reflectance models. *Remote Sensing of Environment*, 88, 363-373.
- Smolander, S., & Stenberg, P. (2005), Simple parameterizations of the radiation budget of uniform broadleaved and coniferous canopies. *Remote Sensing of Environment*, 94, 355-363.

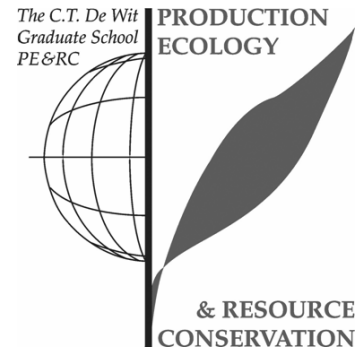




## PE&RC PhD Education Statement Form

---

With the educational activities listed below the PhD candidate has complied with the educational requirements set by the C.T. de Wit Graduate School for Production Ecology and Resource Conservation (PE&RC) which comprises of a minimum total of 22 credits (= 32 ECTS = 22 weeks of activities)



### **Review of Literature (3 credits)**

- Mendel University of Agriculture and Forestry Brno (1999-2000)
- Wageningen University (2001-2002)

### **Writing of Project Proposal (5 credits)**

- Remote sensing of multiple stress response of Norway spruce forests (2001-2002)

### **Post-Graduate Courses (2 credits)**

- Remote Sensing: Focus on Forest Ecosystems (2000)

### **Deficiency, Refresh, Brush-up and General Courses (1 credit)**

- ENVI & IDL programming (2006)

### **PhD Discussion Groups (5 credits)**

- Forest and conservation ecology (2002-2006)
- Statistics, mathematics and modelling (2004-2006)

### **PE&RC Annual Meetings, Seminars and Introduction Days (1 credit)**

- PE&RC workshop – ‘Plant spectrophotometry: applications and basic research’ (2002)
- PE&RC seminar – ‘Computational modelling for plant biology’ (2006)
- 

### **International Symposia, Workshops and Conferences (4 credits)**

- Second SPECTRA workshop, Noordwijk (2003)
- The 4<sup>th</sup> Workshop on Imaging Spectroscopy, Warsaw (2005)
- The 9<sup>th</sup> ISPMRS, Beijing (2005)
- ISPRS Mid-term Symposium 2006, Enschede (2006)
- 

### **Laboratory Training and Working Visits (3 credits)**

- Radiative transfer in forest canopy, CESBIO (Toulouse, France) (2003)
- Operating AISA Eagle VNIR airborne sensor, SPECIM (Finland) (2004)

## Curriculum Vitae

---

Name Malenovský  
First name Zbyněk  
Date of birth February 6<sup>th</sup>, 1975  
Place of birth Hodonín, Czechoslovakia (Czech Republic nowadays)  
Nationality Czech  
Address Velkomoravská 10, 695 01 Hodonín (Czech Republic)

### Education and training

1989-1993 Gymnasium Hodonín (Czech Republic)  
May 12<sup>th</sup>, 1993 – final examination  
1993-1994 Masaryk University Brno (Czech Republic), Faculty of Natural Sciences (subject: Nature and environmental protection)  
1994-1998 Palacky University Olomouc (Czech Republic), Faculty of Natural Sciences (subject: Nature and environmental protection)  
September 26<sup>th</sup>, 1996 – Bachelor diploma in Environmental protection  
September 9<sup>th</sup>, 1998 – Master diploma in Environmental protection  
1998-2000 Mendel University of Agriculture and Forestry Brno (Czech Republic), PhD study (discontinued)  
2000-2001 Wageningen University (The Netherlands), NUFFIC scholarship (Huygens Programme)  
2001-2002 Wageningen University (The Netherlands), MSc. thesis ‘Investigation of functional parts and status of Norway spruce crowns using spectral remote sensing information’  
2002-2006 Wageningen University (The Netherlands), PhD thesis ‘Quantitative remote sensing of Norway spruce (*Picea abies* (L.) Karst.): Spectroscopy from needles to crowns to canopies’

### Professional experience

1999 Ecole supérieure d'agriculture de Purpan (Toulouse, France), visiting scholar  
2004 Centre d'Etudes Spatiales de la Biosphère (UPS-CNES-CNRS-IRD, Toulouse, France), visiting scholar  
2001-2006 Institute of Systems Biology and Ecology (Academy of Sciences of the Czech Republic), research assistant

## List of publications

---

### Peer reviewed journals

- Malenovský Z.**, 2001. Possibilities of using satellite data for mapping the vegetation formation types in the forested area of Mediterranean region; *Journal of Forest Science*, 47, 114-123.
- Malenovský Z.**, Clevers J.G.P.W., Arkimaa H, Kuosmanen V., Cudlín P., Polák T., 2003. Spectral differences of the functional crown parts and status of Norway spruce trees studied using remote sensing. *Ekologia (Bratislava)*, 22, Supplement 1/2003: 207-210.
- Lhotáková Z. , Albrechtová J., **Malenovský Z.**, Rock B.N. Polák T., Cudlín P., 2006. Does the orientation of Norway spruce (*Picea abies* /L./ Karst.) branches within sunlit crown part influence the heterogeneity of biochemical, structural and spectral characteristics of needles? *Environmental and Experimental Botany*, accepted\*\*.
- Malenovský Z.**, Albrechtová J., Lhotáková Z., Zurita-Milla R., Clevers J.G.P.W., Schaepman M.E., Cudlín P., 2006. Applicability of the PROSPECT model for Norway spruce needles. *International Journal of Remote Sensing*, in press††.
- Malenovský Z.**, Bartholomeus H.M., Acerbi-Junior F.W., Schopfer J.T., Painter T. H., Epema G.F., Bregt A.K., 2005. Scaling dimensions in spectroscopy of soil and vegetation. *International Journal of Applied Earth Observation and Geoinformation*, accepted.
- Malenovský Z.**, Homolová L., Martin E., Gastellu-Etchegorry J. P., Pokorný R., Kaplan V., Zurita-Milla R., Schaepman, M. E., Clevers J.G.P.W., 2006. Mapping the chlorophyll concentration of Norway spruce canopy using high spatial resolution imaging spectroscopy. *Remote Sensing of Environment*, in preparation‡‡.
- Malenovský Z.**, Lhotáková Z., Albrechtová J., Clevers J. G. P. W., Schaepman M. E., Cudlín P. (2006c), Differences in leaf optical properties of environmentally stressed Norway spruce (*Picea abies* (L.) Karst.) crowns. *Trees – Structure and Function*, in preparation.
- Malenovský Z.**, Martin E., Homolová L., Gastellu-Etchegorry J.-P., Zurita-Milla R., Schaepman M.E., Pokorný R., Clevers J.G.P.W., Cudlín P., 2006. Influence of woody elements of a Norway spruce canopy on nadir reflectance simulated by the DART model at very high spatial resolution. *Remote Sensing of Environment*, accepted.
- Malenovský Z.**, Ufer C.M., Lhotáková Z., Clevers J.G.P.W., Schaepman M.E., Albrechtová J., Cudlín P., 2006. Area under curve Normalized to Maximal Band depth between 650-725 nm: A new hyperspectral index for chlorophyll estimation of a forest canopy. *EARSel eProceedings*, 5(2), 161-172.

---

\*\* Accepted – papers accepted for publication.

†† In press – papers awaiting printing.

‡‡ In preparation – papers in preparation for submission to a journal.

## Conference and workshop contributions

- Malenovský Z.**, Clevers J.G.P.W., Arkimaa H., Kuosmanen V., Cudlín P., Polák T.: Spectral differences of the functional crown parts and status of Norway spruce trees studied using remote sensing information, 20th Int. Meeting IUFRO, Long term air pollution effect on forest ecosystems, Zvolen, Slovakia, 30.8.-1.9.2002.
- Malenovský Z.**, Martin E., Gastellu-Etchegorry J.P., Cudlín P., Clevers J.G.P.W.: Heterogeneity description improvements of spruce crown architecture simulated using the 3-D radiative transfer model DART, CD-ROM of Proceedings of Second SPECTRA Workshop, ESTEC, Noordwijk, The Netherlands, 28.-30.11.2003, ISSN 1022-6656.
- Cudlín P., **Malenovský Z.**, Krám P., Jonášová M., Havlíček F.: Influence of geological substrate on Norway spruce health status in western Bohemia. International Conference Acid Rain 2005, Prague, Czech Republic, 12.6.-17.6.2005.
- Homolová L., **Malenovský Z.**, Martin E., Pokorný R., Gastellu-Etchegorry J.-P., Schaepman M.E., Cudlín P.: Parameterization of high resolution radiative transfer for Norway spruce forest stand ensuring quality of retrievable biophysical variables. Workshop Ensuring the quality and reliability of land and atmosphere Essential Climate Variables: The EU-25 contribution, Krakow, Poland, 15.12.-16.12. 2005.
- Kooistra L., Clevers J.G.P.W, Schaepman M.E., van Dobben H., Wamelink G.W.W., Sykora K., Holtland J., Batelaan O., Bertels L., Debruyn W., Bogaert J., Schmidt A., Clement J., Bloemmen M., Mucher C.A., van den Hoof C., De Bruin S., Stuiver J., Zurita Milla R., **Malenovský Z.**, Wenting P., Mengesha T., van Oort P.A.J., Liras Laita E., Wamelink G.W.W., Schaepman-Strub G., Hung L.Q. Verbeiren B., Sterckx S.: Linking Biochemical and Biophysical Variables Derived from Imaging Spectrometers to Ecological Models - The HyEco'04 Group Shoot. In Zagajewski B., Sobczak M., (Eds.), Imaging Spectroscopy – New Quality in Environmental Studies. The 4th Workshop on Imaging Spectroscopy, Warsaw University and European Association of Remote Sensing Laboratories (EARSel), Warsaw, Poland, 27.3.-29.3.2005, ISBN 83-89502-41-0.
- Krám P., **Malenovský Z.**, Cudlín P., Shanley J.B.: Contrasting resistance to acidification due to bedrock geochemistry – effects on streamwater chemistry and Norway spruce health status at 21 Czech catchments Int. Conference Acid Rain 2005, Prague, Czech Republic, 12.6.-17.6.2005.
- Malenovský Z.**, Martin E., Gastellu-Etchegorry J.P., Homolová L., Cudlín P., Schaepman M.E., Clevers J.G.P.W: Structure of woody species in radiative transfer. Centre for Geo-Information, First Point Israeli-Dutch Workshop on Spatial, Temporal, and Spectral Scales in Agro-Ecosystems, Wageningen, The Netherlands. 14.9.-15.9.2005.
- Malenovský Z.**, Martin E., Homolová L., Pokorný R., Schaepman M.E., Gastellu-Etchegorry J.-P., Zurita Milla R., Clevers J.G.P.W., Cudlín P.: Influence of forest canopy structure simulated using the Discrete Anisotropic Radiative Transfer (DART) model on the retrieval of spruce stand LAI. In Liang, S., Liu, J., Li, X., Liu, R., Schaepman, M., (Eds.), The 9th International Symposium on Physical Measurements and Signatures in Remote Sensing. Beijing, China, 17.10.-19.10.2005, ISPRS XXXVI(7/W20), ISSN 1682-1750.

---

**Malenovský Z.**, Ufer C., Lhotáková Z., Clevers J.G.P.W., Schaepman M.E., Cudlín P., Albrechtová J.: ANMB650-725 – A new hyperspectral index for chlorophyll estimation of a forest canopy from hyperspectral images. In Zagajewski B., Sobczak M., (Eds.), Imaging Spectroscopy – New Quality in Environmental Studies. The 4th Workshop on Imaging Spectroscopy, Warsaw University and European Association of Remote Sensing Laboratories (EARSeL), Warsaw, Poland, 27.3.-29.3.2005, ISBN 83-89502-41-0.

**Malenovský Z.**, Lhotáková Z., Albrechtová J., Clevers J.G.P.W., Schaepman M.E., Cudlín P.: Variability in leaf optical properties of Norway spruce crowns. In Kerle N., Skidmore A.K., (Eds.), From Pixel to Processes, ISPRS Mid-term Symposium 2006 , Proceedings – CD ROM, WG VII/1: Fundamental Physics and Modelling, Enschede, The Netherlands, 8.5.-11.5.2006.